



# City Research Online

## City, University of London Institutional Repository

---

**Citation:** Das, D. (2019). Mixed formulation for seismic analysis of shear critical reinforced concrete, steel and composite structures. (Unpublished Doctoral thesis, City, University of London)

This is the accepted version of the paper.

This version of the publication may differ from the final published version.

---

**Permanent repository link:** <https://openaccess.city.ac.uk/id/eprint/24180/>

**Link to published version:**

**Copyright:** City Research Online aims to make research outputs of City, University of London available to a wider audience. Copyright and Moral Rights remain with the author(s) and/or copyright holders. URLs from City Research Online may be freely distributed and linked to.

**Reuse:** Copies of full items can be used for personal research or study, educational, or not-for-profit purposes without prior permission or charge. Provided that the authors, title and full bibliographic details are credited, a hyperlink and/or URL is given for the original metadata page and the content is not changed in any way.

**Mixed Formulation for Seismic Analysis of Shear Critical  
Reinforced Concrete, Steel and Composite Structures**

by

Dipankar Das

A dissertation submitted in partial satisfaction of the  
requirements for the degree of  
Doctor of Philosophy

in

Structural Engineering

in the division of

School of Mathematics, Computer Science and Engineering

of the

City, University of London

July 2019

*To my family*

# TABLE OF CONTENTS

LIST OF FIGURES.....	7
ACKNOWLEDGEMENTS.....	17
DECLARATION .....	20
ABSTRACT.....	21
Chapter 1 Introduction.....	24
1.1 General.....	24
1.2 Literature Review.....	26
1.2.1 Reinforced Concrete Members.....	32
1.2.2 Steel Members .....	46
1.2.3 Steel-Concrete Composite Members .....	53
1.3 Objectives and Scope .....	63
Chapter 2 Shear Critical Frame Element – Mixed Formulation .....	68
2.1 Overview.....	68
2.2 Element Kinematics .....	73
2.3 Section Kinematics.....	75
2.4 Equilibrium .....	77
2.5 Compatibility .....	78
2.6 Constitutive Laws.....	79
2.7 Variational Formulation .....	80
2.8 Material Model.....	87
2.8.1 Overview .....	87
2.8.2 Reinforced Concrete .....	95
2.8.2.1 Concrete – Biaxial.....	96

2.8.3	Steel .....	103
2.8.3.1	Steel - Biaxial .....	103
2.8.3.1.1	J2 Plasticity Model.....	105
2.8.3.1.2	Generalized Plasticity Model .....	110
2.9	Stability Criteria and State Determination .....	118
2.9.1	Stability Criteria.....	118
2.9.2	State Determination.....	121
2.10	Implementation .....	125
 Chapter 3 Correlation Studies – Shear Critical RC and Steel		
	Components .....	126
3.1	Overview.....	126
3.2	RC Beams .....	126
3.2.1	Beams by Vecchio and Shim (2004) .....	126
3.3	RC Columns.....	143
3.3.1	Columns by Xiao, Priestley and Seible (1993) .....	143
3.3.2	Column by Arakawa, Arai and Mizoguchi (1989).....	162
3.3.3	Column by Imai and Yamamoto (1986) .....	164
3.4	RC Shear Walls.....	166
3.4.1	Walls by Lefas, Kotsovos and Ambraseys (1990) .....	166
3.4.2	Walls by Tran and Wallace (2015).....	175
3.5	Steel Shear Beams.....	187
3.5.1	Shear Link by Hjelmstad and Popov (1983) – Monotonic Loading .....	187
3.5.2	Shear Link by Hjelmstad and Popov (1983) – Cyclic Loading	190

Chapter 4 Shear Critical Composite Element – Displacement and Mixed Formulation.....	193
4.1 Overview.....	193
4.2 Element Kinematics .....	194
4.3 Section Kinematics.....	197
4.4 Equilibrium .....	199
4.5 Compatibility .....	201
4.6 Constitutive Law .....	202
4.7 Variational Formulation .....	203
4.7.1 Displacement-based Formulation .....	203
4.7.1.1 State Determination.....	209
4.7.2 Mixed-based Formulation .....	211
4.7.2.1 Stability Criteria.....	217
4.7.2.2 State Determination.....	220
Chapter 5 Correlation Studies – Shear Critical Steel-Concrete Composite Components.....	224
5.1 Overview.....	224
5.2 SC Sandwiched Beam – Numerical Study.....	225
5.3 SC Sandwiched Beam by Leng and Song (2016) .....	234
5.4 SC Composite Beam by Nie, Xiao and Chen (2004) .....	236
Chapter 6 Shear Critical Frame Element –Mixed Formulation considering Geometric Nonlinearity .....	251
6.1 Overview.....	251
6.2 Element Kinematics .....	252
6.3 Section Kinematics.....	255

6.4 Equilibrium .....	257
6.5 Compatibility .....	258
6.6 Constitutive Law .....	259
6.7 Variational Formulation .....	259
6.7.1 Mixed-based Formulation .....	259
6.7.1.1 Stability Criteria.....	265
6.7.1.2 State Determination.....	265
Chapter 7 Correlation Studies – Shear Critical RC Component considering P-Delta Effect.....	267
7.1 Overview.....	267
7.2 RC Columns.....	268
7.2.1 Column by Barrera, Bonet, Romero and Miguel (2011) ....	268
7.2.2 Column by Legeron and Paultre (2000).....	275
7.2.3 Column by Caballero-Morrison, Bonet, Navarro-Gregori and Martí-Vargas (2012) .....	277
7.2.4 Column by Bae and Bayrak (2008) .....	280
Chapter 8 Summary and Conclusions .....	295
8.1 Summary.....	295
8.2 Conclusions.....	299
8.3 Recommendations for Future Research .....	303
Appendix A .....	305
Appendix B .....	308
Bibliography.....	322

## LIST OF FIGURES

2-1	Basic reference system without rigid body modes .....	73
2-2	Element nodal deformations .....	74
2-3	Section differential equilibrium .....	77
2-4	Linear Plasticity Model .....	94
2-5	Applied principal stresses and reinforcement directions of RC element .....	96
2-6	Generalized Plasticity Model .....	111
3-1	Geometry of A1, A2 and A3 beams .....	127
3-2	Cross-sections of A1, A2 and A3 beams .....	128
3-3	Load-Deflection Response of Beam A1 .....	129
3-4	Load-Deflection Response of Beam A2 .....	129
3-5	Load-Deflection Response of Beam A3 .....	130
3-6	Effect of Integration Points on Load-Deflection Response of Beam A1 .....	131
3-7	Variation of Shear Deformation along length of Beam A1 .....	131
3-8	Variation of Shear Force along length of Beam A1 .....	132
3-9	Variation of Bending Moment along length of Beam A1 .....	132
3-10	Variation of Curvature along length of Beam A1 .....	133
3-11	Principle Compressive Strain- Load Response at Loading Point of Beam A1 .....	133
3-12	Axial Strain- Load Response at Loading Point of Beam A1 .....	134

3-13	Effect of Integration Points on Load-Deflection Response of Beam A2	.....134
3-14	Variation of Shear Deformation along length of Beam A2	.135
3-15	Variation of Shear Force along length of Beam A2	.....135
3-16	Variation of Bending Moment along length of Beam A2	.....136
3-17	Variation of Curvature along length of Beam A2	.....136
3-18	Principle Compressive Strain- Load Response at Loading Point of Beam A2	.....137
3-19	Axial Strain- Load Response at Loading Point of Beam A2	.137
3-20	Effect of Integration Points on Load-Deflection Response of Beam A3	.....138
3-21	Variation of Shear Deformation along length of Beam A3	.138
3-22	Variation of Shear Force along length of Beam A3	.....139
3-23	Variation of Bending Moment along length of Beam A3	.....139
3-24	Variation of Curvature along length of Beam A3	.....140
3-25	Principle Compressive Strain- Load Response at Loading Point of Beam A3	.....140
3-26	Axial Strain- Load Response at Loading Point of Beam A3	.141
3-27	Geometry of RC Columns R1, R3 and R5	.....144
3-28	Cross-sections of R1, R3 and R5 Columns	.....145
3-29	Lateral Load-Deflection Response of Column R1	.....146
3-30	Lateral Load-Deflection Response of Column R3	.....147

3-31	Lateral Load-Deflection Response of Column R5	.....147
3-32	Lateral Load-Shear Deformation Response of Column R1	..148
3-33	Variation of Shear Deformation along length of Column R1	..149
3-34	Variation of Shear Force along length of Column R1	.....149
3-35	Lateral Load-Curvature Response of Column R1	.....150
3-36	Variation of Curvature along length of Column R1	.....150
3-37	Variation of Bending Moment along length of Column R1	151
3-38	Principle Compressive Strain – Loading Response of concrete fibre of Column R1	.....151
3-39	Axial Strain – Loading Response of longitudinal Rebar of Column R1	.....152
3-40	Lateral Load-Shear Deformation Response of Column R3	152
3-41	Loading-Axial Strain Response of Stirrup of Column R3 at Base Section	.....153
3-42	Loading-Principle Compressive Strain Response of Concrete Fibre of Column R3 at Base Section	.....153
3-43	Loading-Axial Strain Response of longitudinal Rebar of Column R3 .....	.....154
3-44	Loading-Principle Tensile Strain Response of Concrete Fibre of Column R3	.....154
3-45	Lateral Load-Shear Deformation Response of Column R5	..155
3-46	Lateral Load-Curvature Response of Column R5	.....155

3-47	Lateral Load-Displacement Response of Column R5	.....156
3-48	Effect of Number of Elements on Lateral Load-Displacement Response of Column R1	.....156
3-49	Effect of Number of Elements on Lateral Load-Displacement Response of Column R3	.....157
3-50	Loading-Principle Compressive Strain Response of Concrete Fibre of Column R5	.....157
3-51	Loading-Axial Strain Response of Stirrup of Column R5 at Base Section	.....158
3-52	Loading-Axial Strain Response of longitudinal Rebar of Column R5	.....158
3-53	Loading-Principle Tensile Strain Response of Concrete Fibre of Column R5	.....159
3-54	Lateral Load-Deflection Response of column OA5	.....163
3-55	Lateral Load-Deflection Response of column OA5 comparing with mixed flexure element	.....163
3-56	Lateral Load-Deflection Response	.....165
3-57	Lateral Load-Deflection Response comparing with mixed flexure element	.....165
3-58	Geometry of RC Walls SW21 and SW22	.....167
3-59	Lateral Load-Deflection Response of Wall SW21	.....168
3-60	Lateral Load-Deflection Response of Wall SW22	.....169

3-61	Variation of Shear Deformation along length of Wall SW21	170
3-62	Variation of Curvature along length of Wall SW21 .....	170
3-63	Principle Compressive Strain – Loading Response of Concrete Fibre of Wall SW21 .....	171
3-64	Axial Strain – Loading Response of Rebar Fibre of Wall SW21 ..	171
3-65	Principle Tensile Strain – Loading Response of Concrete Fibre of Wall SW21 .....	172
3-66	Principle Compressive Strain – Loading Response of Concrete Fibre of Wall SW22 .....	172
3-67	Axial Strain – Loading Response of Rebar Fibre of Wall SW22	173
3-68	Axial Strain – Loading Response of Rebar of Wall SW22 .....	173
3-69	Axial Strain – Loading Response of Rebar Comparison between the walls .....	174
3-70	Lateral Load-Deflection Response of Wall RW-A15-P10-S78....	177
3-71	Lateral Load-Deflection Response of Wall RW-A15-P2.5-S64...	177
3-72	Lateral Load-Shear Deformation Response .....	178
3-73	Lateral Load-Curvature Response .....	179
3-74	Vertical-Horizontal Displacement Response .....	179
3-75	Curvature-Horizontal Displacement Response .....	180
3-76	Loading-Axial Strain Response of Rightmost vertical Rebar at base section .....	180

3-77	Loading-Axial Strain Response of Rightmost horizontal Rebar at base section .....	181
3-78	Loading-Axial Strain Response of Rightmost horizontal Rebar at 316 mm above base section .....	181
3-79	Variation of Axial Strain of Rightmost horizontal Rebar along height of wall .....	182
3-80	Variation of Accumulated Plastic Tensile Strain of Rightmost vertical Rebar along height of wall .....	182
3-81	Variation of Principle Strain of Rightmost Concrete Fibre along height of wall RW-A15-P10-S78 at positive excursion .....	183
3-82	Variation of Principle Strain of Rightmost Concrete Fibre along height of wall RW-A15-P2.5-S64 at positive excursion .....	183
3-83	Cross-sections of Specimen 4 .....	188
3-84	Monotonic Load-Deflection Response of Specimen 4 .....	190
3-85	Cyclic Load-Deflection Response of Specimen 4 .....	192
4-1	Basic reference system without rigid body modes .....	195
4-2	Element nodal deformations .....	196
4-3	Section differential equilibrium .....	199
5-1	Geometry of Sandwiched Beam .....	228
5-2	Load-Deflection Response .....	230
5-3	Curvature distribution (minimum potential energy principle).....	230
5-4	Curvature distribution (HR variational principle) .....	231

5-5	Bending moment distribution (HR variational principle)	.....232
5-6	Bending moment distribution (minimum potential energy principle).....	232
5-7	Slip distribution (minimum potential energy principle)	.....233
5-8	Slip distribution (HR variational principle)	.....234
5-9	Bottom plate axial force distribution (minimum potential energy principle)	.....235
5-10	Bottom plate axial force distribution (HR variational principle)...	235
5-11	Load-Deflection Response of SCS beam JZ3.5-1	.....238
5-12	Cross-section of Composite Beam CBS-2	.....240
5-13	Load-Deflection Response of SC beam CBS-2	.....241
5-14	Shear Force distribution along the length of Beam	.....243
5-15	Shear Deformation distribution along the length of Beam	.....243
5-16	Interface Slip Distribution along the Length of Beam	.....244
5-17	Axial Deformation distribution along the length of Beam in Steel Section	.....245
5-18	Axial Deformation distribution along the length of Beam in Concrete Section	.....245
5-19	Shear Crack Angle distribution along the length of Beam in Middle fibre of Concrete Section	.....246
5-20	Axial Force distribution along the length of Beam in Steel Section	.....247

5-21	Axial Force distribution along the length of Beam in Concrete Section.....	248
5-22	Curvature-Loading Response at loading point .....	248
5-23	Principle Compressive Strain-Loading Response of top concrete fibre at loading point .....	249
5-24	Axial Strain-Loading Response of bottom rebar of concrete deck at loading point .....	249
5-25	Axial Strain-Loading Response of top rebar of concrete deck at loading point .....	250
6-1	Basic reference system without rigid body modes .....	255
6-2	Element nodal deformations .....	256
6-3	Section differential equilibrium .....	259
7-1	Geometry of Column Specimen .....	271
7-2	Cross-section of Column H60-10.5-C0-2-30 .....	271
7-3	Load-Deflection Response of Column H60-10.5-C0-2-30 .....	272
7-4	Load-Moment Response at Loading Point Section .....	273
7-5	Load-Curvature Response at Loading Point Section .....	274
7-6	Load-Strain Response at Loading Point Section .....	274
7-7	Load-Stress Response of bottommost Longitudinal Rebar at Loading Point .....	275
7-8	Stress-Strain Response of bottommost Longitudinal Rebar at Loading Point .....	275

7-9	Deformed Shape at 16.56 kN at post-peak region	.....276
7-10	Load-Deflection Response of Specimen 5	.....278
7-11	Geometry of Column Specimen	.....280
7-12	Cross-section of Column NF60L05V2S600	.....280
7-13	Load-Deflection Response of Column NF60L05V2S600	.....281
7-14	Cross-section of Column S17-3UT	.....283
7-15	Load-Deflection Response of Column S17-3UT	.....284
7-16	Cyclic Envelops	.....286
7-17	Reduction of Peak Shear Resistance due to P-Delta Effect (%)	..287
7-18	Moment-Loading Response at base section	.....287
7-19	Moment-Peak Loading Response at base section for positive excursion	.....288
7-20	Shear Force-Loading Response at base section	.....288
7-21	Shear Force-Peak Loading Response at base section for positive excursion	.....289
7-22	Curvature-Loading Response at base section	.....289
7-23	Curvature-Peak Loading Response at base section for positive excursion	.....290
7-24	Curvature-Peak Loading Response at 447 mm from base section for positive excursion	.....290
7-25	Stirrup Strain-Peak Loading Response at base section for positive excursion	.....291

7-26	Stirrup Strain -Peak Loading Response at 447 mm from base section for positive excursion .....	291
7-27	Principle Strain-Peak Loading Response of Rightmost Concrete Fibre at base section for positive excursion .....	292
7-28	Principle Strain-Peak Loading Response of Rightmost Concrete Fibre at 447 mm from base section for positive excursion .....	292
7-29	Axial Strain-Peak Loading Response of Rightmost vertical Steel Rebar at base section for positive excursion .....	293
7-30	Axial Strain-Peak Loading Response of Rightmost vertical Steel Rebar at 447 mm from base section for positive excursion .....	293
7-31	Axial Strain-Peak Loading Response of Rightmost vertical Steel Rebar at base section for negative excursion .....	294
7-32	Axial Strain-Peak Loading Response of Rightmost vertical Steel Rebar at 447 mm from base section for negative excursion .....	294
B-1	Monotonic non-softened and softened stress–strain curve .....	310
B-2	Cyclic Softened Compression Stress-Strain Relation .....	312
B-3	Cyclic Tensile Stress-Strain Relation (Ayoub, 1999) .....	316
B-4	Menegotto-Pinto model .....	320

## **ACKNOWLEDGEMENTS**

I would like to express my sincere gratitude to my advisor Professor Ashraf Ayoub for his mentorship and continuous encouragement throughout my research work. I thank him for giving me the freedom of pursuing research and consistently helping me to remain focused. Accomplishing this arduous task would have not been possible without his continuous trust and kind patience with me.

I am grateful to Professor Andreas Kappos for helping me to secure the three years University Doctoral Studentship in the City, University of London. It was not possible to pursue this research work without this scholarship. My heartfelt thanks to him for being my second supervisor and providing me an opportunity to fulfil my dream.

I would like to thank the members of my dissertation committee: Professor Yong Lu of the University of Edinburgh and Dr Panagiotis Mergos of the City, University of London for serving as external and internal examiners respectively and for their valuable time and kind attention. A special thanks to Dr Feng Fu for agreeing to serve as Chair of the committee.

I would also like to thank Postgraduate Research Course Officers Ms Nathalie Chatelain and Ms Savita Mary Afonso for their support during the

course of study. Especially, the issuing of various required documents for visa processing promptly, is greatly appreciated.

I am especially thankful to Professor Yogendra Singh of Indian Institute of Technology Roorkee, for being my mentor and friend since the days of my master degree. I would also like to thank Professor Anupam Chakrabarti of Indian Institute of Technology Roorkee, for his constant motivation towards pursuing higher studies since my undergraduate days in Civil Engineering.

I would remain indebted always to my wonderful wife, [REDACTED], for standing by my side during these difficult years. It was virtually impossible to continue this research work without her compromise, sacrifice, support and love. My heartfelt thanks will never be enough to her for leaving a very secured and comfortable life in Mumbai to accompany me to continue my passion and fulfil my dream.

This acknowledgement would be incomplete without expressing my deepest gratitude to my parents, [REDACTED], for their love and support throughout my entire life. Their immense effort to raise and educate us will always be inspirational and has helped me to become a responsible father.

I would also like to thank my mother in-law, late father in-law and brother in-law, [REDACTED], for their support and encouragement.

I am also grateful to have my sister, [REDACTED], brother in-law, [REDACTED], my elder brother, [REDACTED], and sister in-law, [REDACTED], for their love and continuous support. Unwavering guidance and encouragement of my elder brother throughout my life has been the backbone of my entire education.

I would also like to thank my colleagues in the City, University of London for helping me in the early days in UK and spending quality time with me in various occasions. A special thank goes to my friends who were the best witnesses of my struggles and have been my best support.

Finally, this research work would have not been complete without the immeasurable support of my [REDACTED] daughter, [REDACTED], who is our inspiration and source of happiness.

## **DECLARATION**

I grant powers of discretion to the University Librarian to allow this dissertation to be copied in whole or in part without further reference to me. This permission covers only single copies made for study purposes, subject to normal conditions of acknowledgements.

## **ABSTRACT**

### **Mixed Formulation for Seismic Analysis of Shear Critical Reinforced Concrete, Steel and Composite Structures**

by

Dipankar Das

Doctor of Philosophy in Structural Engineering

School of Mathematics, Computer Science and Engineering

City, University of London

Professor Ashraf Ayoub, Supervisor

This study presents the formulation of new two-dimensional frame finite element models for the analysis of shear-critical reinforced concrete, steel and steel-concrete composite structural members considering the interaction of axial force, bending moment and shear force under monotonic and cyclic loading conditions. The elements are developed by following a variational approach with consistent linearization of the governing equations. Shear deformation is considered through the Timoshenko-based section kinematics. Distributed inelasticity at the element and section levels are considered through section integration points along the length of the element and material fibre discretization across the cross-section respectively. Multi-axial stress states due to crack-induced anisotropy in reinforced concrete fibres is simulated through a fixed crack smeared softened membrane model which is based on the stress equilibrium, the strain compatibility and the constitutive relationships of materials. 2d J2 plasticity and generalized plasticity models with radial return mapping algorithm are implemented for structural steel fibres under

monotonic and cyclic loading conditions respectively to accommodate the interaction among the multiaxial stress states. Three types of frame elements are formulated, namely a shear frame element which is applicable for both shear critical reinforced concrete and steel members, a composite shear beam element considering coupling between bond-slip and shear deformation, and a shear critical frame element considering both material and geometric nonlinearity.

The new shear beam element formulations for reinforced concrete and steel members are based on a two-field mixed formulation where both section forces and displacements are simultaneously approximated within the element through independent interpolation functions. New displacement shape function has been developed, which can alleviate the shear locking issue for displacement-based formulation and also, satisfy the new stability criteria for two-field mixed-based formulation considering shear deformation. The element is validated through correlation studies with experimental results of shear-critical RC beams, columns, walls and steel beams for monotonic and cyclic loading conditions.

The new shear beam element formulations for steel-concrete composite members with deformable shear connectors are based on a displacement and two-field mixed formulations, where the transfer of forces between

steel and concrete is modelled by distributed spring elements. New stability criteria has been proposed for shear critical inelastic composite mixed-based formulation with partial interaction. The element is validated through correlation studies with experimental results of shear-critical Steel-Concrete (SC) composite beams for monotonic loading conditions.

This research work concludes with the development of a new shear beam element under large displacements which is based on two-field mixed formulations. The corotational formulation is used to describe the large displacement at the element nodal level and degenerated Green-Lagrange strain measures are used at the basic element level. Since the development of consistent state determination of fibre element formulation three decades ago, this is the first shear fibre beam element formulation which can reasonably reproduce the experimentally-observed post-peak softening region of shear force-shear deformation curve of RC columns. The element is validated through correlation studies with experimental results of P-Delta dominated flexure-shear critical RC columns under monotonic and cyclic loading conditions.

# Chapter 1 Introduction

## 1.1 General

In today's engineering practice, it has become imperative to have a robust and reliable numerical model to design new structures and to assess existing structures for the purpose of rehabilitation to achieve the desirable seismic performance following the performance based seismic design philosophy. This inelastic analysis-driven design process requires the global load-deformation response of the structures under moderate to high seismic risk to determine various damage states, which in turn are controlled by the failure modes of the individual components of the structures. The failure mode of individual components depends on the material, structural detailing, geometry and multi-axial stress state present in the system under the application of external input energy in the form of load and deflection. Traditionally, axial-flexure interaction has been studied extensively because of its determinate nature of stress condition, while the shear deformation brings an internal indeterminacy in the stress condition which requires the extra compatibility conditions to reach a unique solution, has made the research complex for several decades.

Continuum finite element analysis is best suited for the simulation of multi-axial stress states present in the system as the degrees of freedom of continuum elements can capture the nonlinear variation of deformations

along all the three directions of the geometry simultaneously. However, it needs huge numbers of degrees of freedom to reach the converged deformation and consequently stress conditions, which makes it very expensive for analysing global structures. Therefore continuum finite element analysis is suitable for simulation of local regions where accuracy cannot be achieved by using macroscopic models which use various assumptions to find the numerical solution of global structures with reasonable accuracy yet more efficient and much less computational and associative cost.

This research work develops various new two-dimensional beam-column frame elements considering axial-flexure-shear interaction through implementing multi-axial constitutive material models for reinforced concrete and steel. Several elements have been developed for reinforced concrete, steel and steel-concrete composite members with partial interaction for monotonic and cyclic loading. The frame elements have been further extended to include large displacement effects on cyclic response of reinforced concrete members. Two types of functional are used to formulate these elements i.e. potential energy and Hellinger- Reissner functional. Performance evaluation of developed inelastic frame element formulation with respect to accuracy, efficiency and robustness is essential to satisfy two conditions together: 1. Equilibrium of force in the interior

and 2. Displacement compatibility with the adjacent elements. Accuracy is a measure of the degree of agreement between the numerical and experimental measured response of structural members. Robustness refers to its numerical stability while efficiency refers to the computational cost of the whole member simulation. Elements developed based on mixed based formulations exhibits more robust and accurate behaviour than that of displacement-based formulations and are quite efficient for inelastic seismic analysis of large structural systems throughout the loading history.

## **1.2 Literature Review**

The literature review will deal with various frame element formulations which have been developed by various researchers throughout the world. We will focus on particularly those elements which have the capability to simulate axial-flexure-shear interaction considering both geometric linear and non-linear formulations for reinforced concrete, steel and steel-concrete composite members under monotonic and cyclic loading conditions.

Conventional frame element formulations need two ingredients. The first one is the variational functional which relates internal and external energy of the system. The other one is the section level kinematics which connects states of stress and strain at the section and the material fibres. By varying these two ingredients several frame element formulations can be

developed. For example, if the section level kinematics follows Euler-Bernoulli beam theory which assumes plane sections before deformation remain plane and normal to the deformed axis of the beam after deformation, beam element formulations based on this type of section level hypothesis are suitable to simulate the experimentally observed behaviour of flexure critical members. On the other hand, if the section level kinematics follows Timoshenko beam theory which assumes plane sections before deformation remain plane but not normal to the deformed axis of the beam after deformation, beam element formulations based on this type of section level hypothesis are suitable to simulate the experimentally observed behaviour of shear critical members. There are other types of section level kinematics available in the literature such as higher order beam theory which removes the restriction imposed in the Timoshenko beam theory i.e. the constant shear strain and stress across the section depth which violates the mechanical boundary conditions at the top and bottom fibres of the section. This type of higher deformation theory assumes parabolic distribution of shear stress and strain across the section depth in priority and is particularly suitable for the analysis of the system up to the linear elastic material state. The true variation of the shear stress or strain along the section depth is not a known entity at the start of the analysis as it depends on the evolving material states (Vecchio et al.(1988)). Therefore, more generalized material state dependent section kinematics have been

used to simulate the shear behaviour for particularly reinforced concrete members under monotonic loading conditions. This type of formulations need to satisfy the partial differential equation of equilibrium at the material fibre level and a coupling approach between the section and fibre level (Bairan et al. (2006a)), which may introduce convergence issues and prevents them to implement cyclic loading conditions which poses additional challenges to simulate the unloading and reloading stiffness degradation with crack opening and closing phenomenon.

There are different types of elements that have been developed by varying the variational functional. For example, if the element formulation is based on potential energy functional, we termed it as displacement based formulation as the principle argument of this functional is nodal displacement. In this formulation, we need to have only displacement based shape functions which are required to satisfy the property of the shape functions and the compatibility conditions in its strong form. This type of formulation is computationally expensive and needs a huge number of elements to simulate the stress variables and inelastic section deformations along the length of the member. On the contrary, if the element formulation is based on complementary energy functional, we termed it as force based formulation as the principle argument of this functional is nodal forces. In this formulation, we need to have only force based shape functions which

are required to satisfy equilibrium between the applied nodal force and sections forces which in turn need to satisfy the differential equilibrium equations at section level in its strong form. This type of formulation is computationally cheap and superior to that of displacement based formulation as the inelastic section deformations are determined from the equilibrated force shape functions. However, there is a limitation of the force based formulation i.e. they are suitable for the applications where the section forces can be obtained from the available equilibrium equations i.e. the system must be internally statically determinate. If this criteria fails, then additional assumptions will come into picture and the original differential equation of equilibrium will not get satisfied in its strong form and the formulation consequently lose its credibility for not fulfilling its most powerful characteristics.

There are other alternative element formulations where we use both nodal displacement and force as principle arguments and consequently we need to have both displacement and force shape functions. This type of formulation is known as Hellinger-Reissner formulation and does not need any subsidiary conditions to fulfil compared to its counterparts such displacement and force based formulations. However, both shape functions needs to pass stability criteria for HR formulations which makes it very useful for the applications where the internal section forces cannot be

determined from the available equilibrium equations. This gives an additional advantage over force based formulations as HR formulations can be applied for internally statically indeterminate system. However, cautions needs to be adopted to choose judiciously both the displacement and force shape functions.

Element formulations are not self-sufficient. Solver and element formulations work together. They provide information such as element resistance and stiffness matrix to the solver and the solver assembles this information for all the elements and solve for the principle nodal argument. However, most solvers can handle only nodal displacements as a principle argument. Therefore, the assembled system always follows the displacement based formulation. It has to be noted that when we use a variational functional for element formulation, the functional is applied to the assembled elements not to a particular single element. It introduces an inconsistency for force based formulations which has only force nodal degrees of freedom at the element level. Therefore, force based formulations are not variationally a consistent formulation. On the other hand, HR formulation has nodal displacement degrees of freedom, which makes it compatible to the solver once the nodal force degrees of freedom gets statically condensed out. However, both force based and HR formulations use complementary energy term which needs the

determination of fibre strain from the fibre stress. In reality, we have material constitutive law from the experiments which are strain driven material. This introduces a residual term which gets dissipated through the internal element iteration and therefore makes these formulations variationally consistent from the term of strain energy perspective (Hjelmstad et al. (2005)). Moreover, there is another mixed based formulation available in the literature i.e. three-field Hu-Washizu variational functional which needs three independent arguments. In this formulation, when the section deformations and the nodal force get statically condensed out, the state determinate procedure follows the force based formulation.

In the following, we will present various element formulations developed by researchers throughout the world for reinforced concrete, steel and steel-concrete composite members limited to those elements which are able to capture the axial-flexure-shear interaction. We will focus only on those element formulations which are based on distributed inelasticity at the element and section levels considered through section integration points along the length of the element and material fibre discretization across the cross-section respectively. Both available geometric linear and nonlinear element formulations will be discussed.

Apart from distributed inelasticity approach there are two other types of inelastic element formulation available in the literature i.e. concentrated inelasticity models and spread inelasticity models. Interested readers are referred to Filippou et al. (2004) and Zimos (2017) who have offered extensive review and formulation of these types of models respectively. The challenge of these kinds of elements are to simulate the interaction among various response variables along with huge experimental calibration required to define section levels generalized force-deformation curves for different loading and boundary conditions.

### **1.2.1 Reinforced Concrete Members**

Flexure-shear interaction arises due to crack induced anisotropic behaviour present in the concrete for its very different non-linear response in tension and compression. This effect reduces the shear resisting capacity primarily because the induced principle tensile strain reduce the compressive strength of the material and at the same time diagonal cracks make the system more flexible and consequently reduces the shear stiffness of the reinforced concrete beams. The effect of shear on flexure introduces an additional stress into the longitudinal bars in beam depending on the position in a section, whereas the effect of flexure on shear introduces an additional stress in the tie bars once the inclined crack forms (particularly evident on shear failure of slender reinforced wall in the later stage of cyclic loading history). Therefore, simulation of flexure shear interaction is essential to

capture the experimentally observed global and local responses accurately. Axial forces reduce the flexural strength of reinforced concrete columns, whereas the shear capacity, stiffness and deformation capacity of the columns depend on the nature of axial force and state of applied lateral loading history i.e. its effect on shear behaviour may be completely different before and after the peak shear strength. Axial compressive load may increase the shear strength before the peak shear strength by introducing additional frictional effect whereas after peak shear strength region, it may aggravate the negative shear stiffness as the friction effect will get lost by that time and drop of shear resistance may be faster until the onset of axial failure. After the onset of axial failure, disintegrated parts will move like rigid body motion and remain in contact due to applied axial compression load and consequently shear friction will get developed at major inclined plane and rate of drop of shear resistance will be lesser compared to that of before the onset of axial failure. It is to be noted that, during this post peak shear region p-delta effects contributes a substantial part to reducing the shear resistance along with longitudinal bar buckling under compression, whereas bar fracture substantially reduces the shear resistances with making the system hugely flexible. The above description of shear force resisting process indicates that if we want to capture the whole post-peak range of the shear resistance and shear deformation curve, we need to model large displacement effect, bar buckling and bar fracture

in a rational way along with the right choice of section kinematics as Timoshenko section kinematics will not be valid at this time of loading stage. In the present research work, element formulation considers the large displacement effect with multi-axial constitutive material which can couple the shear deformation with the axial deformation arises due to axial and flexural effect in a rational way.

In the following, we will first discuss those beam element formulations which are formulated based on linear geometry i.e. small deformation theory.

Petrangeli et al.(1999) developed an equilibrium based fibre beam element formulation considering parabolic distribution of shear strain along the section depth. To include axial-flexure-shear interaction, the microplane model for concrete proposed by Bazant et al. (1985) has been implemented. Axial strain in the shear reinforcement is determined from the vertical equilibrium between the stirrup tensile force and concrete compressive force of 2d reinforced concrete fibre. The element is validated with experimental results for cyclic loading conditions (Petrangeli(1999)). Later on Jiang et al. (2010) has extended this element formulation to model the inelastic flexure-shear interaction of moderate aspect ratio reinforced concrete wall with DRAIN-2DX program (Prakash et al. 1993).

Marini et al. (2006) presents a force based fibre beam element formulation considering Timoshenko based section kinematics to include axial-flexure-shear interaction for monotonic and cyclic loading conditions. Ad hoc nonlinear shear force – shear deformation law is used to include the shear effect at the section level. Therefore, true coupling with axial and flexure effect has not been considered at the section level, however due to adopting equilibrated force shape functions which is derived from the solution of governing differential equation of equilibrium at the section level, axial-flexure-shear interaction is achieved at the element level. This study has been able to reproduce the experimentally observed post-peak softening region of shear force-shear deformation curve under cyclic loading condition.

Ceresa et al. (2007) provided a literature review of fibre based element formulations which are able to simulate axial-flexure-shear interaction through various multi-axial material constitutive law such as Strut and Tie models (Guedes et al. (1994), Ranzo et al. (1998) and Martinelli (1998)) , microplane model, smeared crack models (Rahal et al. (1995), Vecchio et al.(1988),Bentz (2000) and Bairan (2006b)), damage models (Kotronis et al. (2005) and Mazars et al. (2006)), etc. All the elements developed up to

this time were based on either displacement based or flexibility based. Interested readers are encouraged to access these research works.

Gregori et al. (2007) proposed a displacement based 3d curved Timoshenko fibre beam element considering axial-flexure-shear-torsion interaction through the modified compression field theory at the material level. Reduced integration has been used to alleviate shear locking phenomenon. The element is validated with experimental results for monotonic loading conditions only.

Saritas et al. (2009) developed a mixed based Timoshenko fibre beam element which can take care of the inelastic axial-flexure-shear interaction through the use of plastic-damage model for concrete material at the fibre level. The special feature of this element is that it is based on three field Hu-Washizu variational principle where equilibrated section forces and discontinuous section deformations are used. This formulation does not need any displacement shape functions. The element is validated with experimental results for both monotonic and cyclic loading conditions. This model is computationally demanding as both section force and section deformation need to be condensed out before sending nodal displacement to the solver. Also, plastic-damage model for concrete can induce

convergence issues during internal iterations of vertical equilibrium at fibre level.

Ceresa et al. (2009) developed a displacement based Timoshenko fibre beam element. This research work considers the coupling of axial-flexure-shear interaction by implementing the Modified Compression field theory at the fibre level. A bubble function has been introduced with the linear shape function to remove the shear locking effect which is a serious issue for displacement based finite elements. The element has been validated for cyclic loading conditions however simulation of post-peak softening region needs additional research in the constitutive models of materials and other associated shear force resisting mechanisms.

Mohr et al. (2010) presented a force based fibre beam element considering flexure-shear interaction through smeared crack models at the material level. The special characteristics of this element formulation are that the variation of shear and vertical strains are determined from the current material states. It is to be noted that the vertical strain is an integral part of the shear resisting mechanism which gets suppressed in case of Timoshenko section kinematics. The element is validated with experimental results for monotonic loading conditions only.

Mullapudi et al. (2010) formulated a force based 2d Timoshenko fibre beam element considering axial-flexure-shear interaction at the material level through the bi-axial softened membrane model. The special characteristic of this element is that smeared shear stress along the inclined crack has been explicitly modelled through the fixed crack softened membrane model. Other valuable contribution of this model is that the smeared stress-strain curve of steel and concrete material along with cracked Poisson ratio before and after the yielding of steel has been successfully implemented. Mullapudi et al. (2013) has extended this element formulation for 3d axial-flexure-shear-torsion interaction with tri-axial concrete material states. These elements are validated with experimental results for both global and local response variables for monotonic, cyclic and dynamic loading conditions.

Guner et al. (2011) developed a displacement based fibre beam element considering flexure-shear interaction at the material level through fibre beam element considering flexure-shear interaction at the material level through modified compression field theory with plastic strain offsets to make the material model applicable for cyclic loading conditions. The element has used parabolic shear strain profile along the section depth. The element is validated through experimental results of shear critical frames under cyclic loading conditions.

Stramandinoli et al. (2012) formulated a 2d displacement based Timoshenko fibre beam element considering flexure-shear interaction at the material level through modified compression field theory. The displacement shape function is used as proposed by Reddy (1997) which is different than the conventional displacement shape function as the flexure and shear rigidity terms are embedded in it. The element is validated with experimental results for monotonic loading conditions only.

Long et al. (2014) proposed a 3d displacement based fibre beam element with degenerated solid elements. Reduced integration method is used to remove shear locking. Axial-flexural-shear interaction is adopted by unified concrete plasticity model along with Hinton concrete model to simulate crack opening and closing phenomenon. The element is validated with experimental results for monotonic loading conditions only.

Li et al. (2016) developed a 3d displacement based Timoshenko fibre beam element considering axial-flexure-shear interaction at the material level through enhanced tri-axial modified compression field theory by incorporating the Poisson effect, plastic deformation and other non-mechanical deformations as strain offset. The element is validated with experimental responses for both one and bi-directional shear loading

conditions. The element is able to capture the pinching effect observed in the experimental tests under bi-directional cyclic shear loading conditions.

Kagermanov et al. (2017) developed a force based fibre beam element considering axial-flexure-shear interaction through a smeared crack orthotropic constitutive model where shear strain components at the crack, arising from deviations between principal and crack directions, are related to shear stresses by means of a shear stiffness term that fully satisfies compatibility and equilibrium conditions. The special feature of the element formulation is that an exact shear strain profile and corresponding shear stress distribution over the cross section has been developed using an averaged form of inter-fibre equilibrium over the cross section and piecewise linear interpolation of the shear strain distribution without considering section warping and distortion produced due to shear deformation. The element is validated with experimental results for monotonic and cyclic loading conditions.

Feng et al. (2017) formulated a displacement based Timoshenko fibre beam element considering flexure-shear interaction at the material level through concrete multidimensional softened damage plasticity model. The concrete material parameters are determined from tensile and compressive fracture energy only without considering steel fracture energy (Pugh et al. (2015)

and Kenawy et al. (2018)) to avoid mesh-sensitivity issue. In addition, the element can capture the anchorage bond-slip (Feng et al. (2018)) which in turn force the joint to rotate and consequently contribute in lateral shear deformation. The stepped bond stress distribution was assumed inside the joint and bond-slip was implicitly considered through modification of uniaxial steel material model due to the derived slip. The element is validated by correlation studies of experimentally observed responses under cyclic loading conditions and able to simulate the pinching effect due to the inclusion of anchorage slip into the element formulation.

Kagermanov et al. (2018) proposed a force based 3d fibre beam element considering axial-flexure-shear-torsion interaction considering 3d fixed crack smeared orthotropic model for concrete material. Unlike his previous study for 2d element with shear strain profile developed from inter-fibre equilibrium, in this 3d element formulation Timoshenko section kinematic has been adopted. Torsional effects are included through the Saint-Venant theory of torsion, which accounts for out of plane displacements perpendicular to the cross section due to warping effects. The element is validated with experimental results for monotonic and cyclic loading conditions.

Hereafter, we will present the element formulations based on large deflections theory. There are three approaches to include the nonlinear geometry effect into the element formulations i.e. the total Lagrangian formulation which uses the undeformed structure as a fixed reference configuration, the updated Lagrangian formulation which uses the last deformed configuration as a reference configuration for the current time step and the corotational formulation which defines a new undeformed reference configuration at every time step whose position is based on the end node coordinates of the deformed element. Most of the research works considering large displacement effect have been concentrating on steel and composite structures.

In the following we will discuss research works which have been carried out for reinforced concrete structure including nonlinear geometry effect.

Long et al. (2013) has developed a 3d displacement based corotational beam element using vectorial rotational variables which are three orthogonal components of normal vector and thus commutative additions are possible in the incremental solution process. The flexure-shear interaction for reinforced concrete material is considered uncoupled in this formulation. The element is validated with experimental results for monotonic loading conditions only.

Gendy et al. (2018) recently developed two fibre beam element formulation considering potential energy and Hellinger-Reissner functional for reinforced concrete components. These element formulations consider the axial-flexure interaction only. The special feature of these element formulations are the implemented numerical robust state determination process and complex uniaxial cyclic constitutive material law for both steel and concrete. The element is validated with experimental results of flexure critical P-delta dominated reinforced concrete specimens for both monotonic and cyclic loading conditions for global and local response variables.

Re et al. (2018) proposed a mixed based 3d corotational fibre beam element formulation considering axial-flexure-shear interaction through 3d damage-plastic concrete material law at the fibre level. Numerical localization issue has been considered at the section level instead of fibre level. The element is based on four-field Hu-Washizu variational principle where the additional field has been introduced to include the cross-section warping effect in the element formulation. Small deformation theory has been adopted in the basic element level. The element is validated with experimental results of flexure critical P-delta dominated reinforced concrete specimen for cyclic loading condition. The main limitation of this

model is that small P-Delta effect cannot be simulated as this formulation does not use any displacement shape function inside the element state determination. More number of elements are required to simulate this characteristics which in turn will make the simulation computationally demanding and expensive. While two-noded Hellinger-Reissner formulation with only single element will be able to simulate both small and large P-Delta effect which are necessary to predict accurate plastic hinge length for slender columns.

From the above literature survey of element formulations of reinforced concrete structures, the following observations can be made:

1. Very limited amount of research works have been concentrated on the axial-flexure-shear interaction at the post-peak softening region of shear force-shear deformation curve. There are plenty of opportunity still remains and huge research work needs to be conducted in future to include various resisting mechanisms such as longitudinal bar buckling and fracture, mechanisms related to determine before and after the onset of axial failure, cyclic damage, robust crack opening and closing phenomena under cyclic loading etc. in the fibre element formulation.

2. So far there are basically three types of fibre element formulations that have been developed which are able to simulate axial-flexure-shear interaction i.e. displacement based, force based and three-field mixed based. There are still lots of scope remaining for other types of element formulation such as hybrid and two field mixed based formulations which may be more efficient and robust.
3. Very limited amount of research work have been conducted for reinforced concrete structures considering geometric nonlinearity effect. Future research work should be concentrated in this area, as P-delta effect is one of the main players to contribute to the drop of shear resistance at the post-peak softening region of shear force-shear deformation curve. Lots of opportunities remain for various types of element formulations to simulate inelastic axial-flexure-shear interaction with large displacement effect.
4. Very limited work has been conducted to handle the numerical localization issue for flexure-shear critical cases. Rational approach to reach the concrete solution of this problem is yet to be established for fibre beam element formulations. In this regard, readers are encouraged to follow the research work by Zimos et al. (2018) for spread plasticity beam element formulations.

5. Currently anchorage-slip effect in fibre element formulations needs the assumption of bond stress/strain distribution inside the joint region. Robust model of anchorage-slip considering bond stress/strain variation inside the connection based on equilibrium, compatibility and constitutive law with inelastic axial-flexure-shear interaction is yet to be developed in fibre element formulations.

### **1.2.2 Steel Members**

Shear force in steel beams is primarily resisted by the developed diagonal tensile and compressive resistance in the web region of the sections. Under compression, web may be subjected to diagonal buckling. To resist or delay the buckling in the web, stiffeners are provided in the shear dominated steel beams such shear links in eccentrically braced frames and hybrid coupled walls. Shear links are designed to control the damage and used it as fuse to reduce the axial compression demand in the bracings so that bracing can resist the axial compressive force without going through buckling and contributes in providing the required global lateral strength, stiffness and stable energy dissipation under cyclic loading conditions. It is therefore utmost important to simulate the shear resisting mechanism of steel beams like shear links considering the axial-flexure-shear interaction through

multi-axial material constitutive law for monotonic and cyclic loading conditions.

There are three types of inelastic element formulation available in the literature i.e. stress resultant models with and without fibre models and pure distributed inelasticity models to simulate axial-flexure-shear interaction. Interested readers are referred to Bosco (2015) for pure stress resultant models and Kanvinde et al. (2015) and Belega et al. (2017) for mixed fibre and stress resultant models. The challenge of these kinds of elements are to simulate the interaction among various response variables along with huge experimental calibration required to define section levels generalized force-deformation curves for different loading, geometry and boundary conditions.

In the following we will discuss the inelastic element formulation for steel members considering axial-flexure-shear interaction with distributed inelasticity approach including geometric nonlinear effect considered through a corotational approach.

Simo et al. (1984) developed a displacement based fibre beam element considering axial-flexure-shear interaction through elastic-plastic material law without considering nonlinear hardening at the fibre level. Reduced

integration has been used to get rid of shear locking. Element is validated with experimental results of shear links for both monotonic and cyclic loading conditions.

Saritas et al. (2009) developed a mixed based Timoshenko fibre beam element which can take care of inelastic axial-flexure-shear interaction through the use of J2 plasticity and generalized plasticity model for steel material at the fibre level. The special feature of this element is that it is based on three field Hu-Washizu variational principle where equilibrated section forces and discontinuous section deformations are used. This formulation does not need any displacement shape functions. The element is validated with experimental results for both monotonic and cyclic loading conditions. This model is computationally demanding as both section force and section deformation need to be condensed out before sending nodal displacement to the solver.

Papachristidis et al. (2010) proposed a force based 3d Timoshenko fibre beam element considering axial-flexure-shear-torsion interaction through closed form 3d J2 plasticity material model at the fibre level developed by Yamada et al. (1968). The special feature of this element formulation is that element kinematics are obtained by natural mode method developed by Argyris et al. (1998). The element is validated with experimental results for monotonic, cyclic and dynamic loading conditions.

Triantafyllou et al. (2011) developed a displacement based Timoshenko beam element considering axial-flexure-shear interaction through multi-axial Bouc-Wen nonlinear material model. Shear locking phenomena has been removed by using the exact shape functions obtained by solving the governing differential equations for linear elastic case as proposed by Rakowski (1990) and Friedman et al. (1993). The element is validated with experimental results of shear critical steel specimens for monotonic, cyclic and dynamic loading conditions.

Alsafadie et al. (2011) developed a 3d mixed based beam element. The cross section is discretized using isoparametric quadratic finite elements with four number of gauss points. Axial-flexure-shear-torsion interaction has been considered through von Mises material models at integration points. Linear shape functions for displacements are used for all the section displacement variables. The element is developed based on two-field Hellinger-Reissner variational principle. Corotational approach has been used to include nonlinear geometry effects. The element is validated with experimental results for monotonic loading condition only.

Soydas et al. (2013) proposed a 3d mixed based fibre beam element considering axial-flexure-shear-torsion interaction through 3d J2 plasticity

model at the fibre level. Three-field Hu-Washizu variational principle has been used. It removes the shear locking phenomena automatically. The element is validated with experimental results of uniform and tapered steel specimens for monotonic loading conditions. This model is computationally demanding as both section force and section deformation need to be condensed out before sending nodal displacement to the solver.

Li et al. (2013) developed a displacement based Timoshenko fibre beam element considering axial-flexure-shear interaction through multi-axial J2 plasticity model. Shear locking phenomena has been removed by using the exact shape functions obtained by solving the governing differential equations for linear elastic case as proposed by Reddy (1997). The element is validated with experimental results for monotonic loading conditions only.

Correia et al. (2015) formulated a 3d force based higher order fibre beam element considering flexure-shear-torsion interaction at the material level through linear J2 plasticity model for steel material (Almeida et al. (2015)). The element is validated with experimental responses for monotonic loading conditions only as the implemented material model may not be suitable for cyclic loading conditions.

Rezaiee-Pajand et al. (2015) developed a 3d force based Timoshenko fibre beam element considering axial-flexure-shear-torsion interaction at the material level through a 3d elastic-plastic material model. Corotational approach has been used to include nonlinear geometry effect. The element is validated with experimental responses for monotonic loading conditions only.

Ding et al. (2018) proposed a displacement based fibre beam element considering axial-flexure-shear interaction at the material level through 2d Chaboche elasto-plastic material model incorporating both nonlinear kinematic and isotropic hardening. The special feature of the element is that it can simulate the flange and axial restraint effect on shear link capacity. The element is validated with experimental responses for both monotonic and cyclic loading conditions.

Silva et al. (2018) developed a displacement based Timoshenko fibre element. Material rigidity dependent displacement shape functions have been used. Material nonlinearity is considered based on the plastic zone method. The special feature of the element is that second order effects (big and small P-delta) and residual stress effect have been considered. Corotational approach has been used to include nonlinear geometry effect.

The element is validated with experimental responses for monotonic loading conditions only.

From the above literature survey of element formulations of steel structures, the following observations can be made:

1. There is no study to simulate the fracture process of steel material at the post hardening stage in the fibre element formulation with axial-flexure-shear interaction.
2. So far there are basically three types of fibre element formulations that have been developed which are able to simulate axial-flexure-shear interaction i.e. displacement based, force based and three-field mixed based. Only one study considers the two-field mixed formulation, however the element formulation cannot be termed as fibre beam element as the cross-section of the element was discretized by finite elements. Therefore, there are still lots of scope remaining for other types of element formulations such as hybrid and two field mixed based formulations which may be more efficient and robust.

3. Two research works have been conducted for steel structures considering geometric nonlinearity effect with axial-flexure-shear interaction. However, there is still an opportunity for various types of other element formulations to simulate inelastic axial-flexure-shear interaction with large displacement effects with robust inelastic constitutive material law.

### **1.2.3 Steel-Concrete Composite Members**

There are several types of steel-concrete composite systems available in the literature. The current research work focuses on two types of composite systems. The first one is the old conventional two-layer steel-concrete composite deck system where concrete slab is connected to the steel beam through shear studs. The other one is quite new compared to the old one i.e. steel-concrete-steel sandwiched systems where two thin steel plates are connected by tie rods integrally and a middle thick concrete layer is sandwiched between the top and bottom steel plates and connected by the shear studs with each steel layer. Shear resisting mechanism in these two types of composite system is different. It was earlier thought that the concrete slab in two-layer composite systems contributes very less amount in the overall shear resistance and hence concrete contribution in shear has not been included in the design standards. However, recent experimental studies (Nie et al. (2004)) has proved that the concrete layer provides 33%

to 56% shear resistance which cannot be neglected and should be included into the design standards in a rational way. On the other hand, shear resistance in three-layer sandwiched systems is mainly coming from thick concrete layer till the formation of full diagonal shear cracks. Later on, shear action gets resisted by the top and bottom steel plate cage connected by the tie rods with the help of shear studs. Therefore, for this kind of sandwiched system, after formation of full diagonal shear cracks, a huge amount of residual shear capacity remains. In both types of composite systems, shear studs deforms due to their finite stiffness and thus transfer the shear force between the concrete and steel layers. Hence, it is imperative that analysis tool should be capable of simulating the experimentally observed material inelasticity and will help to develop the reliable inelastic analysis driven design process for these types of steel-concrete composite systems.

There are mainly two types of analysis procedures used in the previous research works i.e. analytical formulations (Challamel et al. (2011) and Martinelli et al. (2012)) and finite element analysis. The analytical formulations are based on linear elastic material and simple boundary conditions. Therefore, it is difficult to simulate the experimentally observed behaviour through analytical formulations especially when the complex nature of load resisting process with material nonlinearity under multiaxial

stress interactions is involved. On the other hand, finite element analysis can handle this type of behaviour efficiently. There are two types of elements that are generally used in finite element analysis i.e. continuum elements and structural frame elements. Many researchers have performed detailed finite element analysis with continuum elements by using available commercial software to reproduce the experimentally observed responses. However, this type of analysis involves a huge number of degrees of freedom and hence, they are suitable for simulation of local region because of the huge amount of cost associated to analyse the complete global structure. Therefore, frame finite element analysis is the alternative one which has been used by various researchers as they can efficiently simulate both local and global behaviour of complete composite structures with reasonable accuracy and much less computational cost.

In the following, we will discuss the research works which has been carried out considering frame finite elements. Extensive amount of frame finite element studies have been carried out considering axial-flexure interaction in the past. Interested readers are referred to Spacone et al. (2004) and Lee et al. (2015) for flexure critical frame element formulations. The current research work focuses on the simulation of shear critical composite structures. Therefore, in the following we will discuss those frame finite element formulations which are able to simulate axial-flexure-shear

interaction in steel-concrete composite structures considering partial interaction.

We will start our discussion on those frame element formulations which are simulating axial-flexure-shear interaction for linear elastic materials.

Schnabl et al. (2007) developed a strain based Timoshenko composite beam element with partial interaction through the modified principle of virtual work where the strain field vector is the unknown quantity which makes the formulation locking free from both shear and slip perspectives. The element is validated with numerical responses for monotonic loading conditions only.

Da Silva et al. (2009) presented a displacement based Timoshenko composite beam element. Partial interaction is simulated by zero thickness four-node continuum interface elements. The element is validated with numerical responses for monotonic loading condition only.

Hjiaj et al. (2012) proposed a displacement based Timoshenko composite beam element considering a continuous relationship between the interface shear flow and the corresponding slip. Displacement shape functions are derived from the closed-form solution of the governing equations to avoid

curvature and shear locking phenomena. Corotational approach has been used to include nonlinear geometry effect. The element is validated with numerical responses for monotonic loading conditions only.

Chakrabarti et al. (2012) formulated a displacement based higher order composite beam taking into account the effect of longitudinal as well as vertical partial interaction between the adjacent layers. A third order variation of the axial displacement of the fibres over the beam depth is taken to have a parabolic variation of shear stress which is also made zero at the beam top and bottom surfaces. As a result, element formulation becomes free of shear locking problem. Later on, the element formulation has been extended for dynamic response analysis (Chakrabarti et al. (2013)). The elements are validated with numerical responses for monotonic and dynamic loading conditions.

Batista et al. (2013) proposed a Timoshenko composite beam element with partial interaction for multi-layered system. The element formulation is based on the analytical solution of the differential equations of the problem. The developed flexibility matrix from the solution of the differential equations has been used in direct stiffness solver after inverting it. The element is validated with numerical responses of multi-layered specimens for monotonic loading condition only.

Santos et al. (2014) developed an equilibrium-based Timoshenko composite element with partial interaction. The formulation relies on a variational principle of complementary energy involving only force and moment-like variables as fundamental unknown fields. The approximate field variables are selected such that all equilibrium equations hold in strong form. The inter-element equilibrium is enforced by resorting to the Lagrangian multiplier method. The element is validated with numerical responses for monotonic loading condition only.

Taig et al. (2015) formulated a composite beam element with partial interaction by considering generalized beam theory where section warping and distortion are inbuilt into the formulation. Cross sectional analysis has been performed by considering different order of polynomials in interpolation functions of tangential and longitudinal displacements, which in turn affected the tangential and shear membrane stress. The proposed formulation has been validated by comparing the responses of composite box Girder Bridge with that of shell finite element analysis.

Keo et al. (2016) proposed a displacement based composite Timoshenko beam element for the analysis of partially connected shear-deformable multi-layered beams where the slips and shear deformations are considered

as primary variables. This coupled system of differential equations has been solved in closed form and the exact stiffness matrix has been derived using the direct stiffness method.

Hereafter, we will discuss frame element formulations which are able to simulate inelastic axial-flexure-shear interaction:

Zona et al. (2011) developed a displacement based Timoshenko fibre composite beam element considering partial interaction. Incorporation of shear deformation varies in two formulations i.e. in one formulation shear deformation is considered in both concrete and steel layers and in the other one, it is considered only in the steel layer (Ranzi et al. (2007)). Normal and shear stress is uncoupled in the concrete material model. Uniaxial nonlinear model for normal and shear stress components for concrete and steel with von Mises yield condition and elastic-plastic-hardening rebar material models are adopted. The element is validated with experimental responses for monotonic loading conditions only.

Nguyen et al. (2014) proposed a force based Timoshenko beam element considering small deformation theory at the basic frame of reference with partial interaction. Corotational approach has been used to include nonlinear geometry effect. The elastic axial-flexure-shear interaction is

achieved in steel through von Mises plasticity theory with combined isotropic and kinematic hardening rule, while for concrete, flexure and shear behaviour is uncoupled. For tension/compression of concrete 1d elastic-plastic model and for shear, linear elastic model has been adopted. The element is validated with numerical responses for monotonic loading conditions only.

Uddin et al. (2017 & 2018) developed a displacement based composite beam element considering higher order beam theory (Reddy (1984)) and partial interaction. A third order variation of longitudinal displacement of material fibre has been assumed along the depth of the section. Axial-flexure-shear interaction is achieved through von Mises plasticity theory with an isotropic hardening rule for concrete in compression and steel material while a damage mechanics model for concrete in tension. The Green-Lagrange strain vector is used to capture the effect of geometric nonlinearity due to large deformations. The element is validated with numerical and experimental responses for monotonic loading conditions only.

Das et al. (2019) developed a displacement and two-field mixed based Timoshenko fibre composite beam elements considering partial shear interaction. These elements are formulated for three-layer steel-concrete

sandwiched system where shear deformation effect in steel plates are negligible. Inelastic axial-flexure-shear interaction is simulated through smeared fixed crack soften membrane material model for concrete. Numerical performance of developed elements is established by comparing various response variables under monotonic loading conditions only.

From the above literature survey of frame element formulations of steel-concrete composite structures, the following observations can be made:

1. Most of the research works have been performed for linear elastic material considering axial-flexure-shear interaction. It is to be noted that the material undergoes inelastic deformations under seismic loading conditions. Therefore, these elements are not suitable for simulation of inelastic axial-flexure-shear interaction for flexure-shear and shear critical specimens.
2. Very limited amount of research works was recently conducted to include inelastic axial-flexure-shear interaction into the frame element formulation. It is to be noted that plasticity based concrete models are used in these studies. Lots of opportunities remain to implement more efficient and robust concrete constitutive models to simulate multi-axial stress states.

3. So far there are basically two types of fibre element formulations that have been developed which are able to simulate the axial-flexure-shear interaction i.e. displacement based and force based. Therefore, there is still lots of scope remaining for other types of element formulations such as two field and three-field mixed formulations which are more efficient and robust.
4. Two research works have been conducted for composite structures considering geometric nonlinearity effect with axial-flexure-shear interaction. However, there is still opportunity for various types of other element formulations to simulate inelastic axial-flexure-shear interaction with large displacement effect with robust multi-axial inelastic constitutive material laws.
5. Except our own work, there is no frame element formulation available in the literature for three-layer sandwiched composite systems considering inelastic axial-flexure-shear interaction.
6. So far all the research works of composite frame element formulations considering axial-flexure-shear interaction are validated only for monotonic loading condition. Suitability of these elements for cyclic and dynamic loading conditions is questionable. Therefore,

future research works need to be performed to develop element formulations considering robust cyclic multi-axial constitutive laws for materials.

### **1.3 Objectives and Scope**

This research work deals with the inelastic material and nonlinear geometric response of two-dimensional beam elements under consideration of the multi-axial coupling of axial, flexure and shear force for reinforced concrete, steel and steel-concrete composite members.

The main objectives of this research work are as follows:

- To develop several new inelastic fibre beam element formulations following various variational approaches with consistent linearization of the governing equations.
- To develop a new shear beam element formulation for reinforced concrete and steel members based on two-field mixed formulations where both section forces and displacements are simultaneously approximated within the element through independent interpolation functions.

- To implement 2d J2 plasticity and generalized plasticity models with radial return mapping algorithm for structural steel fibres under monotonic and cyclic loading conditions respectively to accommodate the interaction among the multiaxial stress states.
- To develop a new shear beam element formulation for steel-concrete composite members with deformable shear connectors based on displacement and two-field mixed formulations, where partial interaction provided by the shear studs between steel and concrete is modelled by distributed spring elements.
- To develop a new shear beam element based on two-field mixed formulations for reinforced concrete members considering large displacement effects. The corotational formulation is used to describe the large displacement at the element nodal level and Green-Lagrange strain measures are used at the basic element level. Since the development of consistent state determination of fibre element formulation three decades ago, this is the first shear fibre beam element formulation which can reasonably reproduce the experimentally observed post-peak softening region of the shear force-shear deformation curve.

- To validate the developed frame elements with experimental results of shear critical reinforced concrete, steel and steel-concrete composite members for monotonic and cyclic loading conditions.

The dissertation is organized into eight chapters as follows:

Chapter 2 presents the two-field mixed formulation of two dimensional shear critical reinforced concrete and steel members. The chapter starts with the derivation of the variational framework and is followed by the multiaxial constitutive material models. The chapter concludes with the presentation of the stability criteria and state determination of shear critical two-field mixed formulation.

Chapter 3 presents the validation of the developed shear two-field mixed beam element with experimental results of shear critical reinforced concrete beams, columns, walls and steel shear links for monotonic and cyclic loading conditions.

Chapter 4 presents the displacement and two-field mixed formulation of two dimensional shear critical steel-concrete composite members with partial interaction. The chapter starts with the derivation of the displacement based variational framework and is followed by the mixed

based formulation. The chapter concludes with the presentation of the stability criteria and state determination of shear critical two-field mixed formulations.

Chapter 5 presents the validation of the developed shear displacement and two-field mixed beam elements with experimental results of shear critical steel-concrete composite members for monotonic and cyclic loading conditions.

Chapter 6 presents the two-field mixed formulation of two dimensional shear critical reinforced concrete members considering large displacement effects. The chapter starts with the derivation of the variational framework and is followed by the stability criteria and state determination of shear critical two-field mixed formulation considering geometric nonlinearity effects.

Chapter 7 presents the validation of the developed large displacement shear two-field mixed beam element with experimental results of P-delta dominated flexure-shear critical reinforced concrete columns for cyclic loading condition.

Chapter 8 presents the summary and conclusion of the current research work and provides directions for future research works.

# **Chapter 2 Shear Critical Frame Element – Mixed Formulation**

## **2.1 Overview**

This chapter presents a new 2d shear critical frame element based on a two-field Hellinger-Reissner functional considering the constitutive models of reinforced concrete and steel which can accommodate the multi-axial coupling of various stress measures at the fibre level following the three pillars of structural mechanics i.e. compatibility, equilibrium and constitutive models at respective levels.

The following presentation starts with the overview of mixed formulation following the main assumptions of the element formulation and the definition of element, section kinematics, equilibrium, compatibility and constitutive law followed by the derivation of the mixed variational formulation. The finite element discretization results in the consistent resisting force vector and stiffness matrix of the element. It concludes with the incorporation of multi-axial inelastic material response and element state determination process along with stability criteria of the mixed formulation.

Mixed finite element formulations offer an efficient method for determination of element internal resistance forces and tangent stiffness

matrices. There are two types of mixed-based formulations based on the number of independent degree of freedoms. Three field mixed-based formulation (Taylor et al. (2005) and Saritas et al. (2009)) follows de Veubeke (1951)-Hu (1955)-Washizhu (1955) variational principle where nodal displacements, section deformations and section forces are independent fields. State determination of three-field mixed formulation follows the similar process of force-based formulation where section deformation and section force have been condensed out at the element level. Two-field mixed based formulations (Spacone et al. (1996), Neuenhofer et al. (1997), Ayoub (2001), Hjelmstad (2002) and Nukala et al. (2004a, 20004b)) follows Hellinger (1914)-Reissner (1950) variational principle where nodal displacements and section forces are independent fields. Independent interpolation functions are used to determine section deformation and force fields. By choosing the distributions of section forces in a smart way, it is possible to satisfy differential equilibrium equation at the section level. The element deformations from an interpolated displacement field and an interpolated force field are both enforced to be compatible to each other in a variational sense. Selecting accurate force interpolation functions also improves the accuracy of the nonlinear curvature and shear deformation fields. Selection of displacement and force shape functions should satisfy the stability criteria (Ayoub et al. (2000)). The mixed finite element formulations also have a more

complicated force recovery procedure than the displacement-based and force-based formulations. Incorporation of geometric nonlinearity is the least cumbersome in the displacement-based formulations but shear locking issues may arise. In force-based formulation, the formulation becomes complex to simulate the geometric nonlinearity as there is no displacement degrees of freedom available (De Souza, (2000)). On the other hand, it is the mixed formulation that provides the best balance between accurate assessments of nonlinear curvatures along the length along with the capability to include geometric nonlinearity directly in the formulation (Alemdar et al. (2005)).

The element kinematics are based on the assumption of small displacements and is described in a basic or corotational reference system that excludes rigid body modes from the global nodal displacement. Timoshenko based section kinematics has been adopted where shear strains along the section remain constant. This assumption of shear strain violates the fibre level partial differential equation of equilibrium and the actual profile of shear strain depends on section geometry. To overcome these issues, shear correction factor is required for linear elastic material behaviour, however under inelasticity the shear strain distribution is material state dependent and the requirement of shear correction factor is

uncertain. The developed element is free from shear locking which is based only on interpolation of the displacement fields.

The current research work aims to extend the two-field mixed-based formulation by Ayoub et al. (2000) to account for shear critical reinforced concrete and steel members by implementing coupled multi-axial constitutive laws for materials, along with new stability criteria. To achieve this purpose, the following new shape function for transverse displacement varying with cubic function along the length of the element has been developed in our research work. This is the only shape function which can fulfil the stability criteria of two-field HR mixed-based formulation considering Timoshenko-based section kinematics. This shape function also needs to be used either for compatible Displacement-based formulation with mixed-based or higher-order independent new displacement-based formulation considering Timoshenko shear deformation. As a result, we need to use three node beam finite element where the middle degree of freedom will get statically condensed out at the element level before sending the information to the solver.

$$v(x) = \left(1 - \frac{x}{L}\right) * v_1 + \left(\frac{x}{L}\right) * v_2 + \left(\frac{5x}{6} - \frac{3x^2}{2L} + \frac{2x^3}{3L^2}\right) * \theta_1 + \left(-\frac{2x}{3} + \frac{2x^2}{L} - \frac{4x^3}{3L^2}\right) * \theta_2 + \left(-\frac{x}{6} - \frac{x^2}{2L} + \frac{2x^3}{3L^2}\right) * \theta_3 \quad (1)$$

This is the higher order version of Cook (1995) proposed following transverse displacement varying with quadratic function along the length of the element. This shape function has been used by researchers for independent displacement-based formulation with Timoshenko beam theory but it cannot be used for mixed-based formulation as it cannot satisfy the required stability criteria for shear critical beam element.

$$v(x) = \left(1 - \frac{x}{L}\right) * v_1 + \left(\frac{x}{L}\right) * v_2 + \left(\frac{x}{2} - \frac{x^2}{2L}\right) * \theta_1 + \left(-\frac{x}{2} + \frac{x^2}{2L}\right) * \theta_2 \quad (2)$$

The following shape function for axial displacement varying with quadratic function along the length of the element used in our research work:

$$u(x) = \left(1 - \frac{3x}{L} + \frac{2x^2}{L^2}\right) * u_1 + \left(\frac{4x}{L} - \frac{4x^2}{L^2}\right) * u_2 + \left(-\frac{x}{L} + \frac{2x^2}{L^2}\right) * u_3 \quad (3)$$

The following shape function for independent rotation varying with quadratic function along the length of the element used in our research work:

$$\theta(x) = \left(1 - \frac{3x}{L} + \frac{2x^2}{L^2}\right) * \theta_1 + \left(\frac{4x}{L} - \frac{4x^2}{L^2}\right) * \theta_2 + \left(-\frac{x}{L} + \frac{2x^2}{L^2}\right) * \theta_3 \quad (4)$$

## 2.2 Element Kinematics

The axis of the proposed frame element is a straight line joined by nodes I and J in the statically determinate basic reference system in which rigid body displacements are removed by choosing the simple supported boundary conditions as shown in Figure 2-1. The frame element is composed of several sections along its axis. Every section is composed of several fibres which are identified by their position from the reference axis and individual cross-section area.

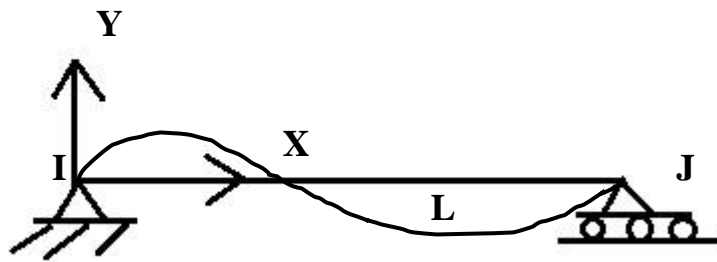


Figure 2-1. Basic reference system without rigid body modes

The section displacement vector  $\mathbf{u}(x)$  collects the two translations  $u(x), v(x)$  in X and Y directions respectively and one rotation  $\theta_z(x)$  about Z axis.

$$\mathbf{u}(x) = [u(x)\theta_z(x) \quad v(x)]^T \quad (5)$$

The element nodal displacement vector  $\mathbf{u}_{IJ}$  collects the nodal displacement with respect to global axes according to the section displacement vector in Equation (5). In the proposed frame element, an additional middle nodal rotational degree of freedom is included which has been statically condensed out at the element level before the assembling process.

$$\mathbf{u}_{IJ} = [u_I v_I \theta_{zI} \quad u_J v_J \theta_{zJ} \theta_{zK}]^T \quad (6)$$

The element deformation vector  $\mathbf{v}$  collects the relative translation  $u$  at node J in X direction, rotations  $\theta_z$  at nodes I and J and middle node k with respect to basic reference axes as shown in the Figure 2-2.

$$\mathbf{v} = [u \quad \theta_{zI} \theta_{zJ} \theta_{zK}]^T \quad (7)$$

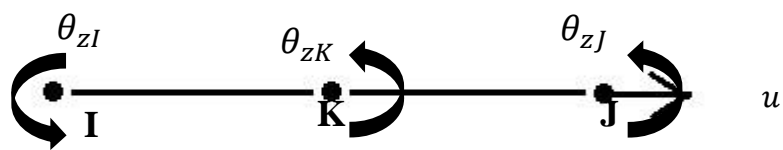


Figure 2-2. Element nodal deformations

The relation between element nodal deformation  $\mathbf{v}$  and displacements  $\mathbf{u}_{IJ}$  can be uniquely determined by compatibility matrix  $\mathbf{a}_c$  with constant

coefficients under linear geometry conditions where  $L$  is the undeformed length of the element.

$$\mathbf{v} = \mathbf{a}_c \mathbf{u}_{IJ} \quad (8)$$

Where

$$\mathbf{a}_c = \begin{bmatrix} 0 & \frac{1}{L} & 1 & 0 & -\frac{1}{L} & 0 & 0 \\ -1 & 0 & 0 & 1 & 0 & 0 & 0 \\ 0 & \frac{1}{L} & 0 & 0 & -\frac{1}{L} & 1 & 0 \\ 0 & \frac{1}{L} & 0 & 0 & -\frac{1}{L} & 0 & 1 \end{bmatrix}$$

### 2.3 Section Kinematics

Under the assumption of Timoshenko beam theory, the displacements  $u^m(x, y)$  of a material point  $m$  with coordinate  $y$  at a section with distance  $x$  from the origin of the reference frame can be represented with the cross-section generalized displacements  $\mathbf{u}(x)$  as follows.

$$u_x^m(x, y) = u(x) - y\theta_z(x) \quad (9)$$

$$v_x^m(x, y) = v(x) \quad (10)$$

The material strain displacement vector  $\boldsymbol{\varepsilon}(x, y)$  can be related with material displacement vector  $u^m(x, y)$  as follows.

$$\varepsilon_{xx} = \frac{\partial u_x^m(x, y)}{\partial x} = \frac{\partial u(x)}{\partial x} - y \frac{\partial \theta_z(x)}{\partial x} \quad (11)$$

$$\varepsilon_{yy} = \frac{\partial v_x^m(x, y)}{\partial y} = \frac{\partial v(x)}{\partial y} = 0 \quad (12)$$

$$2\varepsilon_{xy} = \frac{\partial u_x^m(x, y)}{\partial y} + \frac{\partial v_x^m(x, y)}{\partial x} = -\theta_z(x) + \frac{\partial v(x)}{\partial x} \quad (13)$$

By introducing section the deformation vector  $\mathbf{d}(x)$  which is a function of section displacement vector  $\mathbf{u}(x)$ , we can write down the following equation with the help of section compatibility matrix  $\mathbf{a}_s(y)$ :

$$\boldsymbol{\varepsilon}(x, y) = \mathbf{a}_s(y) \mathbf{d}(x) \quad (14)$$

Where

$$\mathbf{d}(x) = \left[ \frac{\partial u(x)}{\partial x} \quad \frac{\partial \theta_z(x)}{\partial x} \quad \left( -\theta_z(x) + \frac{\partial v(x)}{\partial x} \right) \right]^T$$

$$\mathbf{a}_s(y) = \begin{bmatrix} 1 & -y & 0 \\ 0 & 0 & 1 \end{bmatrix}$$

## 2.4 Equilibrium

The differential equilibrium equation of a segment of length  $dx$  as shown in the Figure 2-3 can be written down as follows:

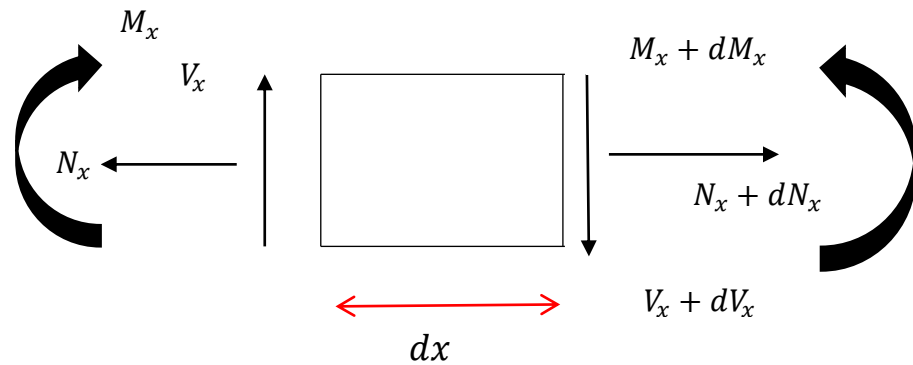


Figure 2-3. Section differential equilibrium

$$\frac{dN_x}{dx} = 0 \quad (15)$$

$$\frac{dM_x}{dx} - V_x = 0 \quad (16)$$

$$\frac{dV_x}{dx} = 0 \quad (17)$$

Where  $N_x, M_x, V_x$  are the axial force, bending moment and shear force respectively.

Writing the equilibrium equations in matrix form:

$$\mathbf{L}^T \mathbf{D}(x) = 0 \quad (18)$$

Where

$$\mathbf{D}(x) = [N_x M_x V_x]^T$$

$$\mathbf{L}^T = \begin{bmatrix} \frac{d}{dx} & 0 & 0 \\ 0 & \frac{d}{dx} & -1 \\ 0 & 0 & \frac{d}{dx} \end{bmatrix}$$

## 2.5 Compatibility

The components of generalized section deformation vector  $\mathbf{d}(x)$  are the axial strain  $\varepsilon_0$  at the reference  $x$  axis, the curvature  $\phi_z$  about the  $z$  axis and shear deformation  $\gamma_y$  in the  $y$  direction respectively:

$$\mathbf{d}(x) = [\varepsilon_0 \phi_z \gamma_y]^T \quad (19)$$

Where

$$\varepsilon_0 = \frac{du(x)}{dx}$$

$$\phi_z = \frac{d\theta_z(x)}{dx}$$

$$\gamma_y = -\theta_z(x) + \frac{dv(x)}{dx}$$

Writing the compatibility equations in matrix form:

$$\mathbf{L}\mathbf{u}(x) - \mathbf{d}(x) = 0 \tag{20}$$

Where

$$\mathbf{L} = \begin{bmatrix} \frac{d}{dx} & 0 & 0 \\ 0 & \frac{d}{dx} & 0 \\ 0 & -1 & \frac{d}{dx} \end{bmatrix}$$

## 2.6 Constitutive Laws

The section constitutive law is as follows:

$$\mathbf{D}(x) = f_{sec}\mathbf{d}(x) \tag{21}$$

Where  $f_{sec}$  is a nonlinear function that describes the section force-deformation relation. The section force-deformation relation is obtained through fibre integration as described in Section 2.8.

## 2.7 Variational Formulation

The formulation of the beam element in this section uses independent generalized stress and displacement interpolation functions in a two-field Hellinger-Reissner (HR) functional which is written in the basic frame of reference as follows:

$$\begin{aligned} \Pi_{HR}(\mathbf{u}, \boldsymbol{\sigma}) = & - \int_v W(\boldsymbol{\sigma}(x, y)) dv + \int_v \boldsymbol{\sigma}^T \boldsymbol{\varepsilon}^u dv - \Pi_{ext}(\mathbf{u}(x)) - \\ & \Pi_{bc}(\mathbf{u}) \end{aligned} \quad (22)$$

where  $W(\boldsymbol{\sigma})$  is the complementary energy function.

In HR variational principle, strain-displacement relation  $\boldsymbol{\varepsilon} = \nabla^s \mathbf{u}(x)$  on  $v$  and displacement boundary condition  $\mathbf{u} = \mathbf{u}^*$  on  $\Gamma_u$ , are satisfied in their strong differential form. Where as, equilibrium conditions  $\mathbf{div} \boldsymbol{\sigma} + \mathbf{b}_o = \mathbf{0}$  on  $v$ , constitutive relation  $\boldsymbol{\sigma} = \boldsymbol{\sigma}(\boldsymbol{\varepsilon})$  on  $v$  and traction boundary conditions  $\mathbf{t} = \mathbf{t}^*$  on  $\Gamma_t$  are satisfied in their integral weak form.

HR energy functional of Eq. (22) can be written without body force and surface traction with section level variables in the following form:

$$\Pi_{HR}(\mathbf{u}, \mathbf{p}) = - \int_L \mathbf{D}^T \mathbf{d}(\mathbf{D}) dx + \int_L \widehat{\mathbf{D}}^T(\mathbf{p}) \mathbf{d}(\mathbf{u}) dx - \mathbf{u}^T \mathbf{P}^* \quad (23)$$

In this formulation, beam section forces  $\widehat{\mathbf{D}}$  are independently determined from element nodal forces  $\mathbf{p}$  as follows:

$$\widehat{\mathbf{D}}(x) = \mathbf{b}(x) \mathbf{p} \quad (24)$$

$$\mathbf{b}(x) = \begin{bmatrix} 1 & 0 & 0 \\ 0 & -\frac{1}{L} & -\frac{1}{L} \\ 0 & \frac{x}{L} - 1 & \frac{x}{L} \end{bmatrix}$$

where  $\mathbf{b}(x)$  is the matrix of force interpolation functions.

Equilibrium matrix  $\mathbf{b}(x)$  satisfies differential equilibrium equation (18) at the section level in its strong form.

The variation of HR energy functional in Eq. (23) can be written in the following form:

$$\delta \Pi_{HR}(\mathbf{u}, \mathbf{p}) = - \int_L \delta \mathbf{D}^T \mathbf{d}(\mathbf{D}) dx + \int_L \delta (\widehat{\mathbf{D}}^T(\mathbf{p}) \mathbf{d}(\mathbf{u})) dx - \delta \mathbf{u}^T \mathbf{P}^* \quad (25)$$

$$\begin{aligned} \delta \Pi_{HR}(\mathbf{u}, \mathbf{p}) = & - \int_L \delta \mathbf{D}^T \mathbf{d}(\mathbf{D}) dx + \int_L \delta (\widehat{\mathbf{D}}^T(\mathbf{p})) \mathbf{d}(\mathbf{u}) dx + \\ & \int_L (\widehat{\mathbf{D}}^T(\mathbf{p})) \delta(\mathbf{d}(\mathbf{u})) dx - \delta \mathbf{u}^T \mathbf{P}^* \end{aligned} \quad (26)$$

The solution of the variational in Equation (26) is non-linear under inelastic material conditions, hence the problem needs to be linearized about a state of both principle arguments  $\mathbf{u}^i$  and  $\mathbf{p}^i$  as follows:

$$\begin{aligned} \delta \Pi_{HR}(\mathbf{p}^{i+1}, \mathbf{u}^{i+1}) = & \delta \Pi_{HR}(\mathbf{p}^i, \mathbf{u}^i) + \frac{\partial \delta \Pi_{HR}(\mathbf{p}, \mathbf{u})}{\partial \mathbf{p}} \Big|_{\mathbf{p}^i, \mathbf{u}^i} \Delta \mathbf{p} + \\ & \frac{\partial \delta \Pi_{HR}(\mathbf{p}, \mathbf{u})}{\partial \mathbf{u}} \Big|_{\mathbf{p}^i, \mathbf{u}^i} \Delta \mathbf{u} \end{aligned} \quad (27)$$

Where  $\Delta \mathbf{u}$  and  $\Delta \mathbf{p}$  are the incremental nodal displacement and force vector respectively.

At equilibrium:

$$\delta \Pi_{HR}(\mathbf{p}^{i+1}, \mathbf{u}^{i+1}) = 0 \quad (28)$$

Therefore from Equation (27), we can write the following:

$$\delta \Pi_{HR}(\mathbf{p}^i, \mathbf{u}^i) + \frac{\partial \delta \Pi_{HR}(\mathbf{p}, \mathbf{u})}{\partial \mathbf{p}} \Big|_{\mathbf{p}^i, \mathbf{u}^i} \Delta \mathbf{p} + \frac{\partial \delta \Pi_{HR}(\mathbf{p}, \mathbf{u})}{\partial \mathbf{u}} \Big|_{\mathbf{p}^i, \mathbf{u}^i} \Delta \mathbf{u} = 0 \quad (29)$$

By using Equations (20), (21), and (24), Equation (29) can be written in the following form:

$$\begin{aligned} & \delta \mathbf{u}^T \left[ \int_L \mathbf{B}_s^T(x) \mathbf{b}(x) dx \Delta \mathbf{p} + \int_L \mathbf{B}_s^T \mathbf{D}(x) dx - \mathbf{P}^* \right] + \\ & \delta \mathbf{p}^T \left[ - \int_L \mathbf{b}^T(x) \mathbf{f}_s(x) \mathbf{b}(x) dx \Delta \mathbf{p} + \int_L \mathbf{b}^T(x) \mathbf{B}_s(x) dx \Delta \mathbf{u} + \right. \\ & \left. \int_L \mathbf{b}^T(x) \mathbf{d}(x) dx - \int_L \mathbf{b}^T(x) \widehat{\mathbf{d}}(x) dx \right] = 0 \end{aligned} \quad (30)$$

Where  $\mathbf{f}_s(x)$  is the section flexibility matrix,  $\mathbf{B}_s(x)$  is the strain displacement matrix and  $\widehat{\mathbf{d}}(x)$  is the section deformation vector determined from section force vector  $\widehat{\mathbf{D}}(x)$  with the help of the section flexibility matrix.

From arbitrariness of  $\delta \mathbf{u}$  and  $\delta \mathbf{p}$ , Equation (30) can be written in the following matrix form:

$$\begin{bmatrix} 0 & \int_L \mathbf{B}_s^T \mathbf{b} dx \\ \int_L \mathbf{b}^T \mathbf{B}_s dx & - \int_L \mathbf{b}^T \mathbf{f}_s \mathbf{b} dx \end{bmatrix} \begin{pmatrix} \Delta \mathbf{u} \\ \Delta \mathbf{p} \end{pmatrix} = \begin{pmatrix} \mathbf{P}^* - \int_L \mathbf{B}_s^T \mathbf{D} dx \\ \int_L \mathbf{b}^T (\widehat{\mathbf{d}} - \mathbf{d}) dx \end{pmatrix} \quad (31)$$

Equation (31) can be written in the following concise form:

$$\begin{bmatrix} 0 & \mathbf{G}^T \\ \mathbf{G} & -\mathbf{F}_{c+s} \end{bmatrix} \begin{pmatrix} \Delta \mathbf{u} \\ \Delta \mathbf{p} \end{pmatrix} = \begin{pmatrix} \mathbf{P}^* - \mathbf{P}_{c+s}^r \\ \mathbf{u}^r \end{pmatrix} \quad (32)$$

Here,

$$\mathbf{G} = \begin{bmatrix} 0 & 1 & 0 & 0 \\ 1 & 0 & 0 & 0 \\ 0 & 0 & 1 & 0 \end{bmatrix}$$

Where  $\mathbf{F}_{c+s}$  is the element flexibility matrix and  $\mathbf{u}^r$  is the element residual deformation vector. It is important to note that on convergence, the element residual deformation vector  $\mathbf{u}^r$  reduces to zero inside each element satisfying compatibility.

The two independent fields of the mixed formulation result in different numerical implementation strategies. The first numerical implementation approach preserves the parameters of the element force field as global variables alongside the end node displacements of the beam element. In this case the governing element equations for these variables in Equation (32) are assembled for the structural model and solved simultaneously for the independent parameters of the two fields at the structural level by a suitable non-linear solution strategy. This algorithm enforces continuity at element boundaries by solving for the forces as independent global degrees of freedom. The implementation of this first strategy is less common in finite element analysis as global solver needs to be coded for both

displacement and force variables, and therefore, this algorithm has not been pursued in this research work. Also, it is recommended that force continuity shall be relaxed locally at element level (Zienkiewicz et. al. (1989)) to avoid highly oscillating displacement distribution. The second numerical implementation strategy condenses the internal force fields from the governing element equations in Equation (32) and retains only the end node displacements of the beam element as global variables. This approach relaxes the basic force continuity requirement across inter-element boundaries.

In a nonlinear structural analysis algorithm, computations of the element resisting force vector and the element tangent stiffness matrix corresponding to the given current element nodal displacements and their increments, is known as element state determination process. In this formulation, the force degrees of freedom are condensed out at the element level from Equation (32) resulting in a generalized stiffness matrix as follows:

$$\mathbf{G}^T [\mathbf{F}_{c+s}^{-1}] [\mathbf{G}\Delta\mathbf{u} - \mathbf{u}^r] = \mathbf{P}^* - \mathbf{G}^T \mathbf{P}_{c+s}^r \quad (33)$$

Two alternative solution strategies exist for the element state determination of the mixed beam element based on whether storing of element residual

deformation vector  $\mathbf{u}^r$  in Equation (33) between subsequent global iterations is required or not. A non-iterative solution algorithm where no internal element iteration is necessary as in this algorithm storing element residual deformation is eliminated through the inclusion of  $\mathbf{u}^r$  in the element forces at the basic frame of reference before exiting from the element state determination at each iteration. Whereas for an iterative solution algorithm internal element iteration is necessary until the deformation vector is adjusted to satisfy compatibility at the element level and the element residual deformation vector  $\mathbf{u}^r$  reduces to zero before returning to the global iteration.

In this formulation, the iterative solution algorithm has been adopted and the choice of displacement and force interpolation functions should follow Babuska-Brezzi condition along with principle of limitation (De Veubeke (1965)). However, it has been established by Ayoub et al. (2001) that the principle of limitation criteria is the prime governing criteria to choose the right order of displacement and force interpolation functions to achieve an accurate solution. Detailed step by step procedure for both solution algorithms with stability of mixed formulation are described in Section 2.9.

Once convergence has reached at the element level i.e.  $\mathbf{u}^r$  becomes zero, Equation (33) can be written as following:

$$(\mathbf{G}^T [\mathbf{F}_{c+s}^{-1}] \mathbf{G}) \Delta \mathbf{u} = \mathbf{P}^* - \mathbf{G}^T \mathbf{P}_{c+s}^r \quad (34)$$

$$(\mathbf{K}_{c+s}) \Delta \mathbf{u} = \mathbf{P}^* - \mathbf{G}^T \mathbf{P}_{c+s}^r \quad (35)$$

$$\mathbf{K} \Delta \mathbf{u} = \mathbf{P}^* - \mathbf{P}^r \quad (36)$$

The nodal displacements of the structural model in the global frame of reference are collected in the displacement vector  $\mathbf{U}^g$ . Detailed procedure of mapping structural nodal displacement relative to global coordinates to the element nodal deformation at the basic frame of reference, transformation of element stiffness matrix and resisting forces from basic to global level and assembling of global stiffness matrix and resistance forces of all elements to assembled structural stiffness matrix  $\mathbf{K}^g$  and structural resistance vector  $\mathbf{P}^{gr}$  are described in detail in Filippou et al. (2004).

## 2.8 Material Model

### 2.8.1 Overview

Multi-axial constitutive law for materials are essential to couple normal stresses and shear stress at the material fibre level which in turn help to

account for the interaction of axial force, bending moment and shear force at element section level. This section presents the various types of constitutive models of structural steel and reinforced concrete available in the literature followed by the implemented material models in the current research work.

Reinforced concrete is a composite material which consists of concrete and rebars. The length dimension of rebars is much greater than its cross-sectional dimensions. Therefore in the frame element formulation, uniaxial stress states are considered for the rebars. On the other hand, a multi-axial stress state exists in the concrete material point under combined loading conditions. In the following, we will first describe various modelling strategies available for multi-axial concrete constitutive laws followed by the uniaxial rebar material, and conclude with the multi-axial constitutive law for structural steel.

The strength of concrete in tension is significantly lower than that in compression. It has been experimentally observed that the interaction among multi-axial tensile stress is much less i.e. tensile stress in one direction does not affect the tensile strength in other directions. On the contrary, multi-axial interaction under compressive stress is very prominent and it changes the behaviour of concrete tremendously. Under tensile

loading, concrete cracks and behaves like a tensile softening material although the presence of rebars in concrete converts it to tensile stiffening behaviour by reducing the post-peak negative slope of tensile stress-strain curve; while under multi-axial compressive loading it crushes and behave like a ductile material. Upon unloading from the compressive stress state after crossing the cracking state, concrete exhibits unrecoverable deformation due to the micro cracks and slip at the micro scale level, which makes it to be treated as a plastically deformable material (Ottosen (1977), Chen (1982)) under compressive loading. On the other hand, tensile macro cracks make concrete more flexible and reduces the elastic stiffness of concrete which cannot be represented by plasticity theory, but can be simulated through continuum damage mechanics theory (Kachanov (1958), Mazars (1986), Luccioni et al. (2003)), whereas it is to be noted that concrete dilatancy due to cracked poisson ratio and inelasticity cannot be represented by damage mechanics theory. Therefore, several models have been proposed by combining these two theories for cyclic loading condition as concrete possess the characteristics of both plasticity and damage. Interested readers are referred to notable contributions made by Ju (1989), Lubliner et al. (1989), Faria et al. (1998), Lee et al. (2001), and Wu et al. (2006). However, the experimentally observed compression-softening effect of reinforced concrete in shear has recently been considered in damage plasticity model (Feng et al. (2017)). Like damage-plastic model,

plasticity is combined with theory of fracture mechanics in fracture-plastic model (Bazant et al. (1979), Owen et al. (1983), Cervenka et al. (1998)). In this model, the concrete compressive behaviour is simulated by plasticity theory and tensile behaviour by a fracture model. Currently, Long et al. (2014) has included crack opening and closing rules into the fracture-plastic model. Apart from macroscopic phenomenological approach of modelling concrete, Bazant et al. (1988) developed the microplane model of concrete based on micromechanics of the inelastic phenomena in the material microstructure.

In the above mentioned concrete models, calibration has been conducted by performing experimental tests on concrete specimens only without considering embedded rebars under multi-axial stress states mostly for monotonic loading condition. However, in reality, the presence of rebars affects both the concrete and rebar properties. For this reason, realistic reinforced concrete models have been developed by conducting experiments on reinforced concrete panels under monotonic and cyclic loading conditions by following the three pillars of continuum mechanics i.e. stress equilibrium, strain compatibility and constitutive law of material. These models are known as smeared crack orthotropic models.

In the following, we will discuss various types of smeared crack orthotropic models available in the literature. Unlike other available concrete models, material state determination for smeared crack modes need equivalent uniaxial stress-strain relation of concrete along each axis of orthotropy.

During the past three decades, extensive experimental testing (Vecchio et al. (1981), Vecchio et al. (1986), Belarbi et al. (1994, 1995), Pang et al. (1995), Hsu et al. (1996)) of reinforced concrete membrane panels subjected to in-plane and out-of-plane loads have been carried out throughout the world. The goal was to develop rational theoretical multi-axial models of reinforced concrete based on smeared crack approach. There are several models available based on smeared or average concepts such as Noguchi et al (1983), Rots et al (1985), de Brost et al (1985), Stevens, et al (1987)Noguchi (1992), Shin et al (1992), Izumo et al (1992), Inoue et al (1992) among others. Important advantages over other concrete models are that local bond-slip is embedded into the smeared stress-strain relationship and smeared tension stiffening model is mesh independent (Hsu et al. (1996)). The research group at the University of Toronto, developed three reinforced concrete constitutive models: the compression field theory (Vecchio et al. (1981)) which was not able to take into account tension stiffening effect; the modified compression field theory (Vecchio et

al. (1986)) which can predict the post-peak behaviour by considering a concrete local shear stress in the principal direction along with compression softening due to perpendicular tensile strain, and the disturbed stress field theory (Vecchio(2000)) which is a hybrid rotating-fixed smeared cracked model for cyclic loading condition. The research group at the University of Houston, developed four reinforced concrete constitutive models: the rotating-angle softened truss model (Belarbi et al. (1995), Pang et al. (1995)) which is a rotating crack model that can predict the behaviour up to the ultimate point and able to simulate tension stiffening effect and the effect of concrete on steel stress-strain relationship; the fixed-angle softened truss model (Pang et al. (1996), Hsu et al. (1997)) which is based on the applied principal stresses and can predict the pre-peak behaviour with fixed crack approach with consideration of concrete contribution; and the softened membrane model (Zhu (2000),Hsu et al. (2002)) with cracked concrete Poisson ratios or Hsu/Zhu ratios (Zhu et al. (2001)) to capture the pre-peak as well as the post-peak softening response for monotonic loading and the cyclic softened membrane model (Mansur (2001), Mansur et al. (2005a, 2005b), Hsu et al. (2005)) for reverse cyclic loading condition.

Hereafter, we will present an overview of various types of constitutive material models used to simulate structural steel under multi-axial stress states.

Steel is considered a ductile material which can undergo significant plastic deformations without losing its equal strength in tension and compression. It also exhibits strain hardening; however modelling of it depends on the type of applied loading on the system. Strain hardening in structural steel material under multi-axial stress state is a complex phenomenon like strain softening of concrete material. There are two types of strain hardening phenomena observed in the experimental tests of structural steel i.e. isotropic strain hardening where the centre of yield surface remains at the origin and kinematic strain hardening (Figure 2-4) where the centre of yield surface moves along the direction of the plastic strain rate throughout the loading history. For reverse cyclic loading conditions, combined isotropic and kinematic hardening needs to be considered to simulate the experimentally observed Bauschinger effect. There are mainly four types of material models used to simulate rate-independent plasticity problems i.e. linear plasticity, nonlinear kinematic hardening plasticity, bounding surface plasticity and generalized plasticity. Linear plasticity is the well-known J2 plasticity model (Figure 2-4) in its simplest form. The model is based on linear evolutionary rules for both the plastic strain rate and the kinematic hardening which results in a piecewise linear stress-strain relation. Nonlinear kinematic hardening plasticity (Armstrong et al. (1965), Chaboche (1986)) is based on the use of nonlinear kinematic hardening

rules and bounding surface plasticity models (Dafalias et al. (1975), Krieg (1975), Dafalias (1986)) where plastic stiffness is a function of the distance between the loading surface and limit (bounding) surface. On the other hand, generalized plasticity (Auricchio et al. (1992), Lubliner (1993)) is based on the use of

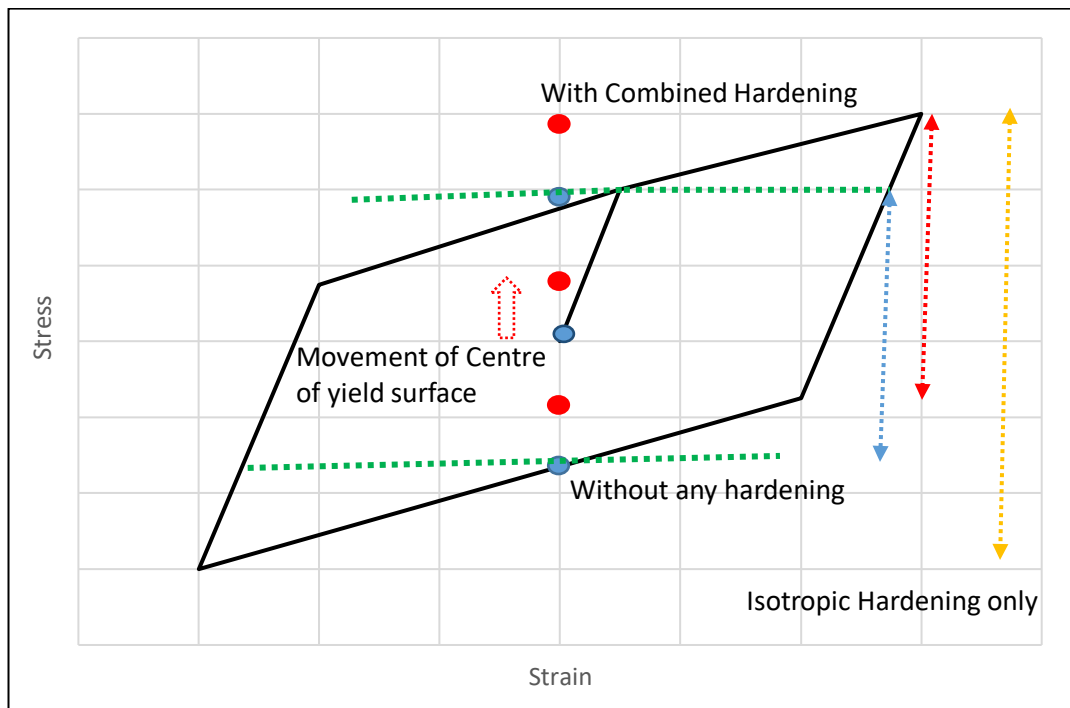


Figure 2-4. Linear Plasticity Model

nonlinear evolutionary equations for the plastic strain rate. The numerical implementation of plasticity models requires the numerical integration of the rate constitutive equations over a discrete sequence of time steps in the incremental-iterative framework. The outcome of adopted integration algorithm is a nonlinear response function i.e. stress tensor which is a function of the strain history up to the current time step. In order to

preserve the quadratic rate of asymptotic convergence, elasto-plastic tangent over a typical time step must be obtained by consistent linearization of the response function. To achieve this goal, the radial return mapping algorithm (Wilkins (1964)) provides an effective and robust integration scheme of the rate constitutive equations through the discrete enforcement of limit equation. It is an elastic-predictor plastic-corrector algorithm which has two parts. In the first part, a purely elastic trial state is computed and in the second part, a plastic correction is computed using the calculated trial state as an initial condition. Interested readers are referred to Simo et al. (1998) for additional discussion.

In the following, we will first discuss the implemented reinforced concrete models followed by steel multi-axial  $J_2$  and generalized plasticity models of structural steel adopted for monotonic and cyclic loading conditions respectively. The uniaxial material models for concrete and steel have been briefly described in Appendix B.

### **2.8.2 Reinforced Concrete**

In this research work, the softened membrane model has been adopted to simulate the biaxial interaction between normal stress and shear stress at the material fibre level. In the following, we will first present the salient features of the implemented softened membrane model which has been

developed by Zhu (2000) and Hsu et al. (2002). Mullapudi et al. (2010) implemented it into the force-based fibre element formulation.

### 2.8.2.1 Concrete – Biaxial

To formulate the softened membrane model, three coordinate systems are typically assumed as shown in Figure 2-5. The first coordinate system (X, Y) defines the local coordinate of the fibre element at the basic frame of reference; the second coordinate system (1, 2) represents the applied principal stresses of reinforced concrete membrane panel which has an angle  $\theta_1$  with respect to X axis while the third coordinate system ( $X_s, Y_s$ ) represents the rebar coordinate system which has angle  $\theta_s$  with respect to X axis.

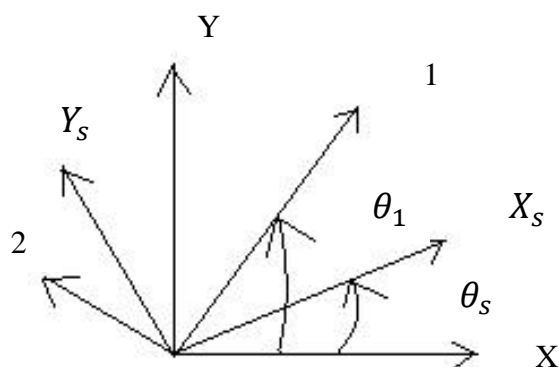


Figure2-5. Applied principal stresses and reinforcement directions of RC element

The stress and strain vectors in X-Y and 1-2 coordinate axes are represented by  $\{\sigma_x \sigma_y \tau_{xy}\}^T$ ,  $\{\varepsilon_x \varepsilon_y \frac{1}{2} \gamma_{xy}\}^T$  and  $\{\sigma_1 \sigma_2 \tau_{12}\}^T$ ,  $\{\varepsilon_1 \varepsilon_2 \frac{1}{2} \gamma_{12}\}^T$  respectively. We have information available in terms of strain vector at X-Y coordinate system and we need to determine the stress vector in X-Y coordinate system along with tangent stiffness of RC panel through the following material state determination process.

The strains are transformed from the X-Y system to 1-2 system through the following transformation matrix:

$$\begin{Bmatrix} \varepsilon_1 \\ \varepsilon_2 \\ \frac{1}{2} \gamma_{12} \end{Bmatrix} = [T(\theta_1)] \begin{Bmatrix} \varepsilon_x \\ \varepsilon_y \\ \frac{1}{2} \gamma_{xy} \end{Bmatrix} \quad (37)$$

Where

$$[T(\theta_1)] = \begin{bmatrix} c^2 & s^2 & 2sc \\ s^2 & c^2 & -2sc \\ -sc & sc & c^2 - s^2 \end{bmatrix}$$

Here,  $c = \cos \theta_1$  and  $s = \sin \theta_1$

The iterative process of determining  $\theta_1$  based on strain state, equilibrium of vertical stress and state of stress can be found in details from Mullapudi et al.(2010).

Biaxial strains in 1-2 system has been transformed into equivalent uniaxial strains at 1-2 system with the help of cracked concrete Poisson ratio which is known as Hsu/Zhu ratio.

$$\begin{pmatrix} \bar{\varepsilon}_1 \\ \bar{\varepsilon}_2 \\ \frac{1}{2}\gamma_{12} \end{pmatrix} = [\mu] \begin{pmatrix} \varepsilon_1 \\ \varepsilon_2 \\ \frac{1}{2}\gamma_{12} \end{pmatrix} \quad (38)$$

Where

$$[\mu] = \begin{bmatrix} \frac{1}{1-\mu_{12}\mu_{21}} & \frac{\mu_{12}}{1-\mu_{12}\mu_{21}} & 0 \\ \frac{\mu_{21}}{1-\mu_{12}\mu_{21}} & \frac{1}{1-\mu_{12}\mu_{21}} & 0 \\ 0 & 0 & 1 \end{bmatrix}$$

Here,  $\mu_{12}$  represents the effect of compression strain in the 2-direction on the tensile strain in the 1-direction and  $\mu_{21}$  represents the effect of tensile strain in the 1-direction on the compression strain in the 2-direction. Zhu et al. (2002) has proposed the following equations of Poisson ratios for cracked concrete based on the biaxial experimental tests on RC panels:

$$\mu_{12} = 0.2 + 850\varepsilon_{sf} \quad \text{if } \varepsilon_{sf} \leq \varepsilon_y \quad (39)$$

$$\mu_{12} = 1.9 \quad \text{if } \varepsilon_{sf} > \varepsilon_y \quad (40)$$

$$\mu_{21} = 0.2 \quad \text{before cracking} \quad (41)$$

$$\mu_{21} = 0 \quad \text{after cracking} \quad (42)$$

Where  $\varepsilon_{sf}$  is the strain in the steel bar that yields first and  $\varepsilon_y$  is the yield strain.

Compressive and tensile strength of concrete has been determined from the uniaxial smeared stress-strain curve of concrete. However, compressive strength of concrete depends on material state of stress. For tensile-compressive state, the compressive strength gets softened due to tensile strains acting in the perpendicular direction whereas for compressive-compressive state of stress, the compressive strength gets enhanced due to the compressive stress acting in the perpendicular direction. This enhancement factor of compressive strength has been adopted in this research work following the Vecchio's model (1992) which is a simplified version of Kupfer et al. (1969) biaxial compression strength envelope. However, the tensile strength of concrete gets influenced in a very minimal way due to the presence of perpendicular tensile strength.

Hsu and Zhu (2001) derived a softening equation in the tension-compression region, which is implemented in the current model, and is based on panel testing as proposed by Hsu et al. (1995) and Belarbi and Hsu (1995). The equation for compressive strength reduction factor proposed by Hsu and Zhu (2001) is:

$$\zeta = \left( \frac{5.8}{\sqrt{\hat{f}_c(MPa)}} \leq 0.9 \right) \left( \frac{1}{\sqrt{1+400\bar{\varepsilon}_1}} \right) \left( 1 - \frac{|\beta|}{24^\circ} \right) \quad (43)$$

Where,

$$\beta = 0.5 \tan^{-1} \left( \frac{\gamma_{12}}{\varepsilon_1 - \varepsilon_2} \right)$$

The softening coefficient  $\zeta$  value is limited to 0.9, because the uniaxial concrete compressive strength  $\hat{f}_c$  is calculated from standard cylinder test, while from the panel experiments at the University of Houston it was observed that the concrete strength does not reach  $\hat{f}_c$ . The reason is due to size effect, loading rate effect, and shape factor which have ample effect on the concrete compressive strength  $\hat{f}_c$ . The ultimate stress in the orthogonal directions is therefore  $\zeta \hat{f}_c$  at a softened strain  $\zeta \varepsilon_0$ , where  $\zeta$  is the softening coefficient,  $\beta$  is the deviation angle which is the difference between the applied stress angle  $\alpha_1$  and the rotating angle  $\alpha_r$ ,  $\bar{\varepsilon}_1$  is the lateral tensile

strain,  $\varepsilon_0$  is the concrete strain at peak compressive strength  $\hat{f}_c$  and  $\zeta\hat{f}_c$  is the softened concrete compressive strength,  $\varepsilon_1$  is the bi-axial strain of concrete in principal direction 1,  $\varepsilon_2$  is the bi-axial strain of concrete in principal direction 2 and  $\gamma_{12}$  is shearing strain in applied principal co-ordinate system 1-2.

Once the strength has been determined in the equivalent uniaxial 1-2 coordinates system, we can determine shear strength and stiffness (G) as follows:

$$G = \frac{\sigma_1 - \sigma_2}{\varepsilon_1 - \varepsilon_2} \quad (44)$$

$$\tau_{12} \text{ at } (t + 1) = \tau_{12} \text{ at } (t) + G \frac{\gamma_{12}}{2} \quad (45)$$

The equivalent uniaxial strain of concrete can be transformed into uniaxial strain of rebars as follows:

$$\begin{pmatrix} \bar{\varepsilon}_{1s} \\ \bar{\varepsilon}_{2s} \\ \frac{1}{2}\gamma_{12} \end{pmatrix} = [T(\theta_s - \theta_1)] \begin{pmatrix} \bar{\varepsilon}_1 \\ \bar{\varepsilon}_2 \\ \frac{1}{2}\gamma_{12} \end{pmatrix} \quad (46)$$

Once we have strength at concrete and steel rebar at their respective co-ordinate systems, we can determine the strength vector of reinforced

concrete panel in X-Y coordinate system from the following equilibrium equations:

$$\begin{Bmatrix} \sigma_x \\ \sigma_y \\ \tau_{xy} \end{Bmatrix} = [T(-\theta_1)] \begin{Bmatrix} \sigma_1 \\ \sigma_2 \\ \tau_{12} \end{Bmatrix} + \sum_i [T(-\theta_{si})] \begin{Bmatrix} \rho_{si}\sigma_{si} \\ 0 \\ 0 \end{Bmatrix} \quad (47)$$

Here,  $\rho_{si}$  is the smeared steel ratio in the direction of  $i$ .

The material stiffness matrix  $[D]$  of reinforced concrete panel in X-Y coordinate system can be determined from equivalent uniaxial stiffness of concrete and steel at their respective coordinate systems as follows.

$$[D] = [D_{concrete}] + [D_{steel}] \quad (48)$$

Where,

$$[D_{concrete}] = [T(-\theta_1)][D_{uniaxial}^{concrete}][\mu][T(\theta_1)]$$

$$[D_{steel}] = \sum_i [T(-\theta_{si})][D_{uniaxial}^{steel_i}][T(\theta_{si} - \theta_1)][\mu][T(\theta_1)]$$

$$[D_{uniaxial}^{concrete}] = \begin{bmatrix} E_{t1} & D_{12} & 0 \\ D_{21} & E_{t2} & 0 \\ 0 & 0 & G \end{bmatrix}$$

Here  $D_{12} = \frac{d\sigma_1}{d\bar{\varepsilon}_2}$  and  $D_{21} = \frac{d\sigma_2}{d\bar{\varepsilon}_1}$  are coupling material stiffness terms which exists only when the material is under tensile-compressive state of strain due to the presence of softening coefficient which is a function of perpendicular tensile strain.

$$[D_{uniaxial}^{steel_i}] = \begin{bmatrix} \rho_{si}E_t & 0 & 0 \\ 0 & 0 & 0 \\ 0 & 0 & 0 \end{bmatrix} \quad (49)$$

### 2.8.3 Steel

In this research work, the J2 model for monotonic loading and generalized plasticity model for cyclic loading has been adopted to simulate the biaxial interaction between normal stress and shear stress at the material fibre level. In the following, we will first present the implemented J2model of steel followed by the salient features of generalized plasticity model. Auricchio et al. (1992) has developed the generalized plasticity model and Saritas et al. (2009) implemented it into the three-field mixed based fibre element formulation.

#### 2.8.3.1 Steel - Biaxial

In case of rate independent small deformation plasticity, we can split the total strain vector  $\boldsymbol{\varepsilon}$  into an elastic component vector  $\boldsymbol{\varepsilon}^e$  and a plastic component vector  $\boldsymbol{\varepsilon}^p$  i.e.  $\boldsymbol{\varepsilon} = \boldsymbol{\varepsilon}^e + \boldsymbol{\varepsilon}^p$ .

The stress ( $\boldsymbol{\sigma}$ ) behaviour of a material can be composed of a stress associated with uniform hydrostatic pressure (volumetric part ‘ $p$ ’) and a stress associated with the resistance of the material to shear distortion (deviatoric part ‘ $s$ ’) which contributes in yielding and plastic flow.

$$p = \frac{1}{3} \text{tr}(\boldsymbol{\sigma}) \quad (50)$$

Where ‘ $tr$ ’ is the trace operator that adds the diagonal terms of stress tensor  $\boldsymbol{\sigma}$ .

With this relation the stress can be written as:

$$\boldsymbol{\sigma} = \boldsymbol{s} + p \cdot \mathbf{1} \quad (51)$$

Where the trace of deviatoric stress is zero and  $\mathbf{1}$  is the rank 2 identity tensor.

The second invariant of deviatoric stress tensor  $\boldsymbol{s}$  is known as  $J_2$ .

Similarly, the strain tensor can be split into volumetric ( $\theta$ ) and deviatoric part ( $\mathbf{e}$ ).

$$\theta = tr(\boldsymbol{\varepsilon}) \quad (52)$$

Where the plastic part of  $\theta$  is zero. With this relation the strain can be written as:

$$\boldsymbol{\varepsilon} = \mathbf{e} + \frac{1}{3}\theta\mathbf{1} \quad (53)$$

The deviatoric strain  $\mathbf{e}$  can also be decomposed into an elastic and plastic part:

$$\mathbf{e} = \mathbf{e}^e + \mathbf{e}^p \quad (54)$$

The elastic behaviour of the material can be described as:

$$\mathbf{s} = 2G(\mathbf{e} - \mathbf{e}^p) \quad (55)$$

Where  $G$  is the shear modulus.

### **2.8.3.1.1 J2 Plasticity Model**

We are using linear isotropic and kinematic hardening rules for the current J2 plasticity model (Figure 2-4). The equations relative to the yield function, plastic flow rule and hardening rules are briefly summarized here.

The yield function is expressed in terms of the deviatoric stress  $\mathbf{s}$ , the back stress variable  $\mathbf{s}_b$  representing the distance of yield surface centre from the origin of deviatoric stress space and linear isotropic hardening modulus  $H_i$ .

$$f(\mathbf{s}, \mathbf{s}_b, H_i) = \|\mathbf{s} - \mathbf{s}_b\| - \sqrt{\frac{2}{3}}(\sigma_y + H_i\beta) \quad (56)$$

Here,  $\sigma_y$  is the uniaxial tensile yield strength and  $\beta$  is the isotropic hardening variable with nature of plastic strain.

The plastic flow rule is:

$$\dot{\mathbf{e}}_p = \alpha \frac{\partial f}{\partial \mathbf{s}} \quad (57)$$

Here  $\alpha$  is known as plastic consistency parameter and  $\frac{\partial f}{\partial \mathbf{s}}$  is the normal to the yield surface which is determined as:

$$\frac{\partial f}{\partial \mathbf{s}} = \frac{(\mathbf{s} - \mathbf{s}_b)}{\|\mathbf{s} - \mathbf{s}_b\|} \quad (58)$$

The hardening rules are:

$$\dot{\beta} = \sqrt{\frac{2}{3}} \alpha \quad (59)$$

$$\dot{\mathbf{s}}_b = \frac{2}{3} \dot{\alpha} H_k \frac{\partial f}{\partial \mathbf{s}} \quad (60)$$

Where  $H_k$  is the kinematic hardening modulus.

The plastic consistency parameter  $\alpha$  satisfies the following Kuhn-Tucker loading and unloading conditions:

$$\dot{\alpha} \geq 0, \quad f \leq 0, \quad \dot{\alpha} f = 0 \quad (61)$$

Also, the following consistency condition needs to be satisfied:

$$\alpha \dot{f} = 0 \quad (62)$$

A step by step summary of the material state determination through the integration of the above mentioned governing equations with the backward-Euler integration scheme which results in a radial return mapping algorithm, is presented below for a single material point. A more

detailed explanation can be found in Simo et al. (1998). The summary focuses on a single iteration  $i$  for reaching vertical stress equilibrium at material point (Klinkel et al. (2002)).

*Step 1:* Determine the elastic trial stress for a given strain vector at time  $(t + 1)$ .

$$\mathbf{e}_{t+1} = \boldsymbol{\varepsilon}_{t+1} - \frac{1}{3}\theta_{t+1}\mathbf{1}$$

$$\mathbf{s}_{t+1} = 2G(\mathbf{e}_{t+1} - \mathbf{e}_t^p)$$

$$\mathbf{s}_{t+1}^{eff,trial} = \mathbf{s}_{t+1} - \mathbf{s}_{b,t}$$

*Step 2:* Compare the trial stress with the yield surface limit.

$$f_{t+1}(\mathbf{s}, \mathbf{s}_b, H_i) = \|\mathbf{s}_{t+1}^{eff,trial}\| - \sqrt{\frac{2}{3}}(\sigma_y + H_i\beta_t)$$

$$\text{If } f_{t+1}(\mathbf{s}, \mathbf{s}_b, H_i) \leq 0$$

Determine elastic tangent matrix as follows:

$$\mathbf{E}_{t+1} = K\mathbf{n}\mathbf{n}^T + 2G(l - l_{vol})$$

Where  $K$  is the bulk modulus.

$$\text{If } f_{t+1}(\mathbf{s}, \mathbf{s}_b, H_i) > 0$$

We will move to step 3 to establish the plastic state.

*Step 3:* Determine consistency parameter and normal to yield surface.

$$\Delta\alpha = \frac{f_{t+1}(\mathbf{s}, \mathbf{s}_b, H_i)}{2G + \frac{2}{3}(H_i + H_k)}$$

$$\frac{\partial f}{\partial \mathbf{s}_{t+1}} = \frac{(\mathbf{s}^{eff,trial}_{t+1})}{\|\mathbf{s}^{eff,trial}_{t+1}\|}$$

*Step 4:* Determine the updated hardening variable, plastic strain and back stress.

$$\beta_{t+1} = \beta_t + \sqrt{\frac{2}{3}}\Delta\alpha$$

$$\mathbf{e}_{t+1}^p = \mathbf{e}_t^p + \Delta\alpha \frac{\partial f}{\partial \mathbf{s}_{t+1}}$$

$$\mathbf{s}_{b,t+1} = \mathbf{s}_{b,t} + \frac{2}{3} H_k \Delta\alpha \frac{\partial f}{\partial \mathbf{s}_{t+1}}$$

*Step 5:* Determine the stress vector and consistent elastic-plastic tangent matrix.

$$\boldsymbol{\sigma}_{t+1} = K\theta_{t+1}\mathbf{1} + \mathbf{s}_{t+1} - 2G\Delta\alpha \frac{\partial f}{\partial \mathbf{s}_{t+1}}$$

$$\mathbf{E}_{t+1} = K(\mathbf{1} * \mathbf{1})$$

$$+ 2G \left[ (1 - \omega) \left( \mathbb{I} - \frac{1}{3} (\mathbf{1} * \mathbf{1}) \right) - \left( \frac{G}{G^p} - \omega \right) \left( \frac{\partial f}{\partial \mathbf{s}_{t+1}} * \frac{\partial f}{\partial \mathbf{s}_{t+1}} \right) \right]$$

Where

$$G^p = G + \frac{H_i + H_k}{3}$$

$$\omega = \frac{2G\Delta\alpha}{\|\mathbf{s}_{t+1}^{eff,trial}\|}$$

### 2.8.3.1.2 Generalized Plasticity Model

The generalized plasticity model has been developed as an alternative to nonlinear hardening kinematic model. Auricchio et al. (1995) discusses the advantages of this model over the nonlinear kinematic hardening model. One of the advantages over J2 plasticity model is that it can simulate the smooth asymptotic transition (Figure 2-6) between elastic and inelastic states during loading stages which has also been observed in the experiment with cyclic and reverse cyclic loading conditions. To achieve this behaviour, an additional limit function  $F$  has been introduced which distinguishes between admissible and non-admissible states.

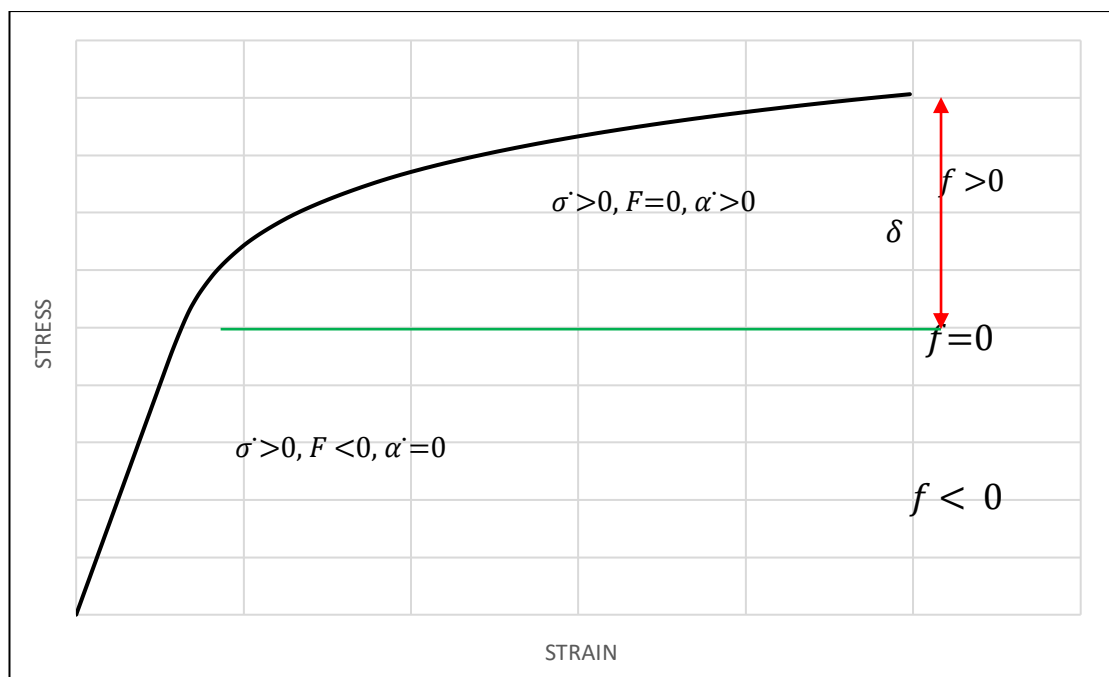


Figure 2-6. Generalized Plasticity Model

The limit function  $F$  has been described as:

$$F = h(f) \left( \frac{df}{d\sigma} : \dot{\boldsymbol{\sigma}} \right) - \dot{\alpha} \quad (63)$$

Where,

$$h(f) = \frac{f}{\varphi(\delta-f) + (H_i + H_k)\delta}$$

Here,  $\varphi$  is the rate of approaching the asymptote and  $\delta$  is the distance between the current and asymptotic radius of yield function.

If  $F \leq 0$ , we have admissible state and if  $F > 0$ , we reach a non-admissible state. The yield function  $f$  distinguishes between elastic state i.e.  $f < 0$  and inelastic states i.e.  $f \geq 0$  which may or may not occur depending on loading or unloading conditions (Figure 2-6).

The limit function is expressed in terms of the deviatoric stress  $\mathbf{s}$ , the back stress variable  $\mathbf{s}_b$  representing the distance of yield surface centre from the origin of deviatoric stress space and linear isotropic hardening modulus  $H_i$ :

$$F(\mathbf{s}, \mathbf{s}_b, H_i) = \|\mathbf{s} - \mathbf{s}_b\| - \sqrt{\frac{2}{3}} (\sigma_y + H_i \beta) \quad (64)$$

Here,  $\sigma_y$  is the uniaxial tensile yield strength and  $\beta$  is the isotropic hardening variable with nature of plastic strain.

The plastic flow rule is:

$$\dot{\mathbf{e}}_p = \alpha \frac{\partial f}{\partial \mathbf{s}} \quad (65)$$

Here  $\alpha$  is known as plastic consistency parameter and  $\frac{\partial f}{\partial \mathbf{s}}$  is the normal to the yield surface which is determined as:

$$\frac{\partial f}{\partial \mathbf{s}} = \frac{(\mathbf{s} - \mathbf{s}_b)}{\|\mathbf{s} - \mathbf{s}_b\|} \quad (66)$$

The hardening rules are:

$$\dot{\beta} = \sqrt{\frac{2}{3}} \alpha \quad (67)$$

$$\dot{\mathbf{s}}_b = \frac{2}{3} \dot{\alpha} H_k \frac{\partial f}{\partial \mathbf{s}} \quad (68)$$

Where  $H_k$  is the kinematic hardening modulus.

The plastic rate parameter  $\alpha$  satisfies the following Kuhn-Tucker loading and unloading conditions.

$$\dot{\alpha} \geq 0, \quad F \leq 0, \quad \dot{\alpha}F = 0 \quad (69)$$

A step by step summary of the material state determination through the integration of the above mentioned governing equations with the backward-Euler integration scheme which results in a radial return mapping algorithm, is presented below for a single material point. A more detailed explanation can be found in Auricchio et al. (1995). The summary focuses on a single iteration  $i$  for reaching vertical stress equilibrium at material point (Klinkel et al. (2002)).

*Step 1:* Determine the elastic trial stress for a given strain vector at time  $(t + 1)$ .

$$\mathbf{e}_{t+1} = \boldsymbol{\varepsilon}_{t+1} - \frac{1}{3}\theta_{t+1}\mathbf{1}$$

$$\mathbf{s}_{t+1} = 2G(\mathbf{e}_{t+1} - \mathbf{e}_t^p)$$

$$\mathbf{s}_{t+1}^{eff,trial} = \mathbf{s}_{t+1} - \mathbf{s}_{b,t}$$

*Step 2:* Compare the trial stress with the yield surface limit.

$$F_{t+1}(\mathbf{s}, \mathbf{s}_b, H_i) = \|\mathbf{s}^{eff,trial}_{t+1}\| - \sqrt{\frac{2}{3}}(\sigma_y + H_i\beta_t)$$

$$A_2 = \|\mathbf{s}^{eff,trial}_{t+1}\| - \|\mathbf{s}^{eff,trial}_t\|$$

If  $f_{t+1}(\mathbf{s}, \mathbf{s}_b, H_i) \leq 0$  OR  $A_2 < 0$

Determine elastic tangent matrix as follows:

$$\mathbf{E}_{t+1} = K\mathbf{nn}^T + 2G(l - l_{vol})$$

Where  $K$  is the bulk modulus.

If  $f_{t+1}(\mathbf{s}, \mathbf{s}_b, H_i) > 0$  OR  $A_2 \geq 0$

We will move to step 3 to establish the plastic state.

*Step 3:* Determine consistency parameter (smallest positive root) and normal to yield surface.

$$\Delta\alpha = \frac{-b(+or -)\sqrt{(b^2 - 4ac)}}{2a}$$

Where,

$$a = 2G_1A_3$$

$$b = A_4 - A_1A_3 + 2G_1A_2$$

$$c = -A_1A_2$$

$$2G_1 = 2G + \frac{2}{3}(H_i + H_k)$$

$$A_1 = F_{t+1}(\mathbf{s}, \mathbf{s}_b, H_i)$$

$$A_3 = \varphi - 2G$$

$$A_4 = (\varphi + H_i + H_k)\delta$$

$$\frac{\partial f}{\partial \mathbf{s}_{t+1}} = \frac{(\mathbf{s}^{eff,trial}_{t+1})}{\|\mathbf{s}^{eff,trial}_{t+1}\|}$$

*Step 4:* Determine the updated hardening variable, plastic strain and back stress.

$$\beta_{t+1} = \beta_t + \sqrt{\frac{2}{3}} \Delta\alpha$$

$$\mathbf{e}_{t+1}^p = \mathbf{e}_t^p + \Delta\alpha \frac{\partial f}{\partial \mathbf{s}_{t+1}}$$

$$\mathbf{s}_{b,t+1} = \mathbf{s}_{b,t} + \frac{2}{3} H_k \Delta\alpha \frac{\partial f}{\partial \mathbf{s}_{t+1}}$$

*Step 5:* Determine the stress vector and consistent elastic-plastic tangent matrix.

$$\boldsymbol{\sigma}_{t+1} = K \theta_{t+1} \mathbf{1} + \mathbf{s}_{t+1} - 2G \Delta\alpha \frac{\partial f}{\partial \mathbf{s}_{t+1}}$$

$$\mathbf{E}_{t+1} = K(\mathbf{1} * \mathbf{1})$$

$$+ 2G \left[ (1 - \omega) \left( \mathbb{I} - \frac{1}{3} (\mathbf{1} * \mathbf{1}) \right) + (\omega - A_w) \left( \frac{\partial f}{\partial \mathbf{s}_{t+1}} * \frac{\partial f}{\partial \mathbf{s}_{t+1}} \right) \right]$$

Where,

$$A_w = \frac{2G(b_1 + b_2)}{2G_1 b_1 - A_3 b_2 + A_4}$$

Where,

$$b_1 = A_2 + A_3\Delta\alpha$$

$$b_2 = A_1 - 2G_1\Delta\alpha$$

$$\omega = \frac{2G\Delta\alpha}{\|\mathbf{s}^{eff,trial}_{t+1}\|}$$

## 2.9 Stability Criteria and State Determination

### 2.9.1 Stability Criteria

The two-field mixed based formulation requires both displacement and force shape functions. However, the order of displacement ( $n_d$ ) and force ( $n_f$ ) shape functions are interconnected through the compatibility and constitutive relations. Proper care should be taken to choose the order and continuity of both shape functions, otherwise non-meaningful results will be produced as observed by Zienkiewicz et al. (1989). According to De Veubeke's principle of limitation (1965), the order of stress quantity should be less than that of strain quantity to maintain the stability of the algorithm.

For flexure critical mixed element formulation, constant axial force distribution along the length of the element without the presence of axially distributed loads, require a linear distribution of axial displacement. Whereas, the linear moment field along the length of the element requires a linear curvature field which in turn requires cubic distribution of the transverse displacement field along the length of the element. Therefore the following relation can be written for flexure critical element as proposed by Ayoub (1999).

For axial field,

$$n_f = n_d - 1 \quad (70)$$

For moment field,

$$n_f = n_d - 2 \quad (71)$$

Using Hermitian polynomial shape function for vertical displacement field, two nodes beam elements will be sufficient to satisfy the principle of limitation stability criteria for flexure critical condition.

For shear critical mixed element formulation, constant axial force distribution along the length of the element without the presence of axially distributed loads, require a linear distribution of axial displacements. Whereas, linear moment field along the length of the element requires a linear curvature field which in turn requires a quadratic distribution of rotation field along the length of the element. Whereas, constant shear force distribution along the length of the element require a cubic transverse displacement field along the length of the element to match the same order of the rotation field. Therefore the following relations are proposed for newly developed shear critical mixed element:

For axial field,

$$n_f = n_d - 1 \quad (72)$$

For moment field,

$$n_f = n_d - 1 \quad (73)$$

For shear field,

$$n_f = n_d - 3 \quad (74)$$

Using quadratic polynomial shape functions for the rotation field, two nodes beam element will not be sufficient to satisfy the principle of limitation stability criteria for shear critical condition. Therefore, one additional middle degree of freedom for the rotation field is a must for shear critical two-field mixed beam element which will get statically condensed out at the element level before the assembling process.

## 2.9.2 State Determination

A step by step summary of the state determination algorithm is presented below for a single element. A more detailed explanation can be found in Ayoub (1999). The summary focuses on a single global iteration  $i$  at the structural degree of freedoms through the Newton-Raphson method with applied load counter  $k$ .

*Step 1:* Determine the incremental structural nodal displacement and its update with respect to the global axes of reference by the solver

$$\Delta \mathbf{U}^{i+1} = [\mathbf{K}^i]^{-1} (\mathbf{P}^{k+1} - \mathbf{P}_R^i) \quad (\text{By the solver})$$

Where

$$\mathbf{P}^{k+1} = \mathbf{P}^k + \Delta\mathbf{P}^{k+1} \quad (\text{Update of applied load vector})$$

$$\mathbf{U}^{i+1} = \mathbf{U}^i + \Delta\mathbf{U}^{i+1} \quad (\text{Update of global nodal displacement vector})$$

*Step 2:* Determine the incremental element nodal deformation and its update with respect to the basic axes of reference with the help of nodal compatibility and extraction of rigid body modes

$$\Delta\mathbf{u}_{IJ_{ele}}^{i+1} = \mathbf{A}_{IJ}\Delta\mathbf{U}^{i+1} \quad (\text{By the solver})$$

$$\Delta\mathbf{v}^{i+1} = \mathbf{a}_c\Delta\mathbf{u}_{IJ_{ele}}^{i+1} \quad (\text{By Element Subroutine})$$

$$\mathbf{v}^{i+1} = \mathbf{v}^i + \Delta\mathbf{v}^{i+1} \quad (\text{Update of element nodal deformation vector})$$

*Step 3:* Determine the incremental element nodal force and its update with respect to the basic axes of reference for a given element nodal deformation vector which remains constant for element iteration loop counter  $j$ .

$$\Delta\mathbf{q}^j = \mathbf{k}_{ele}^{j-1}(\mathbf{G}\Delta\mathbf{v}^{i+1} - \mathbf{u}^{r,j-1})$$

$$\mathbf{q}^{j+1} = \mathbf{q}^j + \Delta\mathbf{q}^j \quad (\text{Update of element nodal force vector})$$

*Step 4:* Determine the incremental section deformation and its update with respect to the basic axes of reference for a given element nodal force vector.

$$\Delta \mathbf{d}^j = [\mathbf{k}_{sec}^{j-1}]^{-1} (\mathbf{b} \Delta \mathbf{q}^j)$$

$$\mathbf{d}^{j+1} = \mathbf{d}^j + \Delta \mathbf{d}^j \quad (\text{Update of section deformation vector})$$

$$\mathbf{q}_{sec}^{j+1} = \mathbf{q}_{sec}^j + (\mathbf{b} \Delta \mathbf{q}^j) \quad (\text{Update of section force vector})$$

*Step 5:* Determine the section tangent stiffness ( $\mathbf{k}_{sec}^{j+1}$ ) and resistance vector ( $\mathbf{p}_{sec}^{j+1}$ ) for a given section deformation vector with mid-point integration rule and material state determination as described in Section 2.8.

*Step 6:* Determine the element residual deformation and flexibility matrix and update the element nodal forces with updated section deformation and forces for the next element iteration until the norm of element nodal energy becomes less than the specified tolerance value to dissipate the element residual deformation.

$$\mathbf{f}_{ele}^{j+1} = \sum \mathbf{b}^T [\mathbf{k}_{sec}^{j+1}]^{-1} \mathbf{b}$$

$\mathbf{u}^{r,j+1} = \mathbf{u}^{r,j} + \sum \mathbf{b}^T [\mathbf{k}_{sec}^{j+1}]^{-1} (\mathbf{q}_{sec}^{j+1} - \mathbf{p}_{sec}^{j+1})$  (Update of element nodal residual deformation vector)

$$\mathbf{q}^{j+2} = \mathbf{q}^{j+1} - [\mathbf{f}_{ele}^{j+1}]^{-1} \mathbf{u}^{r,j+1}$$

$$\mathbf{d}^{j+2} = \mathbf{d}^{j+1} + [\mathbf{k}_{sec}^{j+1}]^{-1} (\mathbf{q}_{sec}^{j+1} - \mathbf{p}_{sec}^{j+1}) - [\mathbf{k}_{sec}^{j+1}]^{-1} (\mathbf{b}[\mathbf{f}_{ele}^{j+1}]^{-1} \mathbf{u}^{r,j+1})$$

$$\mathbf{q}_{sec}^{j+2} = \mathbf{q}_{sec}^{j+1} - (\mathbf{b}[\mathbf{f}_{ele}^{j+1}]^{-1} \mathbf{u}^{r,j+1})$$

*Step 7:* Determine the element stiffness matrix and resistance vector in iteration counter  $i$  for the given nodal element deformation upon the convergence of element compatibility at the basic frame of reference.

$$\mathbf{K}_{ele}^{i+1} = \mathbf{G}^T [\mathbf{f}_{ele}^{j+1}]^{-1} \mathbf{G}$$

$$\mathbf{Q}_{ele}^{i+1} = \mathbf{G}^T \mathbf{q}_{ele}^{i+1}$$

*Step 8:* Determine the element stiffness matrix and resistance vector in iteration counter  $i$  at the global frame of reference.

$$K_{ele,glo}^{i+1} = a_c^T K_{ele}^{i+1} a_c$$

$$Q_{ele,glo}^{i+1} = a_c^T Q_{ele}^{i+1}$$

## 2.10 Implementation

The element subroutines are coded in FORTRAN 90 programming language. FEAP Pv (Taylor, 1989) has been used as global solver for finite element solution. The element formulation needs three frame of reference i.e. global frame of reference for element nodal degrees of freedom with rigid body modes, basic frame of reference for element nodal deformation without rigid body modes and basic frame of reference for element nodal forces. For a given set of element nodal displacement degree of freedoms by the solver, element state determination process becomes responsible to transfer the calculated consistent resistance and stiffness matrix at each frame of reference considering equilibrium, compatibility and multi-axial constitutive models of materials to the solver. Solver iteratively determines the converged value of element nodal displacement degree of freedoms after assembling the various elements information by following principle of potential energy. Required response variables which are stored in history variables in element subroutines, have been reported in the following chapters.

# **Chapter 3 Correlation Studies – Shear Critical RC and Steel Components**

## **3.1 Overview**

This chapter presents several correlation studies of the newly developed frame element based on two-field mixed formulations with the experimental results of shear critical reinforced concrete and steel members under monotonic and cyclic loading conditions.

The correlation studies starts with reinforced concrete beams under monotonic loading condition followed by reinforced concrete columns and walls under cyclic loading conditions. At the end, correlations studies extended to steel shear links under monotonic and cyclic loading conditions to demonstrate the capability of the element formulation with implemented multi-axial material models.

## **3.2 RC Beams**

### **3.2.1 Beams by Vecchio and Shim (2004)**

Vecchio et al. (2004) performed tests on a series of 12 reinforced concrete beams under three point monotonic loading conditions to reproduce the test results of similar beam specimens tested by Bresler et al. (1963). The effect

of span to depth ratio and reinforcement details on the load-deformation response, load capacity and failure mode have been investigated. Three types of failure modes have been observed i.e. diagonal-tension, shear-compression and flexure-compression. Out of these 12 specimens, three specimens A1, A2 and A3 (Figure 3-1) are chosen for the correlation studies. Specimens A1 and A2 which have shear span to depth ratio ( $1800/552=3.3$ ) and ( $2285/552=4.1$ ) respectively failed in a shear-compression mode whereas specimen A3 which has shear span to depth ratio ( $3200/552=5.8$ ) failed in a flexure-compression mode.

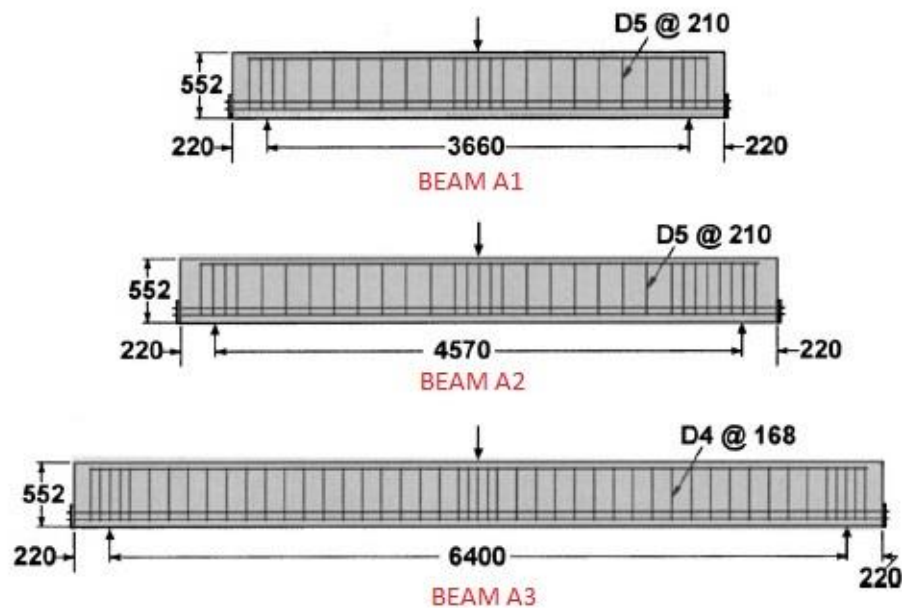


Figure 3-1. Geometry of A1, A2 and A3 beams

The cross-section details of these three specimens are shown in Figure 3-2. All the specimens have same width and depth i.e. 305 mm and 552 mm respectively.

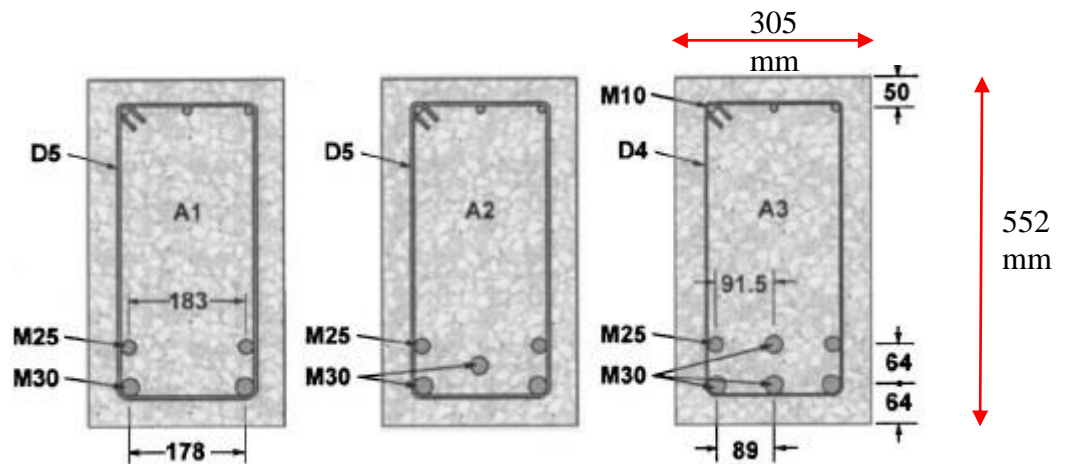


Figure 3-2. Cross-sections of A1, A2 and A3 beams

The tension longitudinal reinforcements M25 and M30 have cross-sectional areas of  $500 \text{ mm}^2$  and  $700 \text{ mm}^2$  with yield strengths of 440 MPa and 436 MPa respectively. Whereas compression longitudinal reinforcements M10 has a cross-sectional area of  $100 \text{ mm}^2$  with yield strength of 315 MPa. Two types of shear reinforcement are used i.e. D4 and D5 which have yield strength of 600 MPa with cross-sectional areas of  $25.7 \text{ mm}^2$  and  $32.2 \text{ mm}^2$  respectively. The spacing of transverse reinforcement along the length of the beams A1 and A2 is 210 mm, whereas for beam A3 it is 168 mm. The concrete compressive strength of beams A1, A2 and A3 are 22.6 MPa, 25.9 MPa and 43.5 MPa respectively.

For three point loading conditions, two beam elements are used to model the entire beam specimen with 5 section integration points in each element. Figures 3-3, 3-4 and 3-5 compare the load versus mid-span deflection response of the models using the proposed beam element with the experimental results of beams A1, A2 and A3 respectively.

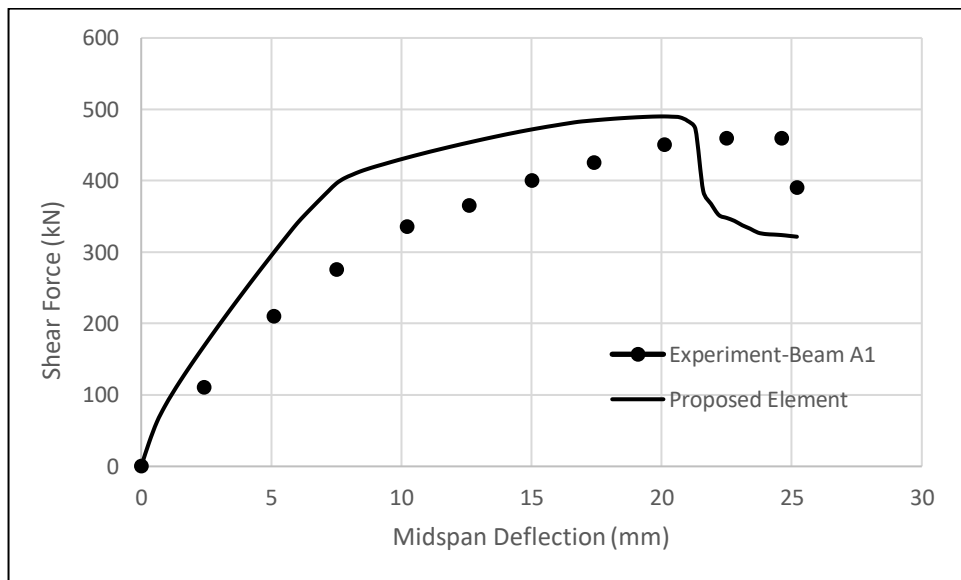


Figure 3-3. Load-Deflection Response of Beam A1

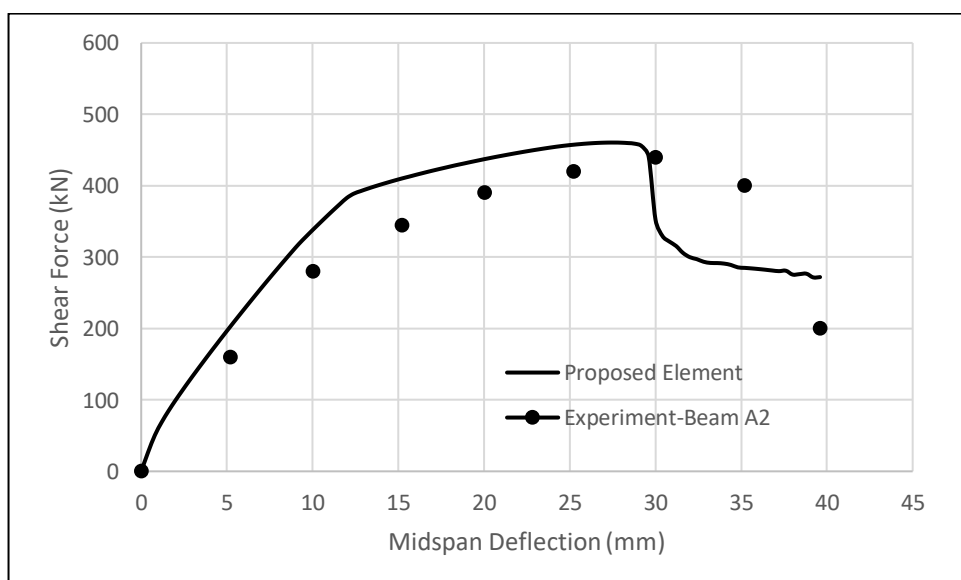


Figure 3-4. Load-Deflection Response of Beam A2

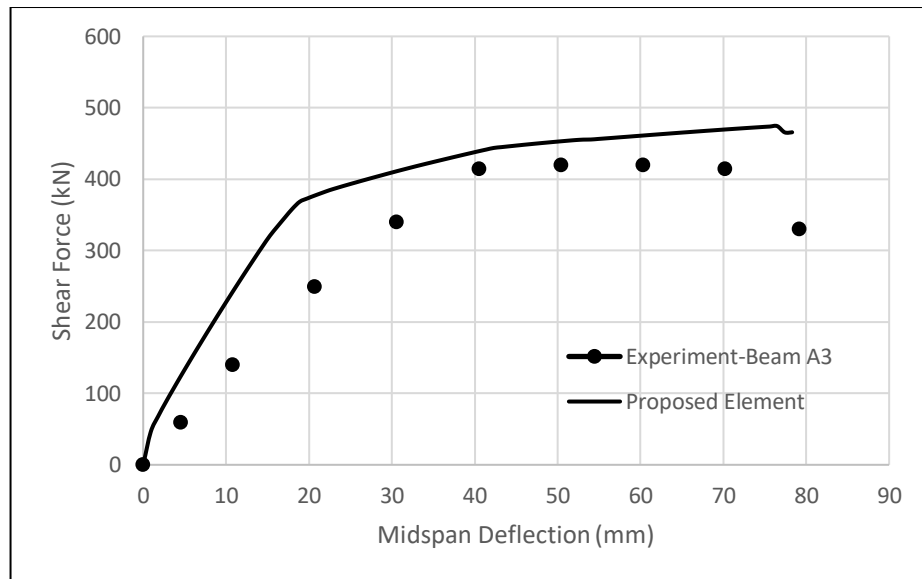


Figure 3-5. Load-Deflection Response of Beam A3

From the above plots, it can be observed that the proposed element reasonably reproduce the overall experimentally observed load-deflection response. However, it has produced a stiffer response at the pre-peak shear strength; whereas, the ultimate shear resistance and shear deformation capacity have been captured well. It is to be noted that with a higher shear span to depth ratio, the shear resistance capacity gets decreased but the shear deformation capacity substantially gets increased.

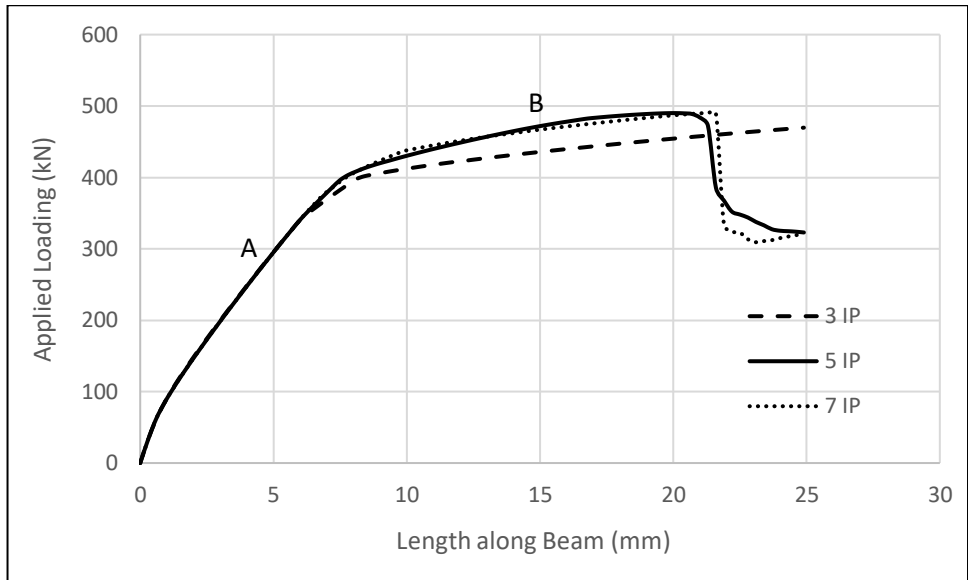


Figure 3-6. Effect of Integration Points on Load-Deflection Response of Beam A1

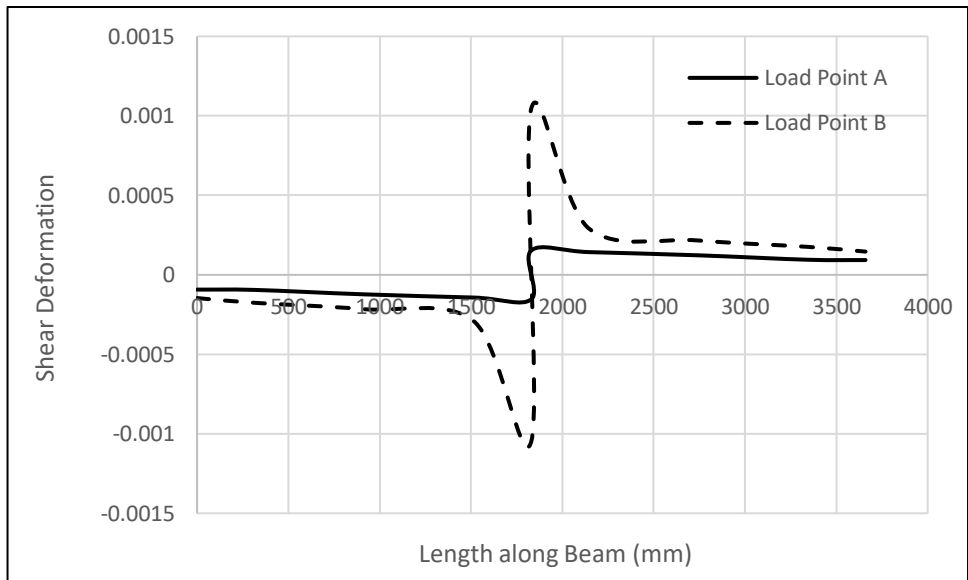


Figure 3-7. Variation of Shear Deformation along length of Beam A1

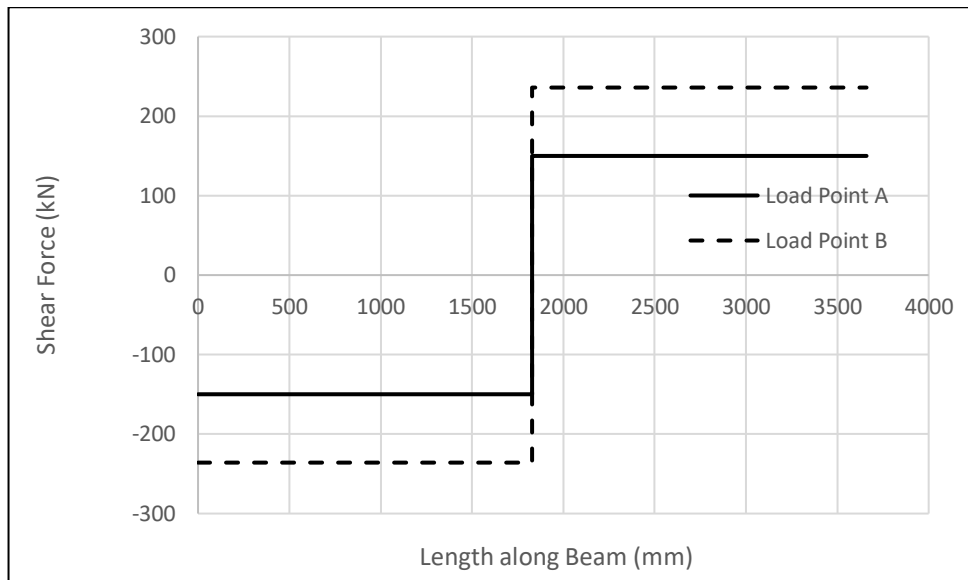


Figure 3-8. Variation of Shear Force along length of Beam A1

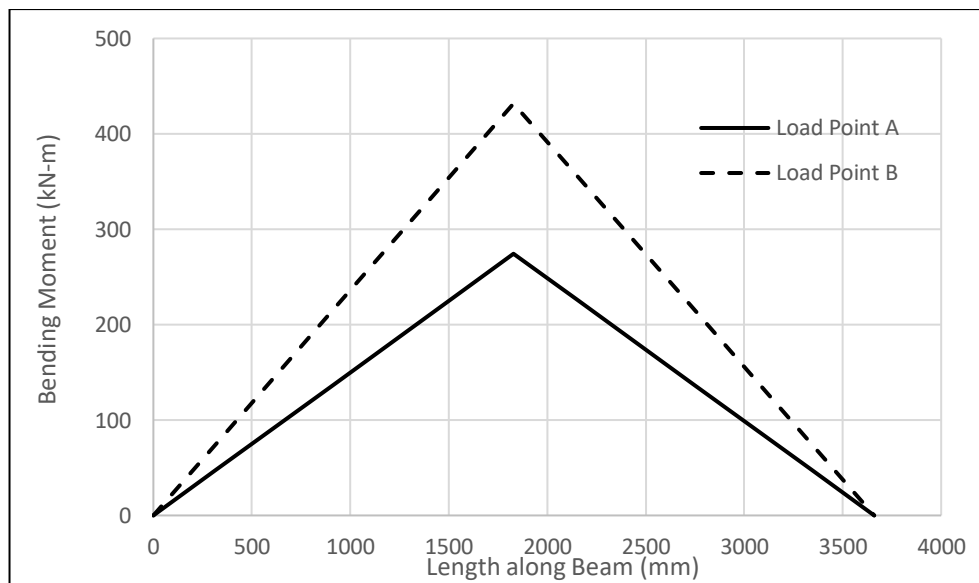


Figure 3-9. Variation of Bending Moment along length of Beam A1

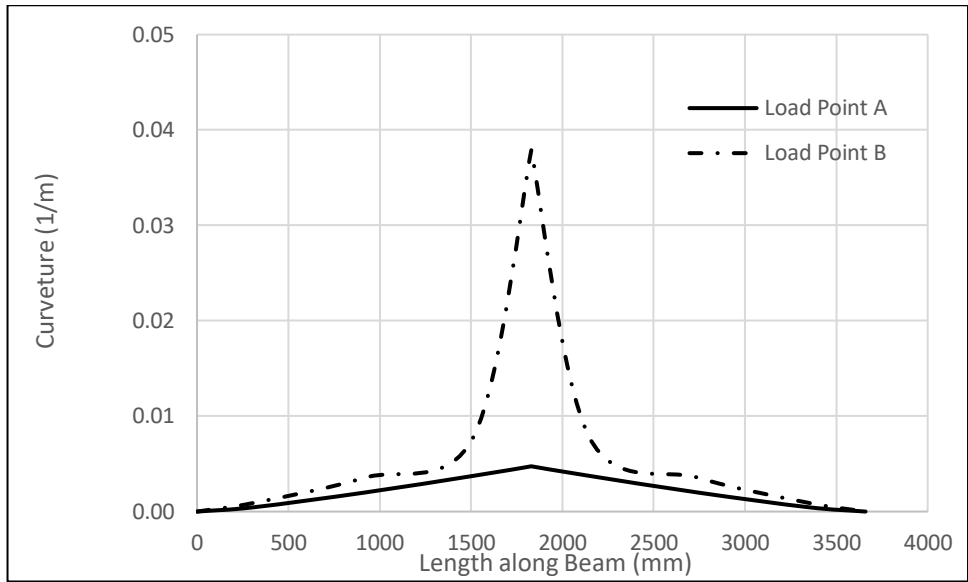


Figure 3-10. Variation of Curvature along length of Beam A1

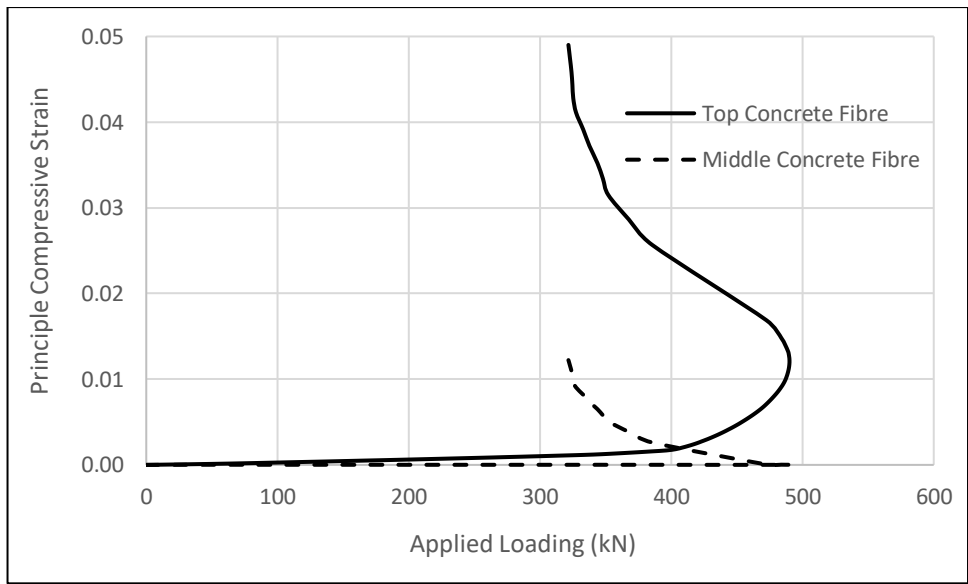


Figure 3-11. Principle Compressive Strain- Load Response at Loading Point of Beam A1

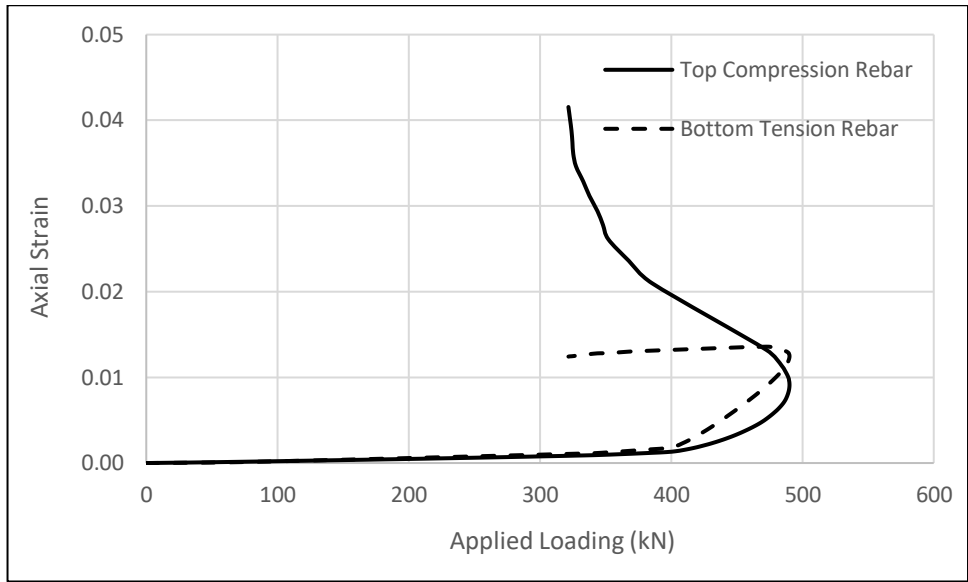


Figure 3-12. Axial Strain- Load Response at Loading Point of Beam A1

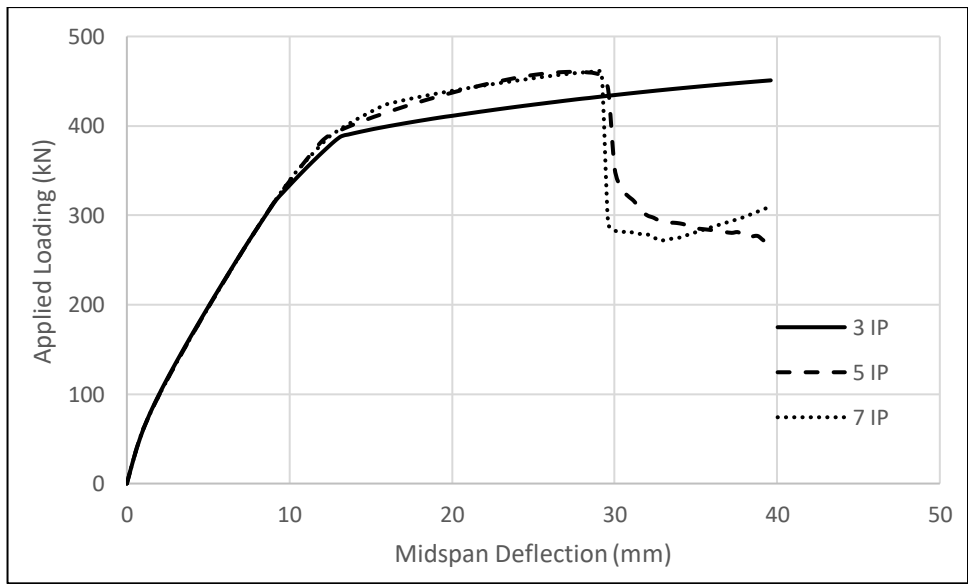


Figure 3-13. Effect of Integration Points on Load-Deflection Response of Beam A2

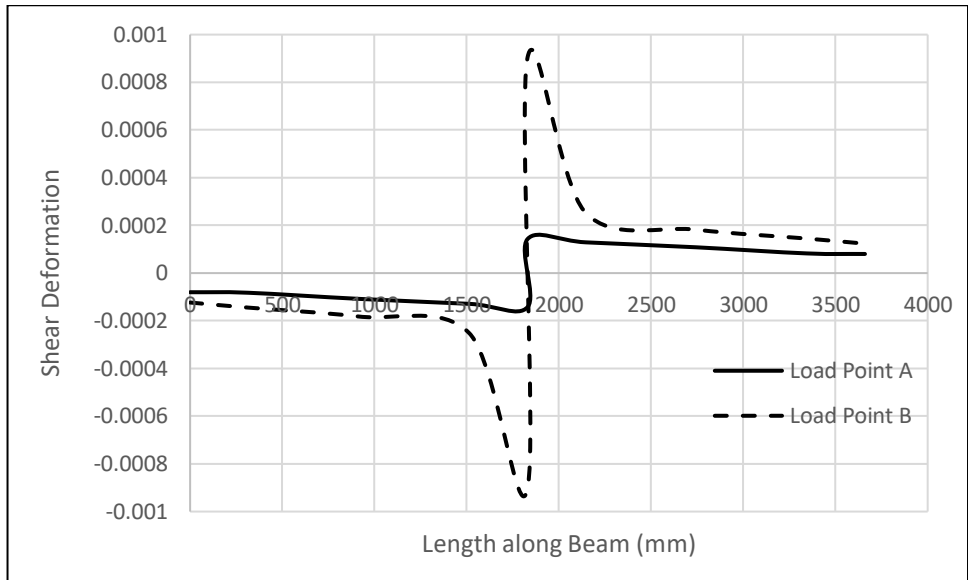


Figure 3-14. Variation of Shear Deformation along length of Beam A2

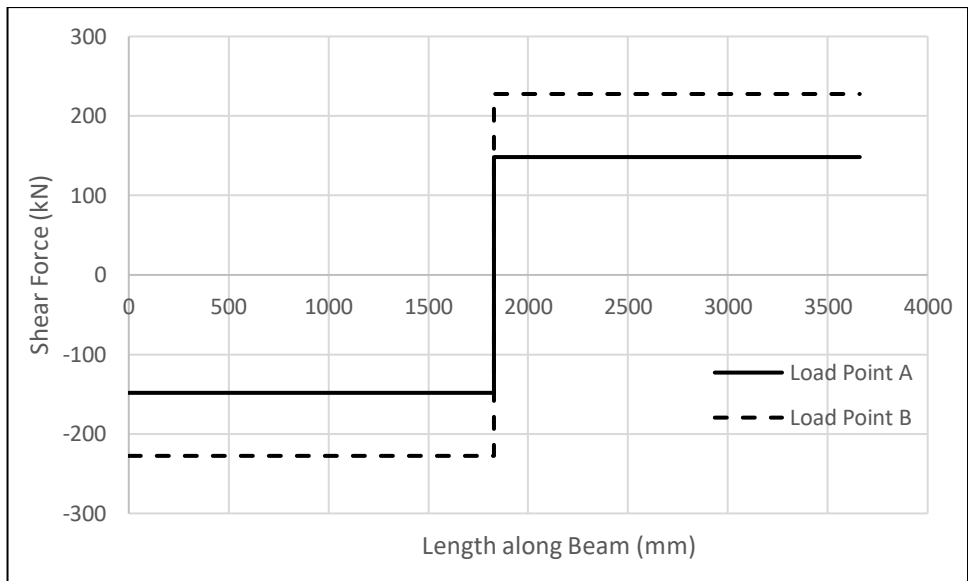


Figure 3-15. Variation of Shear Force along length of Beam A2

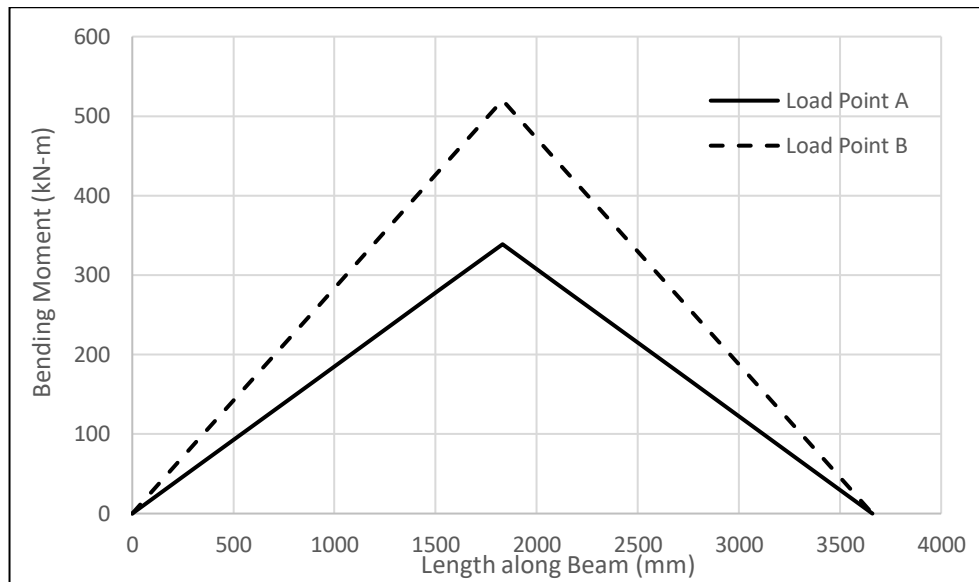


Figure 3-16. Variation of Bending Moment along length of Beam A2

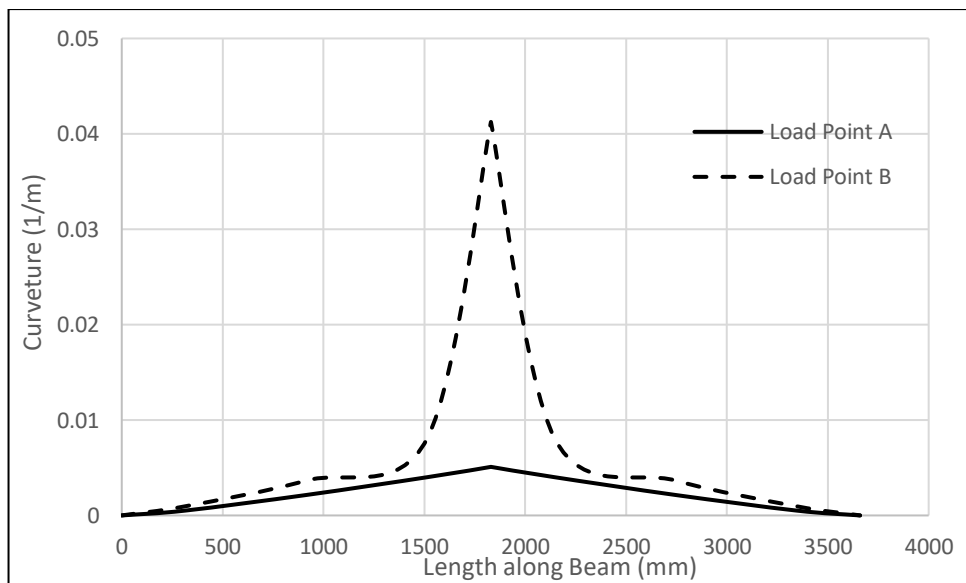


Figure 3-17. Variation of Curvature along length of Beam A2

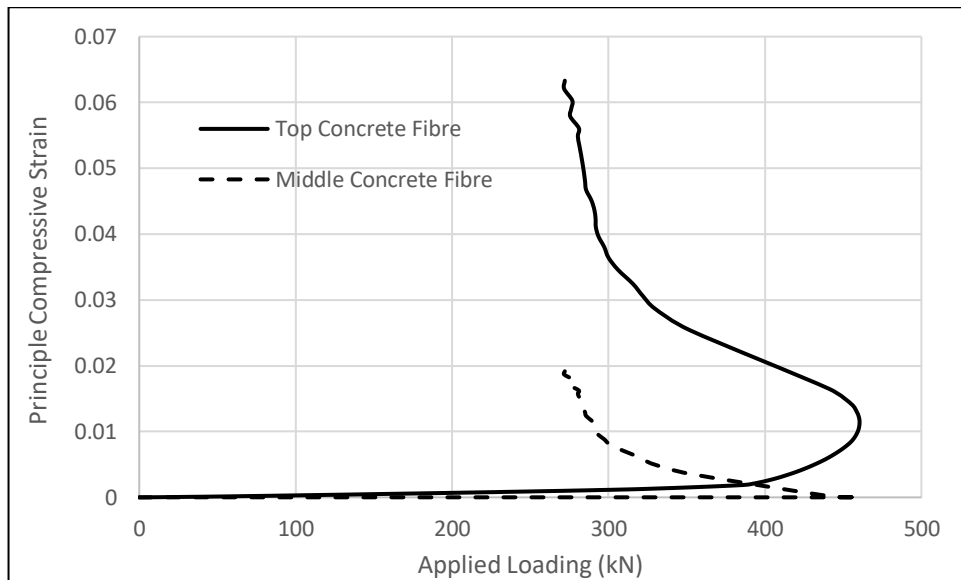


Figure 3-18. Principle Compressive Strain- Load Response at Loading Point of Beam A2

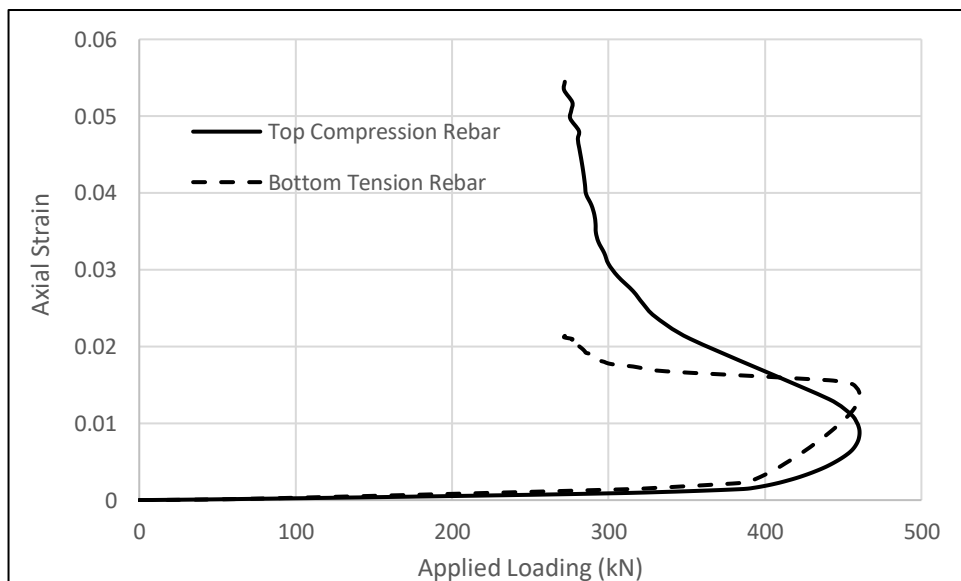


Figure 3-19. Axial Strain- Load Response at Loading Point of Beam A2

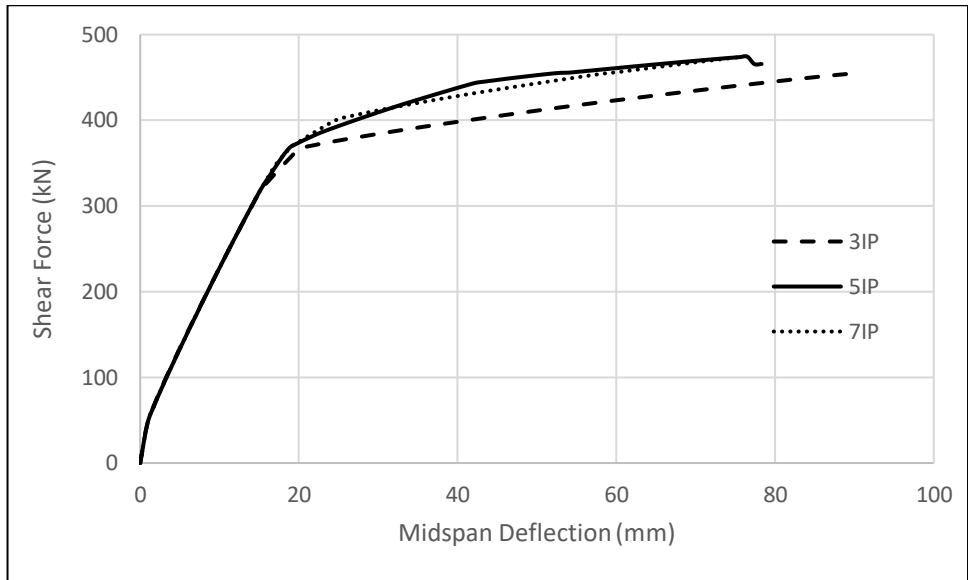


Figure 3-20. Effect of Integration Points on Load-Deflection Response of Beam A3

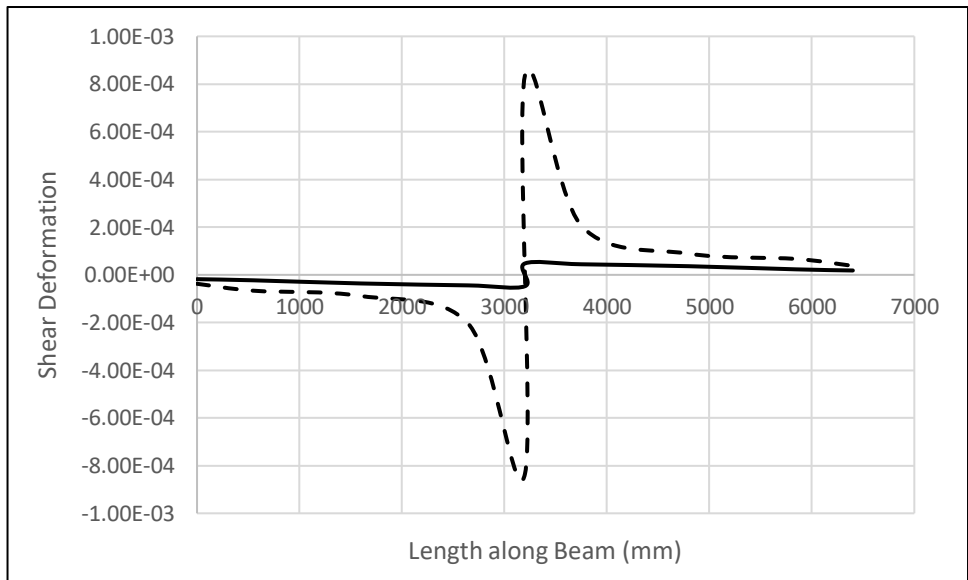


Figure 3-21. Variation of Shear Deformation along length of Beam A3

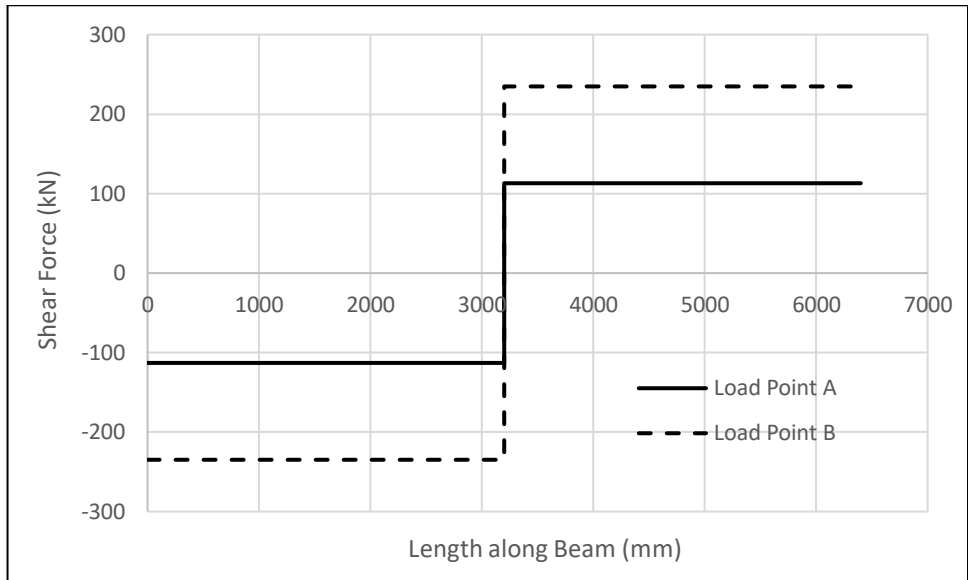


Figure 3-22. Variation of Shear Force along length of Beam A3

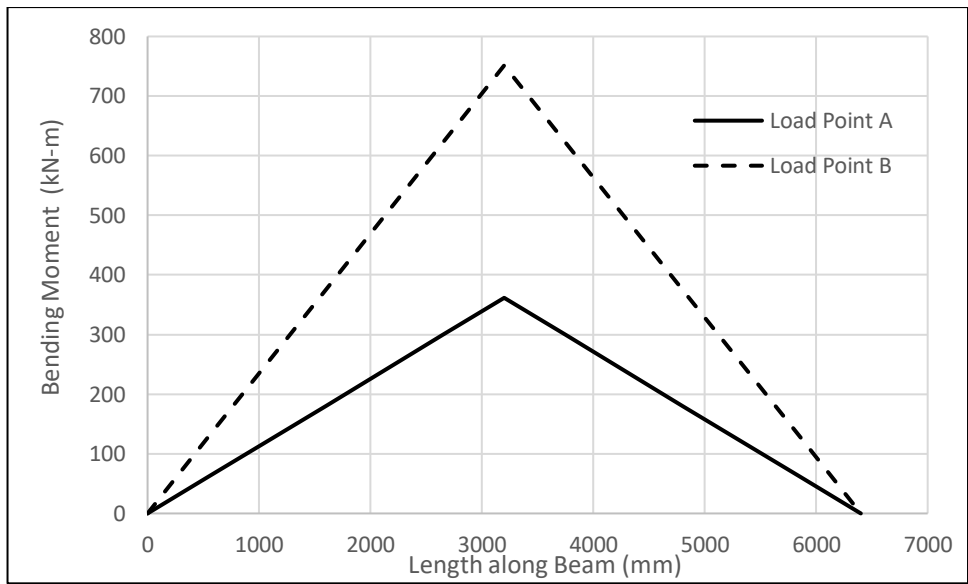


Figure 3-23. Variation of Bending Moment along length of Beam A3

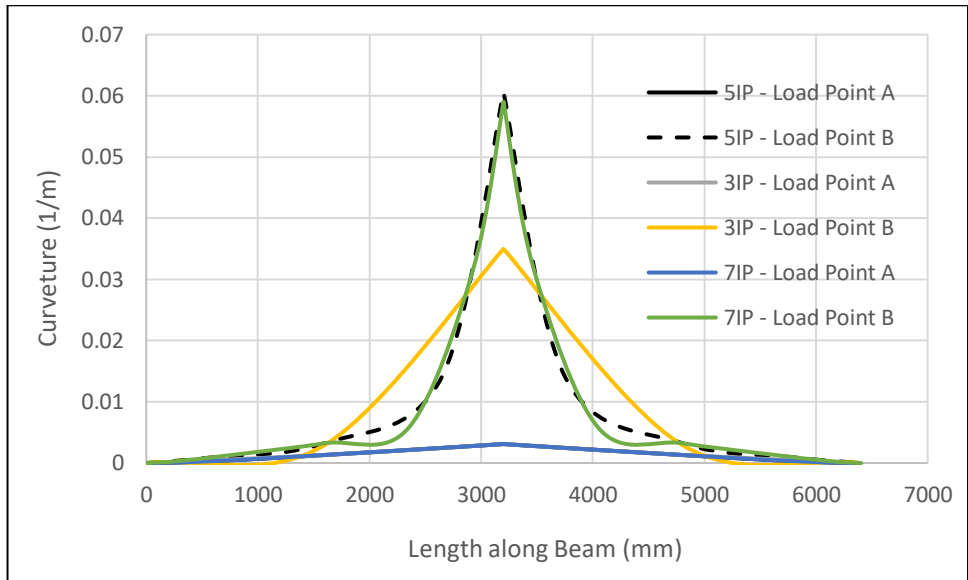


Figure 3-24. Variation of Curvature along length of Beam A3

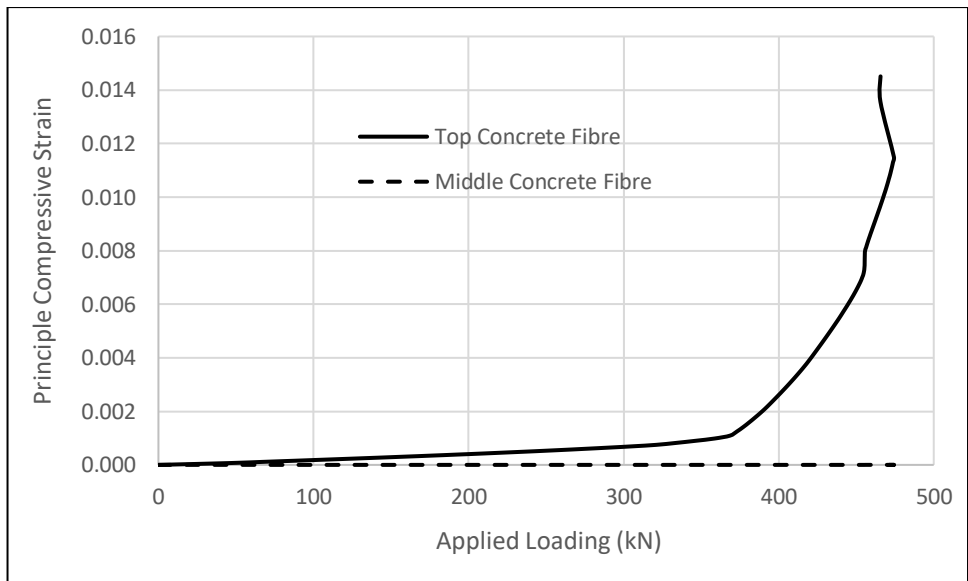


Figure 3-25. Principle Compressive Strain- Load Response at Loading Point of Beam A3

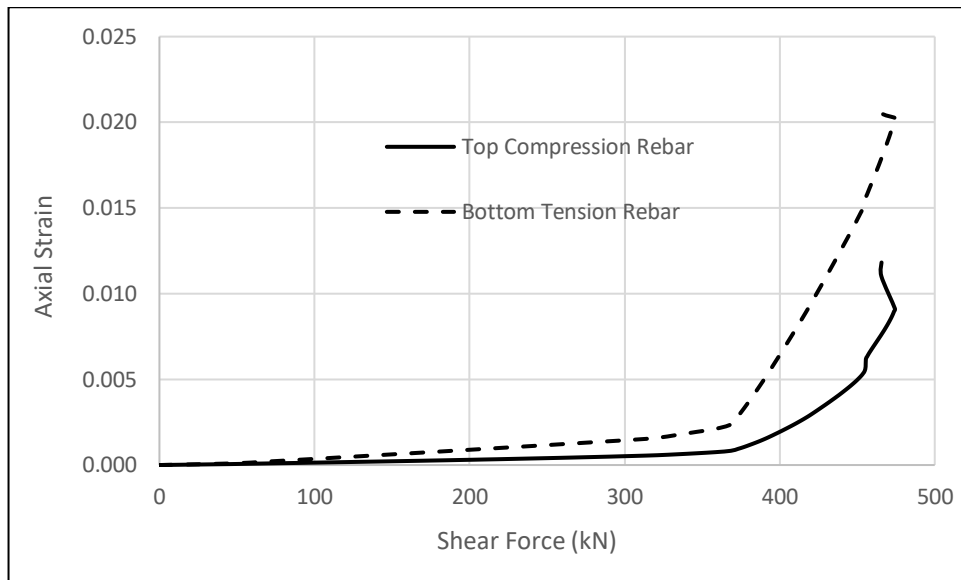


Figure 3-26. Axial Strain- Load Response at Loading Point of Beam A3

Figures 3-6, 3-13, and 3-20 show the effect of integration points on load-deflection response of Beam A1, A2 and A3 respectively. It can be noted that response is not integration point sensitive in elastic state of material. However, in inelastic state of material, capacity gets decreased while 3 no of integration points are used. Moreover, for 5 and 7 no of integration points, almost identical results are obtained. This signifies that proposed mixed beam element would be producing reasonable results if we use minimum 5 no of integration points.

Figures 3-9, 3-16, and 3-23 show the variation of shear deformation along the length of Beam A1, A2 and A3 respectively. It can be noted that in elastic range of material, variation of shear deformation is almost linear and in inelastic state of material, nonlinear variation of shear deformation near

the load point due to flexure-shear interaction has been reported. However, variation of shear force is constant along the half span of the beam as can be observed in the Figures 3-10, 3-17 and 3-24 for Beam A1, A2 and A3 respectively.

Figures 3-9, 3-16, and 3-23 show the variation of bending moment along the length of Beam A1, A2 and A3 respectively. It can be noted that in both elastic and inelastic state of material, variation of moment is linear as expected. However, in elastic state of material, variation of curvature is linear while in inelastic state of material, nonlinear variation of curvature near the load point due to flexure-shear interaction has been reported in the Figures 3-10, 3-17 and 3-24 for Beam A1, A2 and A3 respectively. It can also be noted that accurate variation of curvature in inelastic state of material has not been produced by 3 no of integration points. Moreover, both 5 and 7 no of integration points have produced identical curvature variation in both elastic and inelastic state of material.

Figures 3-11, 3-18, and 3-25 show the principle compressive strain-loading response of top and middle concrete fibres at the loading point of Beam A1, A2 and A3 respectively. It can be noted that for all the beams top concrete fibre reaches substantial amount of compressive strain. However, middle concrete fibre of beam A3 has produced very lesser amount of

compressive strain compared to its counterpart i.e. beam A1 and A2. This signifies that beam A1 and A2 fails in shear compression mode while beam A3 fails in flexure compression mode as observed in the experiments. This can be further substantiated from the Figures 3-12 and 3-19 that the bottom tensile reinforcement strain remains constant at the later stage of loading for beam A1 and A2, which signifies that input energy getting dissipated by the internal shear energy in the shear compression zone and flexural energy generated from the tensile rebar get ceased. However, for beam A3 from Figure 3-26, it can be observed that tensile strain gets increased in the later stage of loading as it fails in flexure mode. It should also be noted that in all the beams the compression rebar has produced comparable amount of strain with that of top compressive concrete fibre to satisfy the compatibility condition.

These observations can conclude that the proposed beam element based on mixed formulation can reasonable reproduce the global and local behaviour along with failure modes observed in the experiments for both flexure and shear critical members.

### **3.3 RC Columns**

#### **3.3.1 Columns by Xiao, Priestley and Seible (1993)**

Xiao et al. (1993) conducted tests on a series of three reinforced concrete columns R1, R3 and R5 (Figure 3-27) under constant axial compressive loading of 507.1 kN with increasing amplitude of lateral displacement cycles at the columns top end. The columns were fixed at both ends and the lateral loading displaced the columns in a double bending curvature mode.

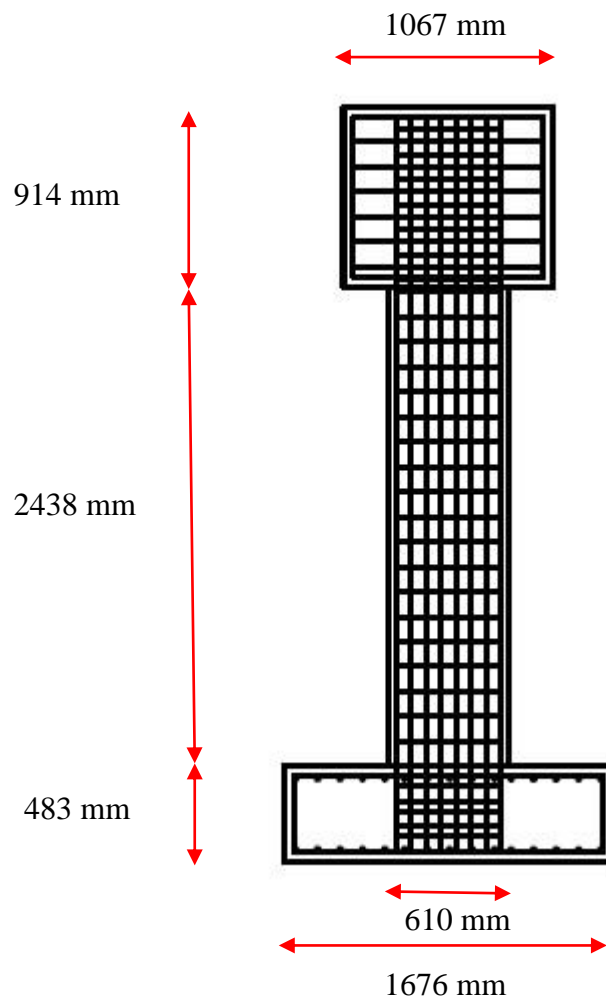


Figure 3-27. Geometry of RC Columns R1, R3 and R5

The cross-section details of these three specimens are shown in Figure 3-28. All the specimens have the same width and depth i.e. 406 mm and 610 mm respectively.

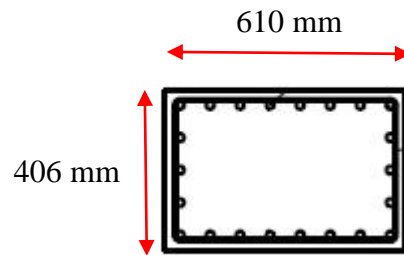


Figure 3-28. Cross-sections of R1, R3 and R5 Columns

22 longitudinal reinforcements of diameter 19.05 mm are uniformly spaced along the perimeter of the columns. Rectangular hoops of diameter 6.35 mm are placed at a spacing of 127 mm along the length of the columns. Concrete compressive strengths of columns R1, R3 and R5 are 37.9 MPa, 34.1 MPa and 32.8 MPa respectively. Yield strengths of longitudinal and transverse reinforcements are 317.2 MPa, 469.5 MPa, 469.5 MPa and 360.6 MPa, 324.0 MPa, 324.0 MPa for columns R1, R3 and R5 respectively. For all columns, peak compressive strain and strain at crushing of concrete material has been considered as 0.002 and 0.02 respectively. The tensile strength of concrete has been taken as  $0.33*(f_c)^{0.5}$ . Unloading stiffness for concrete material is considered as 0.01.

One element has been used to model the entire column specimen with 5 section integration points. Figures 3-29, 3-30 and 3-31 compare the lateral load versus top end deflection response of the models using the proposed beam element with the experimental results of columns R1, R3 and R5 respectively.

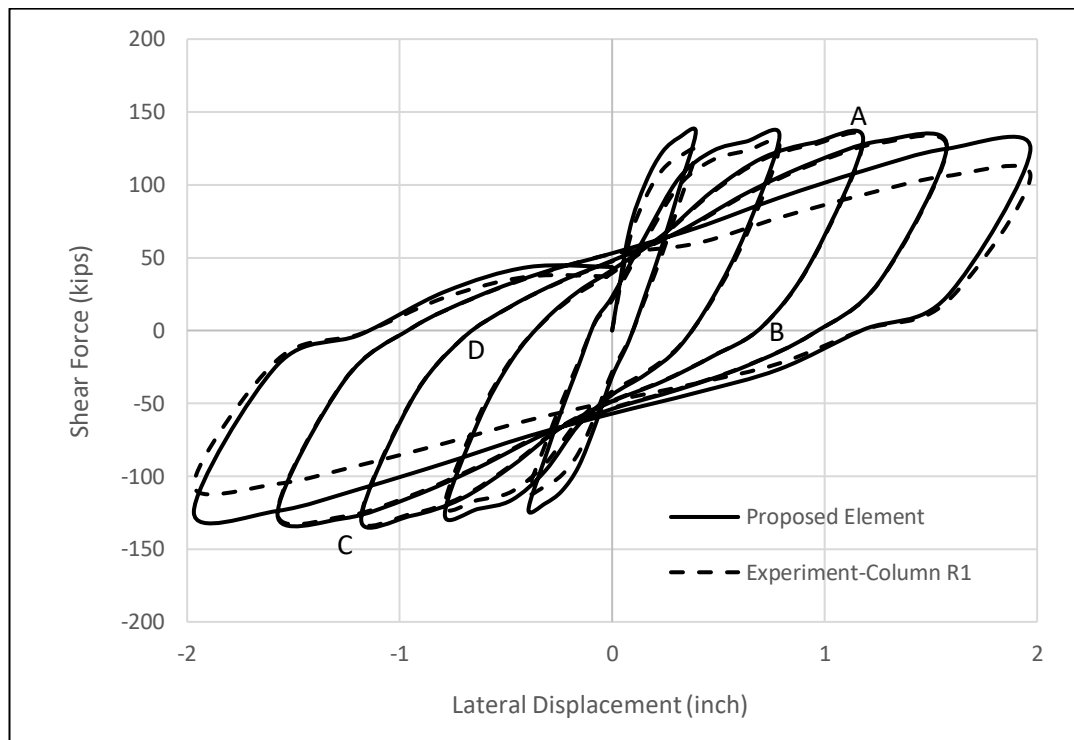


Figure 3-29. Lateral Load-Deflection Response of Column R1

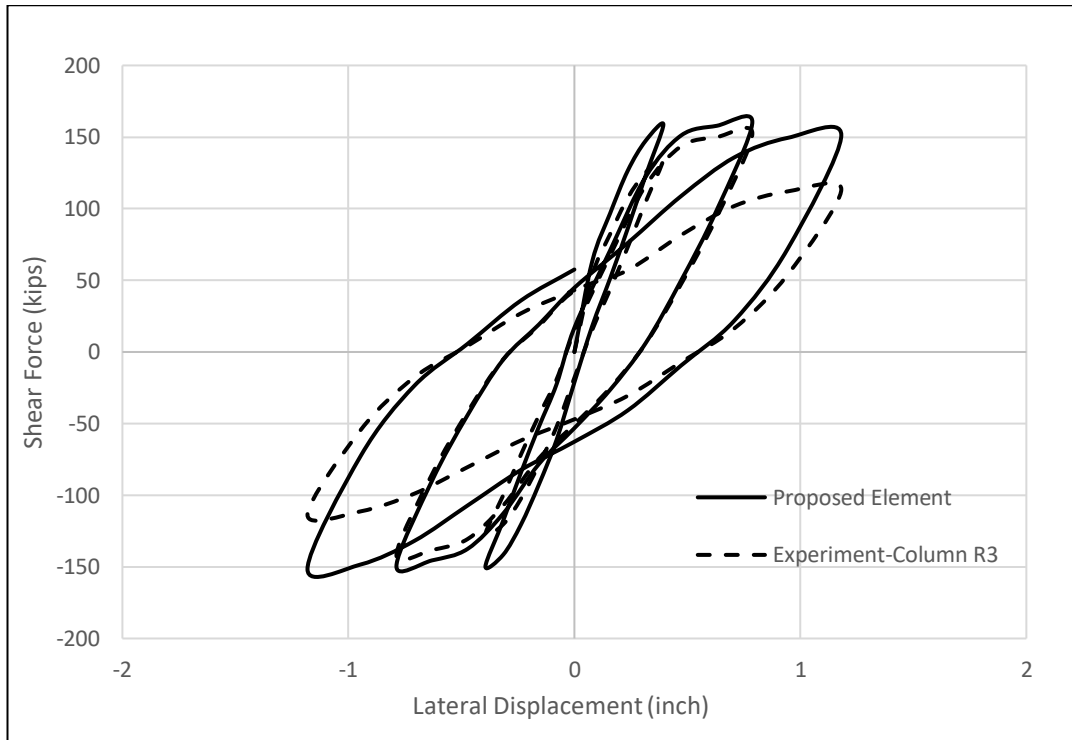


Figure 3-30. Lateral Load-Deflection Response of Column R3

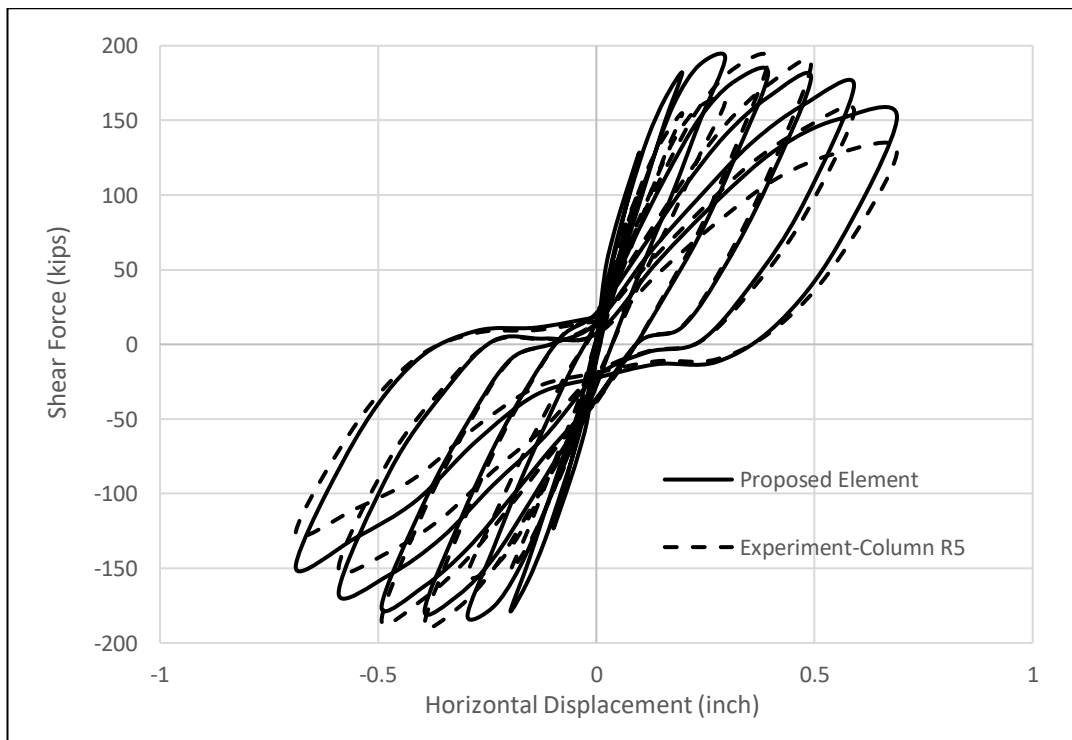


Figure 3-31. Lateral Load-Deflection Response of Column R5

From the above plots, it can be observed that the proposed element reasonably reproduces the overall experimentally observed load-deflection response. However, it has produced a stiffer response at the pre-peak shear strength. Whereas, hysteretic energy and shear deformation capacity have been captured reasonably well for columns R1 and R3, however some divergence in results can be observed for column R5. It is to be noted that the proposed element does not include large displacement effects, bar buckling and fracture, bond failure and spalling of cover concrete. These inelastic actions significantly influence energy dissipation characteristics and shear strength degradation.

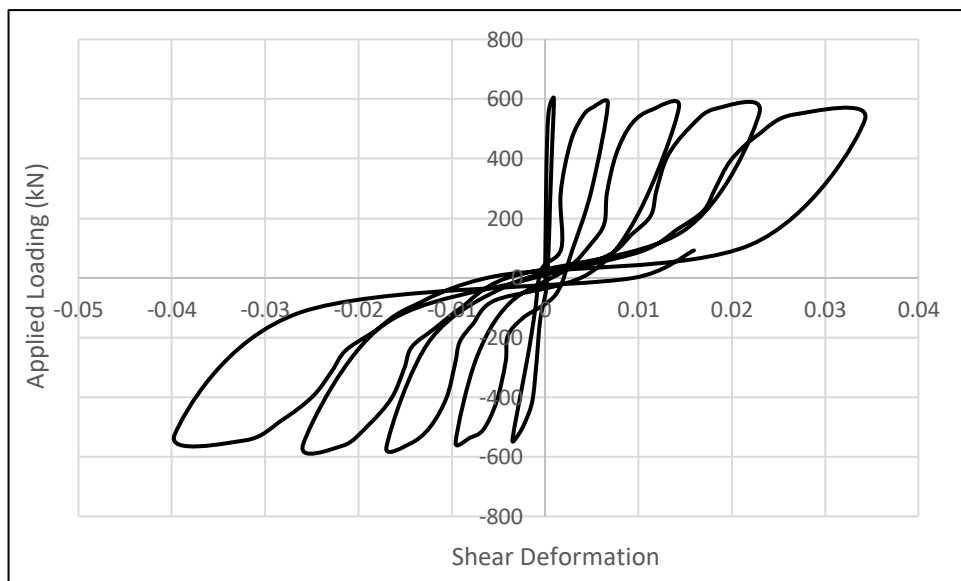


Figure 3-32. Lateral Load-Shear Deformation Response of Column R1

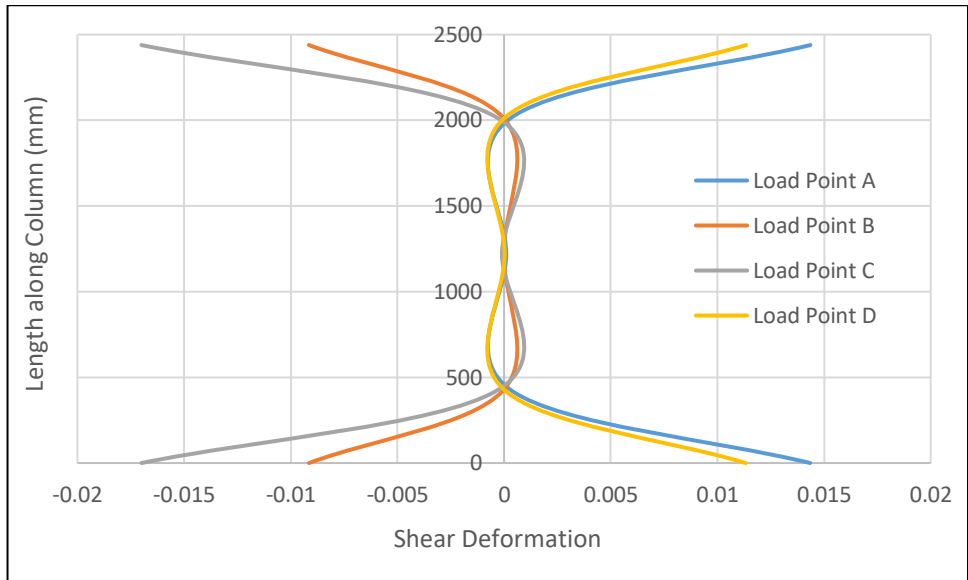


Figure 3-33. Variation of Shear Deformation along length of Column R1

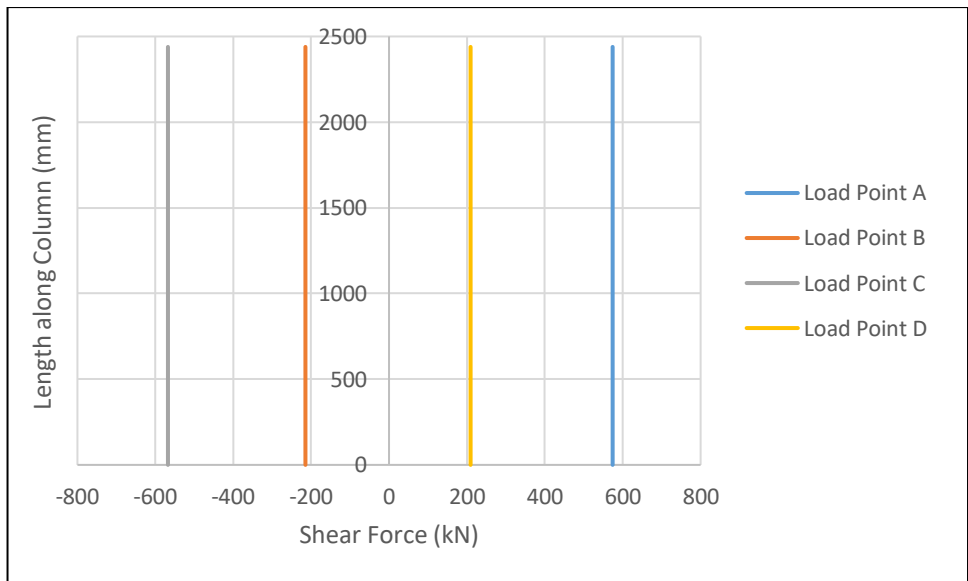


Figure 3-34. Variation of Shear Force along length of Column R1

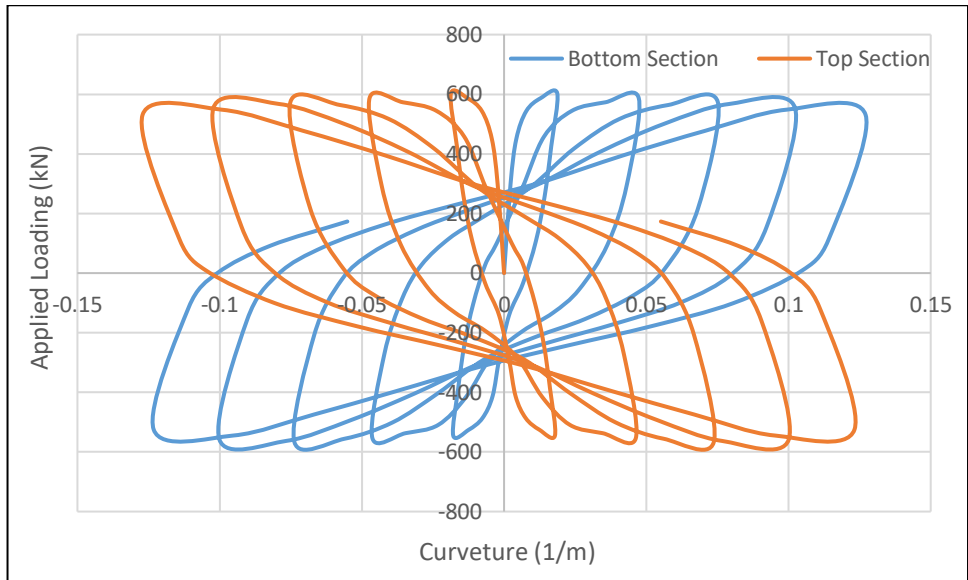


Figure 3-35. Lateral Load-Curvature Response of Column R1

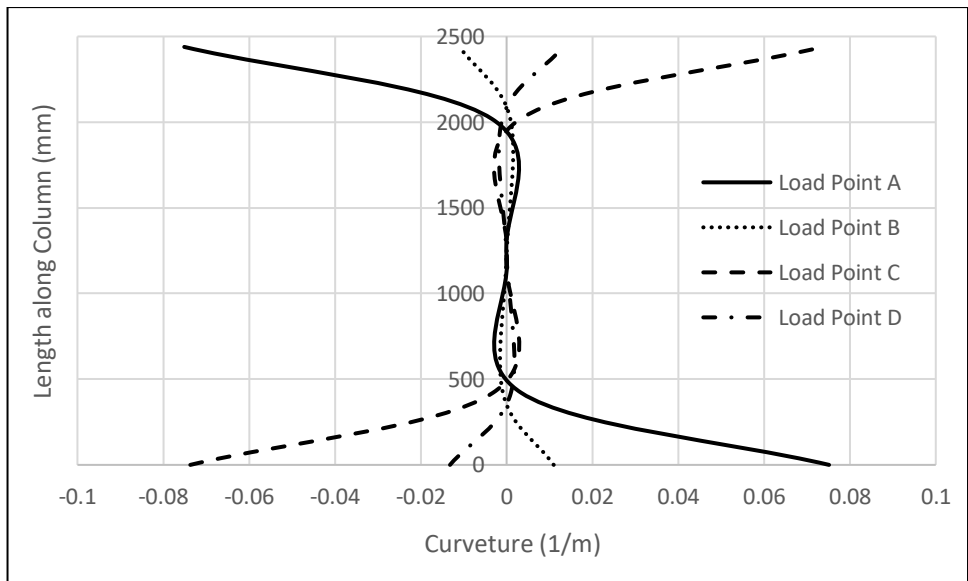


Figure 3-36. Variation of Curvature along length of Column R1

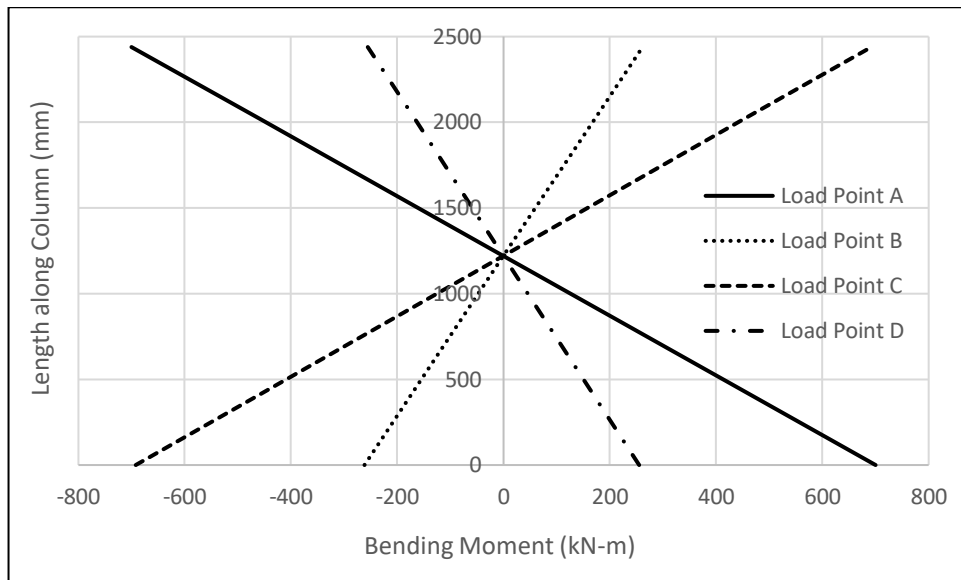


Figure 3-37. Variation of Bending Moment along length of Column R1

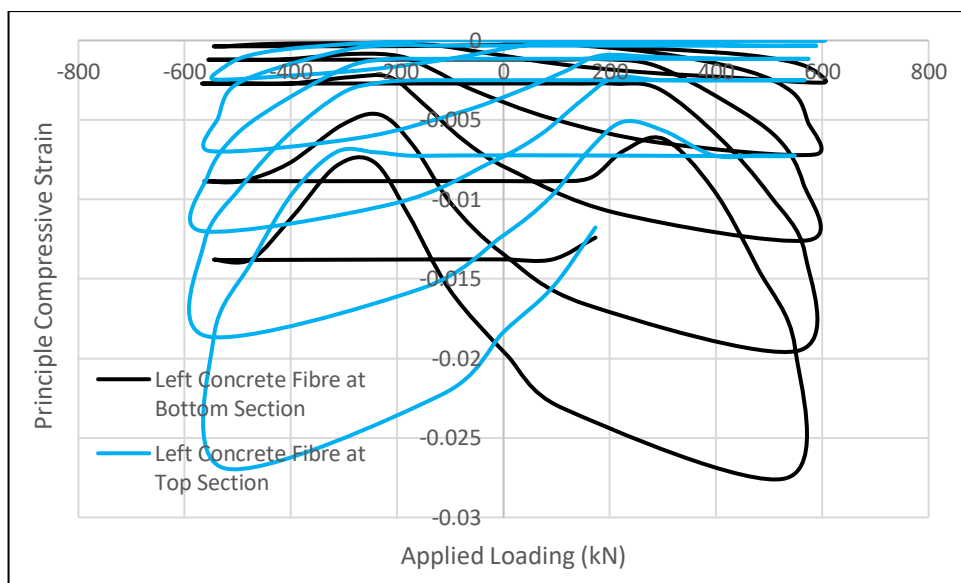


Figure 3-38. Principle Compressive Strain – Loading Response of concrete fibre of Column R1

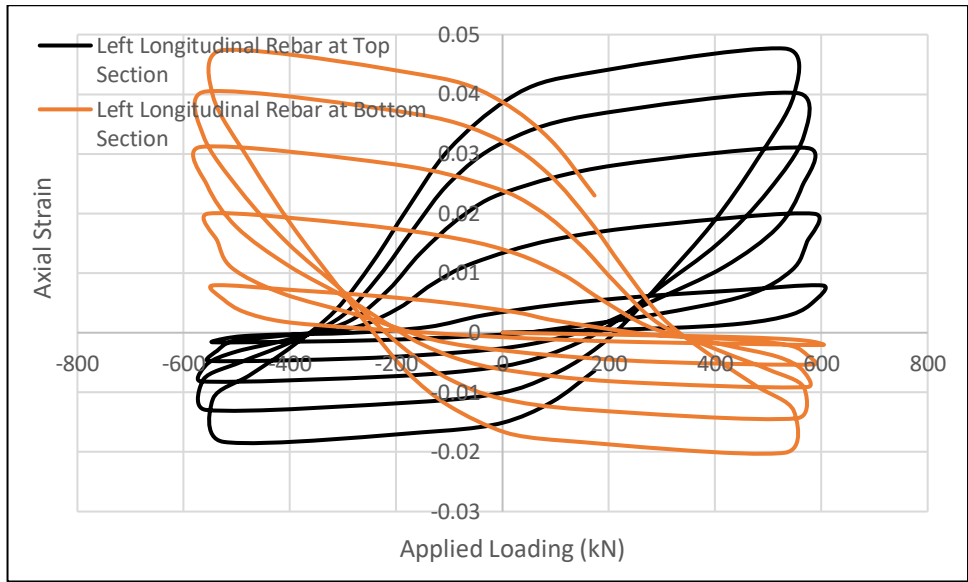


Figure 3-39. Axial Strain – Loading Response of longitudinal Rebar of Column R1

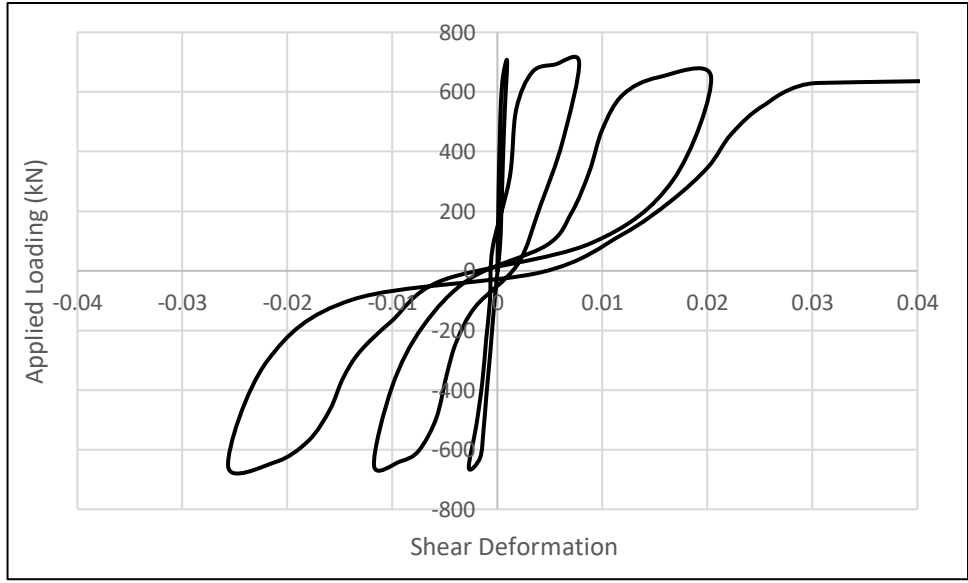


Figure 3-40. Lateral Load-Shear Deformation Response of Column R3

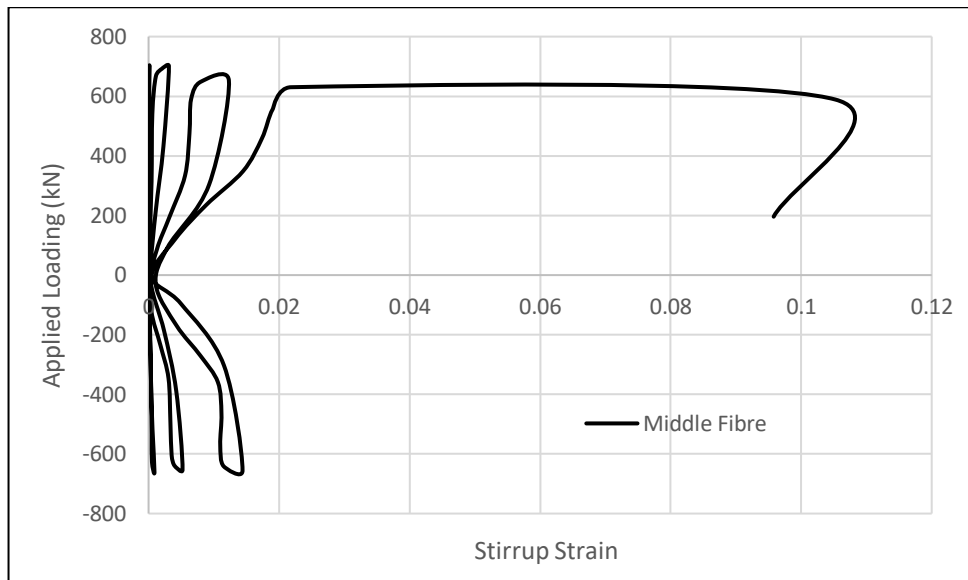


Figure 3-41. Loading-Axial Strain Response of Stirrup of Column R3 at Base Section

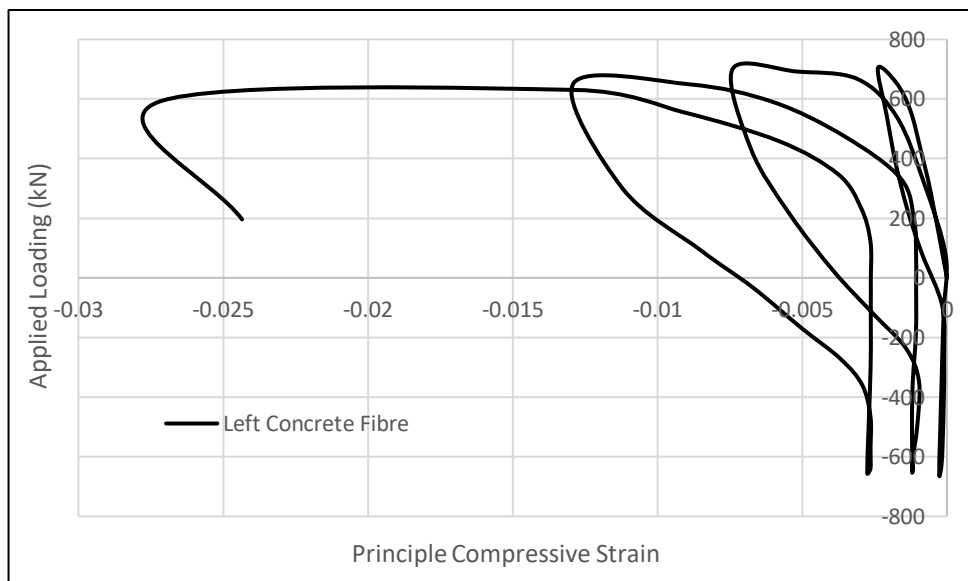


Figure 3-42. Loading-Principle Compressive Strain Response of Concrete Fibre of Column R3 at Base Section

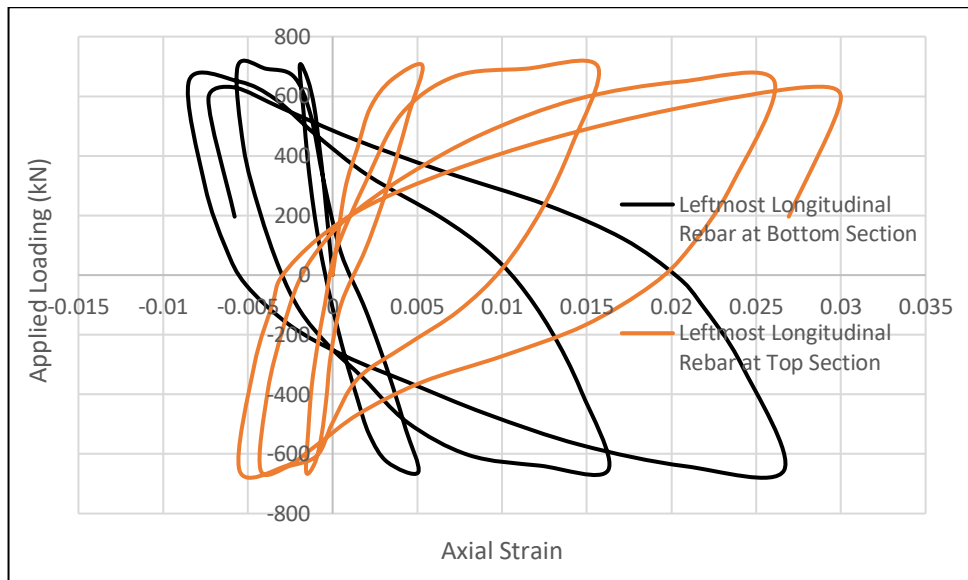


Figure 3-43. Loading-Axial Strain Response of longitudinal Rebar of Column R3

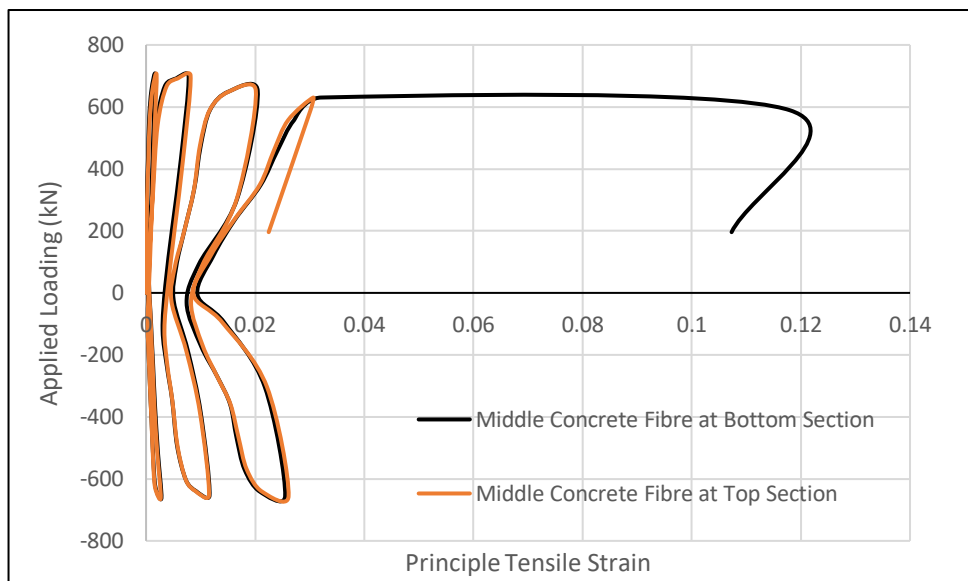


Figure 3-44. Loading-Principle Tensile Strain Response of Concrete Fibre of Column R3

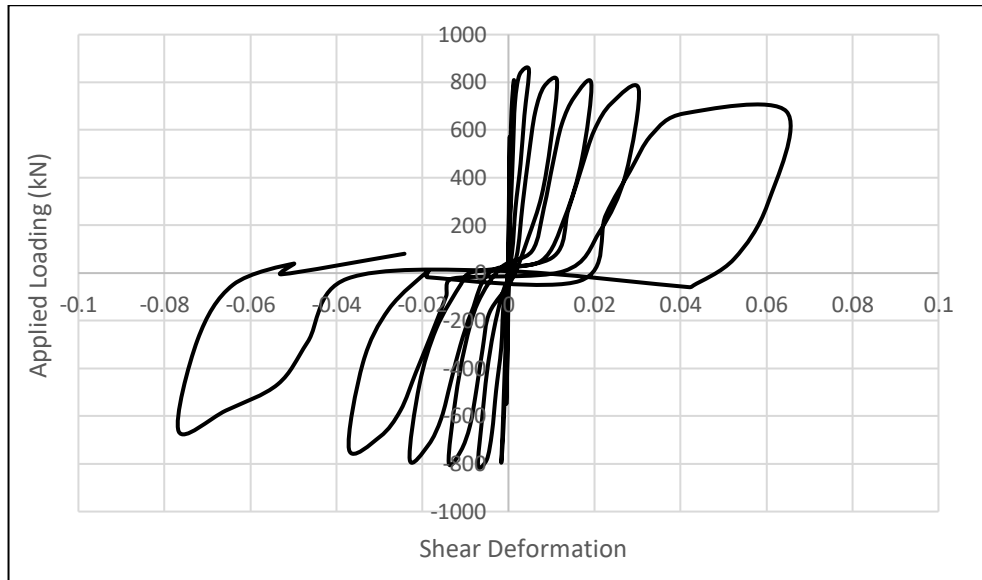


Figure 3-45. Lateral Load-Shear Deformation Response of Column R5

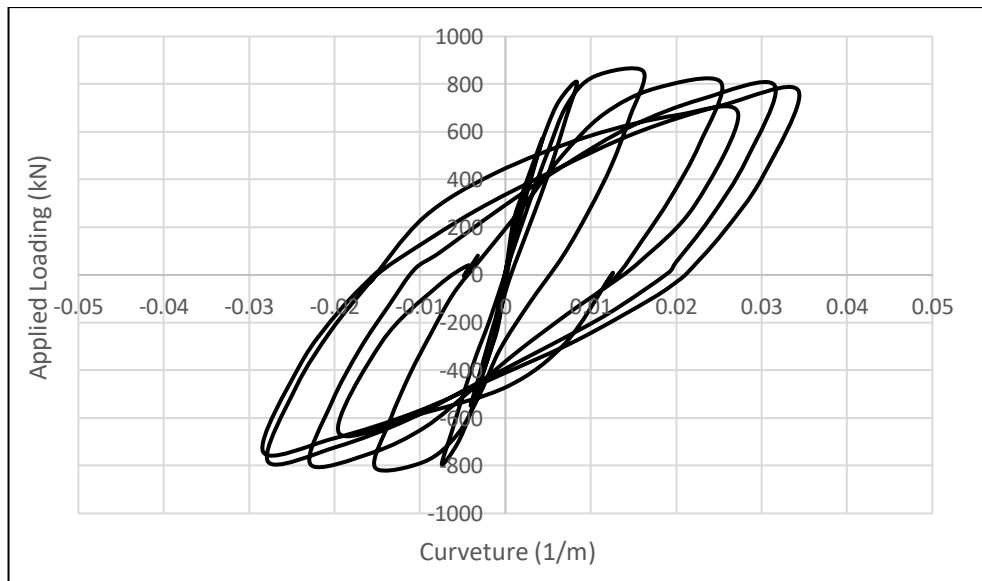


Figure 3-46. Lateral Load-Curvature Response of Column R5

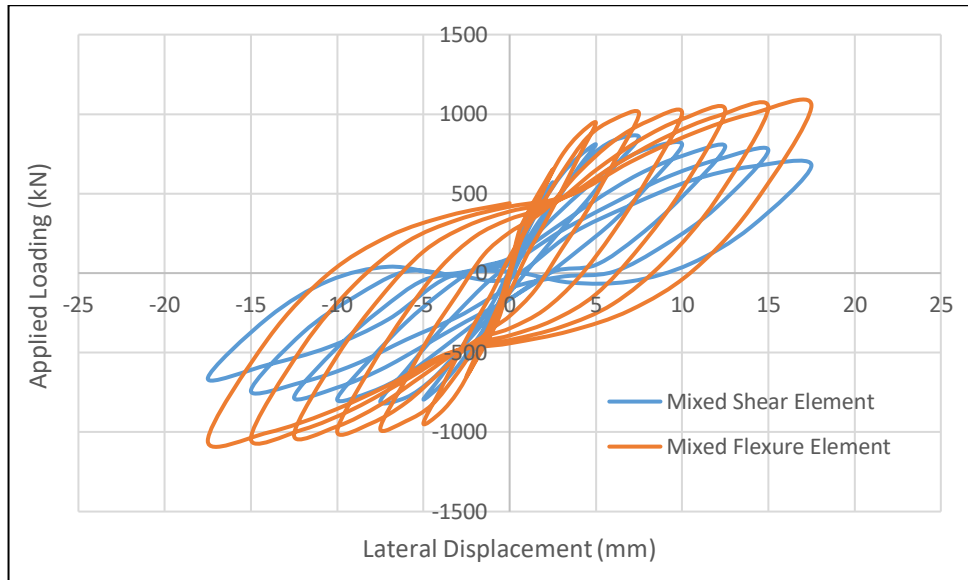


Figure 3-47. Lateral Load-Displacement Response of Column R5

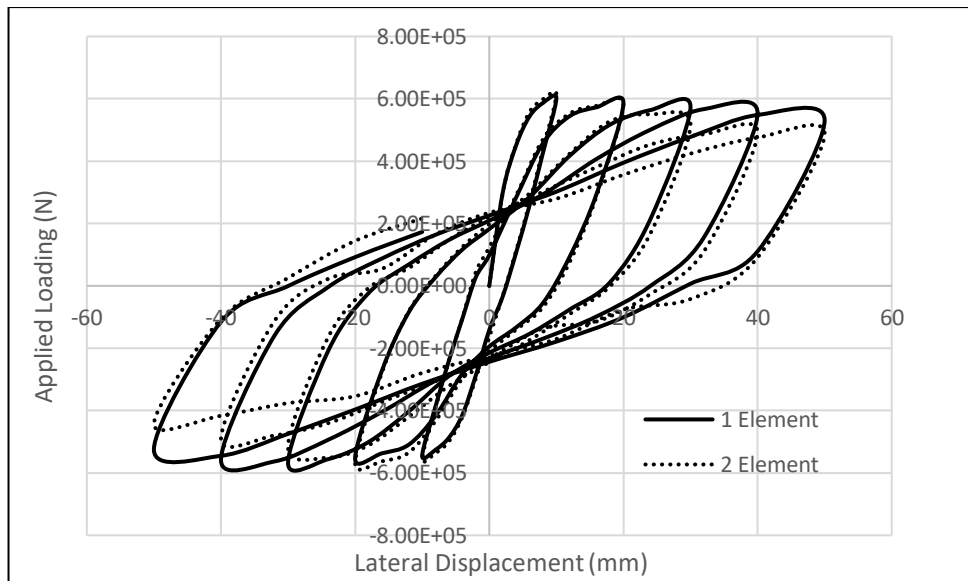


Figure 3-48. Effect of Number of Elements on Lateral Load-Displacement

Response of Column R1

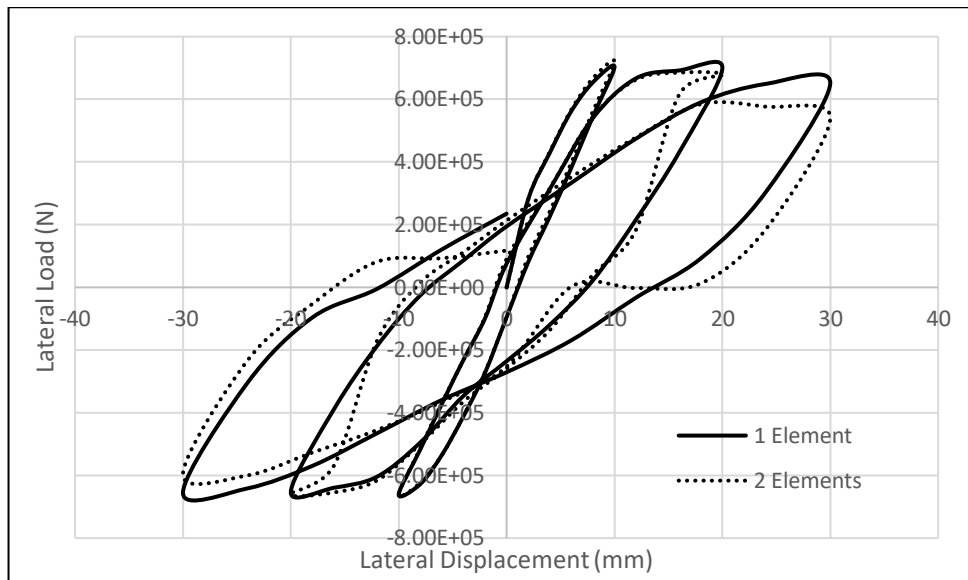


Figure 3-49. Effect of Number of Elements on Lateral Load-Displacement

### Response of Column R3

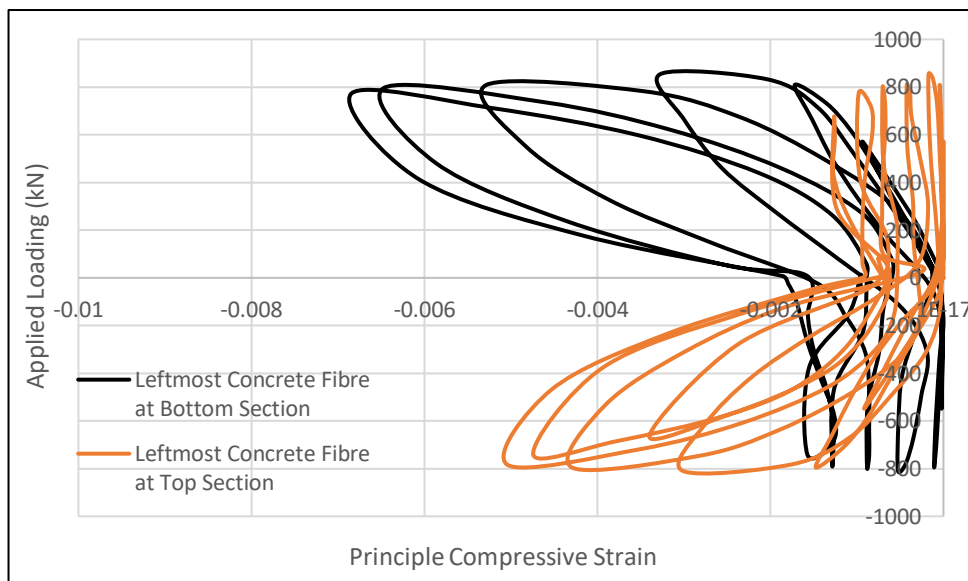


Figure 3-50. Loading-Principle Compressive Strain Response of Concrete

### Fibre of Column R5

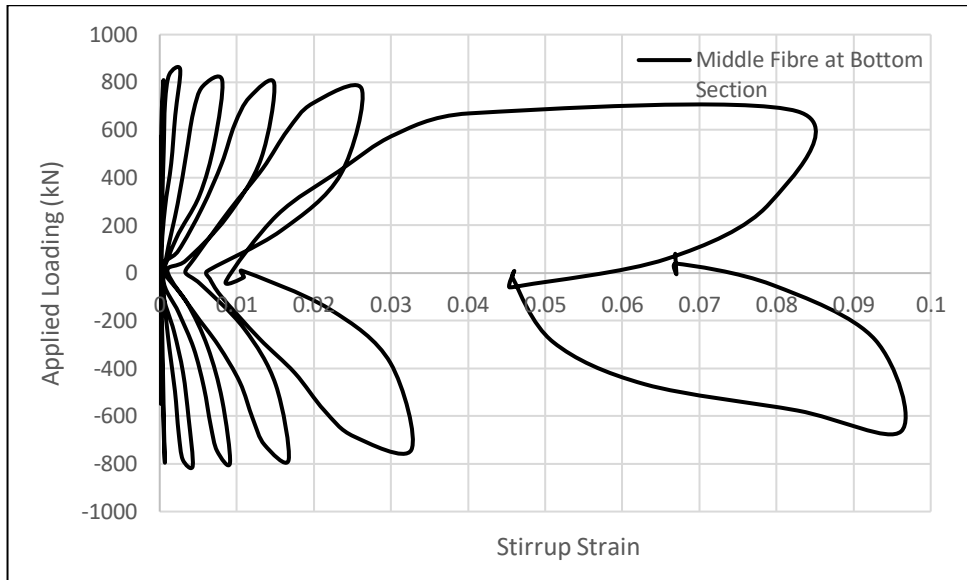


Figure 3-51. Loading-Axial Strain Response of Stirrup of Column R5 at Base Section

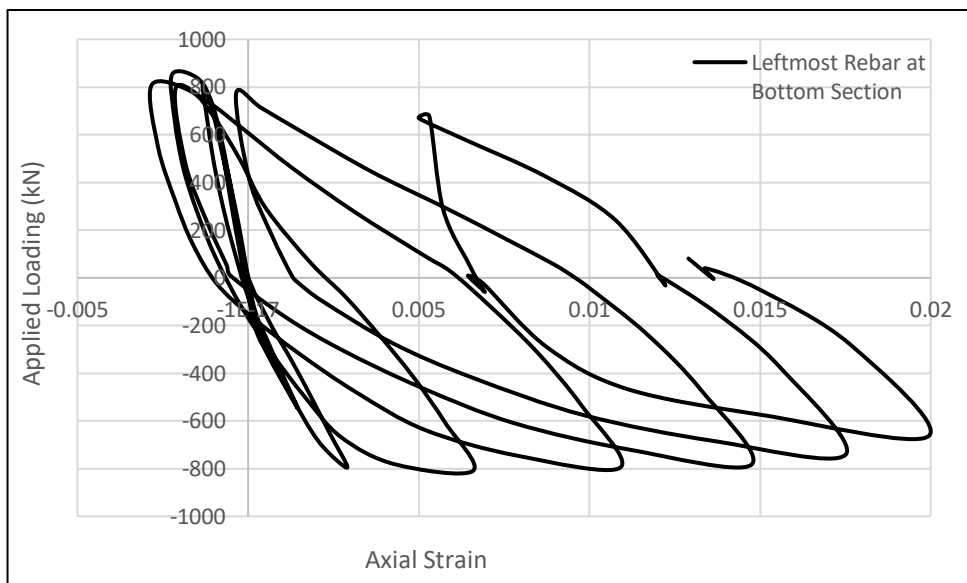


Figure 3-52. Loading-Axial Strain Response of longitudinal Rebar of Column R5

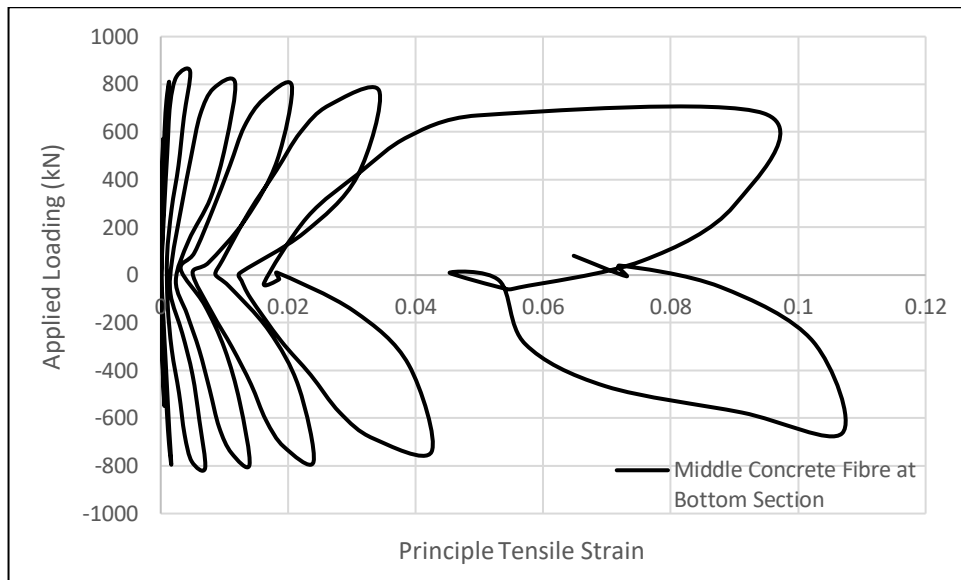


Figure 3-53. Loading-Principle Tensile Strain Response of Concrete Fibre of Column R5

Figures 3-32, 3-40, and 3-45 show the variation of shear deformation along the length of column R1, R3 and R5 respectively. It can be observed that there is almost no residual shear deformation for columns R1 and R3 while for R5 substantial amount of residual shear deformation presents. This gives an indication of pinching behaviour observed in R5 column and larger energy dissipation capacity for R1 and R3 columns. It can also be observed from Figure 3-33 that variation of shear deformation at the top and bottom of the column is nonlinear due to flexure-shear interaction. Figure 3-34 shows the expected constant variation of shear force along the length of the column while Figure 3-37 shows the linear variation of bending moment maximum at the top and bottom due to both ends fixed boundary condition. Figure 3-36 shows the nonlinear variation of curvature

at both ends due to flexure-shear interaction at different loading stages. Figure 3-35 and 3-46 show the load-curvature response of columns R1 and R5. It can be observed that at the later stage of loading curvature gets reduced for column R5 compared to that of R1. This is because of two reasons i.e. the first one is due to reduced moment capacity at the later stage of loading and the second reason is that flexural stiffness does not get reduced or gets ceased as shear deformation becomes fully prominent at the later stage of loading. This signifies that proposed mixed formulation is capable of reproducing flexure (R1) and shear (R5) failure from the section level information also.

Figure 3-47 shows the need of having mixed shear element. Mixed flexure element overestimates the shear capacity and stiffness. Figure 3-48 and 3-49 show the effect of number of elements on load-deflection response. It can be observed that larger number of elements produce lesser shear capacity at the later stage of loading. Future work is needed to fix the issue of mesh objectivity.

From Figures 3-32 and 3-42 show the principle compressive strain in the leftmost concrete fibre for columns R1 and R3. It can be observed that for both columns compressive strain reaches substantial amount at the later stage of loading which indicates huge loss of compressive strength. Also

from Figure 3-33 the axial strain in vertical reinforcement also reaches substantial amount which indicates that the failure in column R1 governs by the flexural mode. However, for column R3 stirrup strain (Figure 3-41) and tensile strain (Figure 3-44) in middle concrete fibre reaches substantial amount at the later stage of loading indicates the behaviour of column R3 gets dominated by the shear failure mode. However, unlike columns R1 and R3, for column R5 the principle compressive strain (Figure 3-50) in the leftmost concrete fibre is substantially less while stirrup strain (Figure 3-51) and tensile strain (Figure 3-53) in the middle concrete fibre are huge which indicates that the failure mode gets controlled by shear from the early stage of loading. As a result, expected pinching behaviour is predominant for R5 due to incremental loss of shear stiffness from the early stage of loading. This shear controlled phenomenon for column R5 from the initial stage loading can also be supported from Figure 3-52 that under positive loading excursion the leftmost vertical rebar reaches lesser amount of compressive strain compared to its counterparts R1 (Figure 3-39) and R3 (Figure 3-43). Largest compressive strain (Figure 3-39) in left vertical rebar should occur for R1 as its failure is governed by flexure mode. For R3, failure mode is governed by flexure-shear which will induce lesser amount of compressive strain (Figure 3-43) in the leftmost vertical rebar. Also, after few cycles of loading, leftmost rebar remains in tensile strain zone even under constant compressive loading which signifies that the unloading

of compressive strain in the rebar happens to satisfy the equilibrium, which is a typical phenomenon for failure almost completely dominated by the shear deformation.

### **3.3.2 Column by Arakawa, Arai and Mizoguchi (1989)**

Arakawa et al. (1989) performed cyclic tests of reinforced concrete columns under constant axial compressive loading of 476 kN with increasing amplitude of lateral displacement cycles at the columns top end. The specimen OA5 failed in a shear mode. The specimen has width and depth both of 180 mm and length of 225 mm. 8 longitudinal reinforcements of diameter 12.7 mm are uniformly spaced along the perimeter of the columns. Square hoops of diameter 4 mm are placed at a spacing of 64.3 mm along the length of the columns. The concrete compressive strength of the column is 33 MPa. Yield strengths of longitudinal and transverse reinforcements are 340 MPa and 249 MPa respectively.

One element has been used to model the entire column specimen with 5 section integration points. Figure 3-54 compares the lateral load versus top end deflection response of the models using the proposed beam element with the experimental results. It can be observed from the plot that the proposed element can capture the loading capacity and pinching effect of hysteretic behaviour reasonably well.

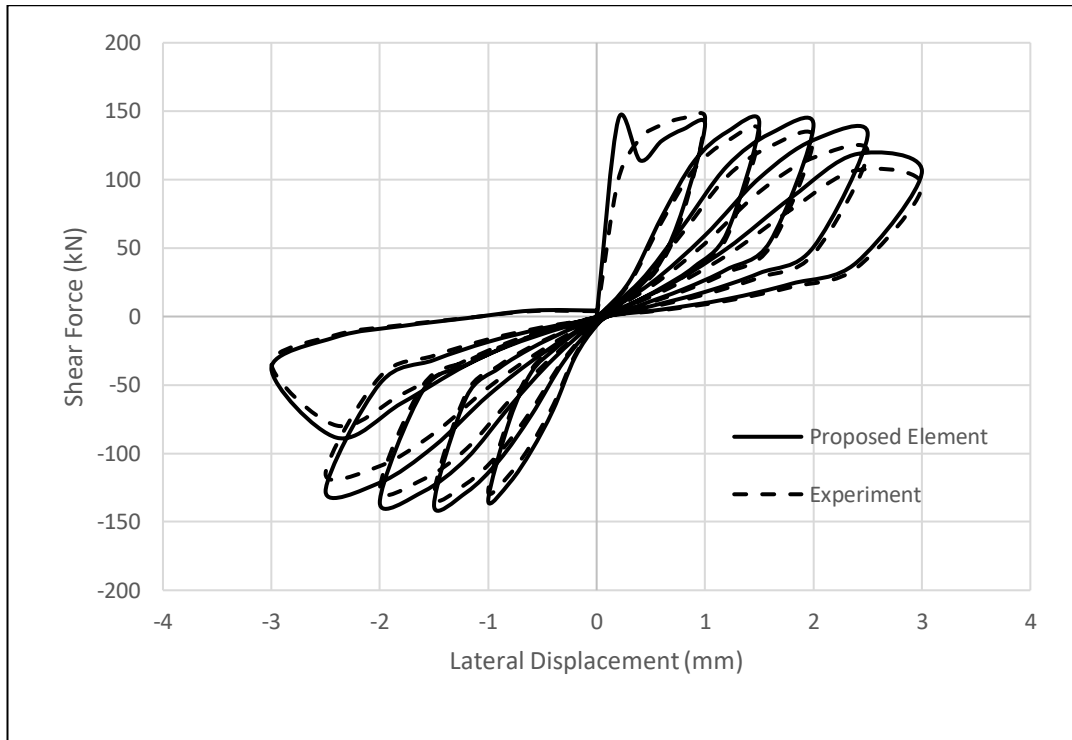


Figure 3-54. Lateral Load-Deflection Response of column OA5

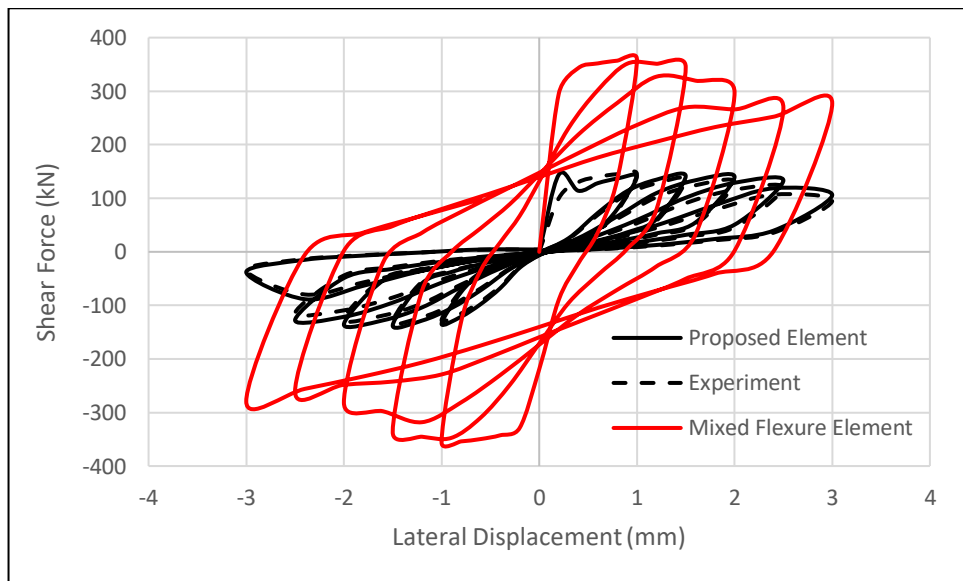


Figure 3-55. Lateral Load-Deflection Response of column OA5 comparing with mixed flexure element

It can be observed from Figure 3-55 that the mixed flexure element overestimates the shear capacity and stiffness both. As a result, we need to

have mixed shear element which can reasonably reproduce experimentally observed load deformation response for shear critical members.

### **3.3.3 Column by Imai and Yamamoto (1986)**

Imai et al. (1986) conducted cyclic test of reinforced concrete columns under constant axial compressive loading of 392 kN with increasing amplitude of lateral displacement cycles at the columns top end. The specimen has width and depth of 400 mm and 500 mm respectively. 14 longitudinal reinforcements of diameter 22 mm are uniformly spaced along the perimeter of the columns. Rectangular hoops of diameter 9 mm are placed at a spacing of 100 mm along the length of the columns. The concrete compressive strength of the column is 27.1 MPa. Yield strengths of longitudinal and transverse reinforcements are 318 MPa and 336 MPa respectively.

One element has been used to model the entire column specimen with 5 section integration points. Figure 3-56 compares the lateral load versus top end deflection response of the models using the proposed beam element with the experimental results. It can be observed from the plot that the proposed element can capture the loading capacity and pinching effect of hysteretic behaviour reasonably well. However, some divergence in results can be observed in the last loading cycle as the shear resisting mechanisms invoked during this loading stage has not been included in the element model.

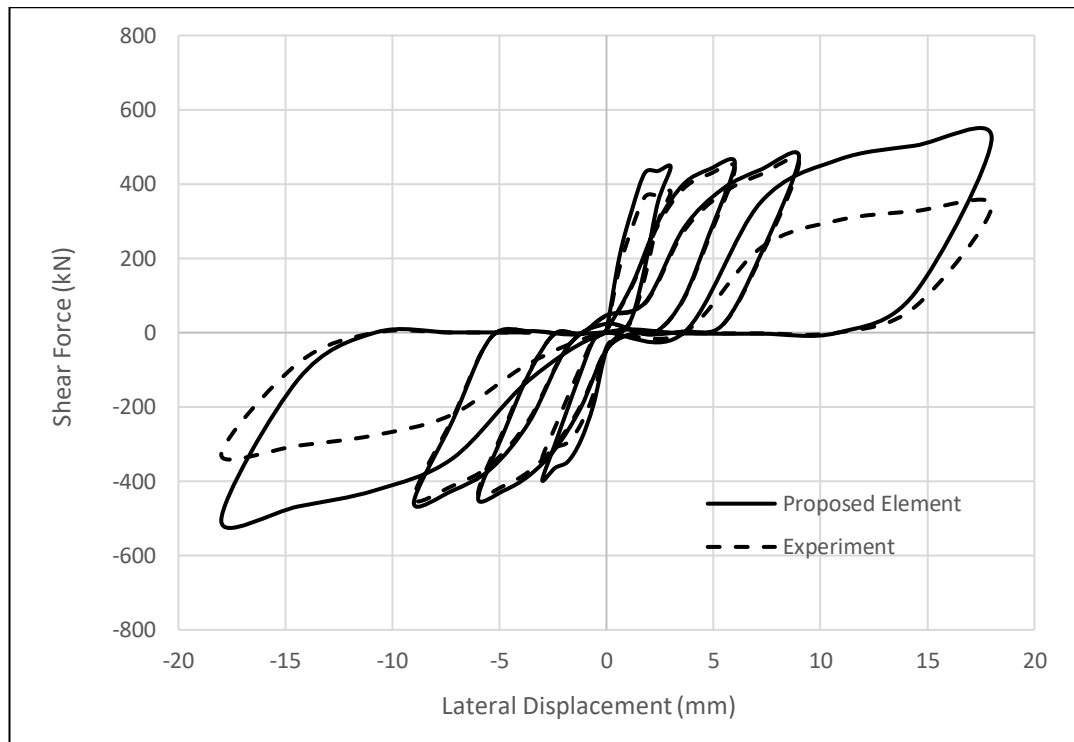


Figure 3-56. Lateral Load-Deflection Response

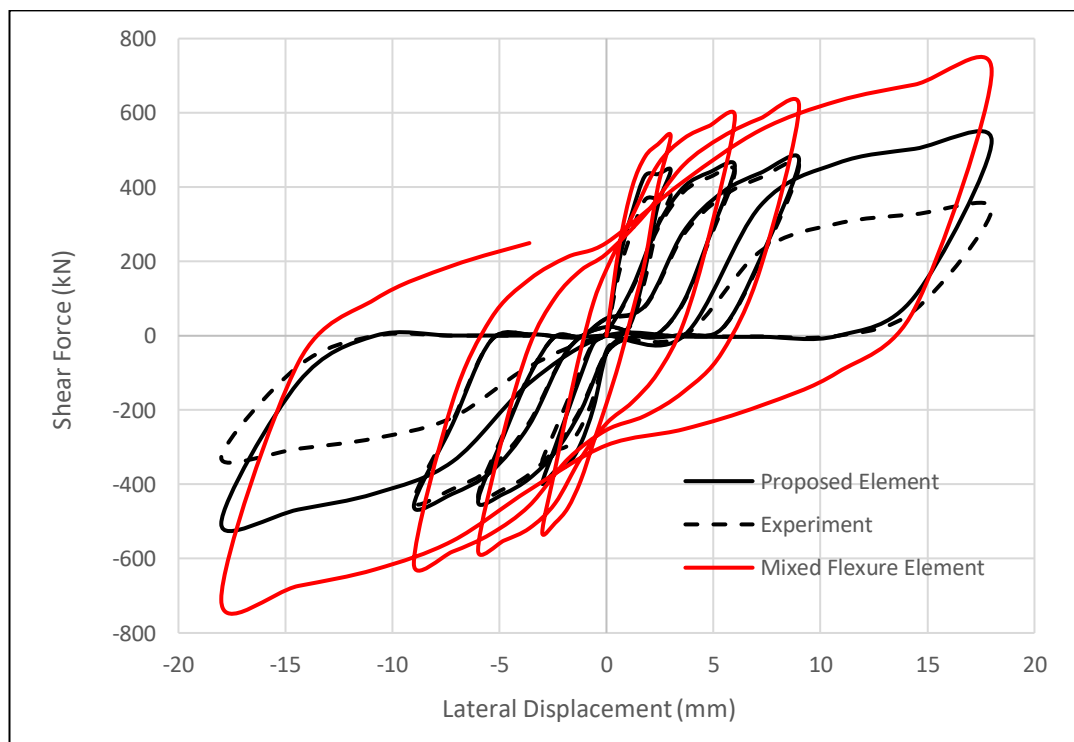


Figure 3-57. Lateral Load-Deflection Response comparing with mixed flexure element

It can be observed from Figure 3-57 that we need to have mixed shear element which can reasonably reproduce experimentally observed load deformation response for shear critical members, while the mixed flexure element overestimates the shear capacity and stiffness both.

## **3.4 RC Shear Walls**

### **3.4.1 Walls by Lefas, Kotsovos and Ambraseys (1990)**

Lefas et al. (1990) performed tests on a series of thirteen reinforced concrete walls with increasing amplitude of lateral displacement monotonically at the walls top end to investigate the effect of several parameters such as height to width ratio, the axial load, the concrete strength and the amount of web horizontal reinforcement on shear resisting mechanisms of RC rectangular walls. The walls were fixed at the bottom end and the lateral loading displaced the walls in a single bending curvature mode. Out of these specimens, two specimens SW21 and SW22 (Figure 3-58) are chosen for correlation studies. Specimens SW21 and SW22 have shear span to depth ratio ( $1300/650=$ ) 2. The thickness of the walls is 65 mm.

The vertical and horizontal reinforcement comprised high-tensile deformed steel bars of 8 mm and 6.25 mm diameter with yield strengths of 470 MPa and 520 MPa respectively. Wall boundary zones are confined with stirrups

of 4 mm mild steel bars with yield strength of 420 MPa. The spacing of horizontal and vertical rebar's are 115 mm and 62 mm respectively. Concrete compressive strengths of walls SW21 and SW22 are 42.8 MPa and 50.6 MPa respectively. Wall SW21 was subjected to lateral load only whereas wall SW22 was subjected to constant axial compressive load of 182 kN with a lateral load monotonically increasing to failure.

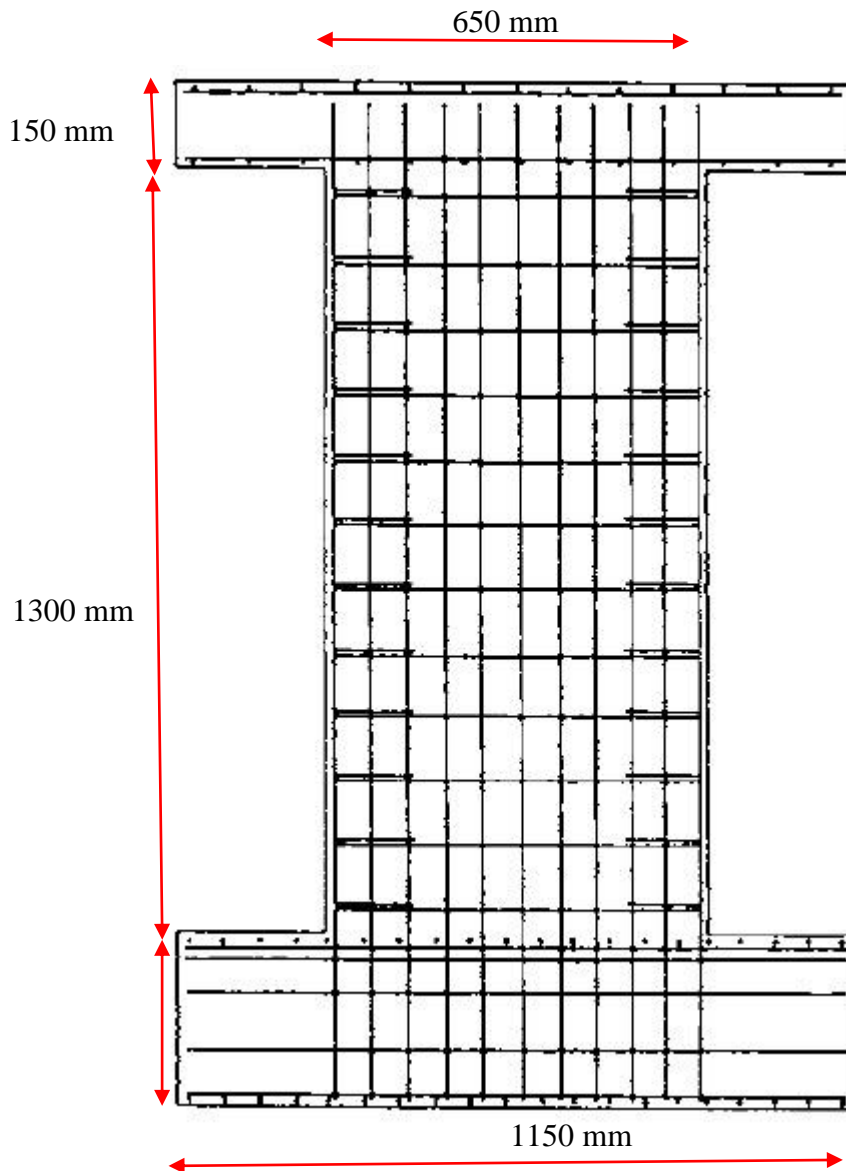


Figure 3-58. Geometry of RC Walls SW21 and SW22

One element has been used to model the entire wall specimen with 5 section integration points. Figures 3-59 and 3-60 compare the lateral load versus top end deflection response of the models using the proposed beam element with the experimental results of walls SW21 and SW22 respectively. The effect of number of elements on load-deflection response has been also reported.

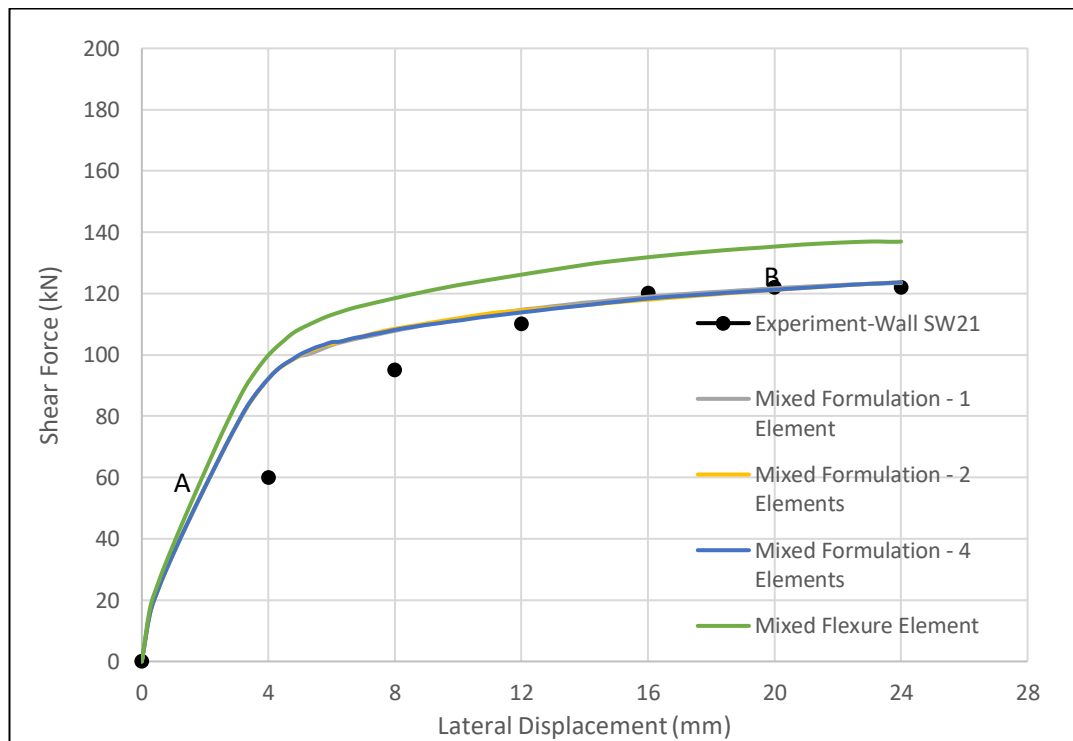


Figure 3-59. Lateral Load-Deflection Response of Wall SW21

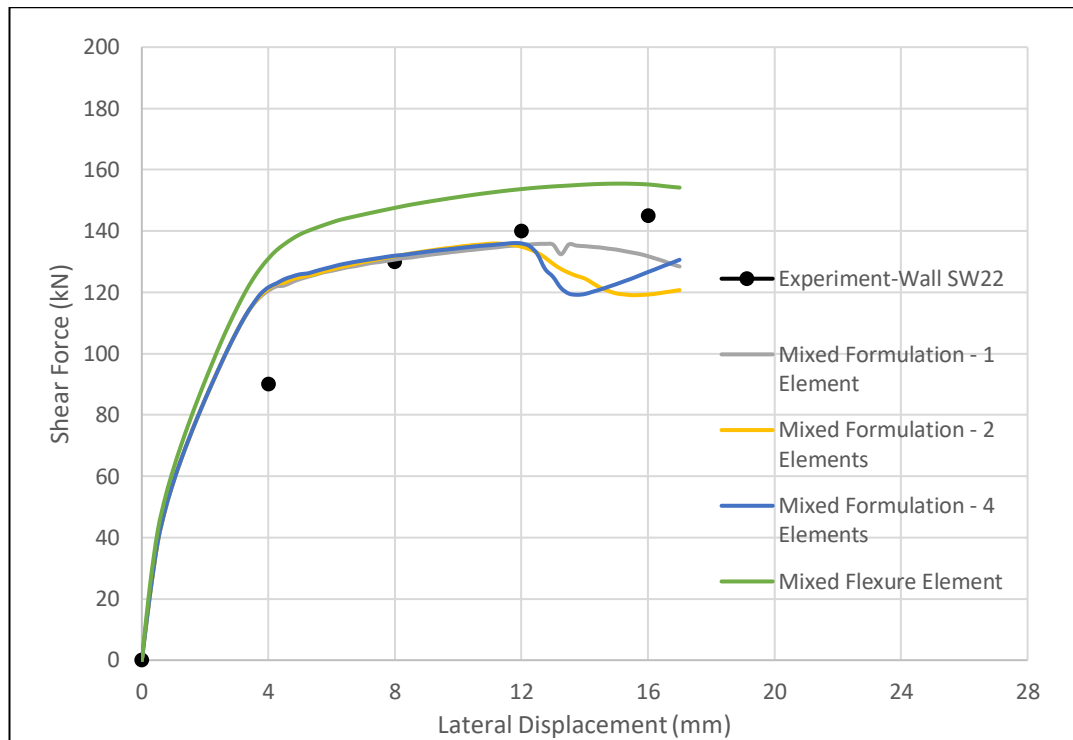


Figure 3-60. Lateral Load-Deflection Response of Wall SW22

From the above plots, it can be observed that the proposed element reasonably reproduce the overall experimentally observed load-deflection response. Pre-peak stiffness has been overestimated. Shear deformation capacity have been captured well. However, it has produced a softer shear strength response slightly. It is to be noted that the axial compressive load has increased the shear resisting capacity with the decrement of shear deformation capacity. It is also to be noted that for wall SW21, number of elements does not affect the load-deflection response in the entire loading duration. However, for wall SW22, the number of elements has affected the response after peak region. This aspect of mesh objectivity shall be investigated in future in more details. It is also to be seen that mixed

flexure element produce higher shear capacity than that of observed in experiments as expected.

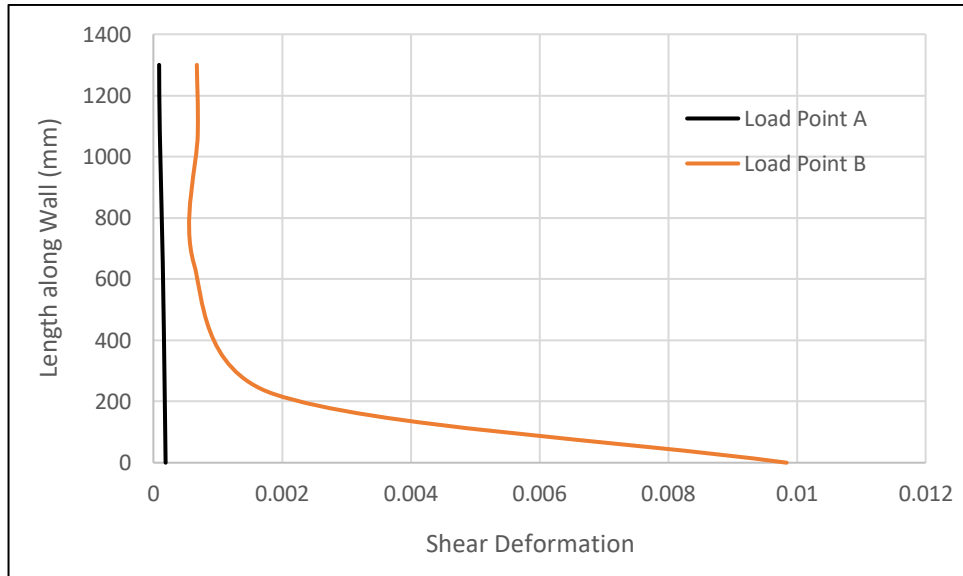


Figure 3-61. Variation of Shear Deformation along length of Wall SW21

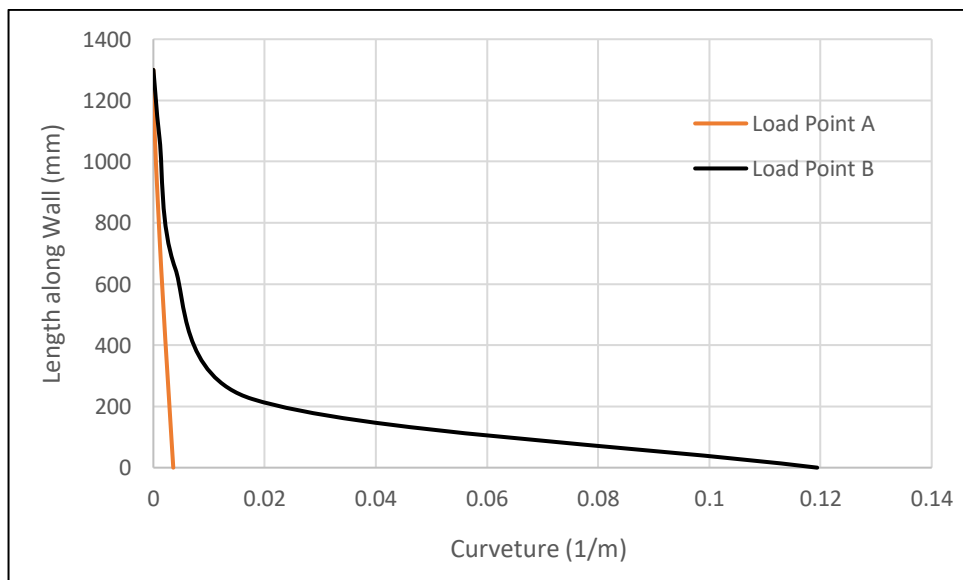


Figure 3-62. Variation of Curvature along length of Wall SW21

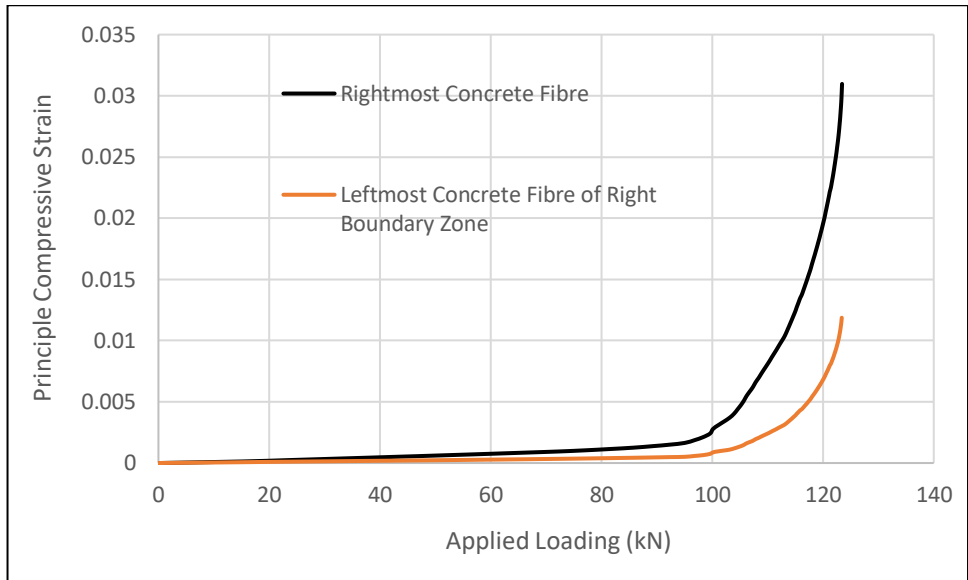


Figure 3-63. Principle Compressive Strain – Loading Response of Concrete Fibre of Wall SW21

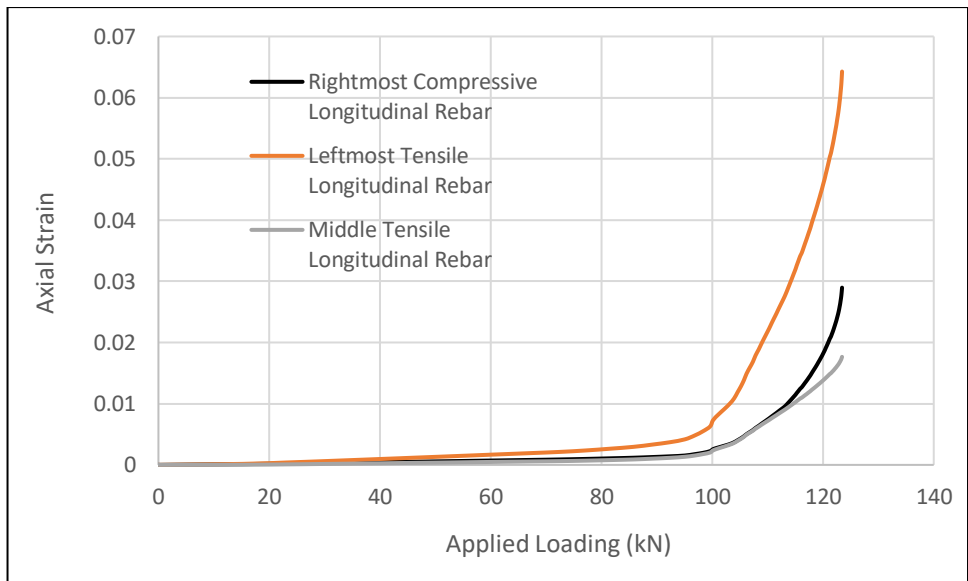


Figure 3-64. Axial Strain – Loading Response of Rebar Fibre of Wall SW21

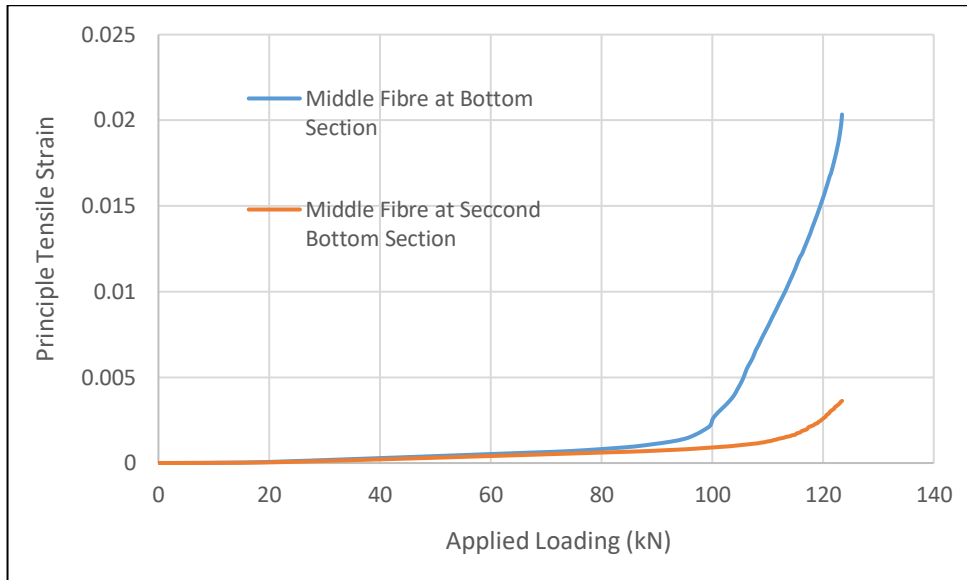


Figure 3-65. Principle Tensile Strain – Loading Response of Concrete Fibre of Wall SW21

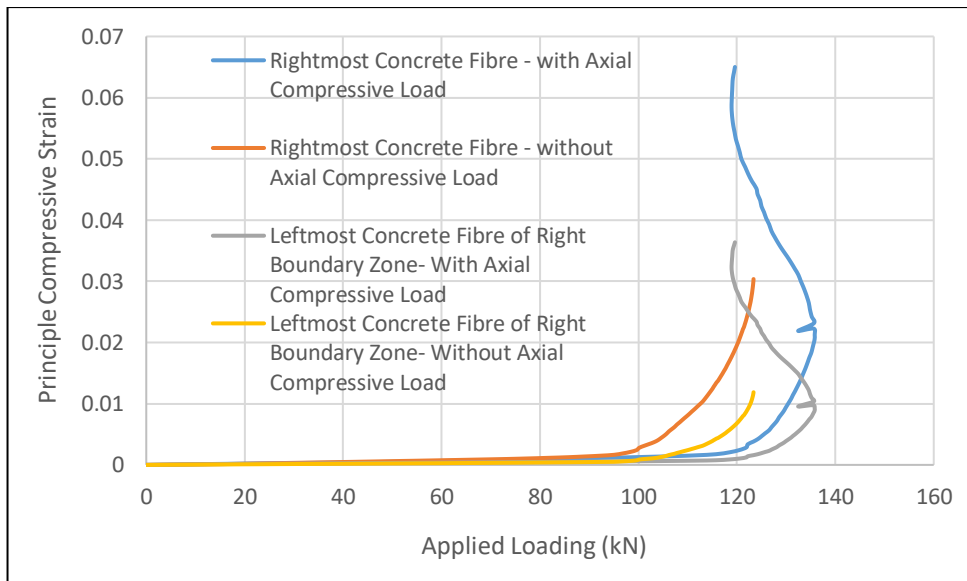


Figure 3-66. Principle Compressive Strain – Loading Response of Concrete Fibre of Wall SW22

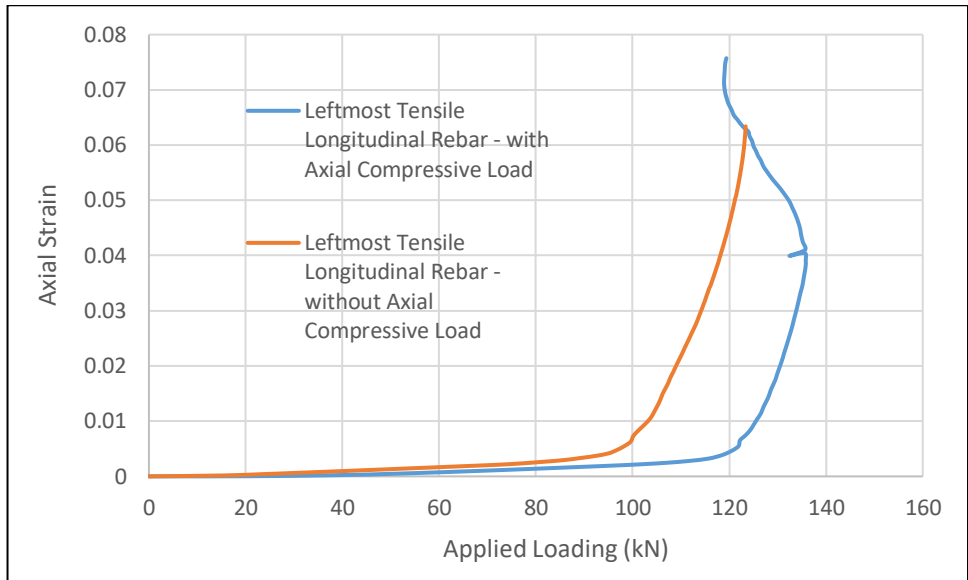


Figure 3-67. Axial Strain – Loading Response of Rebar Fibre of Wall

SW22

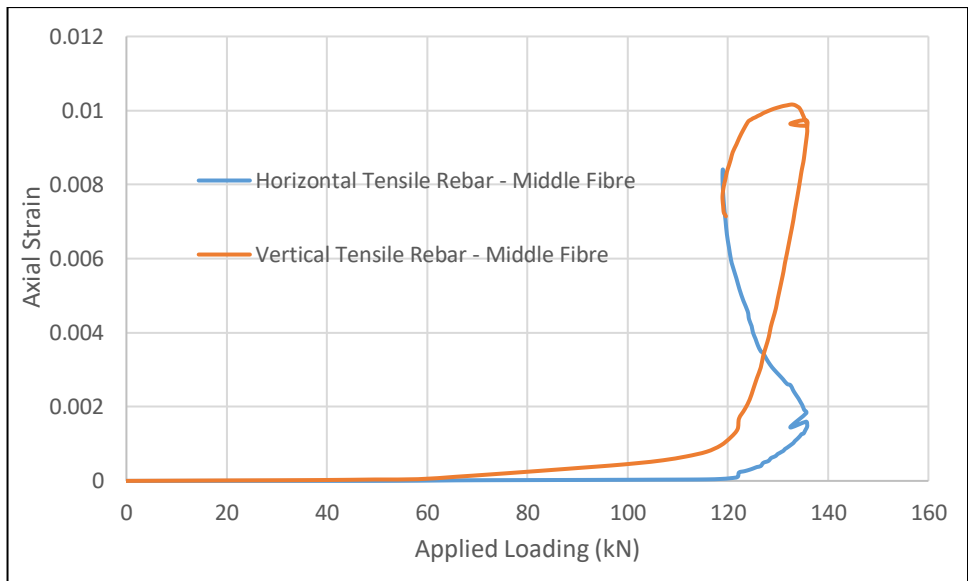


Figure 3-68. Axial Strain – Loading Response of Rebar of Wall SW22

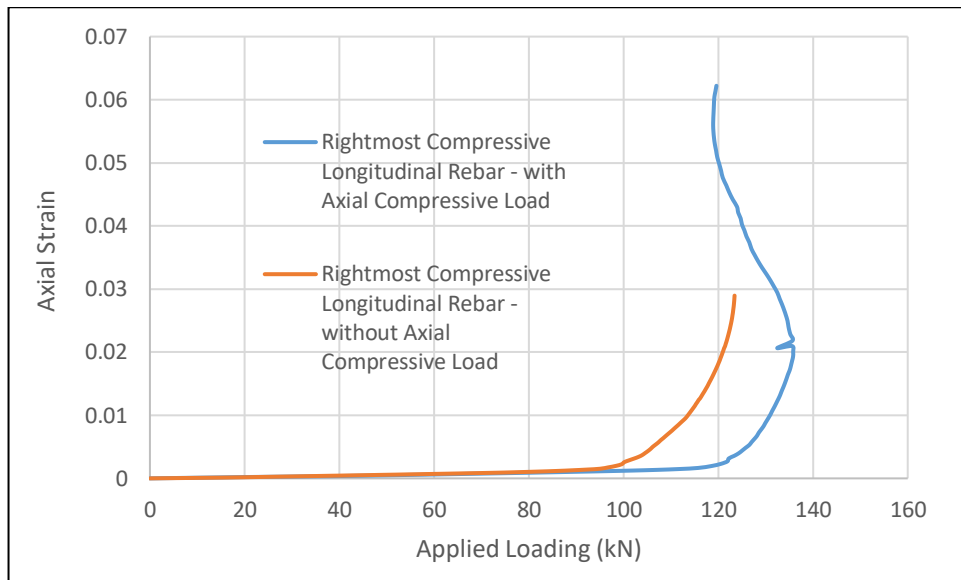


Figure 3-69. Axial Strain – Loading Response of Rebar Comparison between the walls

Figures 3-61 and 3-62 show the variation of shear deformation and curvature along the height of the wall SW21. It can be observed that both section deformations are nonlinear at the bottom section due to shear flexure-interaction as expected.

From the Figures 3-63 and 3-66, it can be observed that concrete fibres have reached substantial amount of compressive strain. However, for axial compressive loading on wall SW22, the compressive strain is more in the concrete fibres than that of wall SW21. From Figures 3-64, 3-67 and 3-69, it can be observed that the rebar strains in extreme left and right direction has reached substantial amount. However, from Figures 3-65 it can be observed that tensile strain in middle concrete fibres reaches substantial

amount of strain which indicates flexure-shear interaction for wall SW21. Also, from Figure 3-68, it can be seen that middle vertical rebar unloads the strain while the horizontal web rebar reaches substantial amount of tensile strain, which also indicates the flexure-shear interaction for wall SW22. It can be concluded that axial compressive loading has helped to initiate early shear mechanism in wall SW22 compared to that of wall SW21.

### **3.4.2 Walls by Tran and Wallace (2015)**

Tran et al. (2015) performed tests on a series of five large-scale cantilever reinforced concrete walls under constant axial compressive load and reversed cyclic lateral loading to investigate the effect of different variables such as wall aspect ratio, axial stress and shear stress on the nonlinear cyclic response of moderate aspect ratio (1.5 to 2.5) reinforced concrete structural walls such as wall deformation capacity and failure modes. Primarily three failure modes have been observed i.e. diagonal tension, web crushing and buckling of boundary vertical reinforcement. Out of these specimens, two specimens RW-A15-P10-S78 and RW-A15-P2.5-S64 are chosen for correlation studies. These specimens have shear span to depth ratio ( $1830/1220=$ ) 1.5. The thickness of the walls is 150 mm.

Both the vertical and horizontal reinforcement comprised steel bars of 9.5 mm with yield strength of 443 MPa in the web region of both walls. The spacing of both horizontal and vertical rebars are 127 mm and 152 mm for walls RW-A15-P10-S78 and RW-A15-P2.5-S64 respectively. In the boundary zones, two types of vertical rebars are used i.e. 4 rebars of diameters of 15.9 mm with yield strength of 474 MPa and 4 rebars of diameters of 19.1 mm with yield strength of 477 MPa for both walls. Boundary zones are confined with stirrups of 6.4 mm steel bars with yield strength of 423 MPa with a spacing of 50 mm along the height of both wall specimens. Concrete compressive strengths of walls RW-A15-P10-S78 and RW-A15-P2.5-S64 are 55.8 MPa and 57.5 MPa respectively. Constant axial compressive loads of 663.2 kN and 170.6 kN are used for walls RW-A15-P10-S78 and RW-A15-P2.5-S64 respectively.

One element has been used to model the entire wall specimen with 5 section integration points. Figures 3-70 and 3-71 compare the lateral load versus top end deflection response of the models using the proposed beam element with the experimental results of walls RW-A15-P10-S78 and RW-A15-P2.5-S64 respectively.

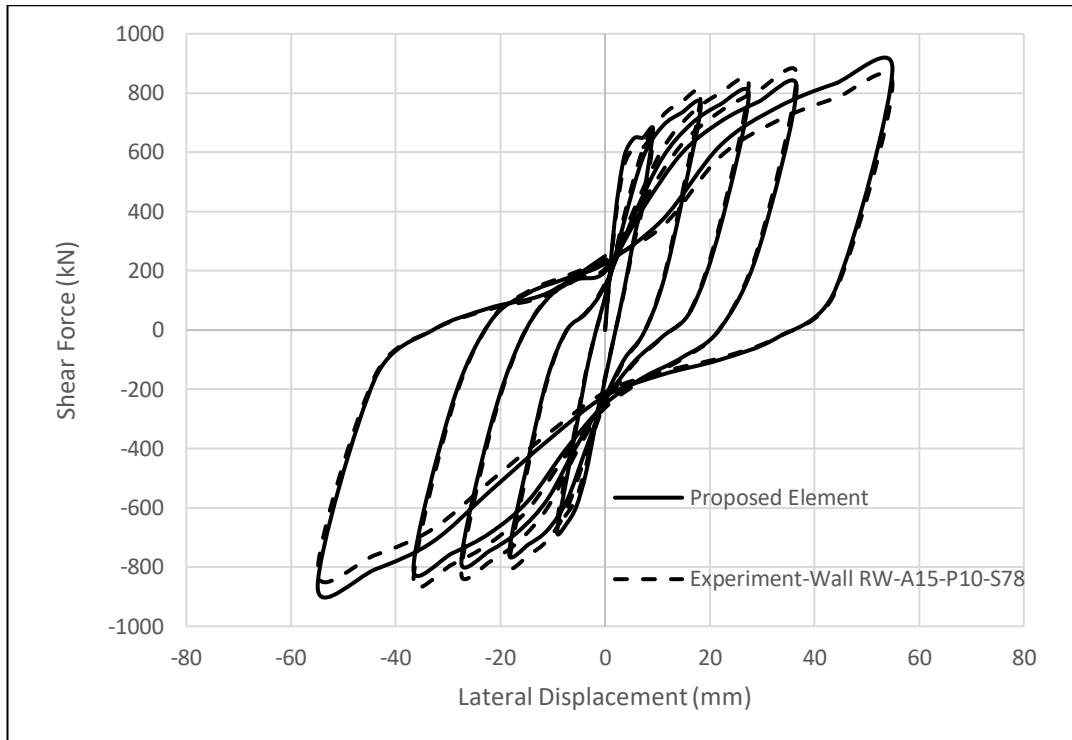


Figure 3-70. Lateral Load-Deflection Response of Wall RW-A15-P10-S78

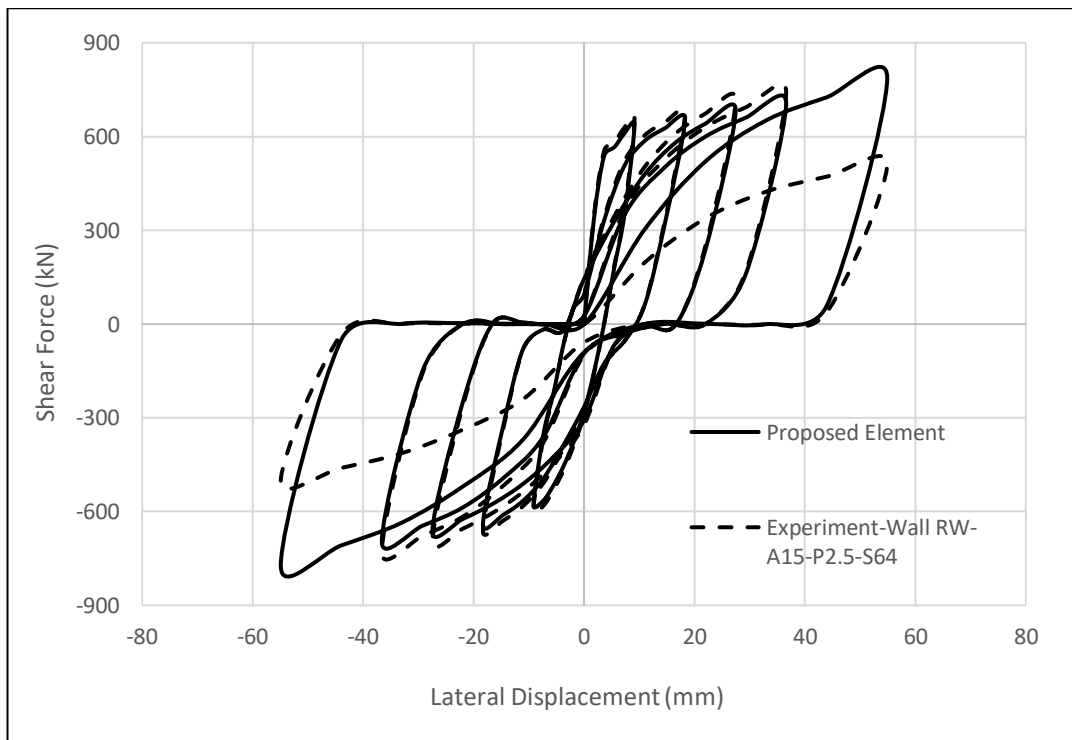


Figure 3-71. Lateral Load-Deflection Response of Wall RW-A15-P2.5-S64

From the above plots, it can be observed that the proposed element reasonably reproduce the overall experimentally observed load-deflection response. Stiffness, shear resistance, shear deformation capacity along with hysteretic behaviour with pinching have been captured well. However, some disagreements of results at the last loading stage are observed due to the reasons explained earlier. It is to be noted that the lower axial compressive load and larger spacing of horizontal and vertical rebars have caused pinching behaviour in wall RW-A15-P2.5-S64 whereas lesser spacing of horizontal and vertical rebars with a higher axial load have helped wall RW-A15-P10-S78 to achieve a stable hysteretic energy.

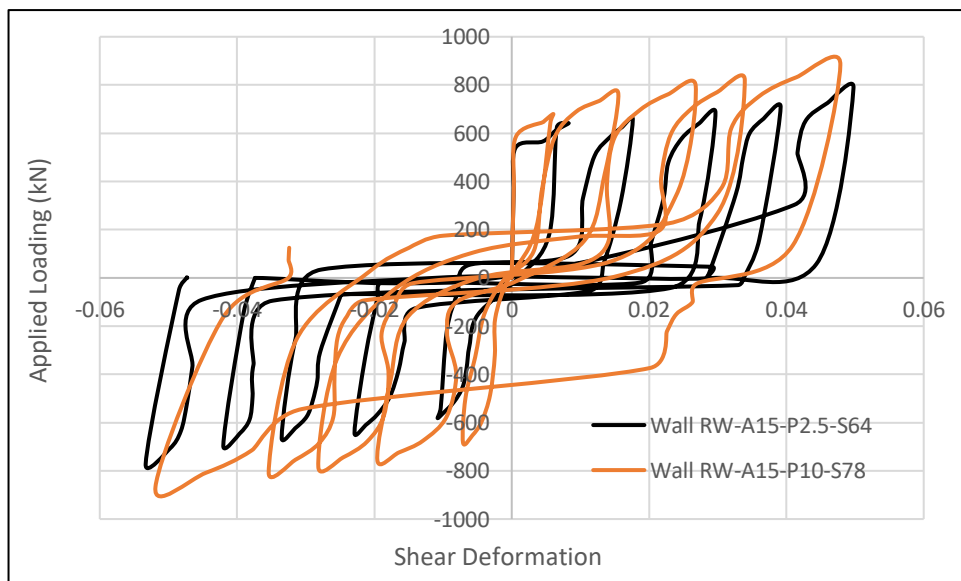


Figure 3-72. Lateral Load-Shear Deformation Response

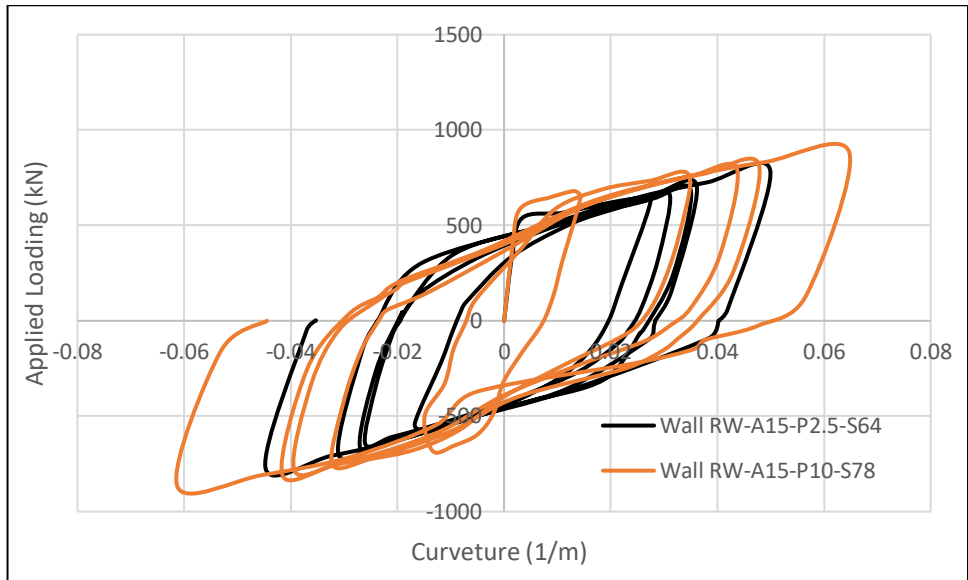


Figure 3-73. Lateral Load-Curvature Response

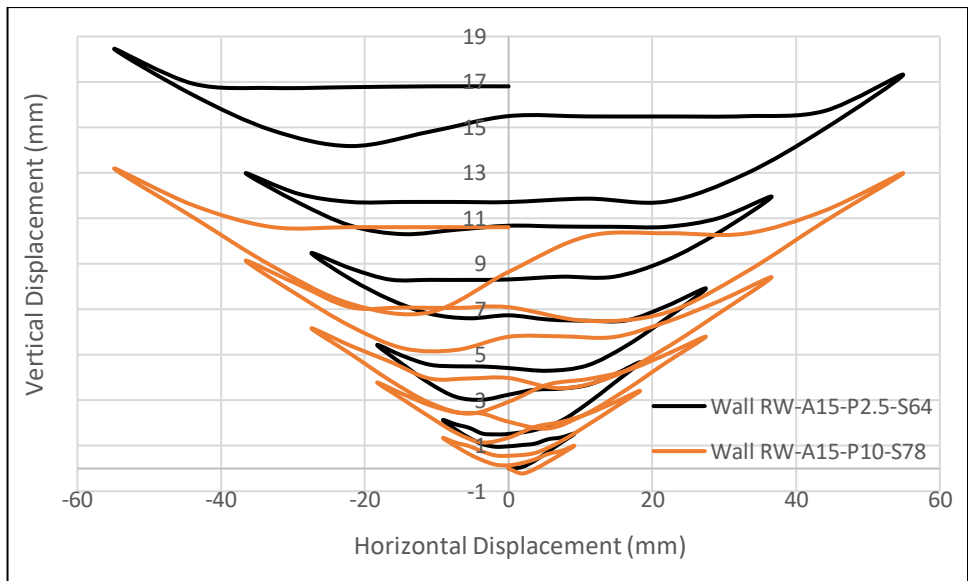


Figure 3-74. Vertical-Horizontal Displacement Response

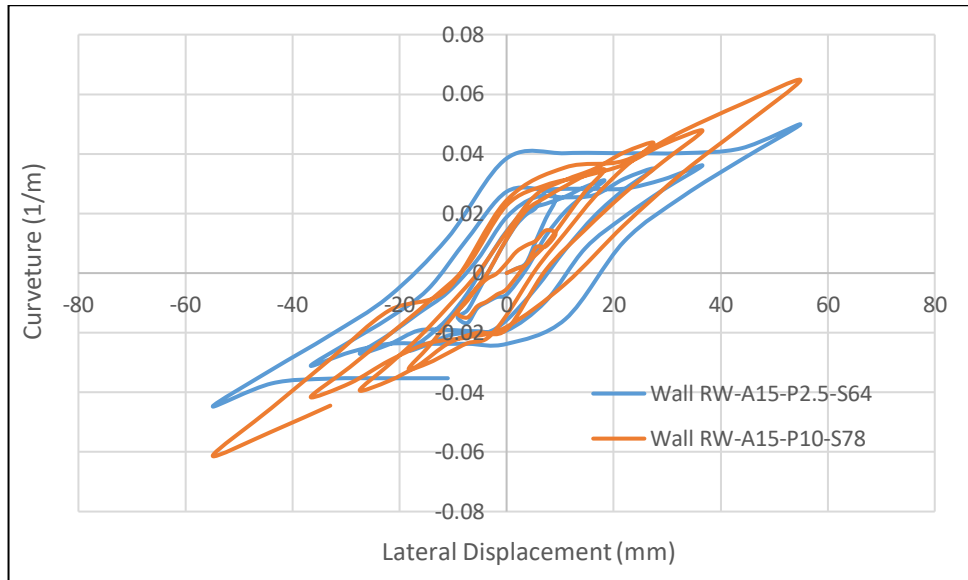


Figure 3-75. Curvature-Horizontal Displacement Response

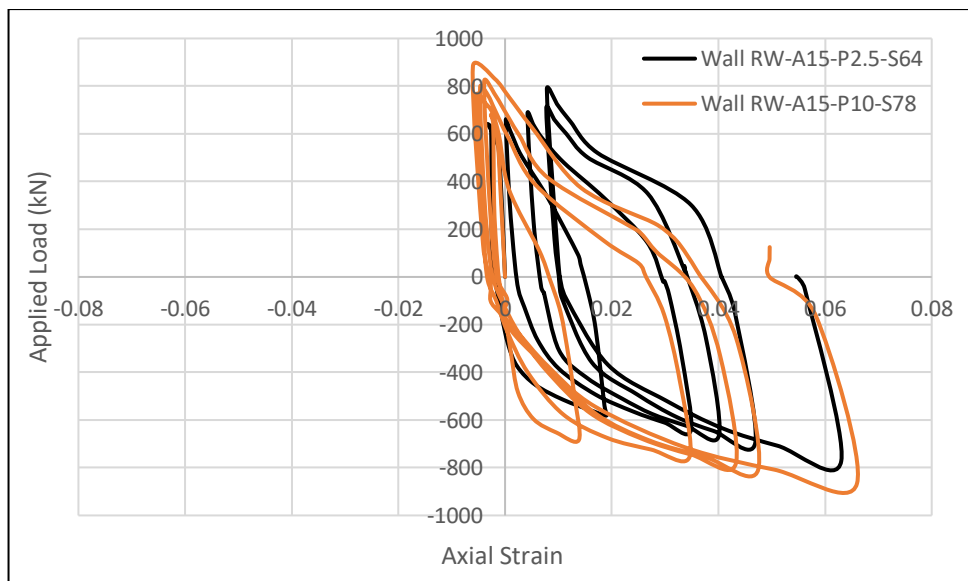


Figure 3-76. Loading-Axial Strain Response of Rightmost vertical Rebar at  
base section

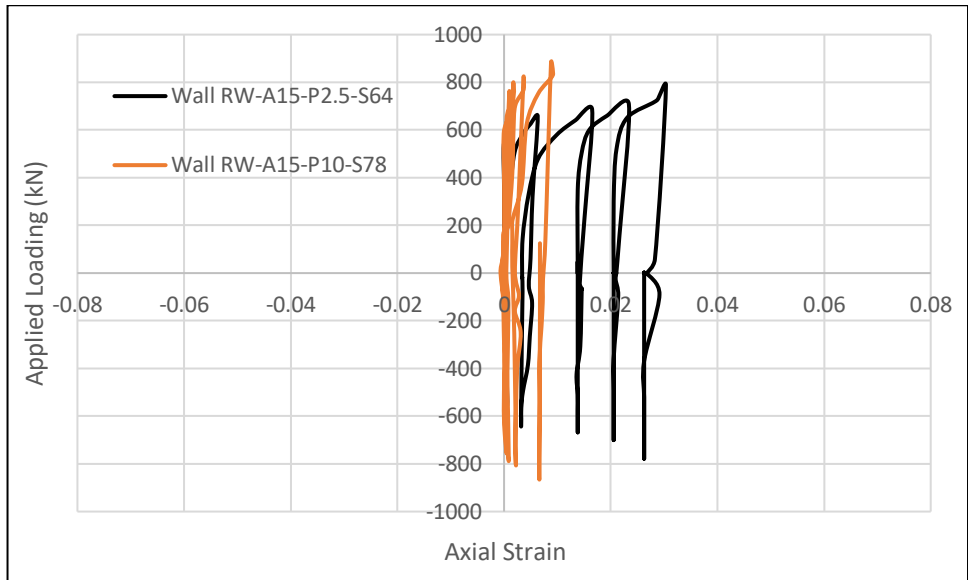


Figure 3-77. Loading-Axial Strain Response of Rightmost horizontal Rebar at base section

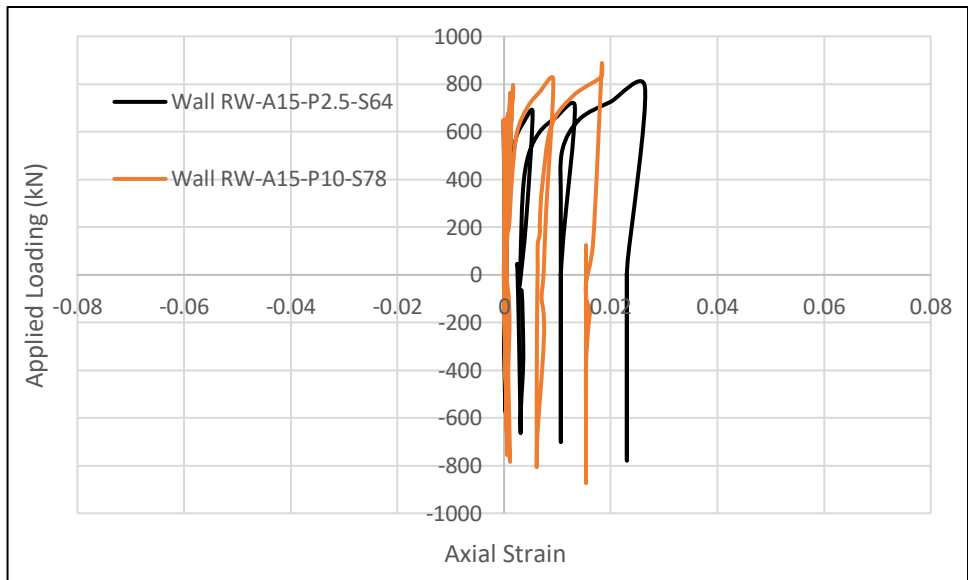


Figure 3-78. Loading-Axial Strain Response of Rightmost horizontal Rebar at 316 mm above base section

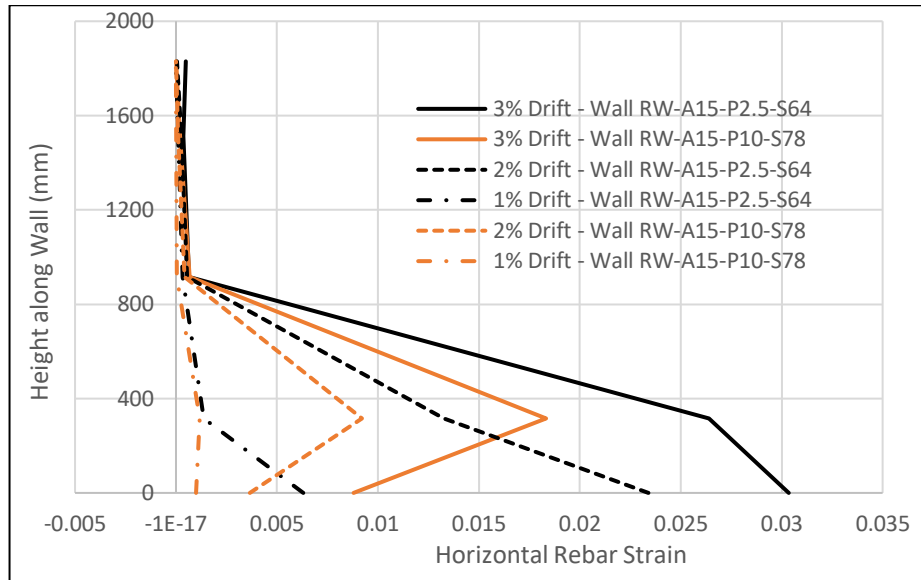


Figure 3-79. Variation of Axial Strain of Rightmost horizontal Rebar along height of wall

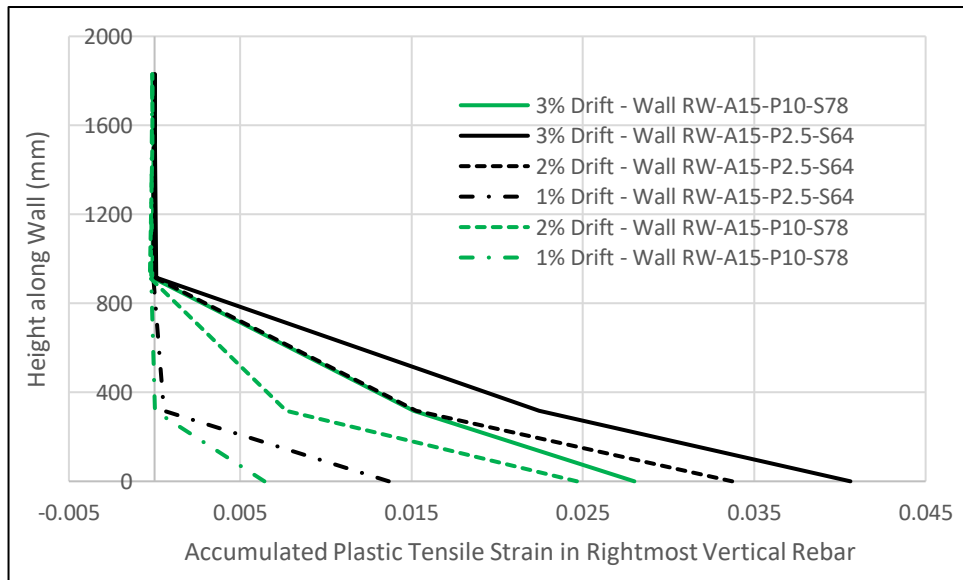


Figure 3-80. Variation of Accumulated Plastic Tensile Strain of Rightmost vertical Rebar along height of wall

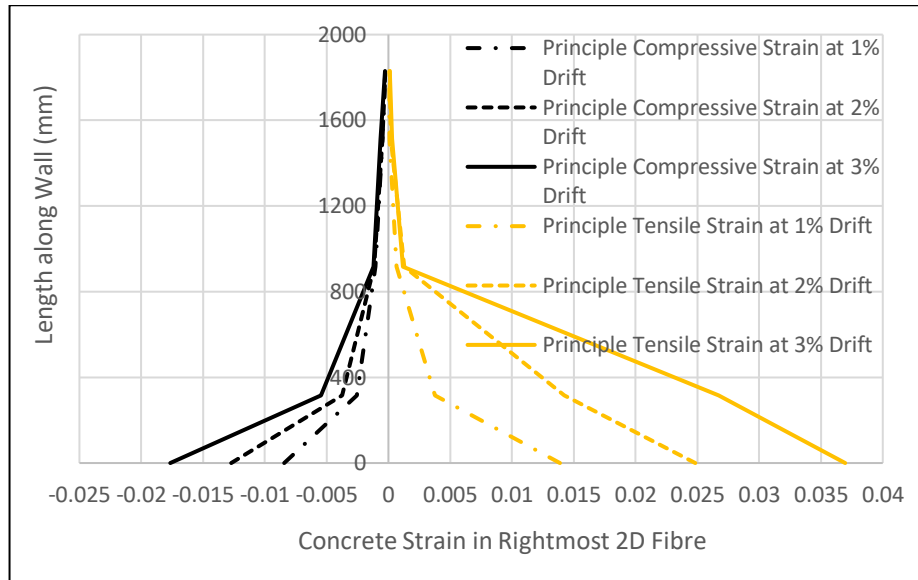


Figure 3-81. Variation of Principle Strain of Rightmost Concrete Fibre along height of wall RW-A15-P10-S78 at positive excursion

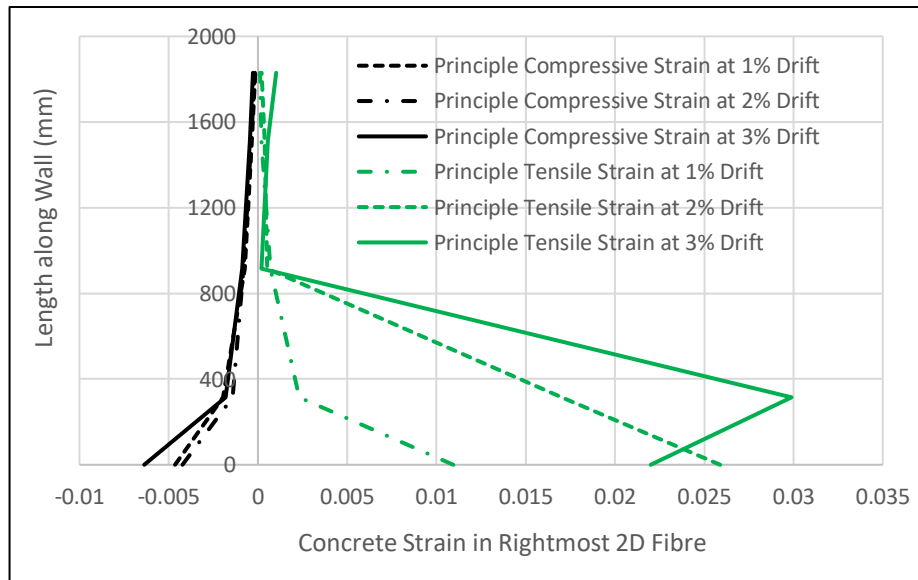


Figure 3-82. Variation of Principle Strain of Rightmost Concrete Fibre along height of wall RW-A15-P2.5-S64 at positive excursion

Figures 3-72 and 3-73 show the load-shear deformation and load-curvature response for both walls. It can be observed that for wall RW-A15-P2.5-S64 residual shear deformation has been observed compared to that of wall RW-A15-P10-S78. Also the curvature response for wall RW-A15-P2.5-S64 is lesser compared to its counterpart in each cycle of loading. These observations supports that failure mode due to shear mechanism gets started early in the wall RW-A15-P2.5-S64 compared to that of wall RW-A15-P10-S78 which has forced to have pinching behaviour in wall RW-A15-P2.5-S64 due to loss of incremental shear stiffness. This can again be supported from the Figure 3-75 that curvature response remain almost constant from the early stage of loading for the wall RW-A15-P2.5-S64 compared to that of wall RW-A15-P10-S78 where curvature response has a slope till the last stage of loading. This phenomenon can also be substantiated from the Figure 3-74 where it can be observed that vertical displacement for wall RW-A15-P2.5-S64 is larger in each cycle of loading than that of wall RW-A15-P10-S78. Lesser axial compressive load in wall RW-A15-P2.5-S64 has aggravated the loss of shear stiffness resulting in pinching behaviour. As a result, more accumulated plastic axial deformation occurs in each cycle of loading, which results in more vertical displacement in wall RW-A15-P2.5-S64 compared to that of wall RW-A15-P10-S78.

From Figure 3-76, it can be observed that under positive loading excursion, the rightmost vertical rebar reaches substantial amount of compressive strain for wall RW-A15-P10-S78. However, for wall RW-A15-P2.5-S64 the induced compressive strain is very less in early stage of loading cycle compared to its counterpart. Moreover, in the later stage of loading cycle, the strain remain in tensile regime signifies that compressive strain in vertical rebar unloads to satisfy the equilibrium. This means that external incremental input energy is getting dissipated almost completely by the incremental shear energy only for wall RW-A15-P2.5-S64. It can also be observed from Figures 3-77 and 3-78 that induced axial strain in the horizontal rebar at the base and second section from the base is larger for wall RW-A15-P2.5-S64 compared to that of wall RW-A15-P10-S78. It means that shear energy becoming responsible to resist the external input energy. This information along with the response in the Figure 3-79, will also help to identify the shear localization zone in the walls particularly when the horizontal rebar exceeds the yield strain indicating the failure controlled by shear mode. From Figure 3-79, it can also be reported that shear deformation gets localized at 316 mm from the base section for wall RW-A15-P10-S78. However, for wall RW-A15-P2.5-S64, shear deformation gets concentrated at the base section. As a result, for wall RW-A15-P10-S78, localized crushing and cracking will happen at 316mm from the base section. On the above, due to having higher axial compressive

loading out of plane bar buckling becomes prominent. However, for wall RW-A15-P2.5-S64, concrete will remain intact at 316mm from the base section and also due to having lesser axial compressive loading, the probability of out of plane bar buckling becomes less. This phenomenon can also be supported from the Figure 3-80 where it can be observed that accumulated plastic tensile strain responsible for initiation of buckling, is larger for wall RW-A15-P2.5-S64 in each drift level compared to that of wall RW-A15-P10-S78. Initiation of in plane buckling becomes prominent for this wall RW-A15-P2.5-S64 due to the concentration of shear mechanism at the base section along with lesser compressive loading and accumulated plastic tensile strain.

From Figures 3-81 and 3-82, it can be observed that the principle compressive strain in the rightmost concrete fibre at the base section for wall RW-A15-P2.5-S64 is substantially lesser compared to that of wall RW-A15-P10-S78. This is because the wall RW-A15-P2.5-S64 is getting subjected to 4 time lesser axial compressive loading. This means that concrete crushing is happening earlier for wall RW-A15-P10-S78 at the boundary zone compared to that of wall RW-A15-P2.5-S64. As a result, initiation of out of plane buckling becomes easier for wall RW-A15-P10-S78 due to higher axial compressive loading. However, for wall RW-A15-

P2.5-S64, concrete crushing gets delayed and in plane buckling of vertical rod starts control the failure mode.

## **3.5 Steel Shear Beams**

### **3.5.1 Shear Link by Hjelmstad and Popov (1983) – Monotonic Loading**

Hjelmstad et al. (1983) has studied the inelastic seismic behaviour of shear links which transfers the forces among connected members by going through flexure-shear deformation in eccentric bracing frame system. Therefore, these short beams are designed to dissipate a large amount of input energy. It is imperative to develop elements which can simulate the inelastic behaviour of shear links as it controls the global behaviour of the whole system. Specimen 4 is adopted for the correlation studies. It is fixed at both ends and is subjected to a vertical displacement at the right support monotonically. The length of the short beam is 28 inch. The cross-section details are shown in Figure 3-83.

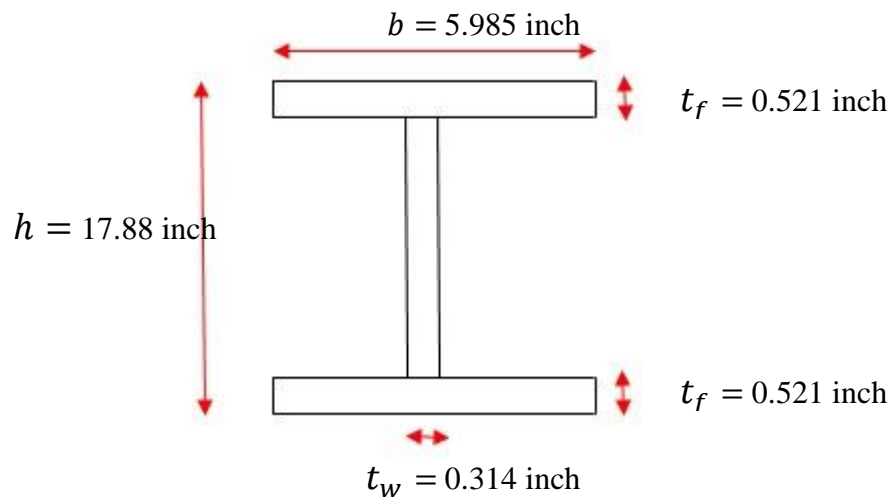


Figure 3-83. Cross-sections of Specimen 4

Both multi-axial models of steel material i.e. J2 plasticity and Generalized plasticity models have been used in the analysis with yield strength of 40 ksi. The Poisson ration used was 0.3. Isotropic hardening ratio of 0.004 and zero kinematic hardening has been considered.

Timoshenko section kinematics produce a uniform shear stress along the section depth. Shear correction factor is needed to handle the discrepancy between the uniform shear stress condition and actual response. It depends on the loading condition, material and geometric properties, and boundary conditions. Higher order beam theory manages this limitation by introducing nonlinear variation of axial displacement in the vertical direction. In this study, a non-uniform shear strain distribution is introduced by following an interpolation function which is multiplied with

generalized shear deformation, as proposed by Saritas et al. (2009), has been adopted.

$$\alpha(y) = \frac{1}{\beta} \left[ (1 + 2\alpha) - 4 \left( \frac{y}{h} \right)^2 \right] \quad (1)$$

Where,

$$\beta = \frac{(1 + 2\alpha)^2 - \frac{2}{3}(1 + 2\alpha) + \frac{1}{5}}{\frac{2}{3}(1 + 3\alpha)}$$

$$\alpha = \frac{2bt_f}{ht_w}$$

One element has been used to model the entire beam specimen with 5 section integration points. Figure 3-84 compare the vertical load versus end deflection response of the models using the proposed beam element with the finite element model by plane stress elements performed by Saritas et al. (2009).

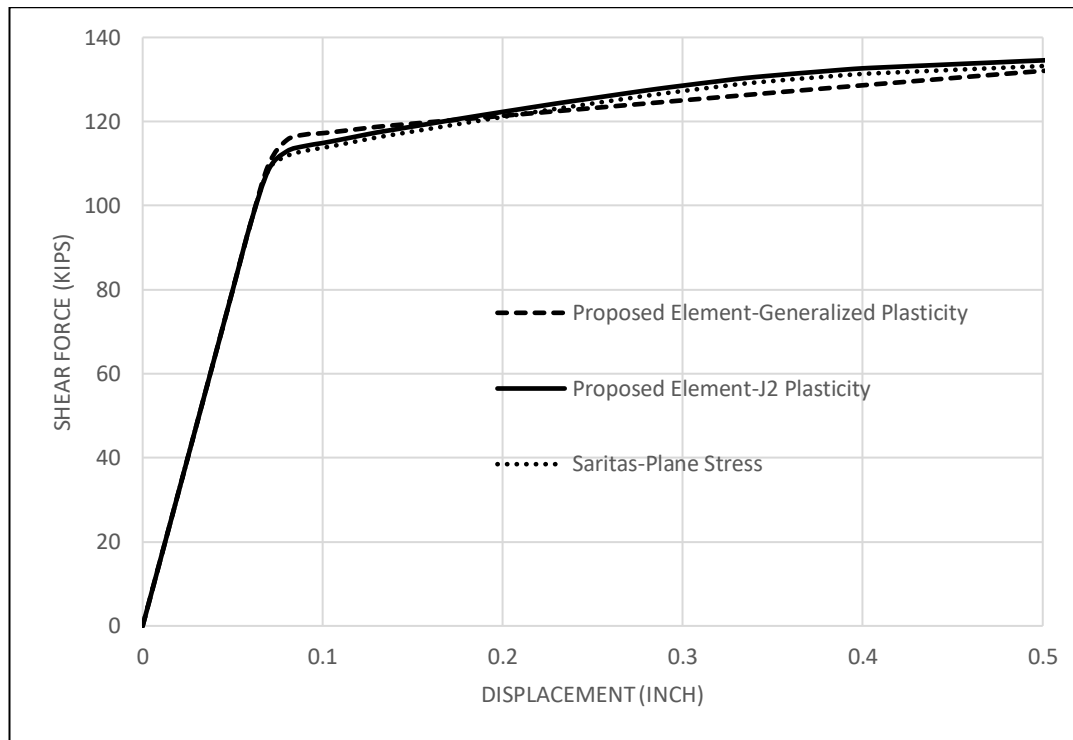


Figure 3-84. Monotonic Load-Deflection Response of Specimen 4

From the above plot, it can be observed that the proposed beam element reasonably reproduce the overall load-deflection response with respect to the expensive finite element model by plane stress elements. Stiffness, shear resistance and shear deformation capacity have been captured well.

### 3.5.2 Shear Link by Hjelmstad and Popov (1983) – Cyclic Loading

Hjelmstad et al. (1983) conducted tests on a series of fifteen short wide-flange steel beams under severe cyclic loading conditions to investigate transverse stiffening arrangement against web buckling and consequently to enhance the energy dissipation capacity. Out of these specimens,

specimen 4 is chosen for the correlation studies because of its stable energy dissipation capacity and the delay in the onset of local buckling. The cross-section details of specimen 4 are shown in Figure 3-83. Generalized plasticity model for steel material is adopted with isotropic hardening ratio of 0.0002 and kinematic hardening ratio of 0.004. The Young's modulus, yield and ultimate strength are taken as 28300 ksi, 39.5 ksi, 60.1 ksi and 28000 ksi, 35 ksi, 58.5 ksi for web and flange regions respectively.

One element has been used to model the entire beam specimen with 5 section integration points. Figure 3-85 compare the vertical load versus end deflection response of the models using the proposed beam element with the experimental results of specimen 4.

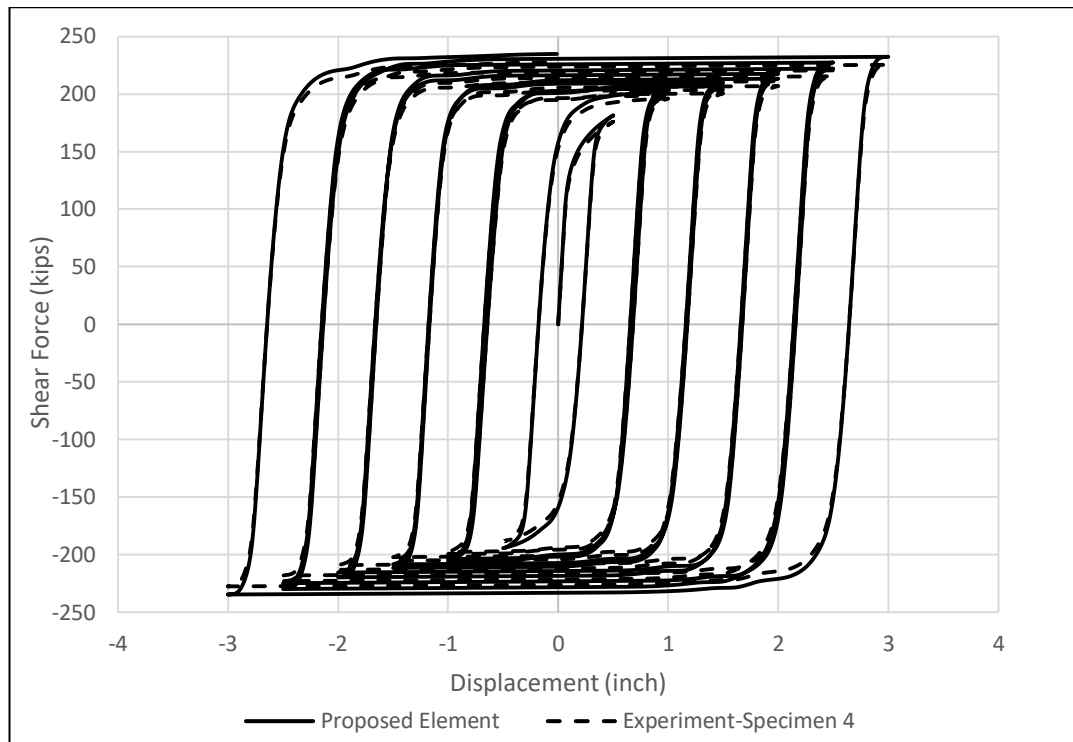


Figure 3-85. Cyclic Load-Deflection Response of Specimen 4

From the above plot, it can be observed that the proposed beam element reasonably reproduces the overall load-deflection response. Stiffness, shear resistance, shear deformation capacity along with hysteretic energy dissipation capacity have been captured well. However, some deviations of unloading stiffness have been observed which may be attributed to the slip of specimen at the restraint locations.

Very similar response has been obtained by Saritas et al. (2009) through the three-field mixed formulation following Hu-Washizhu variational principle.

# **Chapter 4 Shear Critical Composite Element – Displacement and Mixed Formulation**

## **4.1 Overview**

In this chapter, we are going to develop two new shear critical composite frame elements based on distributed inelasticity approach considering the partial interaction between the two mediums i.e. steel and concrete. Unlike other formulations available in the literature, these elements are completed in the sense of constitutive model of materials considering multi-axial coupling among various stress measures and shear deformation in both mediums. Experimentally it has been observed that the shear contribution of concrete layer is not negligible, however it contributes between 30% to 60% of the total shear resisting force which drives to formulate a rational shear element for steel-concrete composite members considering the partial interaction due to the finite stiffness provided by the shear studs. In the following, we will first develop the shear critical displacement-based formulation and then the two-field mixed based formulation with the help of total potential energy and Hellinger-Reissner functional respectively. Currently the contribution of shear resistance from the concrete layer has not been considered in the design of steel-concrete composite members. Therefore, lots of experimental research work has been recently conducted to develop empirical design equations to include the shear contribution of concrete layers in various countries. These distributed inelasticity based

frame element formulations are essential to develop the inelastic analysis driven design process such as performance based design methodology for steel-concrete composite systems with partial interaction.

The current research work aims to extend the two-filed mixed-based formulation by Ayoub et al. (2000) to account for shear critical composite members by implementing coupled multi-axial constitutive laws for materials, along with new stability criteria. To achieve this purpose, the described new shape function (Section 2.1) for transverse displacement varying with cubic function along the length of the element has been used in our research work.

## **4.2 Element Kinematics**

The axis of the proposed composite frame element is a straight line joined by nodes I and J in the statically determinate basic reference system in which rigid body displacements are removed by choosing the simple supported boundary conditions as shown in Figure. 4-1. The frame element is composed of several sections along its axis. Every section is composed of several fibres which are identified by their position from the reference axis and individual cross-section area.

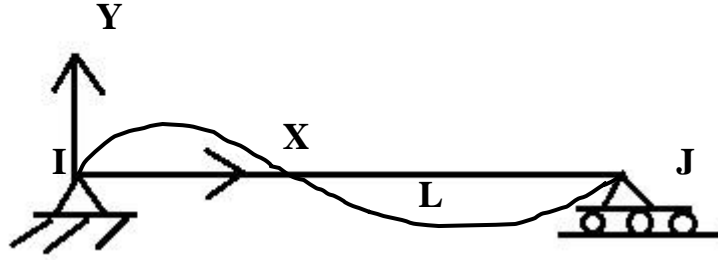


Figure 4-1. Basic reference system without rigid body modes

The section displacement vector  $\mathbf{u}(x)$  collects the two axial translations  $u_s(x), u_c(x)$  in X direction which are axial section displacement passing through the chosen reference axis in steel and concrete layers respectively and one translation  $v(x)$  in Y direction and one rotation  $\theta_z(x)$  about Z axis.

$$\mathbf{u}(x) = [u_s(x) u_c(x) \theta_z(x) \quad v(x)]^T \quad (1)$$

The element nodal displacement vector  $\mathbf{u}_{IJ}$  collects the nodal displacement with respect to global axes according to the section displacement vector in Equation (1). In the proposed composite frame element, an additional middle nodal with axial and rotational degrees of freedom is included, which will be statically condensed out at the element level before the assembling process:

$$\mathbf{u}_{IJ} = [u_I^s \ u_I^c \ v_I \ \theta_{zI} \quad u_J^s \ u_J^c \ v_J \ \theta_{zJ} \quad u_K^s \ u_K^c \ \theta_{zK}]^T \quad (2)$$

The element deformation vector  $\mathbf{v}$  collects the relative translation  $u$  at nodes I, J and K in X direction, rotations  $\theta_z$  at nodes I and J and middle node K with respect to the basic reference axes as shown in the Figure 4-2:

$$\mathbf{v} = [u_{bI}^c u_{bJ}^c u_{bK}^s \theta_{zI} \theta_{zJ} u_{bK}^c u_{bK}^s \theta_{zK}]^T \quad (3)$$

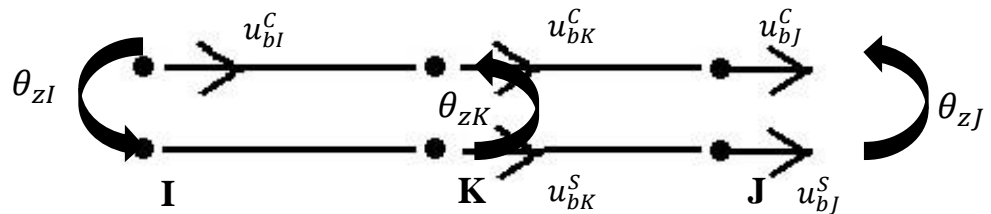


Figure 4-2. Element nodal deformations

The relation between element nodal deformation  $\mathbf{v}$  and displacements  $\mathbf{u}_{IJ}$  can be uniquely determined by the compatibility matrix  $\mathbf{a}_c$  with constant coefficients under linear geometry conditions where  $L$  is the undeformed length of the element:

$$\mathbf{v} = \mathbf{a}_c \mathbf{u}_{IJ} \quad (4)$$

Where,

$$\mathbf{a}_c = \begin{bmatrix} 0 & \frac{1}{L} & 1 & 0 & 0 & -\frac{1}{L} & 0 & 0 & 0 & 0 & 0 \\ -1 & 0 & 0 & 1 & 0 & 0 & 0 & 0 & 0 & 0 & 0 \\ -1 & 0 & 0 & 0 & 1 & 0 & 0 & 0 & 0 & 0 & 0 \\ 0 & \frac{1}{L} & 0 & 0 & 0 & -\frac{1}{L} & 1 & 0 & 0 & 0 & 0 \\ -1 & 0 & 0 & 0 & 0 & 0 & 0 & 1 & 0 & 0 & 0 \\ -1 & 0 & 0 & 0 & 0 & 0 & 0 & 0 & 1 & 0 & 0 \\ -1 & 0 & 0 & 0 & 0 & 0 & 0 & 0 & 0 & 1 & 0 \\ 0 & \frac{1}{L} & 0 & 0 & 0 & -\frac{1}{L} & 0 & 0 & 0 & 0 & 1 \end{bmatrix}$$

### 4.3 Section Kinematics

Under the assumption of a Timoshenko beam theory, the displacements  $\mathbf{u}^m(x, y)$  of a material point  $m$  with coordinate  $y$  at a section with distance  $x$  from the origin of the reference frame can be represented with the cross-section generalized displacements  $\mathbf{u}(x)$  as follows:

$$u_x^{m,s}(x, y) = u_s(x) - y\theta_z(x) \quad (5)$$

$$u_x^{m,c}(x, y) = u_c(x) - y\theta_z(x) \quad (6)$$

$$v_x^m(x, y) = v(x) \quad (7)$$

The material strain displacement vector  $\boldsymbol{\varepsilon}(x, y)$  can be related with the material displacement vector  $\mathbf{u}^m(x, y)$  as follows:

$$\varepsilon_{xx}^s = \frac{\partial u_x^{m,s}(x,y)}{\partial x} = \frac{\partial u_s(x)}{\partial x} - y \frac{\partial \theta_z(x)}{\partial x} \quad (8)$$

$$\varepsilon_{xx}^c = \frac{\partial u_x^{m,c}(x,y)}{\partial x} = \frac{\partial u_c(x)}{\partial x} - y \frac{\partial \theta_z(x)}{\partial x} \quad (9)$$

$$\varepsilon_{yy} = \frac{\partial v_x^m(x,y)}{\partial y} = \frac{\partial v(x)}{\partial y} = 0 \quad (10)$$

$$2\varepsilon_{xy} = \frac{\partial u_x^m(x,y)}{\partial y} + \frac{\partial v_x^m(x,y)}{\partial x} = -\theta_z(x) + \frac{\partial v(x)}{\partial x} \quad (11)$$

By introducing the section deformation vector  $\mathbf{d}(x)$  which is a function of the section displacement vector  $\mathbf{u}(x)$ , we can write down the following equation with the help of section compatibility matrix  $\mathbf{a}_s(y)$ :

$$\boldsymbol{\varepsilon}(x, y) = \mathbf{a}_s(y) \mathbf{d}(x) \quad (12)$$

Where,

$$\mathbf{d}(x) = \left[ \frac{\partial u_s(x)}{\partial x} \quad \frac{\partial u_c(x)}{\partial x} \quad \frac{\partial \theta_z(x)}{\partial x} \quad \left( -\theta_z(x) + \frac{\partial v(x)}{\partial x} \right) \right]^T$$

$$\mathbf{a}_s(y) = \begin{bmatrix} 1 & 0 & -y & 0 \\ 0 & 1 & -y & 0 \\ 0 & 0 & 0 & 1 \end{bmatrix}$$

## 4.4 Equilibrium

The differential equilibrium equation of a segment of length  $dx$  of a composite element with partial interaction as shown in Figure.4-3 can be written down as follows:

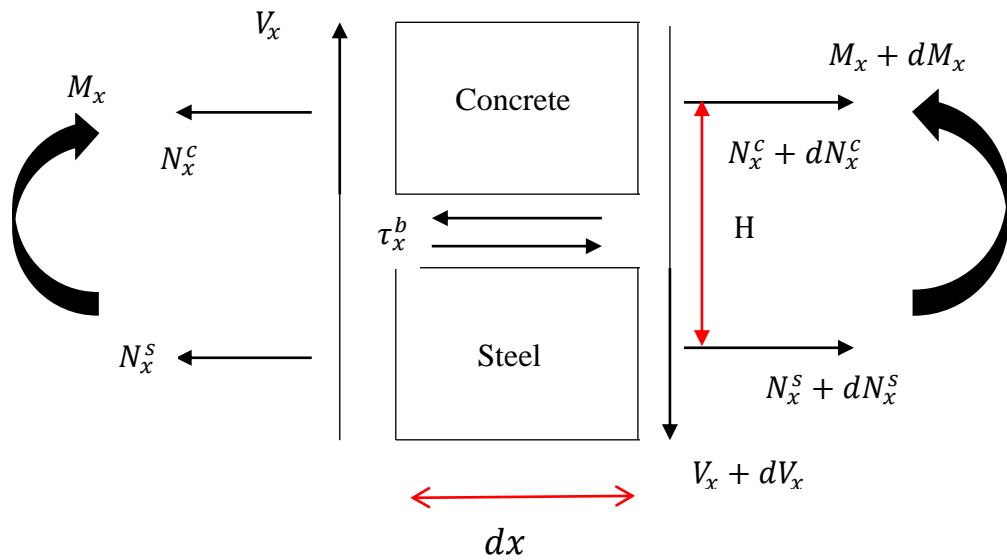


Figure 4-3. Section differential equilibrium

$$\frac{dN_x^s}{dx} + \tau_x^b = 0 \quad (13)$$

$$\frac{dN_x^c}{dx} - \tau_x^b = 0 \quad (14)$$

$$\frac{dM_x}{dx} - V_x - H\tau_x^b = 0 \quad (15)$$

$$\frac{dV_x}{dx} = 0 \quad (16)$$

Where  $N_x^s, N_x^c, M_x, V_x, \tau_x^b$  are the axial force in steel beam, axial force in concrete beam, bending moment, shear force and interface bond force per unit length respectively, and H is the distance between the centroids of steel and concrete beams.

Writing the equilibrium equations in matrix form:

$$\mathbf{L}^T \mathbf{D}(x) - \mathbf{L}_b^T \tau_x^b = 0 \quad (17)$$

Where

$$\mathbf{D}(x) = [N_x^s N_x^c M_x V_x]^T$$

$$\mathbf{L}^T = \begin{bmatrix} \frac{d}{dx} & 0 & 0 & 0 \\ 0 & \frac{d}{dx} & 0 & 0 \\ 0 & 0 & \frac{d}{dx} & -1 \\ 0 & 0 & 0 & \frac{d}{dx} \end{bmatrix}$$

$$\mathbf{L}_b^T = \begin{bmatrix} -1 \\ 1 \\ H \\ 0 \end{bmatrix}$$

## 4.5 Compatibility

The components of generalized section deformation vector  $\mathbf{d}(x)$  are the axial strain  $\varepsilon_0^s$  in steel, the axial strain  $\varepsilon_0^c$  in concrete, the curvature  $\phi_z$  about the z axis and shear deformation  $\gamma_y$  in the y direction respectively:

$$\mathbf{d}(x) = [\varepsilon_0^s \varepsilon_0^c \phi_z \gamma_y]^T \quad (18)$$

Where

$$\varepsilon_0^s = \frac{du_s(x)}{dx}$$

$$\varepsilon_0^c = \frac{du_c(x)}{dx}$$

$$\phi_z = \frac{d\theta_z(x)}{dx}$$

$$\gamma_y = -\theta_z(x) + \frac{dv(x)}{dx}$$

The interface slip  $S(x)$  between the steel beam and concrete slab has been determined as follows:

$$S(x) = \mathbf{L}_b \mathbf{u}(x) \quad (19)$$

Writing the compatibility equations in matrix form:

$$\mathbf{L} \mathbf{u}(x) - \mathbf{d}(x) = 0 \quad (20)$$

Where

$$\mathbf{L} = \begin{bmatrix} \frac{d}{dx} & 0 & 0 & 0 \\ 0 & \frac{d}{dx} & 0 & 0 \\ 0 & 0 & \frac{d}{dx} & 0 \\ 0 & 0 & -1 & \frac{d}{dx} \end{bmatrix}$$

$$\mathbf{L}_b = [-1 \quad 1 \quad H \quad 0]$$

## 4.6 Constitutive Law

The section constitutive law is as follows.

$$\mathbf{D}(x) = f_{sec} \mathbf{d}(x) \quad (21)$$

Where  $f_{sec}$  is a nonlinear function that describes the section force-deformation relation. The section force-deformation relation is obtained through fibre integration as described in Section 2.8.

The bond constitutive law is defined as follows:

$$\tau_x^b = f_{bond} S(x) \quad (22)$$

Where  $f_{bond}$  is a nonlinear function that describes the bond stress-interface slip relation. For the bond-slip constitutive relations, the Eligehausen et al. (1983) law has been used.

## 4.7 Variational Formulation

### 4.7.1 Displacement-based Formulation

Nodal displacements are considered as the primary unknowns in displacement based formulations (Zienkiewicz et al. (1989), Bathe (1996), and Crisfield (1991)). Therefore, element deformations are found from displacement interpolation functions. Cubic Hermitian interpolation

functions for transverse deformation fields produce a linear distribution of curvature along the length of the element. The number of finite elements per member is increased to simulate the nonlinear curvature fields. Element equilibrium is satisfied only in the variational weak sense. Therefore, the element internal forces calculated from the assumed displacement field do not satisfy nodal equilibrium. This also requires decreasing the mesh size by using more finite elements per member. The state determination process uses the strain-displacement relations in connection with displacement interpolation functions to obtain the section deformations that are compatible with the given nodal displacements. It is relatively straightforward to find the resisting forces and section stiffness matrix from the section deformations (section state determination). The integration of the section response over the element length gives the element resisting forces and stiffness matrix, thus completing the state determination process for the element (Izzuddin et al. (1993)). In the case of composite members, the differential axial movement between the steel and concrete media can be determined directly from the deformation fields. Therefore, the bond force can be calculated with the help of the constitutive relation defined for the interface.

The principle of virtual displacements forms the principle of minimum potential energy that uses displacements as the only independent field. The

potential energy functional ( $\Pi_p$ ) is written in terms of independent nodal displacement ( $\mathbf{u}$ ) field in the basic frame of reference which does not include rigid body motions as follows:

$$\Pi_p(\mathbf{u}) = \int_v W(\boldsymbol{\varepsilon}^u(x, y)) dv + \Pi_b(\mathbf{u}(x)) - \Pi_{ext}(\mathbf{u}(x)) - \Pi_{bc}(\mathbf{u}) \quad (23)$$

In Eq. (23),  $\mathbf{u}(x)$  is the section displacement which can be derived from nodal displacement  $\mathbf{u}$ ,  $W(\boldsymbol{\varepsilon})$  is the strain energy function of concrete beam and steel face plate and  $\boldsymbol{\varepsilon}^u$  denotes the strains derived from nodal displacements, ( $\Pi_b$ ) is the strain energy function due to partial bond-slip between these two media, ( $\Pi_{bc}$ ) is the potential energy due to nodal boundary forces and ( $\Pi_{ext}$ ) is the potential energy of the external loading due to body and surface forces and it has the following form:

$$\Pi_{ext} = \int_v \mathbf{u}(x)^T \mathbf{b}_o dv + \int_{\Gamma_t} \mathbf{u}(x)^T \mathbf{t}^* d\Gamma \quad (24)$$

In Eq. (24),  $\mathbf{b}_o$  is the vector of body forces per unit volume and the components of the prescribed external forces per unit area of the boundary are denoted as  $\mathbf{t}^*$ .

In this variational principle, strain-displacement relation  $\boldsymbol{\varepsilon} = \nabla^s \mathbf{u}(x)$  on  $v$ , constitutive relation  $\boldsymbol{\sigma} = \boldsymbol{\sigma}(\boldsymbol{\varepsilon})$  on  $v$ , and displacement boundary condition  $\mathbf{u} = \mathbf{u}^*$  on  $\Gamma_u$  where  $\mathbf{u}^*$  is the imposed displacement, are satisfied in their

strong differential form. Whereas, equilibrium conditions  $\mathbf{div} \boldsymbol{\sigma} + \mathbf{b}_o = \mathbf{0}$  on  $\nu$  and traction boundary conditions  $\mathbf{t} = \mathbf{t}^*$  on  $\Gamma_t$  are satisfied in their integral weak form where the traction  $\mathbf{t} = \boldsymbol{\sigma} \cdot \mathbf{n}$  is the dot product of the stress tensor  $\boldsymbol{\sigma}$  with the outward normal  $\mathbf{n}$  to the boundary.

The domain of the body is denoted by  $\nu$  in Eq. (23) and Eq. (24), while the traction and displacement boundaries are  $\Gamma_t$  and  $\Gamma_u$  respectively. It is assumed that the latter two boundaries are distinct, but the joint set of the two establishes the total boundary surface, i.e.  $\Gamma \in \{\Gamma_u \cup \Gamma_t\}$ .

The potential energy functional of Equation (23) can be written without body force and surface traction with section level variables in the following form:

$$\Pi_p(\mathbf{u}) = \int_L \mathbf{d}^T(x) \mathbf{D}(x) dx + \int_L s^T(x) \tau_x^b(x) dx - \mathbf{u}^T \mathbf{P}^* \quad (25)$$

where  $\mathbf{P}^*$  is the applied nodal boundary forces.

Transformation of this functional from the material level to the section level needs a compatibility condition through appropriate section kinematics. In this formulation, distributed inelasticity at the section level is considered through fibre discretization. Section resisting force and

stiffness are obtained from the integration of the fibre level variables. It is to be noted that by adopting a fibre model, coupling of axial, shear and bending response is a natural process. This is a significant advantage over section based models where coupling needs extra care through plasticity formulation.

The variation of potential energy functional in Equation (25) can be written in the following form:

$$\delta \Pi_p(\mathbf{u}) = \int_L \delta \mathbf{d}^T(x) \mathbf{D}(x) dx + \int_L \delta s^T(x) \tau_x^b(x) dx - \delta \mathbf{u}^T \mathbf{P}^* \quad (26)$$

The solution of the variational in Equation (26) is non-linear under inelastic material conditions, so the problem is linearized about a state  $\mathbf{u}^i$  as follows:

$$\delta \Pi_p(\mathbf{u}^{i+1}) = \delta \Pi_p(\mathbf{u}^i) + \left. \frac{\partial \delta \Pi_p(\mathbf{u})}{\partial \mathbf{u}} \right|_{\mathbf{u}^i} \Delta \mathbf{u} \quad (27)$$

Where  $\Delta \mathbf{u}$  is the incremental nodal displacement vector.

At equilibrium,

$$\delta \Pi_p(\mathbf{u}^{i+1}) = 0 \quad (28)$$

From Equation (27) we get,

$$\delta \Pi_p(\mathbf{u}^i) + \frac{\partial \delta \Pi_p(\mathbf{u})}{\partial u} \Big|_{\mathbf{u}^i} \Delta \mathbf{u} = 0 \quad (29)$$

Equation (29) can be written in the following expanded form:

$$\begin{aligned} & \int_L \delta \mathbf{d}^T(x) \mathbf{D}^i(x) dx + \int_L \delta \mathbf{s}^T(x) \tau_x^{b,i}(x) dx - \delta \mathbf{u}^T \mathbf{P}^* + \\ & \left( \int_L \delta \mathbf{d}^T(x) \frac{\partial \mathbf{D}(x)}{\partial u} dx + \int_L \delta \mathbf{s}^T(x) \frac{\partial \tau_x^b}{\partial u} dx - \delta \mathbf{u}^T \frac{\partial P^*}{\partial u} \right) \Delta \mathbf{u} = 0 \end{aligned} \quad (30)$$

By using Equations (17), (19), (20) and (21) and assuming conservative applied load and from arbitrariness of  $\delta \mathbf{u}$ , Eq. (30) can be written in the following expanded form:

$$\begin{aligned} & \left( \int_L \mathbf{B}_s^T(x) \mathbf{K}_s(x) \mathbf{B}_s(x) dx + \int_L \mathbf{B}_b^T(x) \mathbf{K}_b(x) \mathbf{B}_b(x) dx \right) \Delta \mathbf{u} = \mathbf{P}^* - \\ & \int_L \mathbf{B}_s^T(x) \mathbf{D}^i(x) dx - \int_L \mathbf{B}_b^T(x) \tau_x^{b,i}(x) dx \end{aligned} \quad (31)$$

Where,  $\mathbf{B}_s(x)$  and  $\mathbf{B}_b(x)$  are the strain-displacement and slip-displacement matrix.

Eq. (31) can be written in the following concise form:

$$(K_{c+s} + K_B)\Delta u = P^* - P_{c+s}^r - P_b^r \quad (32)$$

$$K\Delta u = P^* - P^r \quad (33)$$

where  $K$  is the composite element stiffness matrix which consists of combined concrete and steel beam stiffness  $K_{c+s}$  and bond stiffness  $K_B$  and  $P^r$  is the composite element resistance matrix which consists of combined concrete and steel beam resistance  $P_{c+s}^r$  and bond resistance  $P_b^r$ .

#### 4.7.1.1 State Determination

A step by step summary of the state determination algorithm is presented below for a single element. The summary focuses on a single global iteration  $i$  at the structural degree of freedoms through the Newton-Raphson method with applied load counter  $k$ .

*Step 1* to *Step 2* is similar to the section 2.9.2. However, concerned matrixes should be based on this chapter.

*Step 3*: Determine the incremental section deformation and slip and its update with respect to the basic axes of reference for a given element nodal deformation vector:

$$\Delta \mathbf{d}^i = \mathbf{B}_s(x) \Delta \mathbf{v}^{i+1}$$

$$\Delta \mathbf{s}^i = \mathbf{B}_b(x) \Delta \mathbf{v}^{i+1}$$

$$\mathbf{d}^{i+1} = \mathbf{d}^i + \Delta \mathbf{d}^i \quad (\text{Update of section deformation vector})$$

$$\mathbf{s}^{i+1} = \mathbf{s}^i + \Delta \mathbf{s}^i \quad (\text{Update of slip})$$

*Step 4:* Determine the section tangent stiffness ( $\mathbf{k}_{sec}^{i+1}$ ) and resistance vector ( $\mathbf{p}_{sec}^{i+1}$ ) for a given section deformation vector with mid-point integration rule and material state determination as described in Section 2.8. Also, determine bond forces  $\tau_x^{b,i+1}$  and bond stiffness  $\mathbf{K}_b^{i+1}$  from the bond constitutive relations:

*Step 5:* Determine the element stiffness matrix and resistance vector at the basic frame of reference:

$$\mathbf{K}_{ele}^{i+1} = \mathbf{K}_{c+s}^{i+1} + \mathbf{K}_B^{i+1}$$

$$\mathbf{K}_{c+s}^{i+1} = \sum \mathbf{B}_s^T \mathbf{k}_{sec}^{i+1} \mathbf{B}_s$$

$$K_B^{i+1} = \sum B_b^T K_b^{i+1} B_b$$

$$P^{r,i+1} = P_{c+s}^{r,i+1} + P_b^{r,i+1}$$

$$P_{c+s}^{r,i+1} = \sum B_s^T p_{sec}^{i+1}$$

$$P_b^{r,i+1} = \sum B_b^T \tau_x^{b,i+1}$$

*Step 6:* Determine the element stiffness matrix and resistance vector in iteration counter  $i$  at the global frame of reference:

$$K_{ele,glo}^{i+1} = a_c^T K_{ele}^{i+1} a_c$$

$$Q_{ele,glo}^{i+1} = a_c^T P^{r,i+1}$$

### 4.7.2 Mixed-based Formulation

The formulation of the composite beam element in this section uses independent generalized stress and displacement interpolation functions in

a two-field Hellinger-Reissner (HR) functional which is written in the basic frame of reference as follows:

$$\begin{aligned} \Pi_{HR}(\mathbf{u}, \boldsymbol{\sigma}) = & - \int_v W(\boldsymbol{\sigma}(x, y)) dv + \int_v \boldsymbol{\sigma}^T \boldsymbol{\varepsilon}^u dv + \Pi_b(\mathbf{u}(x)) - \\ & \Pi_{ext}(\mathbf{u}(x)) - \Pi_{bc}(\mathbf{u}) \end{aligned} \quad (34)$$

where  $W(\boldsymbol{\sigma})$  is the complementary energy function.

In the HR variational principle, strain-displacement relation  $\boldsymbol{\varepsilon} = \nabla^s \mathbf{u}(x)$  on  $v$  and displacement boundary condition  $\mathbf{u} = \mathbf{u}^*$  on  $\Gamma_u$ , are satisfied in their strong differential form. Whereas, equilibrium conditions  $\mathbf{div} \boldsymbol{\sigma} + \mathbf{b}_o = \mathbf{0}$  on  $v$ , constitutive relation  $\boldsymbol{\sigma} = \boldsymbol{\sigma}(\boldsymbol{\varepsilon})$  on  $v$  and traction boundary conditions  $\mathbf{t} = \mathbf{t}^*$  on  $\Gamma_t$  are satisfied in their integral weak form.

HR energy functional of Equation (34) can be written without body force and surface traction with section level variables in the following form:

$$\begin{aligned} \Pi_{HR}(\mathbf{u}, \mathbf{p}) = & - \int_L \mathbf{D}^T \mathbf{d}(\mathbf{D}) dx + \int_L \widehat{\mathbf{D}}^T(\mathbf{p}) \mathbf{d}(\mathbf{u}) dx + \\ & \int_L \mathbf{s}^T(\mathbf{u}) \tau_x^b dx - \mathbf{u}^T \mathbf{P}^* \end{aligned} \quad (35)$$

In this formulation, beam section forces  $\widehat{\mathbf{D}}$  are independently determined from element nodal forces  $\mathbf{p}$  as follows:

$$\widehat{\mathbf{D}}(x) = \mathbf{b}(x) \mathbf{p} \quad (36)$$

Where  $\mathbf{b}(x)$  is the matrix of force interpolation functions.

It is to be noted that bond forces are determined through bond constitutive relation. Therefore, the equilibrium matrix  $\mathbf{b}(x)$  only satisfies the differential equilibrium Equation (17) partially without the contribution of bond stress. It is in synchronization with HR energy functional as in this variational principle there is no subsidiary condition required. However, composite element formulation based on principle of complementary energy functional loses its most powerful credibility for not satisfying the differential equilibrium equations in its strong form fully.

The variation of HR energy functional in Equation (35) can be written in the following form:

$$\begin{aligned} \delta \Pi_{HR}(\mathbf{u}, \mathbf{p}) = & - \int_L \delta \mathbf{D}^T \mathbf{d}(\mathbf{D}) dx + \int_L \delta (\widehat{\mathbf{D}}^T(\mathbf{p}) \mathbf{d}(\mathbf{u})) dx + \\ & \int_L \delta \mathbf{s}^T(x) \tau_x^b(x) dx - \delta \mathbf{u}^T \mathbf{P}^* \end{aligned} \quad (37)$$

$$\begin{aligned} \delta \Pi_{HR}(\mathbf{u}, \mathbf{p}) = & - \int_L \delta \mathbf{D}^T \mathbf{d}(\mathbf{D}) dx + \int_L \delta(\widehat{\mathbf{D}}^T(\mathbf{p})) \mathbf{d}(\mathbf{u}) dx + \\ & \int_L (\widehat{\mathbf{D}}^T(\mathbf{p})) \delta(\mathbf{d}(\mathbf{u})) dx + \int_L \delta \mathbf{s}^T(x) \tau_x^b(x) dx - \delta \mathbf{u}^T \mathbf{P}^* \end{aligned} \quad (38)$$

The solution of the variational in Equation (38) is non-linear under inelastic material conditions, hence the problem needs to be linearized about a state of both principle arguments  $\mathbf{u}^i$  and  $\mathbf{p}^i$  as follows:

$$\begin{aligned} \delta \Pi_{HR}(\mathbf{p}^{i+1}, \mathbf{u}^{i+1}) = & \delta \Pi_{HR}(\mathbf{p}^i, \mathbf{u}^i) + \frac{\partial \delta \Pi_{HR}(\mathbf{p}, \mathbf{u})}{\partial \mathbf{p}} \Big|_{\mathbf{p}^i, \mathbf{u}^i} \Delta \mathbf{p} + \\ & \frac{\partial \delta \Pi_{HR}(\mathbf{p}, \mathbf{u})}{\partial \mathbf{u}} \Big|_{\mathbf{p}^i, \mathbf{u}^i} \Delta \mathbf{u} \end{aligned} \quad (39)$$

Where  $\Delta \mathbf{u}$  and  $\Delta \mathbf{p}$  are the incremental nodal displacement and force vector respectively.

At equilibrium,

$$\delta \Pi_{HR}(\mathbf{p}^{i+1}, \mathbf{u}^{i+1}) = 0 \quad (40)$$

Therefore from Equation (39), we can write the following:

$$\delta \Pi_{HR}(\mathbf{p}^i, \mathbf{u}^i) + \frac{\partial \delta \Pi_{HR}(\mathbf{p}, \mathbf{u})}{\partial \mathbf{p}} \Big|_{\mathbf{p}^i, \mathbf{u}^i} \Delta \mathbf{p} + \frac{\partial \delta \Pi_{HR}(\mathbf{p}, \mathbf{u})}{\partial \mathbf{u}} \Big|_{\mathbf{p}^i, \mathbf{u}^i} \Delta \mathbf{u} = 0 \quad (41)$$

By using Equations (19), (20), (21), (22) and (36) along with the assumption of conservative external load, Equation (41) can be written in the following form:

$$\begin{aligned}
& \delta \mathbf{u}^T \left[ \int_L \mathbf{B}_s^T(x) \mathbf{b}(x) dx \Delta \mathbf{p} + \int_L \mathbf{B}_b^T(x) \mathbf{K}_b(x) \mathbf{B}_b(x) dx \Delta \mathbf{u} + \right. \\
& \left. \int_L \mathbf{B}_s^T \mathbf{D}(x) dx + \int_L \mathbf{B}_b^T \tau_x^b(x) dx - \mathbf{P}^* \right] + \\
& \delta \mathbf{p}^T \left[ - \int_L \mathbf{b}^T(x) \mathbf{f}_s(x) \mathbf{b}(x) dx \Delta \mathbf{p} + \int_L \mathbf{b}^T(x) \mathbf{B}_s(x) dx \Delta \mathbf{u} + \right. \\
& \left. \int_L \mathbf{b}^T(x) \mathbf{d}(x) dx - \int_L \mathbf{b}^T(x) \widehat{\mathbf{d}}(x) dx \right] = 0
\end{aligned} \tag{42}$$

where  $\mathbf{f}_s(x)$  is the section flexibility matrix and  $\widehat{\mathbf{d}}(x)$  is the section deformation vector determined from section force vector  $\widehat{\mathbf{D}}(x)$  with the help of the section flexibility matrix.

From arbitrariness of  $\delta \mathbf{u}$  and  $\delta \mathbf{p}$ , Eq. (42) can be written in the following matrix form:

$$\begin{aligned}
& \begin{bmatrix} \int_L \mathbf{B}_b^T \mathbf{K}_b \mathbf{B}_b dx & \int_L \mathbf{B}_s^T \mathbf{b} dx \\ \int_L \mathbf{b}^T \mathbf{B}_s dx & - \int_L \mathbf{b}^T \mathbf{f}_s \mathbf{b} dx \end{bmatrix} \begin{pmatrix} \Delta \mathbf{u} \\ \Delta \mathbf{p} \end{pmatrix} = \\
& \begin{pmatrix} \mathbf{P}^* - \int_L \mathbf{B}_s^T \mathbf{D} dx - \int_L \mathbf{B}_b^T \tau_x^b dx \\ \int_L \mathbf{b}^T (\widehat{\mathbf{d}} - \mathbf{d}) dx \end{pmatrix}
\end{aligned} \tag{43}$$

Eq. (43) can be written in the following concise form:

$$\begin{bmatrix} \mathbf{K}_B & \mathbf{G}^T \\ \mathbf{G} & -\mathbf{F}_{c+s} \end{bmatrix} \begin{pmatrix} \Delta \mathbf{u} \\ \Delta \mathbf{p} \end{pmatrix} = \begin{pmatrix} \mathbf{P}^* - \mathbf{P}_{c+s}^r - \mathbf{P}_b^r \\ \mathbf{u}^r \end{pmatrix} \quad (44)$$

where  $\mathbf{F}_{c+s}$  is the element flexibility matrix and  $\mathbf{u}^r$  is the element residual deformation vector. It is important to note that on convergence, the element residual deformation vector  $\mathbf{u}^r$  reduces to zero inside each element satisfying compatibility.

In this formulation, the force degrees of freedom are condensed out at the element level from Equations (44) resulting in a generalized stiffness matrix as follows:

$$\mathbf{G}^T [\mathbf{F}_{c+s}^{-1}] [\mathbf{G} \Delta \mathbf{u} - \mathbf{u}^r] + \mathbf{K}_B \Delta \mathbf{u} = \mathbf{P}^* - \mathbf{G}^T \mathbf{P}_{c+s}^r - \mathbf{P}_b^r \quad (45)$$

Once convergence is reached at element level i.e.  $\mathbf{u}^r$  becomes zero, Equation (45) can be written as follow:

$$(\mathbf{G}^T [\mathbf{F}_{c+s}^{-1}] \mathbf{G} + \mathbf{K}_B) \Delta \mathbf{u} = \mathbf{P}^* - \mathbf{G}^T \mathbf{P}_{c+s}^r - \mathbf{P}_b^r \quad (46)$$

$$(\mathbf{K}_{c+s} + \mathbf{K}_B) \Delta \mathbf{u} = \mathbf{P}^* - \mathbf{G}^T \mathbf{P}_{c+s}^r - \mathbf{P}_b^r \quad (47)$$

$$\mathbf{K}\Delta\mathbf{u} = \mathbf{P}^* - \mathbf{P}^r \quad (48)$$

The nodal displacements of the structural model in the global frame of reference are collected in the displacement vector  $\mathbf{U}^g$ . Detailed procedure of mapping structural nodal displacement relative to global coordinates to the element nodal deformation at the basic frame of reference, transformation of element stiffness matrix and resisting forces from basic to global level and assembling of global stiffness matrix and resistance forces of all elements to the assembled structural stiffness matrix  $\mathbf{K}^g$  and structural resistance vector  $\mathbf{P}^{gr}$  are described in details in Filippou et al. (2004).

#### 4.7.2.1 Stability Criteria

The two-field mixed based formulation requires both displacement and force shape functions. However, the order of displacement ( $n_d$ ) and force ( $n_f$ ) shape functions are interconnected through the compatibility and constitutive relations. Proper care should be taken to choose the order and continuity of both shape functions, otherwise non-meaningful results will be produced as observed by Zienkiewicz et al. (1989). According to De Veubeke's principle of limitation (1965), the order of stress quantity should be less than that of strain quantity to maintain stability of the algorithm.

For flexure critical mixed composite element formulation, a linear axial force distribution along the length of the element without the presence of axially distributed loads, require quadratic distribution of axial displacement. Whereas, a linear moment field along the length of the element requires linear curvature field which in turn requires cubic distribution of the vertical displacement field along the length of the element. Therefore the following relation can be written for flexure critical element as proposed by Ayoub (1999):

For axial field,

$$n_f = n_d - 1 \quad (49)$$

For moment field,

$$n_f = n_d - 2 \quad (50)$$

Using Hermitian polynomial shape functions for the vertical displacement field, two nodes beam element will be sufficient for dependent rotation field to satisfy the principle of limitation stability criteria for flexure critical condition. However, one additional middle degree of freedom for the axial

field will get statically condensed out at the element level before the assembly process.

For shear critical mixed composite element formulation, a linear axial force distribution along the length of the element without the presence of axially distributed loads, require quadratic distribution of axial displacement. Whereas, a linear moment field along the length of the element requires a linear curvature field which in turn requires quadratic distribution of rotation field along the length of the element. Whereas a constant shear force distribution along the length of the element requires a cubic vertical displacement field along the length of the element to match the same order of the rotation field. Therefore the following relations are proposed for the newly developed shear critical mixed element:

For axial field,

$$n_f = n_d - 1 \quad (51)$$

For moment field,

$$n_f = n_d - 1 \quad (52)$$

For shear field,

$$n_f = n_d - 3 \quad (53)$$

Using quadratic polynomial shape functions for axial and rotational fields, two nodes beam element will not be sufficient to satisfy the principle of limitation stability criteria for shear critical condition. Therefore, one additional middle degree of freedom for the axial and rotation field is must for shear critical two-field mixed beam element, which will get statically condensed out at the element level before the assembly process.

#### **4.7.2.2 State Determination**

A step by step summary of the state determination algorithm is presented below for a single composite element. A more detailed explanation can be found in Ayoub (1999). The summary focuses on a single global iteration  $i$  at the structural degrees of freedom through the Newton-Raphson method with applied load counter  $k$ .

*Step 1* to *Step 3* is similar to the section 2.9.2. However, concerned matrixes should be based on this chapter.

*Step 4:* Determine the incremental section deformation and slip and its update with respect to the basic axes of reference for a given element nodal force vector:

$$\Delta \mathbf{d}^j = [\mathbf{k}_{sec}^{j-1}]^{-1} (\mathbf{b} \Delta \mathbf{q}^j)$$

$$\mathbf{d}^{j+1} = \mathbf{d}^j + \Delta \mathbf{d}^j \quad (\text{Update of section deformation vector})$$

$$\mathbf{q}_{sec}^{j+1} = \mathbf{q}_{sec}^j + (\mathbf{b} \Delta \mathbf{q}^j) \quad (\text{Update of section force vector})$$

$$\Delta \mathbf{s}^i = \mathbf{B}_b(x) \Delta \mathbf{v}^{i+1}$$

$$\mathbf{s}^{i+1} = \mathbf{s}^i + \Delta \mathbf{s}^i \quad (\text{Update of slip})$$

*Step 5:* Determine the section tangent stiffness ( $\mathbf{k}_{sec}^{j+1}$ ) and resistance vector ( $\mathbf{p}_{sec}^{j+1}$ ) for a given section deformation vector with mid-point integration rule and material state determination as described in Section 2.8. Also, determine bond forces  $\tau_x^{b,i+1}$  and bond stiffness  $\mathbf{K}_b^{i+1}$  from the bond constitutive relations.

*Step 6:* Determine the element residual deformation and flexibility matrix and update the element nodal forces with updated section deformation and forces for the next element iteration until the norm of element nodal energy becomes less than the specified tolerance value to dissipate the element residual deformation:

$$\mathbf{f}_{ele}^{j+1} = \sum \mathbf{b}^T [\mathbf{k}_{sec}^{j+1}]^{-1} \mathbf{b}$$

$\mathbf{u}^{r,j+1} = \mathbf{u}^{r,j} + \sum \mathbf{b}^T [\mathbf{k}_{sec}^{j+1}]^{-1} (\mathbf{q}_{sec}^{j+1} - \mathbf{p}_{sec}^{j+1})$  (Update of element nodal residual deformation vector)

$$\mathbf{q}^{j+2} = \mathbf{q}^{j+1} - [\mathbf{f}_{ele}^{j+1}]^{-1} \mathbf{u}^{r,j+1}$$

$$\mathbf{d}^{j+2} = \mathbf{d}^{j+1} + [\mathbf{k}_{sec}^{j+1}]^{-1} (\mathbf{q}_{sec}^{j+1} - \mathbf{p}_{sec}^{j+1}) - [\mathbf{k}_{sec}^{j+1}]^{-1} (\mathbf{b} [\mathbf{f}_{ele}^{j+1}]^{-1} \mathbf{u}^{r,j+1})$$

$$\mathbf{q}_{sec}^{j+2} = \mathbf{q}_{sec}^{j+1} - (\mathbf{b} [\mathbf{f}_{ele}^{j+1}]^{-1} \mathbf{u}^{r,j+1})$$

*Step 7:* Determine the element stiffness matrix and resistance vector in iteration counter  $i$  for the given nodal element deformation upon the convergence of element compatibility at the basic frame of reference:

$$K_{ele}^{i+1} = K_{c+s}^{i+1} + K_B^{i+1}$$

$$K_{c+s}^{i+1} = G^T [f_{ele}^{j+1}]^{-1} G$$

$$K_B^{i+1} = \sum B_b^T K_b^{i+1} B_b$$

$$P^{r,i+1} = P_{c+s}^{r,i+1} + P_b^{r,i+1}$$

$$P_{c+s}^{r,i+1} = G^T q_{ele}^{i+1}$$

$$P_b^{r,i+1} = \sum B_b^T \tau_x^{b,i+1}$$

*Step 8:* Determine the element stiffness matrix and resistance vector in iteration counter  $i$  at the global frame of reference:

$$K_{ele,glo}^{i+1} = a_c^T K_{ele}^{i+1} a_c$$

$$Q_{ele,glo}^{i+1} = a_c^T P^{r,i+1}$$

# **Chapter 5 Correlation Studies – Shear Critical Steel-Concrete Composite Components**

## **5.1 Overview**

This chapter presents several correlation studies of the newly developed composite frame elements with partial interaction based on displacement and two-field mixed formulation with the numerical and experimental results of shear critical steel-concrete composite members.

Two different types of composite systems are considered for correlation studies i.e. steel-concrete-steel sandwiched systems and conventional steel-concrete composite bridge deck systems to establish the versatility of the proposed composite beam elements. Steel-concrete sandwiched components have recently gained popularity as efficient and cost effective blast resistance systems because of their larger energy dissipation capacity compared to that of conventional reinforced concrete systems. For these sandwiched systems, the shear stress transfer mechanism between steel face plates and surrounding concrete through shear studs, and the resulting shear slip, play an important role in determination of resistance and deformation capacity. There are mainly two types of analysis procedures used in the previous research work. Many researchers have developed their own analytical formulations based on simple assumptions and tried to

simulate the experimental behaviour. However, the complex nature of load resisting process, which involves material nonlinearity with multi-axial stress interactions, prevents the analytical solution to predict the global and local response throughout the loading histories. Therefore, many researchers have used detailed finite element analysis with continuum elements by using available commercial software to reproduce the experimentally observed responses. However, there is no beam-column fibre element developed to simulate the structural performance of steel-concrete sandwiched beams in the literature.

The correlation studies starts with the numerical and experimental studies of sandwiched steel-concrete composite beams followed by steel-concrete composite bridge deck beams to demonstrate the capability of the composite element formulations with implemented multi-axial material models.

## **5.2 SC Sandwiched Beam– Numerical Study**

In order to evaluate the accuracy and efficiency of the new element formulations, the comparison of the displacement vs. mixed formulation composite beam finite elements is conducted on a sample sandwiched beam problem (Figure 5-1). The beam span is 3000 mm. The beam is under

two points vertical loading 1000 mm away from each end. The shear span to depth ratio is 3.3. The top and bottom plate thickness is 8 mm each. Concrete section depth is 288 mm. The width of the beam section is 300 mm. The diameter of tie bar is 9.5 mm and spaced 240 mm along the length of the beam and 200 mm along the section width. The headed stud diameter is 13 mm and spaced 120 mm along the length of the beam and 100 mm along the section width. The concrete compressive strength is 40 MPa. The yield strength of steel material is 350 MPa and bond strength of shear stud is considered to be 150 MPa.

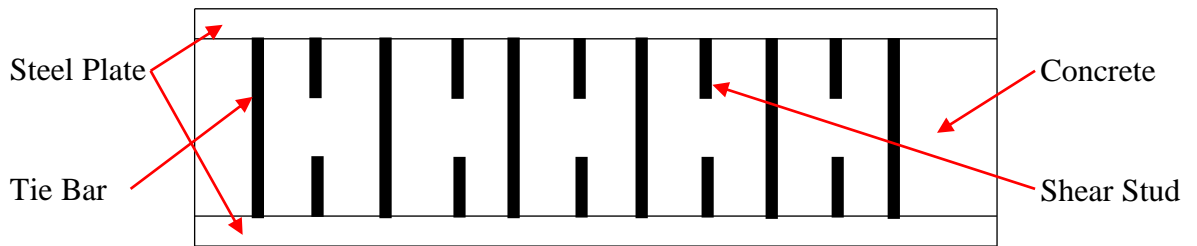


Figure 5-1. Geometry of Sandwiched Beam

It is to be noted that to model sandwiched members, the degrees of freedom at the section and element level need to be adjusted accordingly. Nine and three elements have been used to model the entire beam specimen for displacement and mixed based formulation respectively, with 5 section integration points in each element. For four point bending specimen, we need minimum three number of elements to represent two vertical point

loading on two respective nodes. For mixed based formulation, we have used one element in each span and total three number of elements are used. For displacement based formulation, in each span three number of elements are used i.e. total number of nine elements are used to achieve converged response. It should be noted that choice of number of elements depends on the boundary condition, applied loading condition, convergence and anticipated response information. Figure 5-2 presents the point load versus vertical deflection response of the member with the proposed beam elements.

The curvature distributions at different load stages, for both the minimum potential energy and mixed models are shown in Figure 5-3 and Figure 5-4 respectively. The two load stages A and B are shown in Figure 5-2. The curvature distribution of the displacement-based finite element shows a steep variation in the inelastic zone in the region near the point of application of vertical loads. Since the minimum potential energy model assumes a linear curvature field along the length of the member, it fails to represent the curvature distribution in the inelastic zone with few elements as shown in Figure 5-3. However, the mixed finite element model successfully represents the curvature distribution as shown in Figure 5-4 with just three elements, since section deformations are determined from equilibrated section forces.

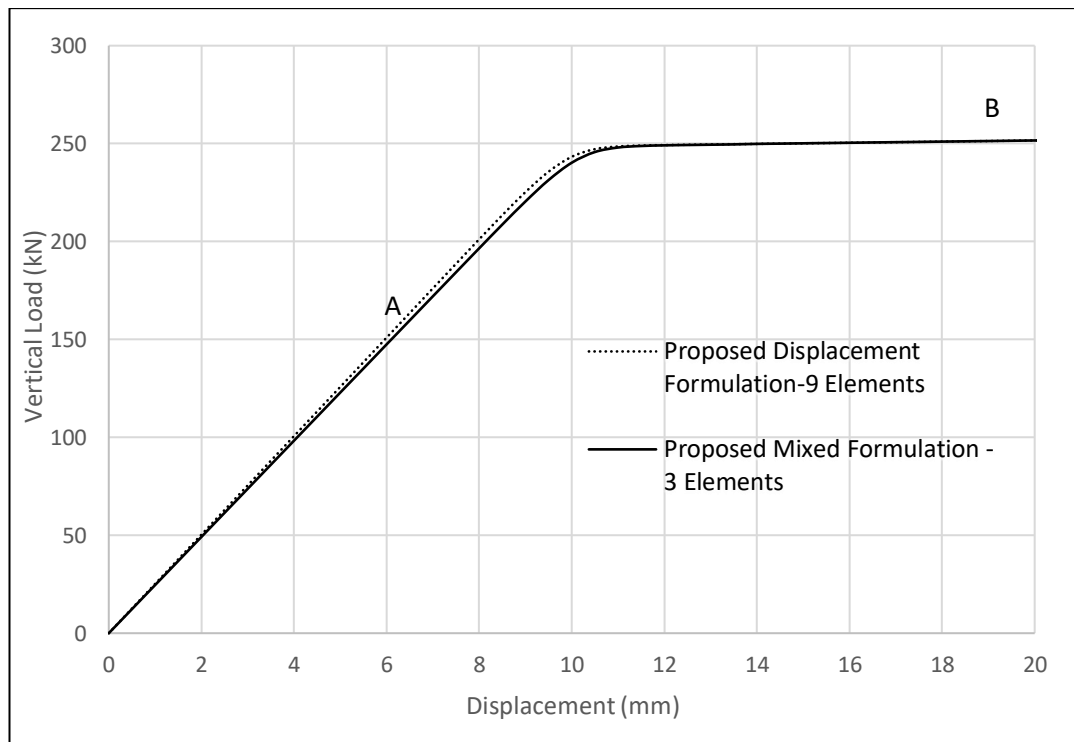


Figure 5-2. Load-Deflection Response

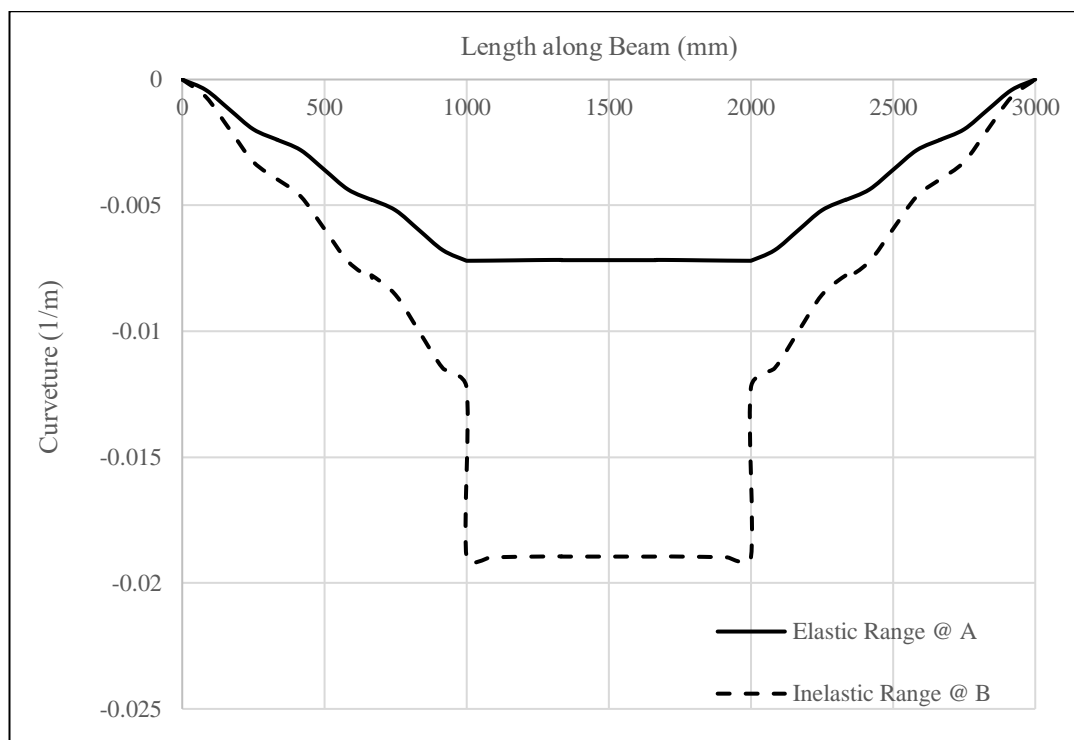


Figure 5-3. Curvature distribution (minimum potential energy principle)

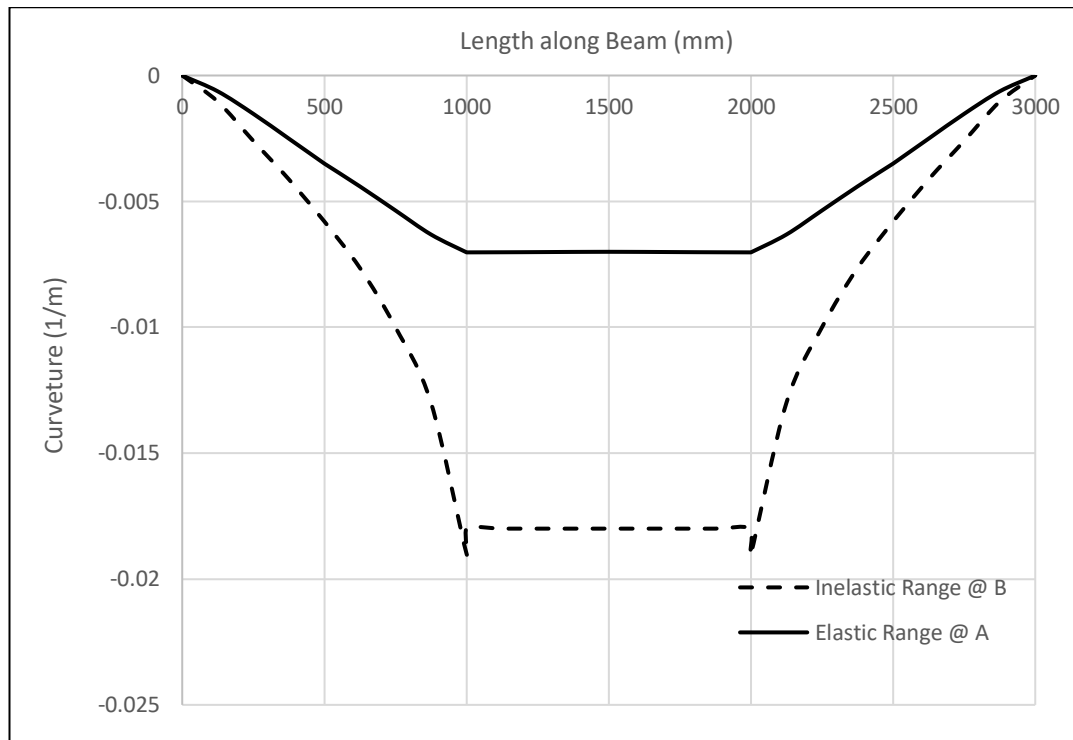


Figure 5-4. Curvature distribution (HR variational principle)

Figures 5-5 and 5-6 show the bending moment distributions for both models. The exact total resisting moment is linear in the absence of any distributed loads, irrespective of the presence of bond shear forces at the interface levels. The mixed model predicts the exact linear moment distribution as shown in Figure 5-5 at both elastic and inelastic zones, while the minimum potential energy model predicts a moment distribution which exhibits jumps at element boundaries as shown in Figure 5-6.

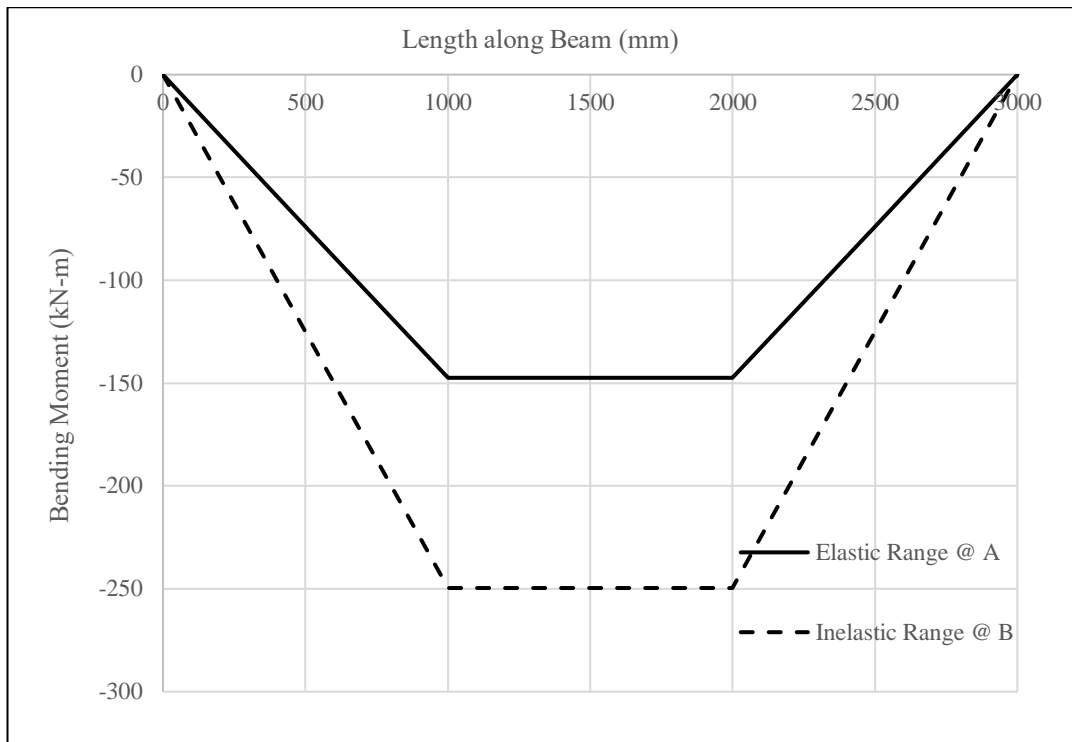


Figure 5-5. Bending moment distribution (HR variational principle)

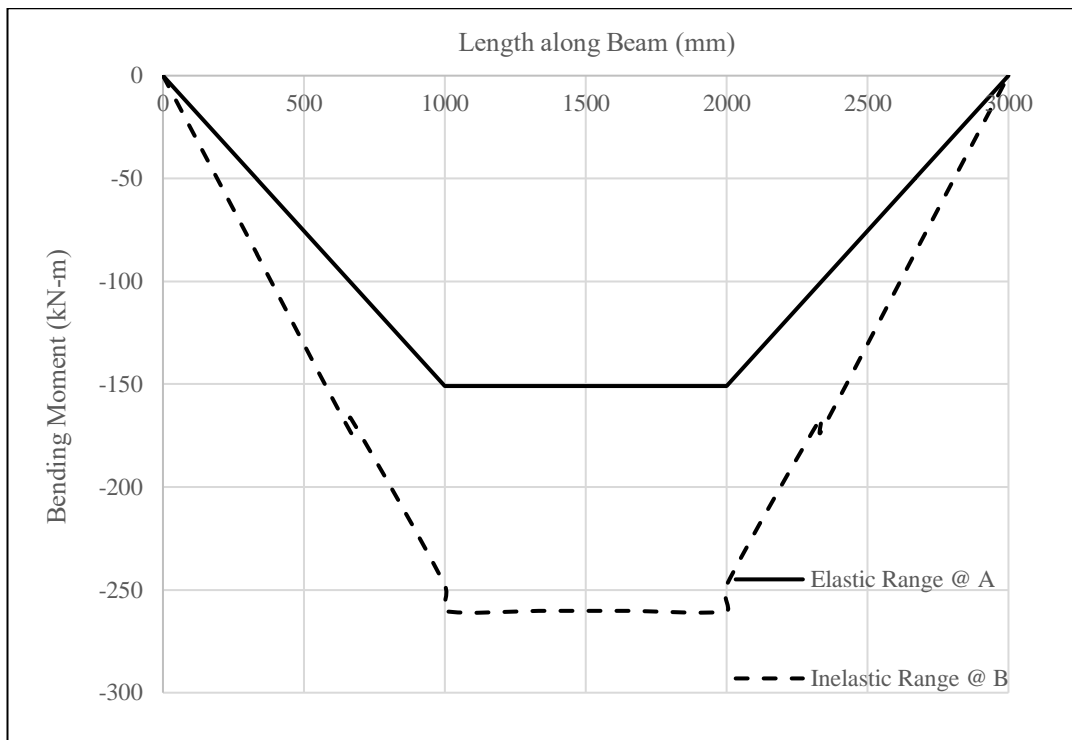


Figure 5-6. Bending moment distribution (minimum potential energy principle)

However, both minimum potential energy and mixed sandwiched models represent the slip distribution very well as shown in Figure 5-7 and Figure 5-8 respectively as both formulations determines slip values from displacement degrees of freedom.

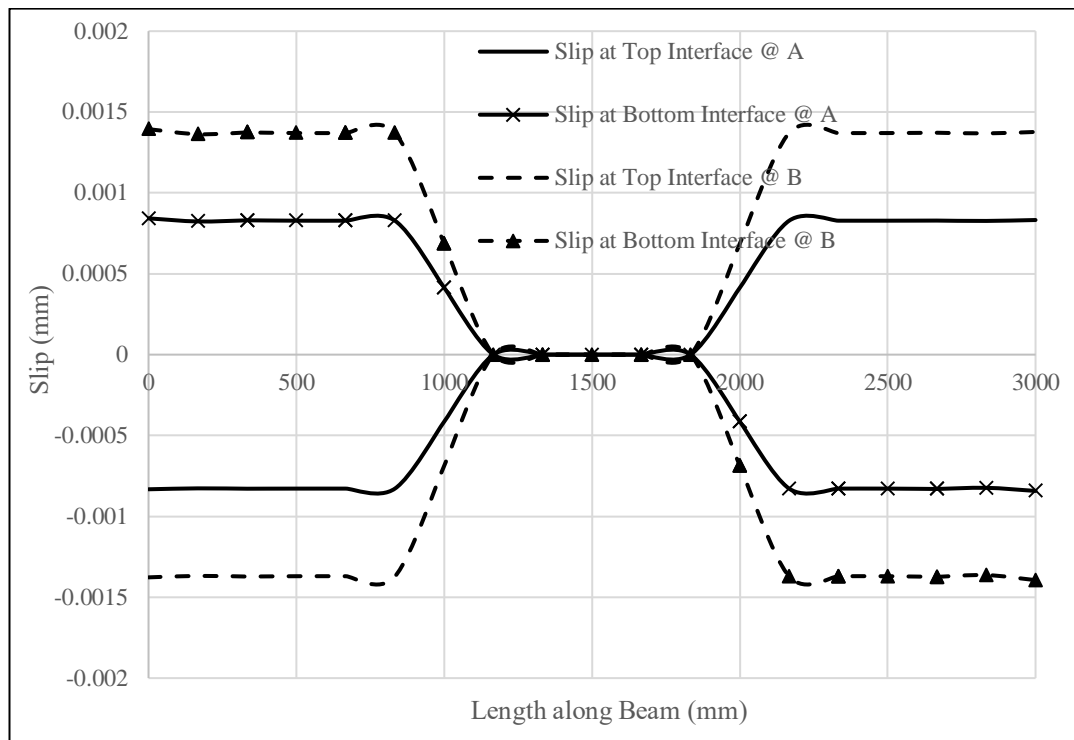


Figure 5-7. Slip distribution (minimum potential energy principle)

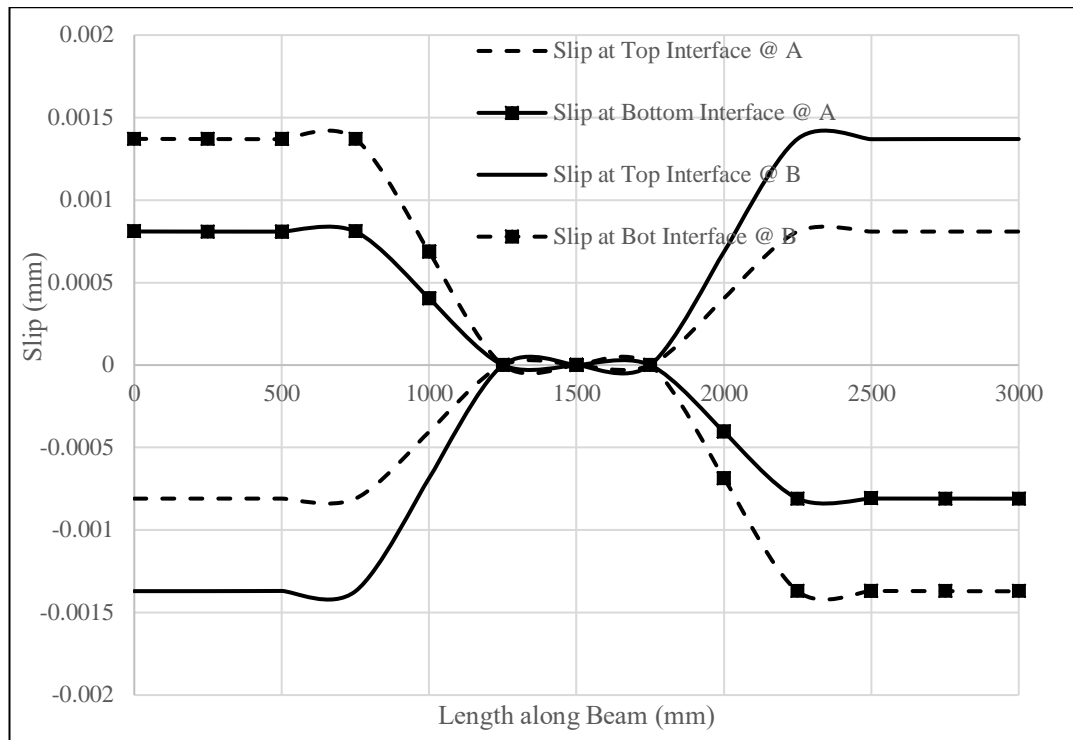


Figure 5-8. Slip distribution (HR variational principle)

Figures 5-9 and 5-10 show the bottom plate axial force distributions for both models. The mixed model clearly better predicts the axial force distribution than the minimum potential energy model which also exhibits nonlinearity and jumps at element boundaries.

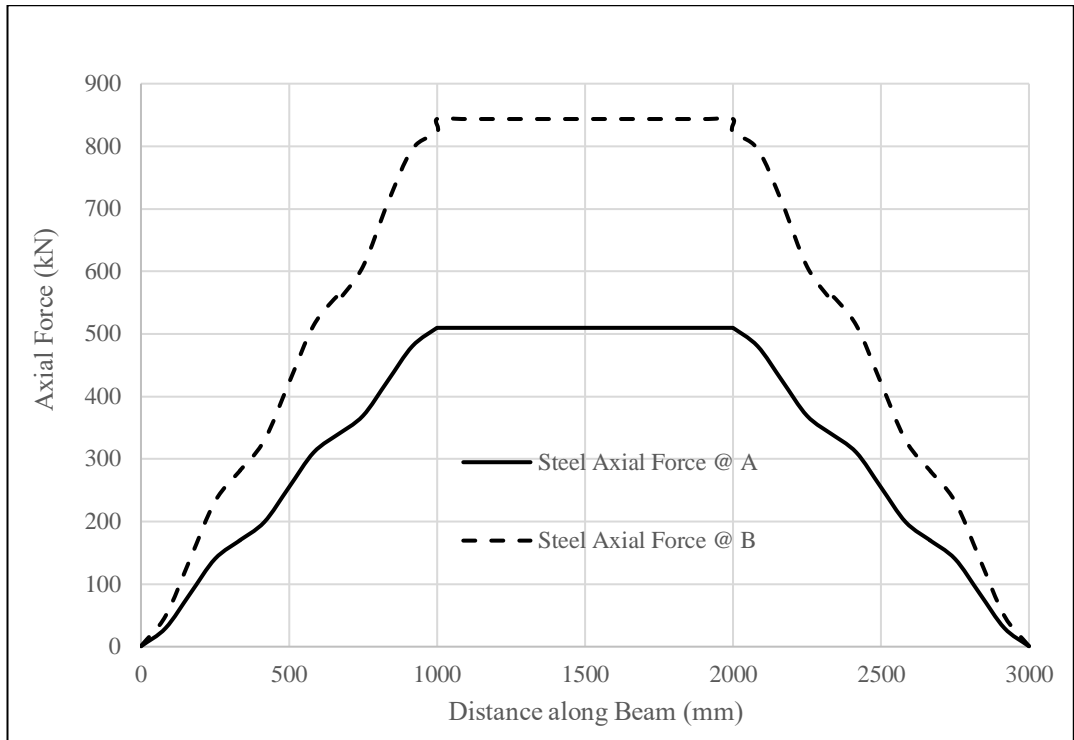


Figure 5-9. Bottom plate axial force distribution (minimum potential energy principle)

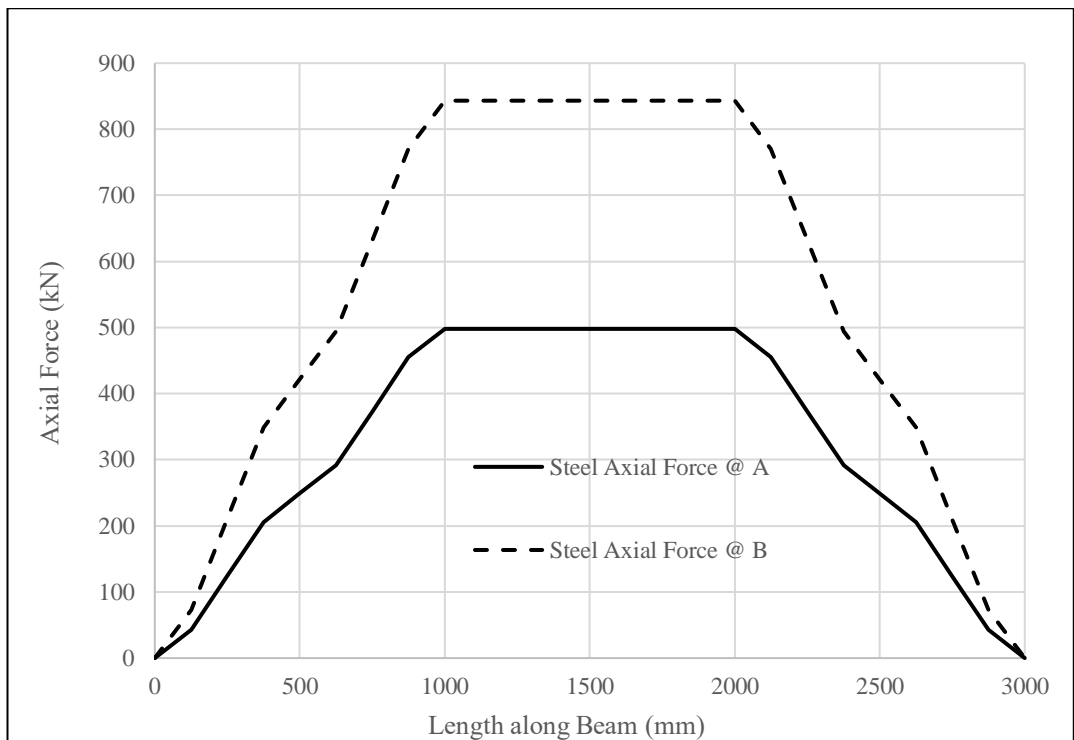


Figure 5-10. Bottom plate axial force distribution (HR variational principle)

This numerical example has established that the newly developed mixed element formulation is more accurate, efficient and computationally less expensive than the element formulation based on the principle of minimum potential energy.

### **5.3 SC Sandwiched Beam by Leng and Song (2016)**

Leng et al. (2016) performed tests on a series of 9 steel-concrete-steel sandwiched beams with shear span to depth ratio ranging from 2.5 to 3.5 under four point monotonic loading conditions to study the effect of shear span to depth ratio, the diameter and spacing of the vertical tie bars and stud connectors on the load-deformation response and failure modes of the composite beams. All beams failed in a vertical shear pattern, which was initiated from the tension plate failure near the critical crack, and tensile yielding of the tie bars after critical diagonal cracking. Slippage and separation between the bottom steel plate and concrete near the end of the critical diagonal crack has been observed in the experiment while the spacing of shear studs in the shear span is large.

Out of these specimens, the sandwiched beam JZ3.5-1 is chosen for the purpose of the correlation study. The beam span is 2600 mm. The beam is under two point vertical loading 1050 mm away from each end. The shear span to depth ratio is 3.5. The top and bottom plate thickness is 6 mm each.

The depth and width of the beam section is both 300 mm. The diameter of tie bar is 9.5 mm and spaced 240 mm along the length of the beam and 200 mm along the section width. The headed stud diameter is 13 mm and spaced 120 mm along the length of the beam and 100 mm along the section width. The concrete compressive strength is 40 MPa. The yield strength of steel plate, tie bar and shear stud are 350 MPa, 295 MPa and 365 MPa respectively. Bond strength of shear studs is considered as 146 MPa.

Sixteen and four elements have been used to model the entire sandwiched beam specimen for displacement and mixed based formulation respectively, with 5 section integration points in each element. Figure 5-11 presents the vertical load versus mid deflection response of the member with the proposed composite beam elements.

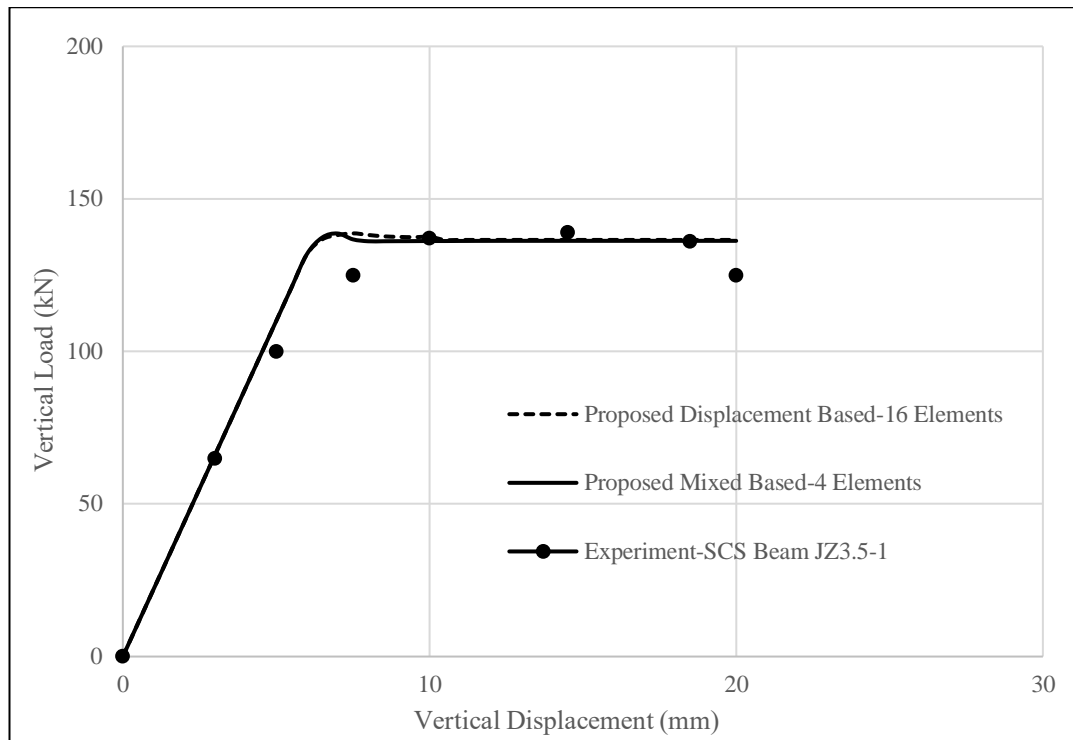


Figure 5-11. Load-Deflection Response of SCS beam JZ3.5-1

From the above plot, it can be observed that the proposed composite beam element formulations have reasonably reproduced the overall experimentally observed load-deflection response. However, it has produced stiffer response at the pre-peak shear strength slightly whereas, the ultimate shear resistance and shear deformation capacity have been captured well.

#### 5.4 SC Composite Beam by Nie, Xiao and Chen (2004)

Nie et al. (2004) conducted tests on a series of 16 steel-concrete composite beams under four point static loading conditions to investigate the effect of

shear span aspect ratio, the width and thickness of the concrete flanges on shear resisting mechanisms and the strength of composite beams. It has been concluded that the concrete shear contribution by concrete flange is 33% to 56% of the applied total ultimate shear, which motivated the development of composite beam element with partial interaction considering inelastic axial-flexure-shear interaction in both concrete and steel materials. Two types of shear failure modes in the concrete flange have been observed in the experiment i.e. diagonal tension failure and diagonal shear crushing. Shear yielding followed by local buckling in the web of steel sections has also been observed in the experiment for those specimens which failed in a shear mode.

Out of these specimens, the composite beam CBS-2 in which a shear failure mode has been observed in the experiment, is chosen for the purpose of the correlation study. The beam span is 2800 mm. The beam is under two point vertical loading 600 mm away from each end. The shear span to depth ratio is 2.0. Cross-section details of the composite beam are shown in Figure 5-12. The width and depth of concrete flange is 680 mm and 100 mm respectively. Reinforcement in the concrete flange along the composite beam axial direction and section width direction are provided with 100 mm spacing and a diameter of 6 mm.

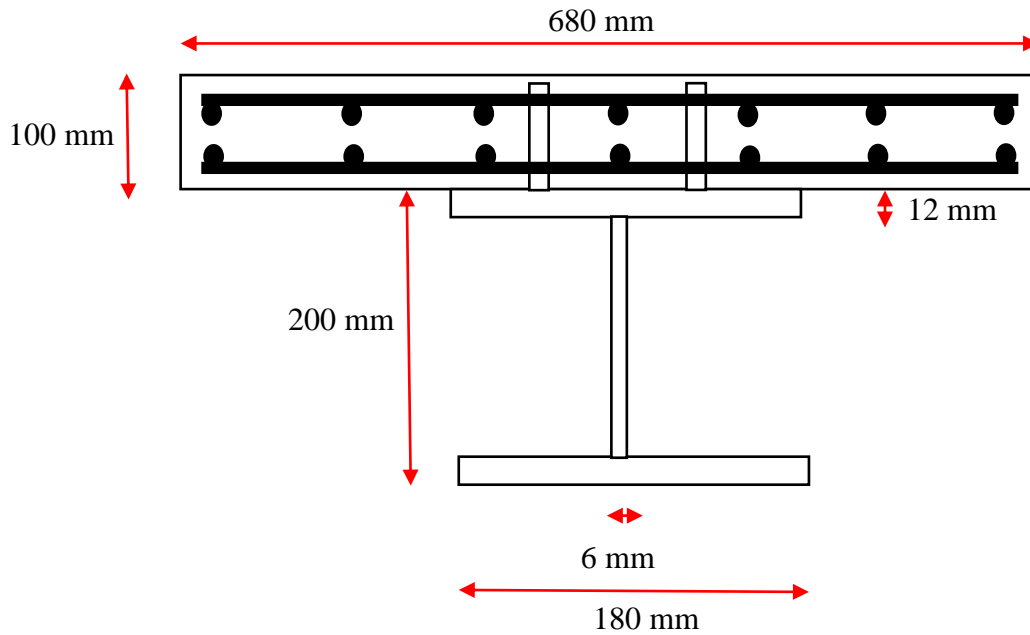


Figure 5-12. Cross-section of Composite Beam CBS-2

The headed stud diameter is 8 mm and spaced 90 mm along the length of the beam and 80 mm along the section width. The concrete compressive strength is 30.06 MPa. The yield strength of steel material in the web and flange regions are 340 MPa and 273 MPa respectively. Bond strength of shear stud is considered as 346 MPa.

Four elements have been used to model the entire composite beam specimen for mixed based formulation with 5 section integration points in each element. Figure 5-13 presents the vertical load versus mid deflection response of the member with the proposed composite beam element.

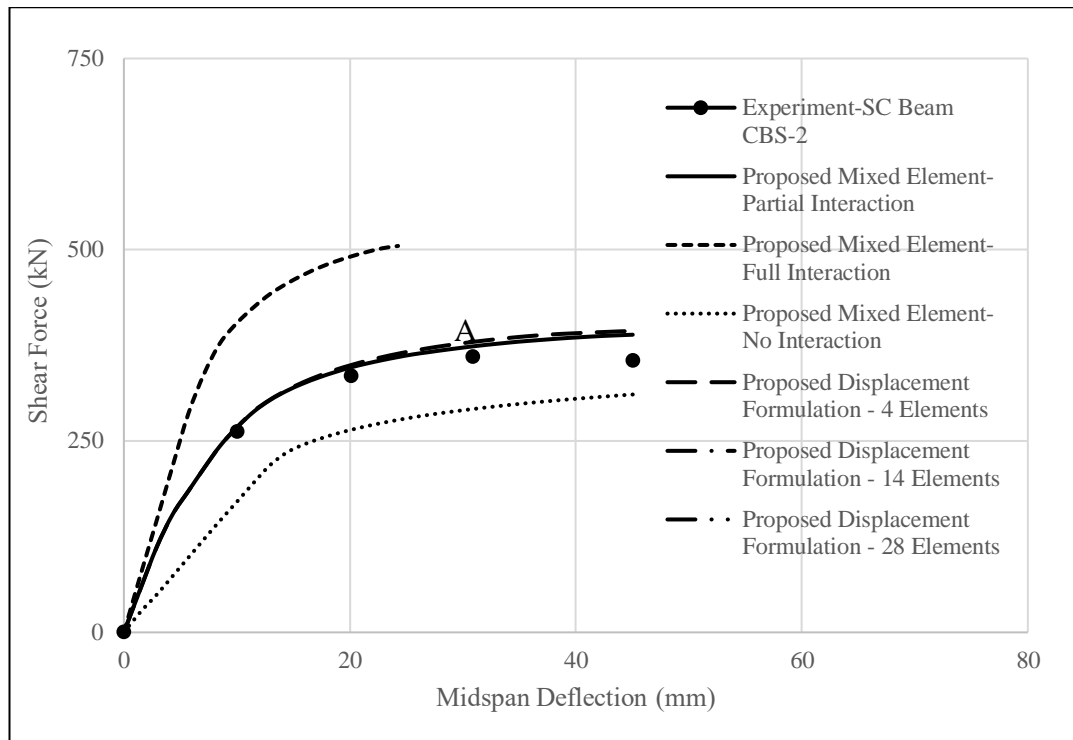


Figure 5-13. Load-Deflection Response of SC beam CBS-2

From the above plot, it can be observed that the proposed composite beam element formulation with partial interaction has reasonably reproduced the overall experimentally observed load-deflection response. Shear stiffness, ultimate shear resistance and shear deformation capacity have been captured well. It is also to be noted that shear resistance capacity gets increased while shear deformation capacity gets decreased when we consider full interaction by increasing the bond stiffness of shear studs. An opposite behaviour can also be observed while we reduce the bond stiffness significantly low for the no interaction situation. These observations once again emphasize the necessity to the formulation of shear critical composite frame element with partial interaction to simulate the shear behaviour

accurately which in turn will help to develop an inelastic analysis-driven design process of composite members. It can also be observed that 4, 14 and 28 elements with displacement based formulation and 4 elements for mixed based formulation produce essentially the same global load-deflection response under four point loading conditions.

Figure 5-14 and 5-15 show the shear force and deformation distribution along the length of the beam in the inelastic zone of the load-deflection response i.e. point A in Figure 5-13 respectively. It can be observed that both displacement and mixed formulation have excellently produced a smooth variation of shear force and deformation along the length of the beam. Similar observation of shear force distribution has also been reported by Zona et al.(2011) with displacement based formulation.

Figure 5-16 shows the interface slip distribution along the length of the beam in the inelastic zone of load-deflection response i.e. point A in Figure 5-13. It can be observed that both displacement and mixed formulation has essentially produced almost same distribution of relative slip along the length of the beam as the slip field has been determined from nodal displacement degrees of freedom for both the formulations.

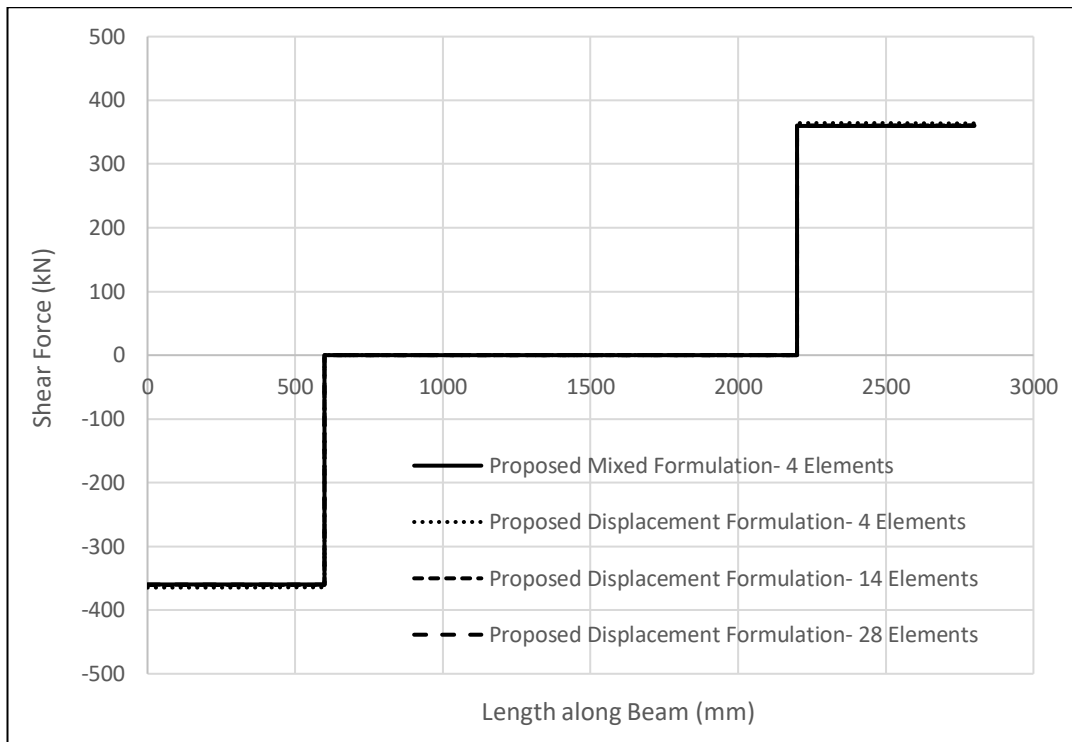


Figure 5-14. Shear Force distribution along the length of Beam

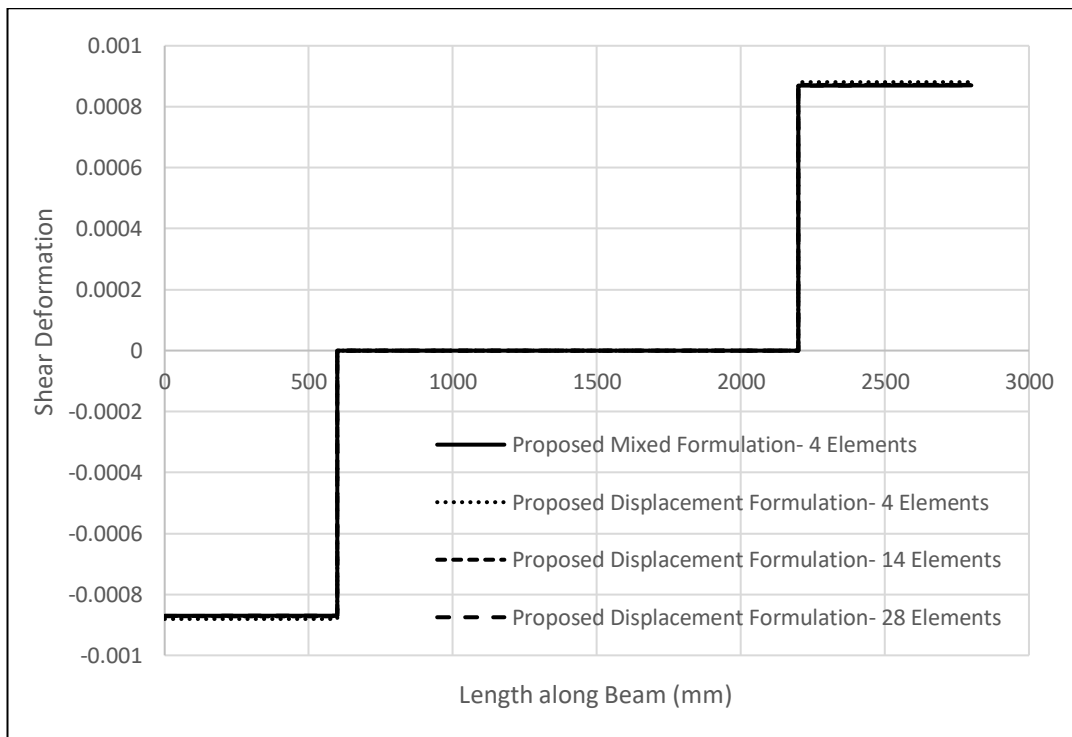


Figure 5-15. Shear Deformation distribution along the length of Beam

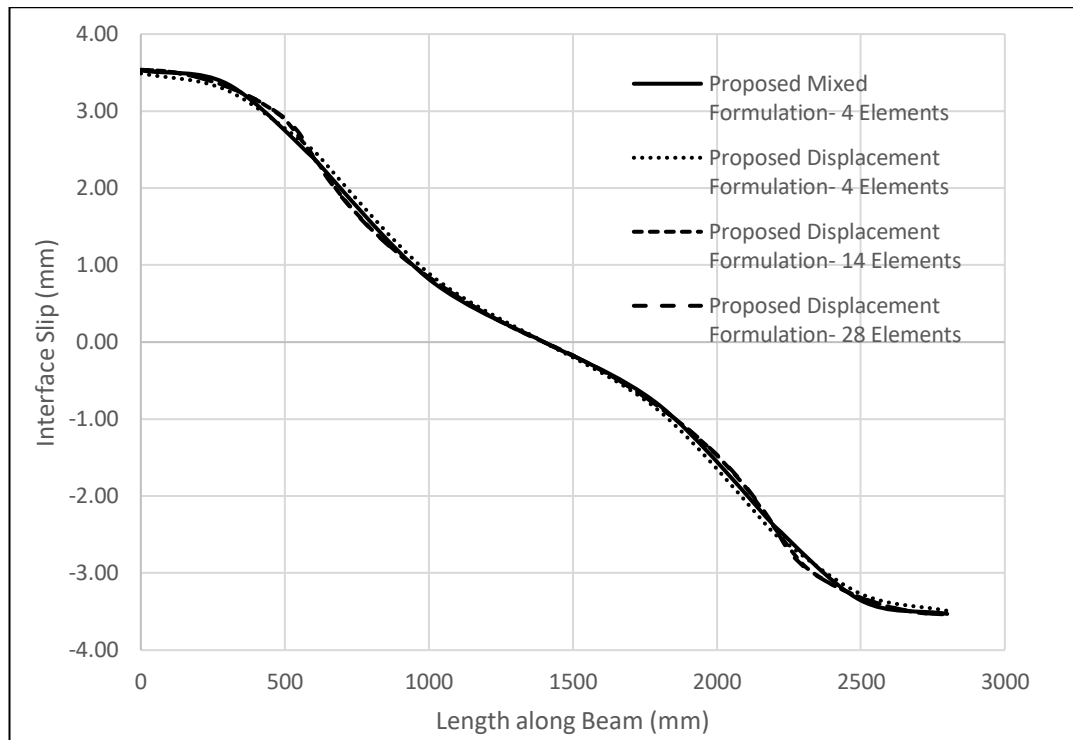


Figure 5-16. Interface Slip Distribution along the Length of Beam

Figure 5-17 and 5-18 show axial deformation distribution along the length of the beam in the inelastic zone of load-deflection response i.e. point A in Figure 5-13 for steel and concrete section respectively. It can be observed that the mixed formulation with 4 elements, has excellently produced an inelastic variation of axial deformation at the applied loading region as expected. However, the displacement based formulation has shown a reasonable performance when the number of elements has been increased to 28. It is to be noted that larger number of elements are required to successfully simulate the local response for displacement based formulations compared to that of the global response.

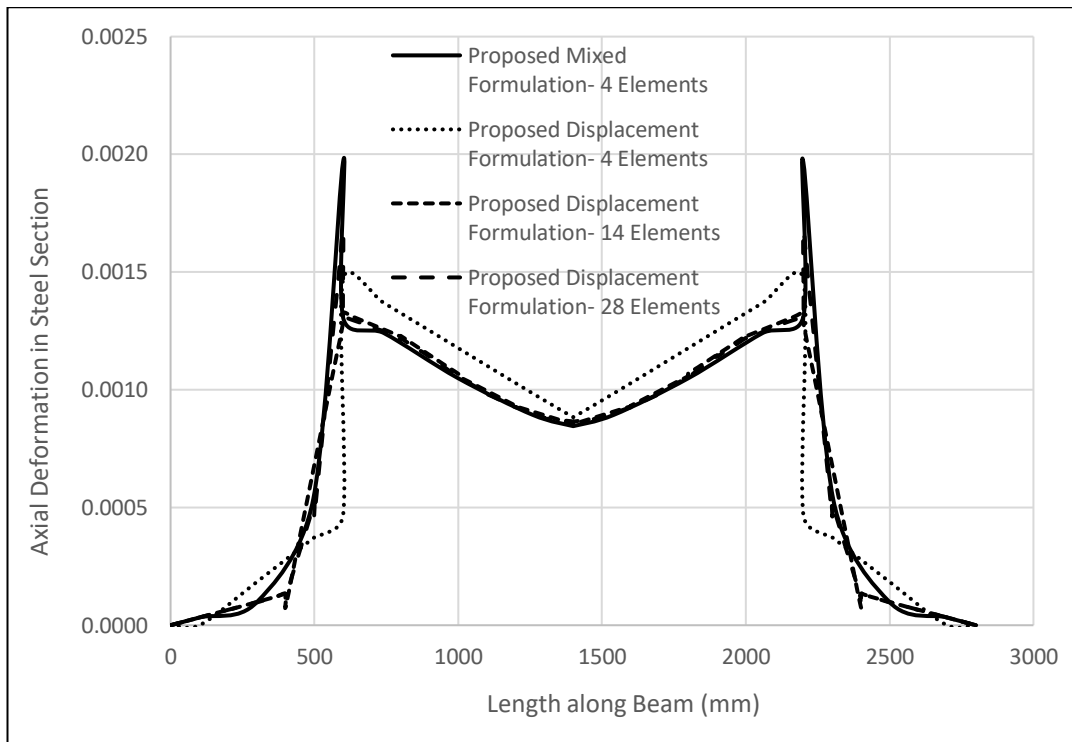


Figure 5-17. Axial Deformation distribution along the length of Beam in Steel Section

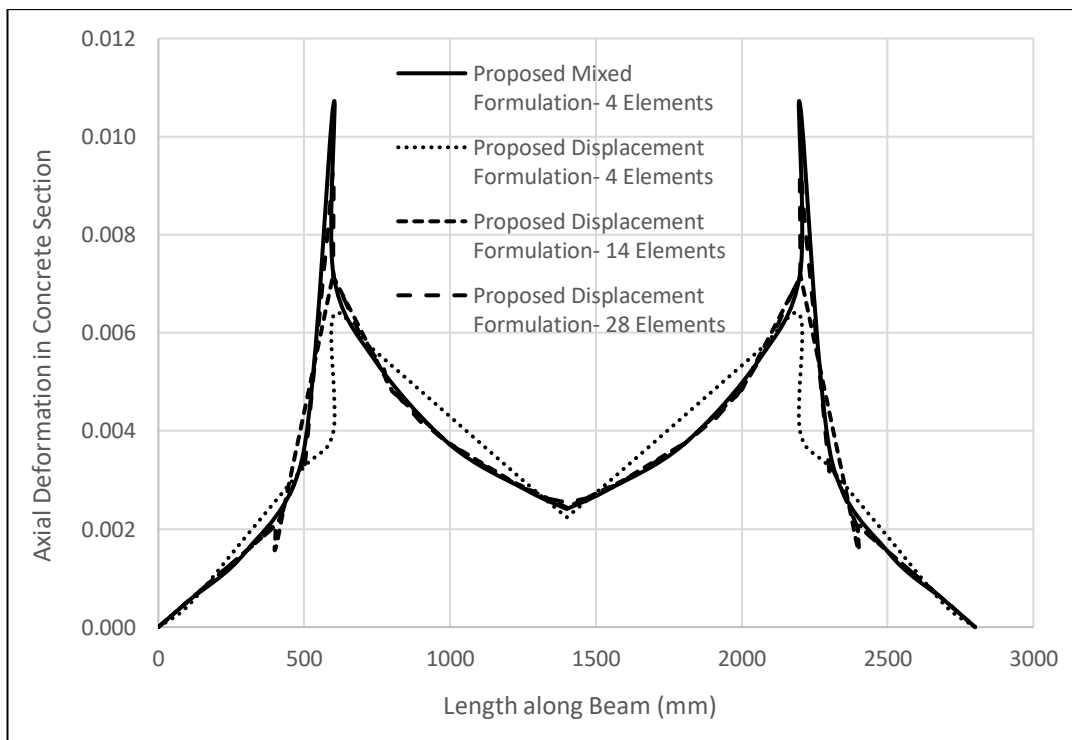


Figure 5-18. Axial Deformation distribution along the length of Beam in Concrete Section

Figure 5-19 shows the shear crack angle distribution along the length of the beam in the inelastic zone of the load-deflection response i.e. point A in Figure 5-13 for the middle fibre of the concrete section. It can be observed that the mixed formulation has excellently produced the accurate variation of shear crack angle at the applied loading region as observed in the experiment. However, the displacement based formulation has shown a reasonable performance when the number of elements has been increased.

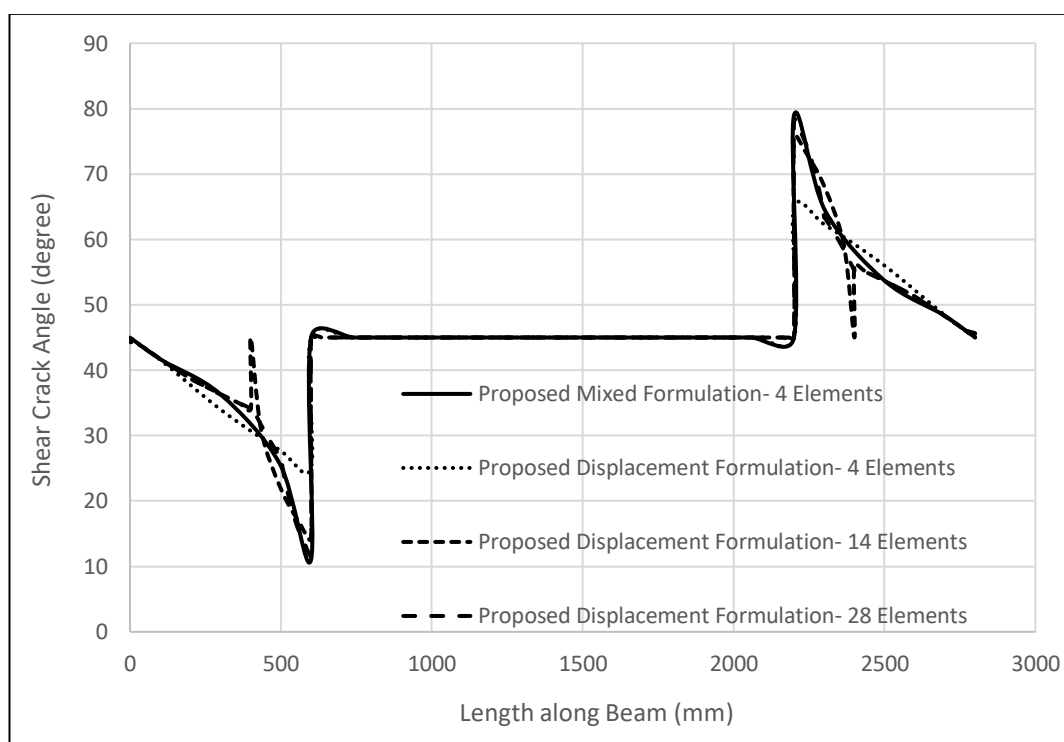


Figure 5-19. Shear Crack Angle distribution along the length of Beam in Middle fibre of Concrete Section

Figure 5-20 and 5-21 show axial force distribution along the length of the beam in the inelastic zone of load-deflection response i.e. point A in Figure 5-13 for steel and concrete section respectively. It can be observed that the mixed formulation with 4 elements, has excellently produced a smooth

linear variation of axial force along with exact equilibrium between steel and concrete axial section force. However the displacement based formulation has shown a jump at the element boundaries and reasonable performance has been achieved when the number of elements has been increased to 28. It is to be noted that larger number of elements are required to successfully simulate the local response for displacement based formulations compared to that of the global response. The aforementioned results have verified the superiority of mixed-based formulation relative to displacement-based formulation.

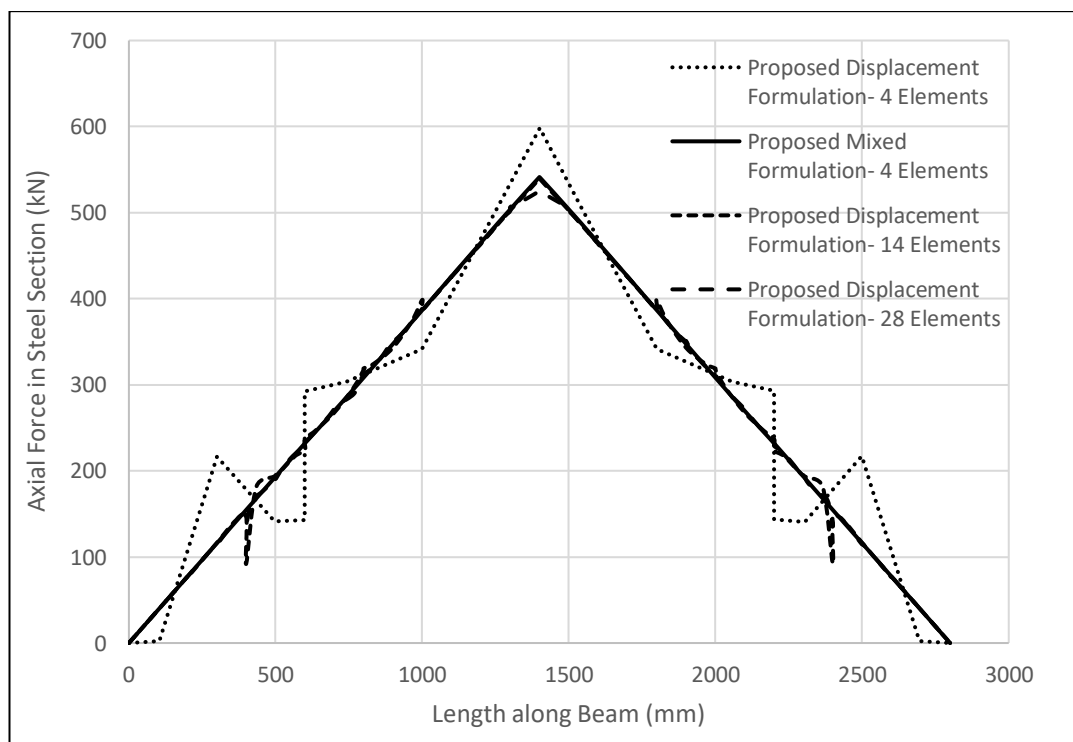


Figure 5-20. Axial Force distribution along the length of Beam in Steel Section

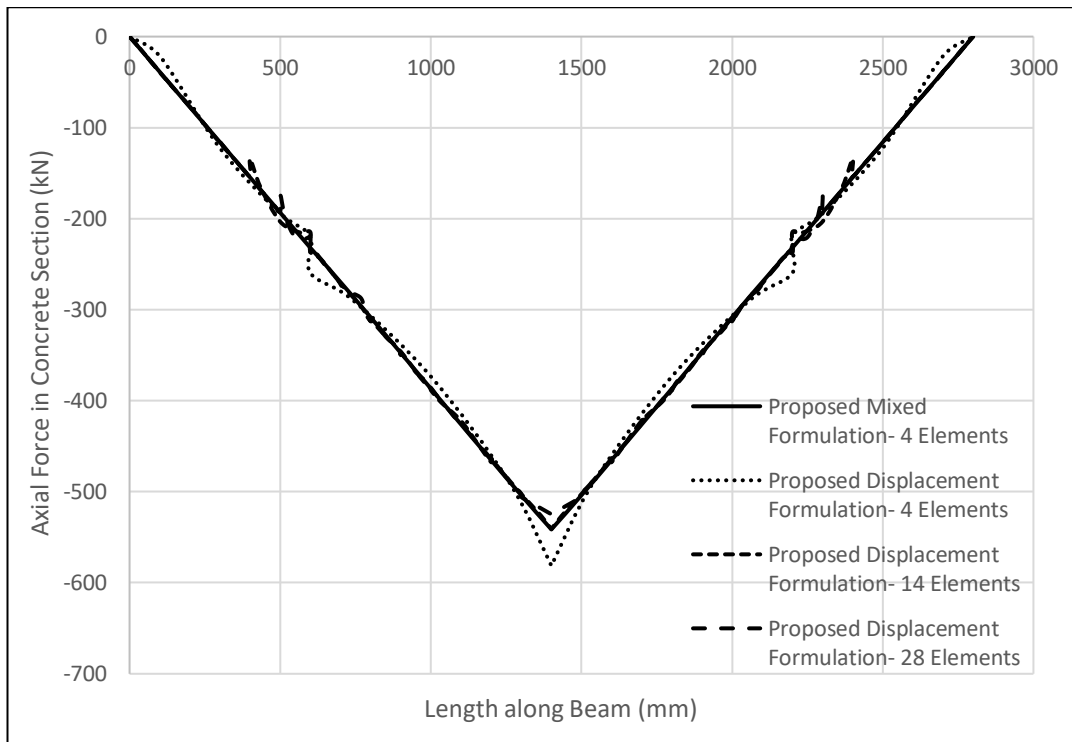


Figure 5-21. Axial Force distribution along the length of Beam in Concrete Section

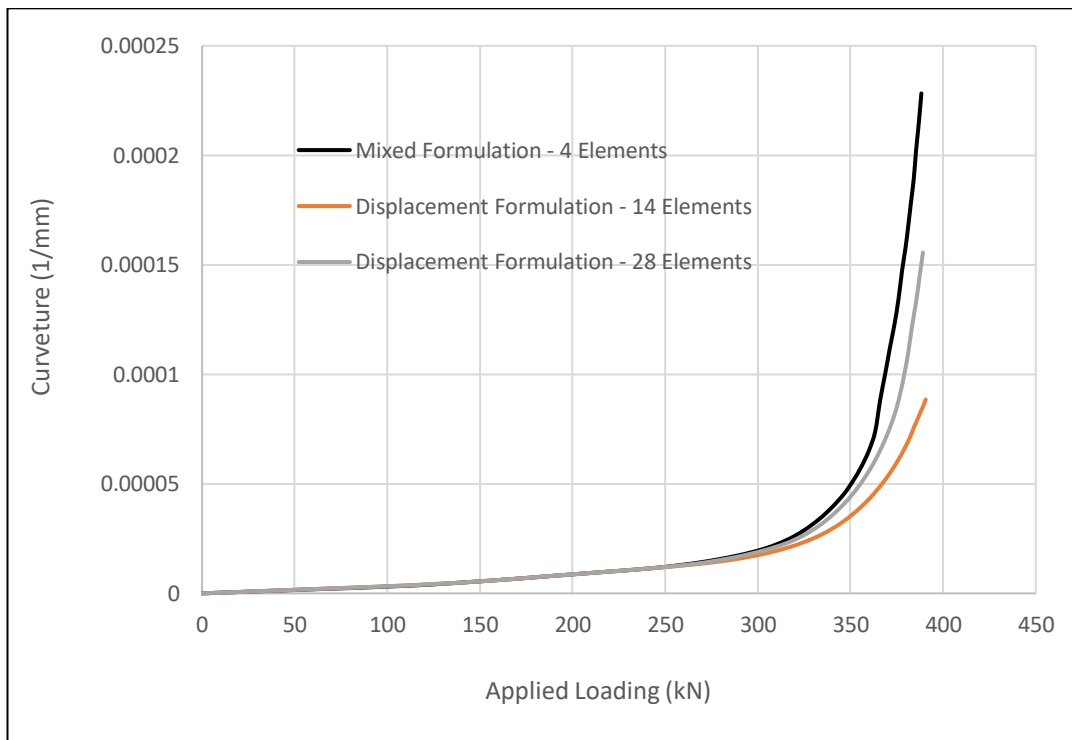


Figure 5-22. Curvature-Loading Response at loading point

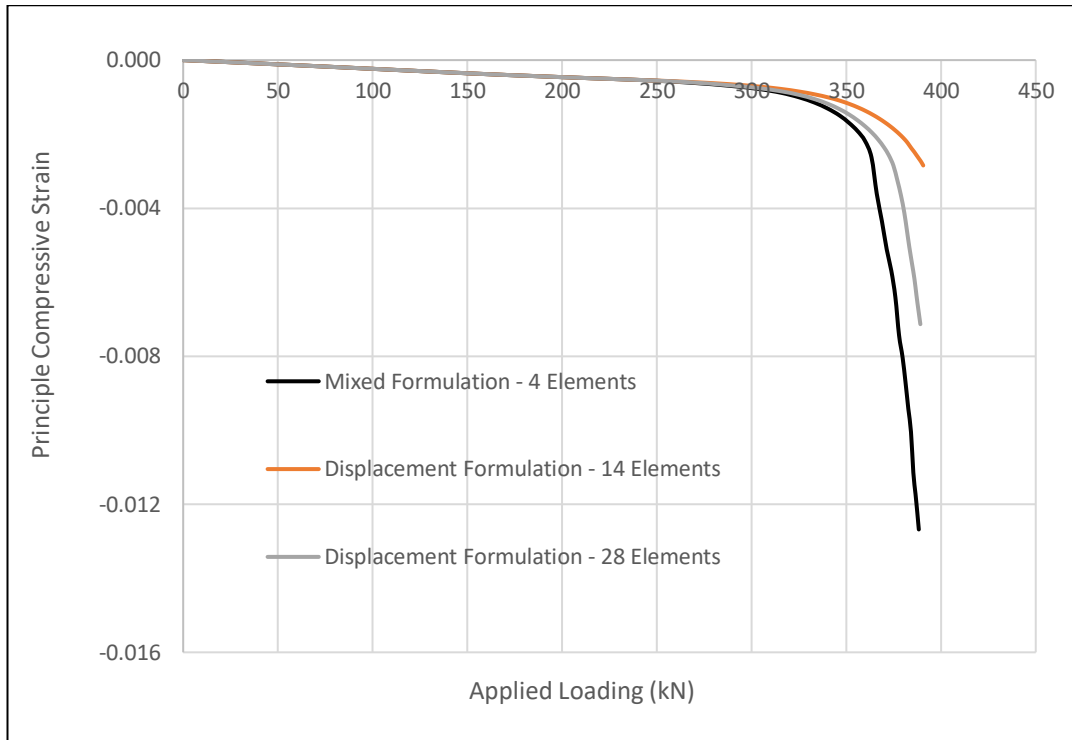


Figure 5-23. Principle Compressive Strain-Loading Response of top concrete fibre at loading point

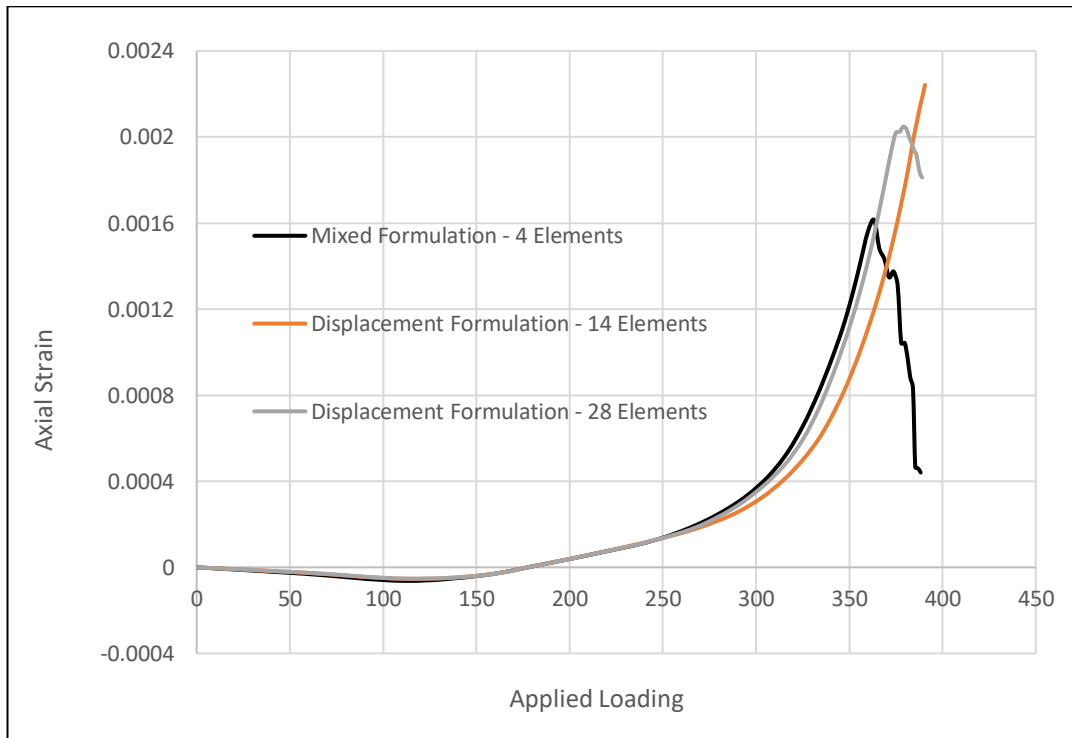


Figure 5-24. Axial Strain-Loading Response of bottom rebar of concrete deck at loading point

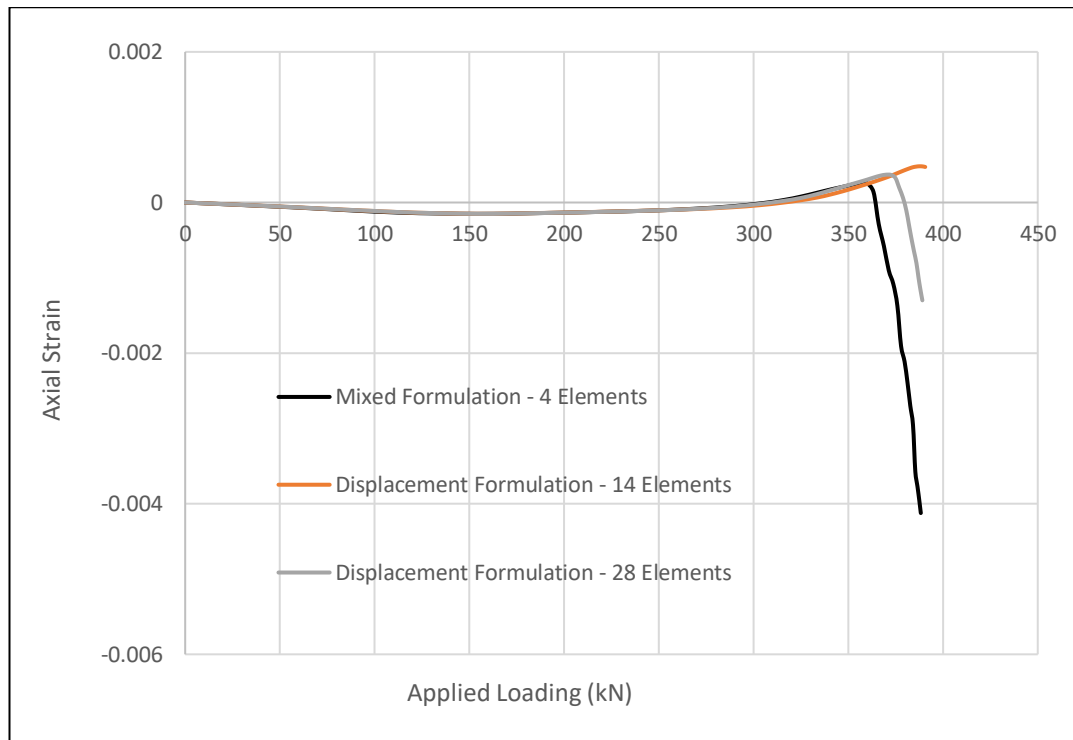


Figure 5-25. Axial Strain-Loading Response of top rebar of concrete deck at loading point

Figure 5-22 shows the curvature-loading response at the loading point. It can be observed that mixed formulation with 4 elements excellently produced localized curvature distribution compared to that of displacement based formulation with 28 elements.

From Figure 5-23, it can be observed that principle compressive strain of top concrete fibre in the concrete deck reach substantial amount value. Displacement based formulation is not able to produce the result even with 28 elements compared to its counterpart.

Figure 5-24 shows the axial strain-loading response of bottom rebar in the concrete deck at loading point. It can be observed that strain does not exceed the yield limit and it gets unloaded at the later stage of loading. This signifies that flexural action does not dominate in the concrete deck. Shear energy resist the external input energy. This local behaviour has been excellently produced by the mixed formulation. Displacement based formulation is not able to reproduce this kind of local behaviour even with large number of elements.

Figure 5-25 shows the axial strain-loading response in the compression rebar at the concrete section. It is to be noted from Figure 5-21 that concrete section remains under compressive stress condition. It should be realized that compressive strain in the top rebar gets unloaded at the later stage of loading. As a result, the rebar reaches in the tensile zone and also the peak amount of compressive strain is substantially less than that of top concrete fibre (Figure 5-23). This observation indicates that the flexure energy in the concrete deck does not play important role at the later stage of loading as the shear energy dominates and resists the external input energy.

These results confirm that proposed mixed formulation is capable of simulating the global and local behaviour of shear critical composite beams

along with failure modes. Moreover, inherent limitations of displacement based formulation to reproduce local behaviour even with large number of elements is a warning sign. The need of mixed based shear composite element which can successfully reproduce local behaviour and will help to formulate inelastic analysis driven design process, has been established through this research work.

# **Chapter 6 Shear Critical Frame Element – Mixed Formulation considering Geometric Nonlinearity**

## **6.1 Overview**

In this chapter, we are going to develop a new shear critical frame element based on distributed inelasticity approach considering large displacement effects. Experimentally it has been observed that under seismic loading condition, P-Delta effect is predominant after the peak shear strength softening zone. Also, for other loading scenario such as impact and blast loading conditions where flexurally-designed members fail in a shear mode, the effect of large displacement is inevitable on load-deformation response of members. Therefore, it is imperative to develop a frame element which can simulate large displacement effects with material inelasticity considering shear deformation. In the following, we will first discuss the element kinematics following the corotational approach and then section kinematics by adopting the degenerated form of Green-Lagrange strain measures. Later on, we will discuss the variational formulation of the two-field mixed based formulation with the help of Hellinger-Reissner functional. Stability criteria needed for mixed formulation along with detailed state determination process will also be discussed. It is to be noted that the newly developed distributed inelasticity based frame element considering large displacement effects with shear

deformation is a one step forward to develop an inelastic analysis-driven design process such as the performance based design methodology for reinforced concrete and steel systems in a more rational way.

The current research work aims to extend the newly developed two-field mixed-based formulation for shear critical reinforced concrete members by implementing coupled multi-axial constitutive laws for materials, along with new stability criteria (Chapter 2) to account for geometric nonlinearity effect. To achieve this purpose, the described new shape function (Section 2.1) for transverse displacement varying with cubic function along the length of the element has been used in our research work.

## **6.2 Element Kinematics**

The axis of the proposed frame element is a straight line joined by nodes I and J in the statically determinate basic reference system in which rigid body displacements are removed by choosing the simple supported boundary conditions as shown in Figure. 6-1. The frame element is composed of several sections along its axis. Every section is composed of several fibres which are identified by their position from the reference axis and individual cross-section area.

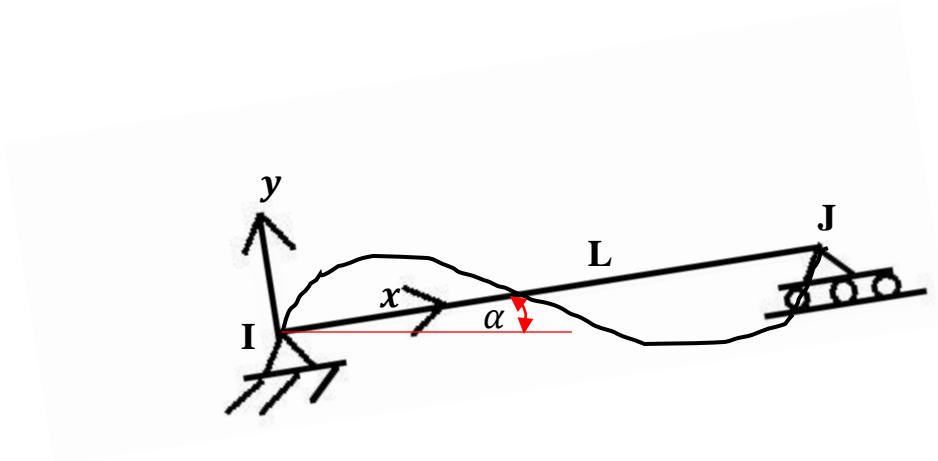


Figure 6-1. Basic reference system without rigid body modes

The section displacement vector  $\mathbf{u}(x)$  collects the two translations  $u(x), v(x)$  in  $x$  and  $y$  directions respectively and one rotation  $\theta_z(x)$  about  $z$  axis.

$$\mathbf{u}(x) = [u(x)\theta_z(x) \quad v(x)]^T \quad (1)$$

The element nodal displacement vector  $\mathbf{u}_{IJ}$  collects the nodal displacement with respect to the global axes according to the section displacement vector in Equation (1). In the proposed frame element an additional middle nodal rotational degree of freedom is included which has been statically condensed out at the element level before the assembly process.

$$\mathbf{u}_{IJ} = [u_I v_I \theta_{zI} \quad u_J v_J \theta_{zJ} \theta_{zK}]^T \quad (2)$$

The element deformation vector  $\mathbf{v}$  collects the relative translation  $u$  at node J in  $x$  direction, rotations  $\theta_z$  at nodes I and J and middle node k with respect to the basic reference axes as shown in Figure. 6-2.

$$\mathbf{v} = [u \ \theta_{zI} \ \theta_{zJ} \ \theta_{zK}]^T \quad (3)$$

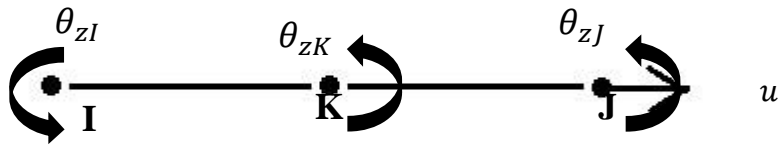


Figure 6-2. Element nodal deformations

The relation between element nodal deformation  $\mathbf{v}$  and displacements  $\mathbf{u}_{IJ}$  can be uniquely determined by the compatibility matrix  $\mathbf{a}_c$  under deformed geometry conditions where  $L$  is the deformed length of the element.

$$\mathbf{v} = \mathbf{a}_c \mathbf{u}_{IJ} \quad (4)$$

Where,

$$\mathbf{a}_c = \begin{bmatrix} -\frac{1}{L} \sin \alpha & \frac{1}{L} \cos \alpha & 1 & \frac{1}{L} \sin \alpha & -\frac{1}{L} \cos \alpha & 0 & 0 \\ -\cos \alpha & -\sin \alpha & 0 & \cos \alpha & \sin \alpha & 0 & 0 \\ -\frac{1}{L} \sin \alpha & \frac{1}{L} \cos \alpha & 0 & \frac{1}{L} \sin \alpha & -\frac{1}{L} \cos \alpha & 1 & 0 \\ -\frac{1}{L} \sin \alpha & \frac{1}{L} \cos \alpha & 0 & \frac{1}{L} \sin \alpha & -\frac{1}{L} \cos \alpha & 0 & 1 \end{bmatrix}$$

Where,

$$L = \sqrt{((x_2 - x_1) + (u_J - u_I))^2 + ((y_2 - y_1) + (v_J - v_I))^2}$$

$$\sin \alpha = \frac{(y_2 - y_1) + (v_J - v_I)}{L}$$

$$\cos \alpha = \frac{(x_2 - x_1) + (u_J - u_I)}{L}$$

$(x_1, y_1)$  and  $(x_2, y_2)$  are initial co-ordinates of node I and J respectively.

### 6.3 Section Kinematics

Under the assumption of a Timoshenko beam theory, the displacements  $u^m(x, y)$  of a material point  $m$  with coordinate  $y$  at a section with distance  $x$  from the origin of the reference frame can be represented with the cross-section generalized displacements  $\mathbf{u}(x)$  as follows:

$$u_x^m(x, y) = u(x) - y\theta_z(x) \quad (5)$$

$$v_x^m(x, y) = v(x) \quad (6)$$

The material strain displacement vector  $\boldsymbol{\varepsilon}(x, y)$  following the degenerated form of Green-Lagrange strain measures, can be related with material displacement vector  $u^m(x, y)$  as follows:

$$\varepsilon_{xx} = \frac{\partial u_x^m(x, y)}{\partial x} + \frac{1}{2} \left( \frac{\partial v(x)}{\partial x} \right)^2 = \frac{\partial u(x)}{\partial x} + \frac{1}{2} \left( \frac{\partial v(x)}{\partial x} \right)^2 - y \frac{\partial \theta_z(x)}{\partial x} \quad (7)$$

$$\varepsilon_{yy} = \frac{\partial v_x^m(x, y)}{\partial y} = \frac{\partial v(x)}{\partial y} = 0 \quad (8)$$

$$2\varepsilon_{xy} = \frac{\partial u_x^m(x, y)}{\partial y} + \frac{\partial v_x^m(x, y)}{\partial x} = -\theta_z(x) + \frac{\partial v(x)}{\partial x} \quad (9)$$

By introducing the section deformation vector  $\mathbf{d}(x)$  which is a function of section displacement vector  $\mathbf{u}(x)$ , we can write down the following equation with the help of section compatibility matrix  $\mathbf{a}_s(y)$ :

$$\boldsymbol{\varepsilon}(x, y) = \mathbf{a}_s(y) \mathbf{d}(x) \quad (10)$$

Where,

$$\mathbf{d}(x) = \left[ \frac{\partial u(x)}{\partial x} + \frac{1}{2} \left( \frac{\partial v(x)}{\partial x} \right)^2 \frac{\partial \theta_z(x)}{\partial x} \quad \left( -\theta_z(x) + \frac{\partial v(x)}{\partial x} \right) \right]^T$$

$$\mathbf{a}_s(y) = \begin{bmatrix} 1 & -y & 0 \\ 0 & 0 & 1 \end{bmatrix}$$

## 6.4 Equilibrium

The differential equilibrium equation of a segment of length  $dx$  as shown in Figure.6-3 can be written down as follows:

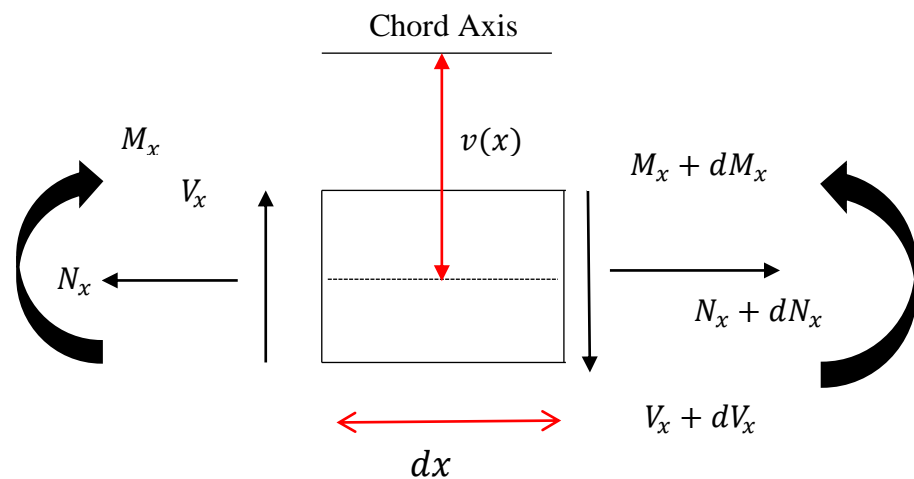


Figure 6-3. Section differential equilibrium

$$\frac{dN_x}{dx} = 0 \tag{11}$$

$$\frac{dM_x}{dx} - V_x = 0 \quad (12)$$

$$\frac{dV_x}{dx} - \frac{d}{dx} \left( N_x \frac{dv(x)}{dx} \right) = 0 \quad (13)$$

Where  $N_x, M_x, V_x$  are axial force, bending moment and shear force respectively.

## 6.5 Compatibility

The components of generalized section deformation vector  $\mathbf{d}(x)$  are the axial strain  $\varepsilon_0$  at the reference  $x$  axis, the curvature  $\phi_z$  about the  $z$  axis and shear deformation  $\gamma_y$  in the  $y$  direction respectively following the degenerated form of Green-Lagrange strain measure:

$$\mathbf{d}(x) = [\varepsilon_0 \phi_z \gamma_y]^T \quad (14)$$

Where

$$\varepsilon_0 = \frac{du(x)}{dx} + \frac{1}{2} \left( \frac{\partial v(x)}{\partial x} \right)^2$$

$$\phi_z = \frac{d\theta_z(x)}{dx}$$

$$\gamma_y = -\theta_z(x) + \frac{dv(x)}{dx}$$

## 6.6 Constitutive Law

The section constitutive law is as follows.

$$\mathbf{D}(x) = f_{sec} \mathbf{d}(x) \tag{15}$$

Where  $f_{sec}$  is a nonlinear function that describes the section force deformation relation. The section force deformation relation is obtained through fibre integration as described in Section 2.8.

## 6.7 Variational Formulation

### 6.7.1 Mixed-based Formulation

The formulation of the beam element in this section uses independent generalized stress and displacement interpolation functions in a two-field Hellinger-Reissner (HR) functional which is written in the basic frame of reference as follows:

$$\begin{aligned} \Pi_{HR}(\mathbf{u}, \boldsymbol{\sigma}) = & - \int_v W(\boldsymbol{\sigma}(x, y)) dv + \int_v \boldsymbol{\sigma}^T \boldsymbol{\varepsilon}^u dv - \Pi_{ext}(\mathbf{u}(x)) - \\ & \Pi_{bc}(\mathbf{u}) \end{aligned} \quad (16)$$

where  $W(\boldsymbol{\sigma})$  is the complementary energy function.

In HR variational principle, strain-displacement relation  $\boldsymbol{\varepsilon} = \nabla^s \mathbf{u}(x)$  on  $v$  and displacement boundary condition  $\mathbf{u} = \mathbf{u}^*$  on  $\Gamma_u$ , are satisfied in their strong differential form. Whereas, equilibrium conditions  $\mathbf{div} \boldsymbol{\sigma} + \mathbf{b}_o = \mathbf{0}$  on  $v$ , constitutive relation  $\boldsymbol{\sigma} = \boldsymbol{\sigma}(\boldsymbol{\varepsilon})$  on  $v$  and traction boundary conditions  $\mathbf{t} = \mathbf{t}^*$  on  $\Gamma_t$  are satisfied in their integral weak form.

HR energy functional of Eq. (16) can be written without body force and surface traction with section level variables in the following form:

$$\Pi_{HR}(\mathbf{u}, \mathbf{p}) = - \int_L \mathbf{D}^T \mathbf{d}(\mathbf{D}) dx + \int_L \widehat{\mathbf{D}}^T(\mathbf{p}) \mathbf{d}(\mathbf{u}) dx - \mathbf{u}^T \mathbf{P}^* \quad (17)$$

In this formulation, beam section forces  $\widehat{\mathbf{D}}$  are independently determined from element nodal forces  $\mathbf{p}$  as follows:

$$\widehat{\mathbf{D}}(x) = \mathbf{b}(x) \mathbf{p} \quad (18)$$

where  $\mathbf{b}(x)$  is the matrix of force interpolation functions.

The variation of HR energy functional in Eq. (17) can be written in the following form:

$$\delta \Pi_{HR}(\mathbf{u}, \mathbf{p}) = - \int_L \delta \mathbf{D}^T \mathbf{d}(\mathbf{D}) dx + \int_L \delta(\widehat{\mathbf{D}}^T(\mathbf{p}) \mathbf{d}(\mathbf{u})) dx - \delta \mathbf{u}^T \mathbf{P}^* \quad (19)$$

$$\begin{aligned} \delta \Pi_{HR}(\mathbf{u}, \mathbf{p}) = & - \int_L \delta \mathbf{D}^T \mathbf{d}(\mathbf{D}) dx + \int_L \delta(\widehat{\mathbf{D}}^T(\mathbf{p})) \mathbf{d}(\mathbf{u}) dx + \\ & \int_L (\widehat{\mathbf{D}}^T(\mathbf{p})) \delta(\mathbf{d}(\mathbf{u})) dx - \delta \mathbf{u}^T \mathbf{P}^* \end{aligned} \quad (20)$$

The solution of the variational in Eq. (20) is non-linear under inelastic material conditions, hence the problem needs to be linearized about a state of both principle arguments  $\mathbf{u}^i$  and  $\mathbf{p}^i$  as follows:

$$\begin{aligned} \delta \Pi_{HR}(\mathbf{p}^{i+1}, \mathbf{u}^{i+1}) = & \delta \Pi_{HR}(\mathbf{p}^i, \mathbf{u}^i) + \frac{\partial \delta \Pi_{HR}(\mathbf{p}, \mathbf{u})}{\partial \mathbf{p}} \Big|_{\mathbf{p}^i, \mathbf{u}^i} \Delta \mathbf{p} + \\ & \frac{\partial \delta \Pi_{HR}(\mathbf{p}, \mathbf{u})}{\partial \mathbf{u}} \Big|_{\mathbf{p}^i, \mathbf{u}^i} \Delta \mathbf{u} \end{aligned} \quad (21)$$

Where  $\Delta \mathbf{u}$  and  $\Delta \mathbf{p}$  are the incremental nodal displacement and force vector respectively.

At equilibrium,

$$\delta \Pi_{HR}(\mathbf{p}^{i+1}, \mathbf{u}^{i+1}) = 0 \quad (22)$$

Therefore from Equation (21), we can write as follows,

$$\delta \Pi_{HR}(\mathbf{p}^i, \mathbf{u}^i) + \frac{\partial \delta \Pi_{HR}(\mathbf{p}, \mathbf{u})}{\partial \mathbf{p}} \Big|_{\mathbf{p}^i, \mathbf{u}^i} \Delta \mathbf{p} + \frac{\partial \delta \Pi_{HR}(\mathbf{p}, \mathbf{u})}{\partial \mathbf{u}} \Big|_{\mathbf{p}^i, \mathbf{u}^i} \Delta \mathbf{u} = 0 \quad (23)$$

By using Equations (14), (15), and (18), Equation (23) can be written in the following form:

$$\begin{aligned} \delta \mathbf{u}^T \left[ \int_L \mathbf{B}_s^T(x) \mathbf{b}(x) dx \Delta \mathbf{p} + \int_L \mathbf{B}_s^T \mathbf{D}(x) dx + \int_L \frac{\partial}{\partial \mathbf{u}} (\mathbf{B}_s^T \mathbf{b}(x)) \mathbf{p} dx \Delta \mathbf{u} - \right. \\ \left. \mathbf{P}^* \right] + \delta \mathbf{p}^T \left[ - \int_L \mathbf{b}^T(x) \mathbf{f}_s(x) \mathbf{b}(x) dx \Delta \mathbf{p} + \int_L \mathbf{b}^T(x) \mathbf{B}_s(x) dx \Delta \mathbf{u} + \right. \\ \left. \int_L \mathbf{b}^T(x) \mathbf{d}(x) dx - \int_L \mathbf{b}^T(x) \widehat{\mathbf{d}}(x) dx \right] = 0 \quad (24) \end{aligned}$$

Where  $\mathbf{f}_s(x)$  is the section flexibility matrix,  $\mathbf{B}_s(x)$  is the strain displacement matrix which is a function of  $\mathbf{u}(x)$ , and  $\widehat{\mathbf{d}}(x)$  is the section deformation vector determined from section force vector  $\widehat{\mathbf{D}}(x)$  with the help of the section flexibility matrix.

From arbitrariness of  $\delta \mathbf{u}$  and  $\delta \mathbf{p}$ , Equation (24) can be written in the following matrix form:

$$\begin{bmatrix} \int_L \frac{\partial}{\partial u} (\mathbf{B}_s^T \mathbf{b}(x)) \mathbf{p} dx & \int_L \mathbf{B}_s^T \mathbf{b} dx \\ \int_L \mathbf{b}^T \mathbf{B}_s dx & - \int_L \mathbf{b}^T \mathbf{f}_s \mathbf{b} dx \end{bmatrix} \begin{pmatrix} \Delta \mathbf{u} \\ \Delta \mathbf{p} \end{pmatrix} = \begin{pmatrix} \mathbf{P}^* - \int_L \mathbf{B}_s^T \mathbf{D} dx \\ \int_L \mathbf{b}^T (\hat{\mathbf{d}} - \mathbf{d}) dx \end{pmatrix} \quad (25)$$

Equation (25) can be written in the following concise form:

$$\begin{bmatrix} \mathbf{K}_{ig} & \mathbf{G}^T \\ \mathbf{G} & -\mathbf{F}_{c+s} \end{bmatrix} \begin{pmatrix} \Delta \mathbf{u} \\ \Delta \mathbf{p} \end{pmatrix} = \begin{pmatrix} \mathbf{P}^* - \mathbf{P}_{c+s}^r \\ \mathbf{u}^r \end{pmatrix} \quad (26)$$

Where  $\mathbf{F}_{c+s}$  is the element flexibility matrix and  $\mathbf{u}^r$  is the element residual deformation vector and  $\mathbf{K}_{ig}$  is the internal geometric stiffness matrix. Here,

$$\mathbf{G} = \begin{bmatrix} (\frac{19}{180}L\theta_{z1} - \frac{11}{180}L\theta_{zj} - \frac{2}{45}L\theta_{zk}) & 1 & (-\frac{11}{180}L\theta_{z1} + \frac{19}{180}L\theta_{zj} - \frac{2}{45}L\theta_{zk}) & (-\frac{2}{45}L\theta_{z1} - \frac{2}{45}L\theta_{zj} + \frac{4}{45}L\theta_{zk}) \\ & & 1 & 0 & 0 & 0 \\ & & 0 & 0 & 1 & 0 \end{bmatrix}$$

$$\mathbf{K}_{ig} = \begin{bmatrix} \frac{19}{180}LP_a & 0 & -\frac{11}{180}LP_a & -\frac{2}{45}LP_a \\ & 0 & 0 & 0 \\ -\frac{11}{180}LP_a & 0 & \frac{19}{180}LP_a & -\frac{2}{45}LP_a \\ -\frac{2}{45}LP_a & 0 & -\frac{2}{45}LP_a & \frac{4}{45}LP_a \end{bmatrix}$$

Here,  $P_a$  is the nodal axial force at node J in the basic frame of reference of deformation. It is important to note that at convergence, the element residual deformation vector  $\mathbf{u}^r$  reduces to zero inside each element satisfying compatibility. In this formulation, the force degrees of freedom are condensed out at the element level from Equation (26) resulting in a generalized stiffness matrix as follows:

$$[\mathbf{K}_{ig} + \mathbf{G}^T [\mathbf{F}_{c+s}^{-1}] \mathbf{G}] \Delta \mathbf{u} + \mathbf{G}^T [\mathbf{F}_{c+s}^{-1}] [-\mathbf{u}^r] = \mathbf{P}^* - \mathbf{G}^T \mathbf{P}_{c+s}^r \quad (27)$$

Once convergence is reached at the element level i.e.  $\mathbf{u}^r$  becomes zero, Equation (27) can be written as following:

$$(\mathbf{K}_{ig} + \mathbf{G}^T [\mathbf{F}_{c+s}^{-1}] \mathbf{G}) \Delta \mathbf{u} = \mathbf{P}^* - \mathbf{G}^T \mathbf{P}_{c+s}^r \quad (28)$$

$$(\mathbf{K}_{c+s}) \Delta \mathbf{u} = \mathbf{P}^* - \mathbf{G}^T \mathbf{P}_{c+s}^r \quad (29)$$

$$\mathbf{K} \Delta \mathbf{u} = \mathbf{P}^* - \mathbf{P}^r \quad (30)$$

The nodal displacements of the structural model in the global frame of reference are collected in the displacement vector  $\mathbf{U}^g$ . Detailed procedure of mapping structural nodal displacements relative to global coordinates to the element nodal deformations at the basic frame of reference, transformation

of element stiffness matrix and resisting forces from the basic to the global level and assembling of global stiffness matrix and resistance forces of all elements to assembled structural stiffness matrix  $\mathbf{K}^g$  and structural resistance vector  $\mathbf{P}^{gr}$  are described in details in Filippou et al. (2004).

#### **6.7.1.1 Stability Criteria**

*Stability criteria* is similar to the section 2.9.1.

#### **6.7.1.2 State Determination**

A step by step summary of the state determination algorithm is presented below for a single element with large displacement effects. The summary focuses on a single global iteration  $i$  at the structural degree of freedoms through the Newton-Raphson method with applied load counter  $k$ .

*Step 1* to *Step 6* is similar to the section 2.9.2. However, concerned matrixes should be based on this chapter.

*Step 7*: Determine the element stiffness matrix including internal geometric stiffness matrix and resistance vector in iteration counter  $i$  for the given nodal element deformation upon the convergence of element compatibility at the basic frame of reference:

$$\mathbf{K}_{ele}^{i+1} = \mathbf{G}^T [\mathbf{f}_{ele}^{j+1}]^{-1} \mathbf{G} + \mathbf{K}_{ig}$$

$$\mathbf{Q}_{ele}^{i+1} = \mathbf{G}^T \mathbf{q}_{ele}^{i+1}$$

*Step 8:* Determine the element stiffness matrix including external geometric stiffness matrix  $\mathbf{K}_{og}$  and resistance vector in iteration counter  $i$  at the global frame of reference:

$$\mathbf{K}_{ele,glo}^{i+1} = \mathbf{a}_c^T \mathbf{K}_{ele}^{i+1} \mathbf{a}_c + \mathbf{K}_{og}$$

$$\mathbf{K}_{og} = \left[ \frac{\partial \mathbf{a}_c}{\partial \mathbf{u}} \right]^T \mathbf{Q}_{ele}^{i+1} \quad (\text{Provided in Appendix A})$$

$$\mathbf{Q}_{ele,glo}^{i+1} = \mathbf{a}_c^T \mathbf{Q}_{ele}^{i+1}$$

# **Chapter 7 Correlation Studies – Shear Critical RC Component considering P-Delta Effect**

## **7.1 Overview**

This chapter presents several correlation studies of the newly developed shear critical frame element with large displacement effects based on two-filed mixed formulation with the experimental results of reinforced concrete members for monotonic and cyclic loading conditions.

The correlation studies starts with flexure critical reinforced concrete columns under monotonic loading conditions followed by reinforced concrete columns under cyclic loading conditions. In the end, correlations studies extended to shear critical reinforced concrete columns under cyclic loading conditions to demonstrate the capability of the element formulation to simulate the post-peak softening region of load versus displacement response.

## **7.2 RC Columns**

### **7.2.1 Column by Barrera, Bonet, Romero and Miguel (2011)**

Barrera et al. (2011) performed tests on a series of 44 reinforced concrete columns (Figure 7-1) under constant axial compressive loading and monotonically increasing amplitude of lateral force to study the behaviour of slender (shear span ratio  $>6.5$ ) columns by using high strength concrete. The effect of several variables such as strength of concrete (30 MPa, 60MPa and 90 MPa), shear span ratio (7.5, 10.5 and 15), axial load level and longitudinal and transversal reinforcement ratio on the strength and deformation capacity of the columns were studied. Two types of failure modes are reported i.e. failure mode due to ultimate strength of the section and failure mode due to instability. Out of these specimens, column H60-10.5-C0-2-30 is chosen for the correlation study as this specimen (shear span to depth ratio 10.5) fails in flexural compression of concrete, and reinforcement bar buckling has not been observed in the experiment. The specimen has been subjected to a constant axial load of 432 kN.

The cross-section details of this specimen are shown in Figure 7-2. The specimen has width and depth of 150 mm and 140 mm respectively.

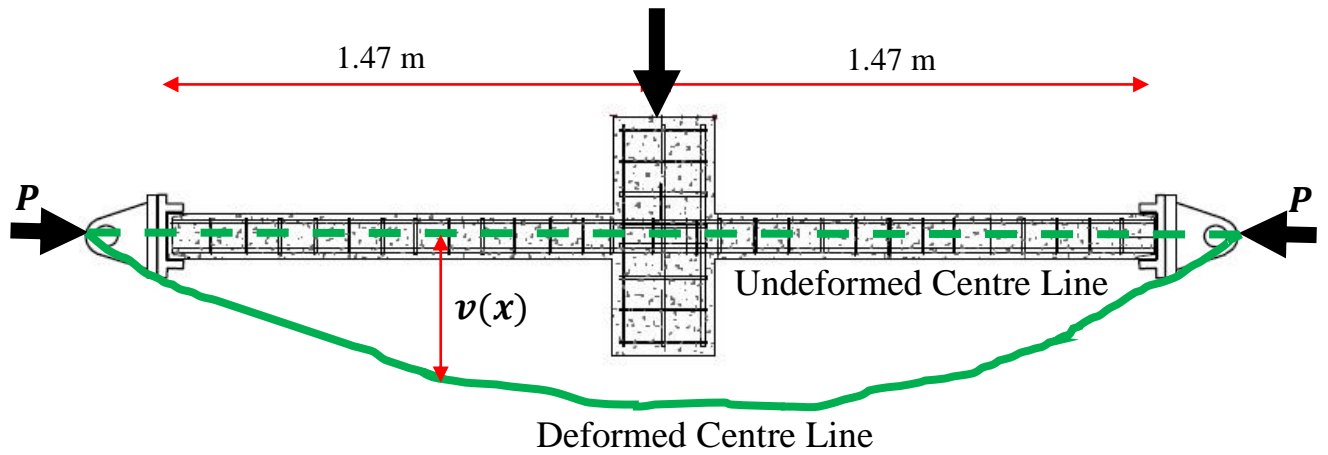


Figure 7-1. Geometry of Column Specimen

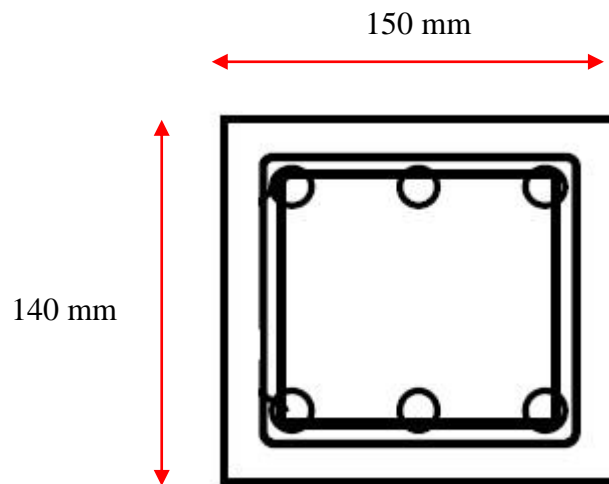


Figure 7-2. Cross-section of ColumnH60-10.5-C0-2-30

6 longitudinal reinforcements of diameter 10 mm are uniformly spaced along the perimeter of the columns. Rectangular hoops of diameter 6 mm are placed at a spacing of 100 mm along the length of the columns.

Concrete compressive strength of the column is 60.5 MPa. Yield strengths of longitudinal and transverse reinforcements are 537 MPa and 500 MPa respectively. Peak compressive strain and strain at crushing of concrete material has been considered as 0.0025 and 0.09 respectively. The tensile strength of concrete has been taken as  $0.33*(f_c)^{0.5}$ . Unloading stiffness for concrete material is considered as 0.01. Similar values of these variables have also been considered by Gendy et al. (2018).

Two elements have been used to model the entire column specimen with 5 section integration points in each element. Figure 7-3 compares the shear force versus mid deflection response of the model using the proposed beam element with the experimental results of column H60-10.5-C0-2-30.

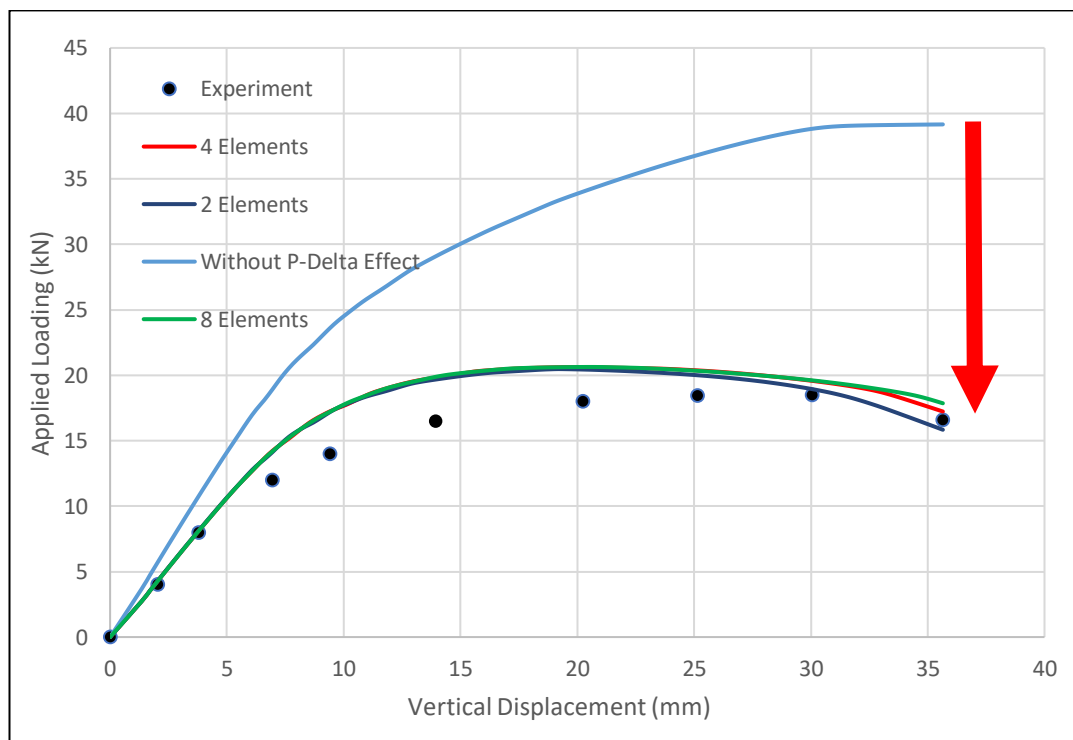


Figure 7-3. Load-Deflection Response of Column H60-10.5-C0-2-30

From the above plot, it can be observed that the proposed element with large displacement effects excellently reproduced the overall experimentally observed load-deflection response. However, the element without P-Delta effects has overestimated the shear strength and stiffness as expected. Therefore, it is imperative to develop a beam element considering geometric nonlinearity to model the behaviour of slender reinforced concrete columns. It can also be noted that 2, 4 and 8 elements have produced almost same response except in the last stage of loading with little deviation.

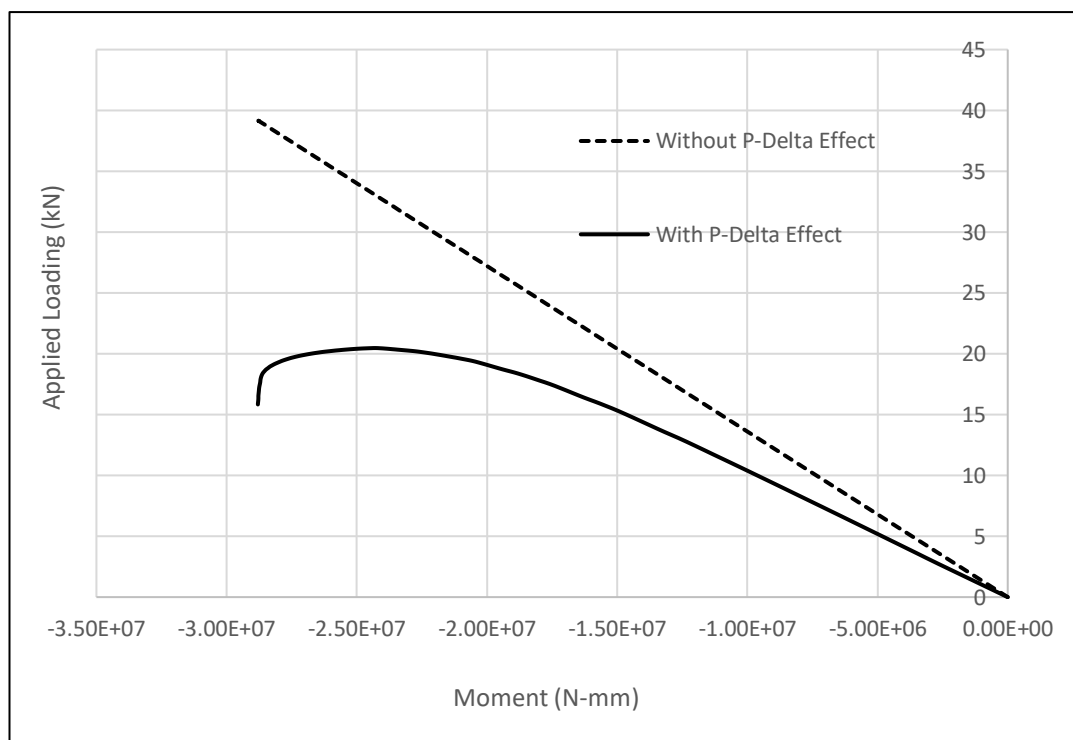


Figure 7-4. Load-Moment Response at Loading Point Section

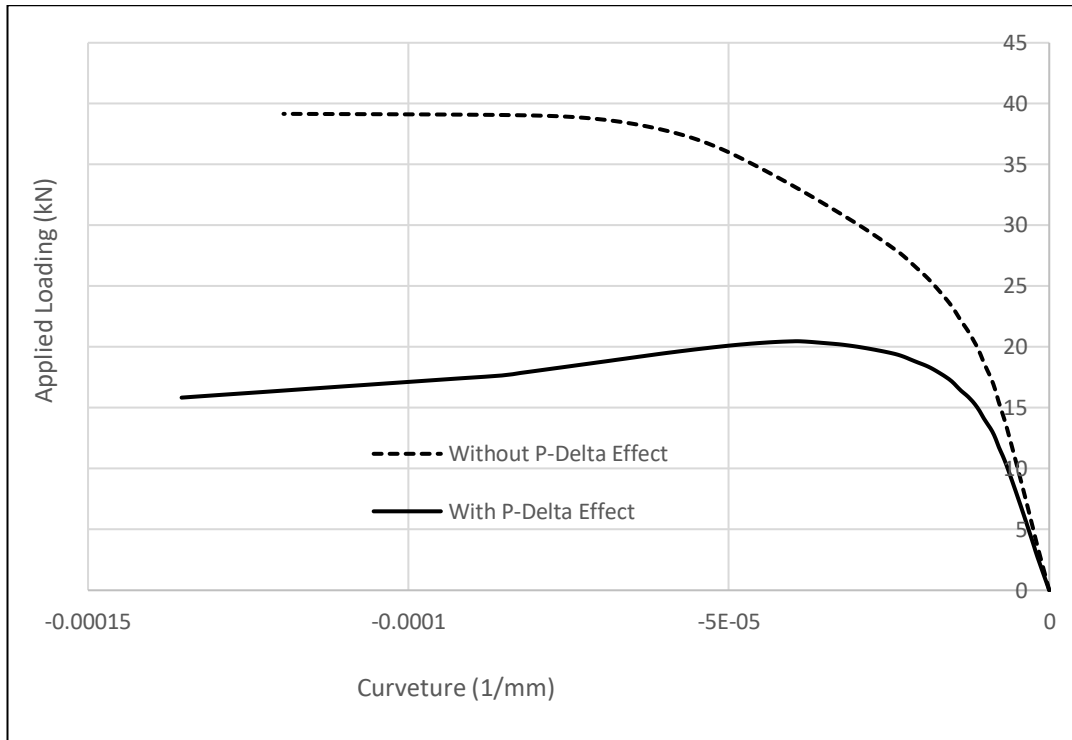


Figure 7-5. Load-Curvature Response at Loading Point Section

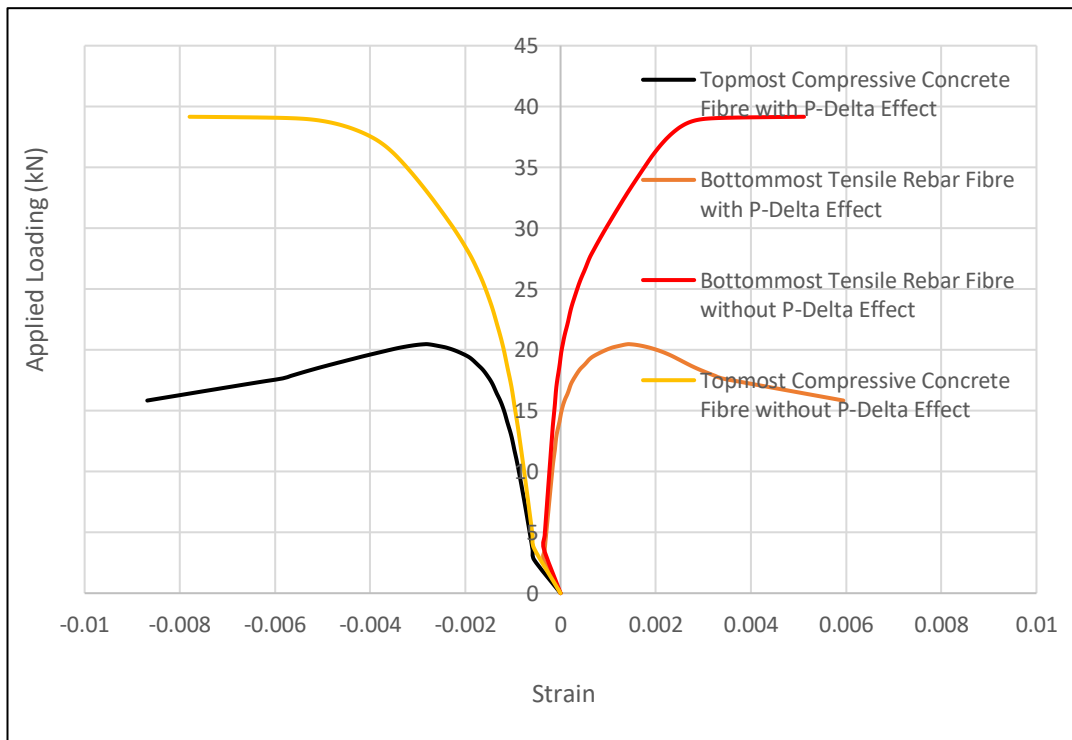


Figure 7-6. Load-Strain Response at Loading Point Section

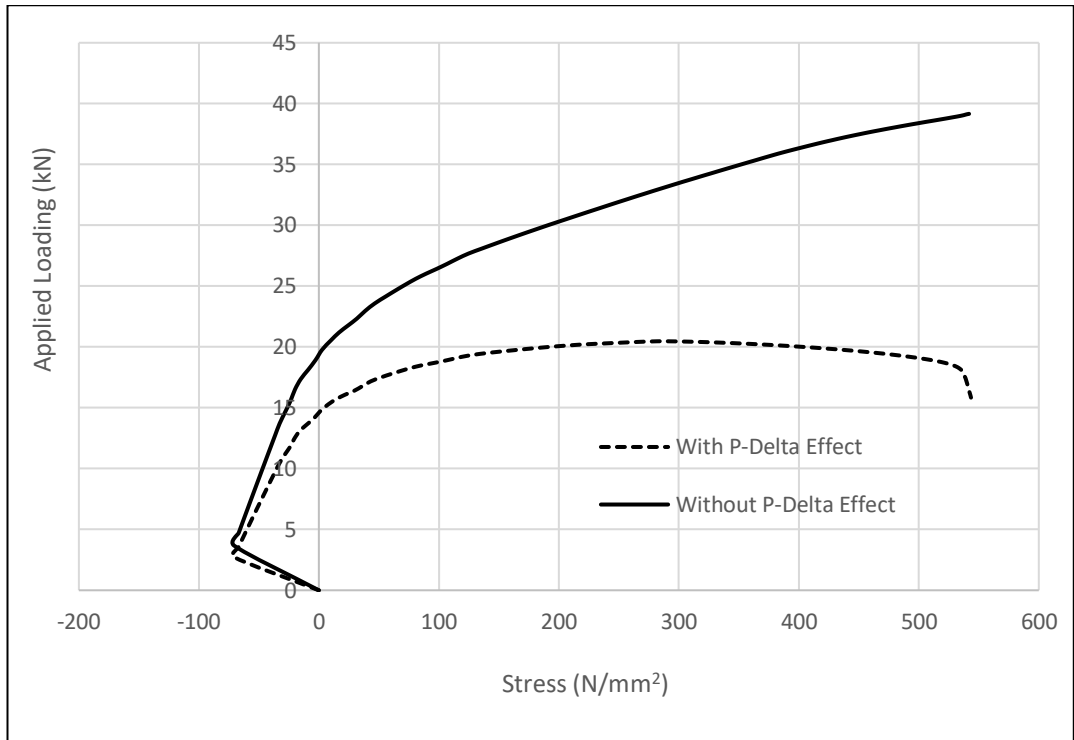


Figure 7-7. Load-Stress Response of bottommost Longitudinal Rebar at Loading Point

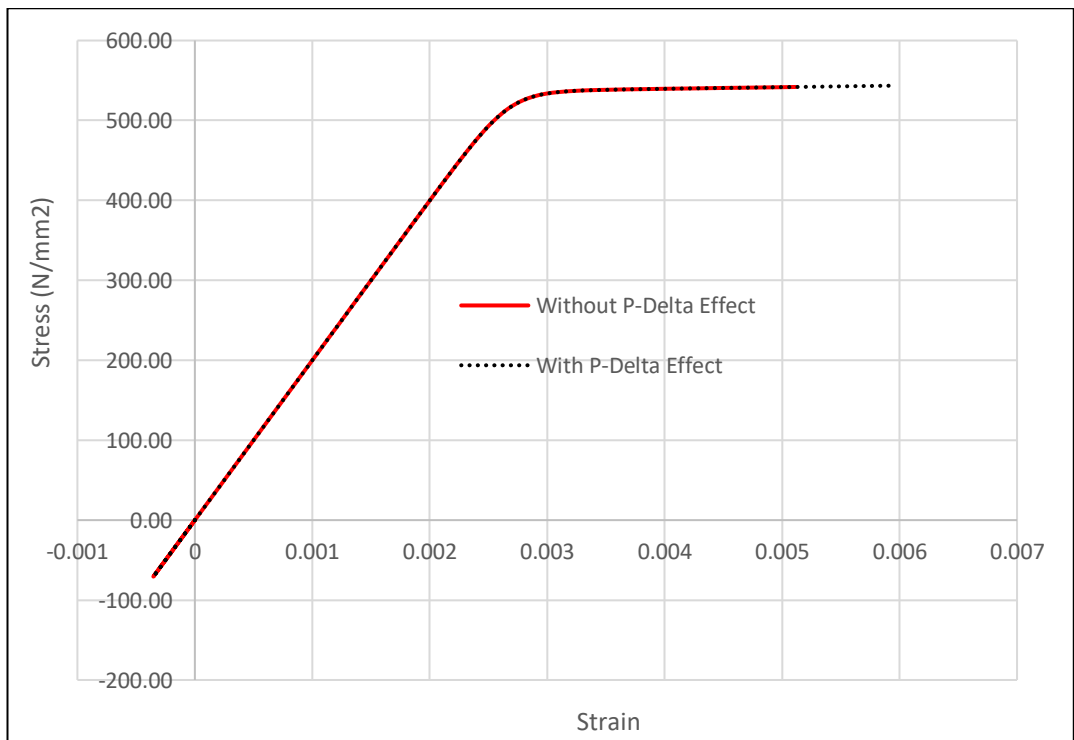


Figure 7-8. Stress-Strain Response of bottommost Longitudinal Rebar at Loading Point

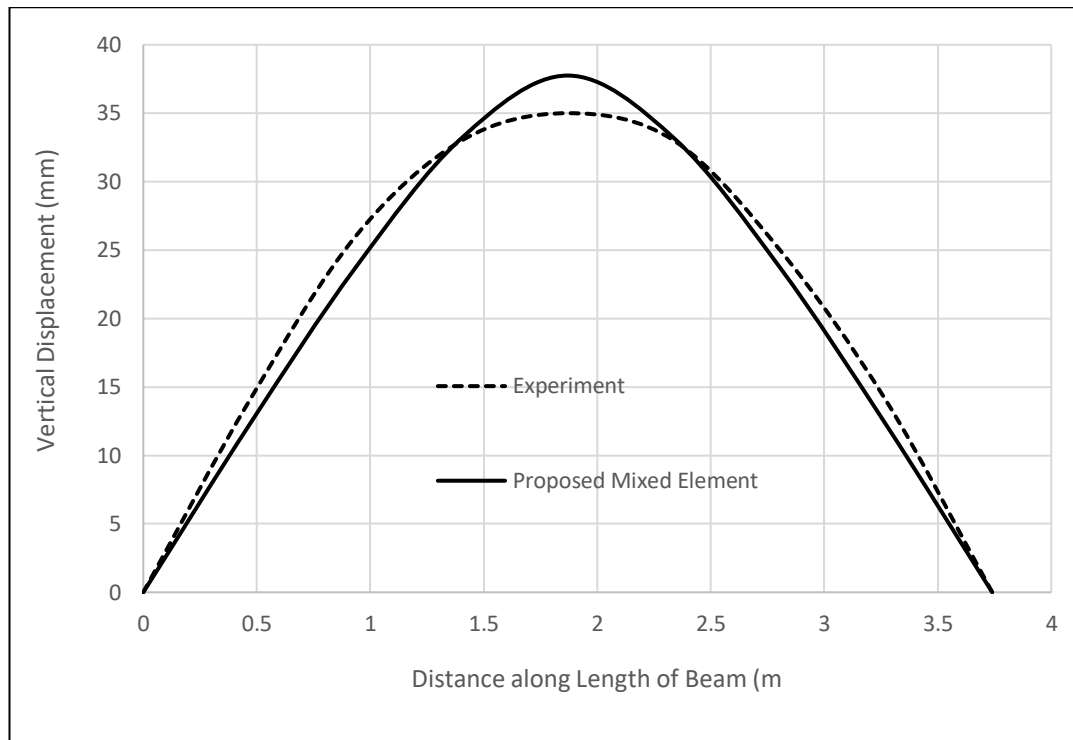


Figure 7-9. Deformed Shape at 16.56 kN at post-peak region

Figures 7-4 and 7-5 show the load- moment and load-curvature response at the loading point. It can be observed that under 20 Kn of loading both moment and curvature is larger when we consider P-Delta effect as expected. It can also be seen from Figure 7-6 that top concrete fibre and bottom rebar reaches higher strain values at 20 Kn loading stage while we consider P-delta effect. Also, at the last stage of loading, bottom tensile rebar and top concrete fibre reaches substantial amount of strain which makes the specimen fails in flexural compression. Similarly from Figure 7-7 stress in the bottom tensile rebar has also reached higher stress value at 20 Kn of loading stage. It can also be noted that during initial stage of loading, compressive strain gets induced in the bottom rebar due to applied

compressive loading. Figure 7-8 shows the stress-strain plot of the bottom tensile rebar where it can be observed that strain at constant stress gets increased at the later stage of loading while P-Delta effect becomes prominent. It can also be observed from the Figure 7-9 that the proposed mixed element has reasonably reproduced the variation of the vertical displacement along the length of the column at 16.56 Kn.

### **7.2.2 Column by Legeron and Paultre (2000)**

Legeron et al. (2000) performed tests on a series of 6 large-scale cantilever reinforced high strength concrete columns (shear span ratio = 6.56) under constant axial compressive load and reverse cyclic lateral loading to investigate primarily the effect of axial load on seismic behaviour of slender columns. Out of these columns, Specimen 5 is chosen for the correlation study. The specimen has been subjected to a constant axial load of 2400 kN.

The specimen has width and depth both of 305 mm and length of 2000 mm. 4 corner longitudinal reinforcements of diameter 19.5 mm and 4 intermediate longitudinal reinforcements of diameter 16 mm are uniformly spaced along the perimeter of the columns. Square hoops of diameter 11.3 mm are placed at a spacing of 130 mm along the length of the columns.

The concrete compressive strength of the column is 97.7 MPa. Yield strengths of corner and middle longitudinal and transverse reinforcements are 430 MPa, 494 MPa and 391 MPa respectively.

One element has been used to model the entire column specimen with 5 section integration points. Figure 7-10 compares the lateral load versus top end deflection response of the models using the proposed beam element with the experimental result.

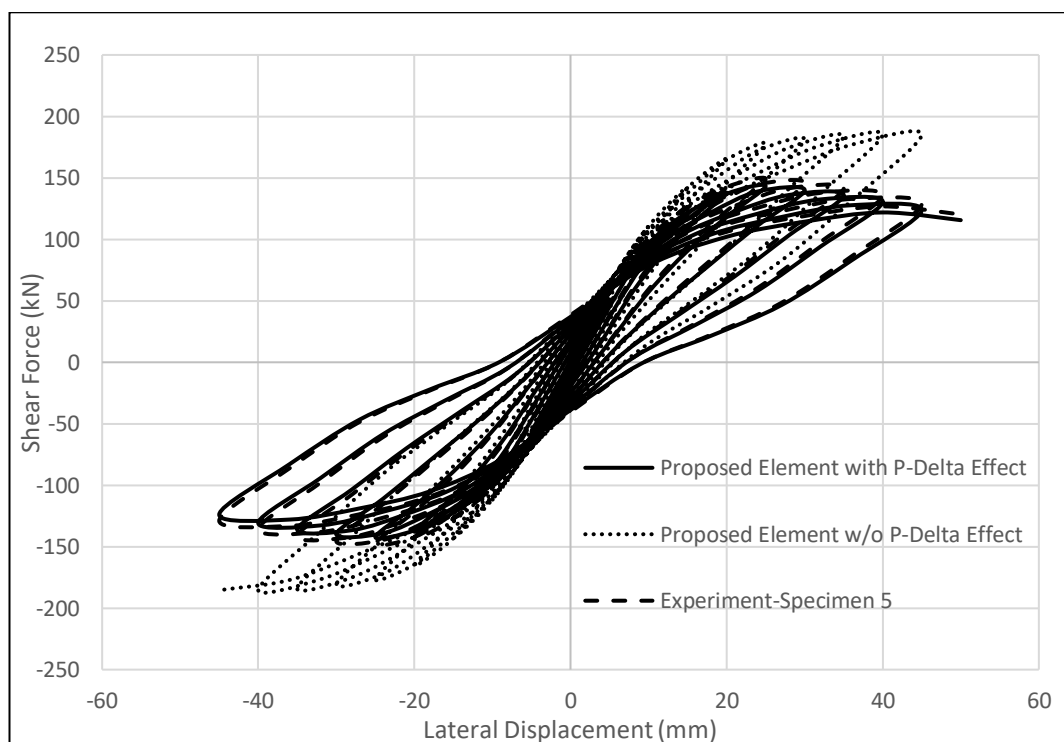


Figure 7-10. Load-Deflection Response of Specimen 5

From the above plot, it can be observed that the proposed element without P-Delta effects overestimates the shear strength and stiffness as expected.

Whereas the proposed element with P-Delta effect has exceptionally reproduced the overall experimentally observed load-deflection response. Stiffness, shear resistance, shear deformation capacity along with hysteretic behaviour have been captured very well.

### **7.2.3 Column by Caballero-Morrison, Bonet, Navarro-Gregoriand Martí-Vargas (2012)**

Caballero-Morrison et al.(2012) conducted tests on a series of 14 reinforced concrete columns (Figure 7-11) under constant axial compressive loading and cyclic lateral force to study the behaviour of slender (shear span ratio 5 to 10) columns. The effect of several variables such as slenderness, axial load level, transverse reinforcement ratio and volumetric steel-fibre ratio on the strength and deformation capacity of the columns was studied.

Out of these specimens, column NF60L05V2S600is chosen for the correlation study as this specimen (shear span to depth ratio 5.77) has stirrups spacing of 600 mm along the length of the column. Shear failure occurred in this specimen after stirrup yielding, spalling of concrete cover and buckling of longitudinal bars. The specimen has been subjected to a constant axial load of 420.6 kN.

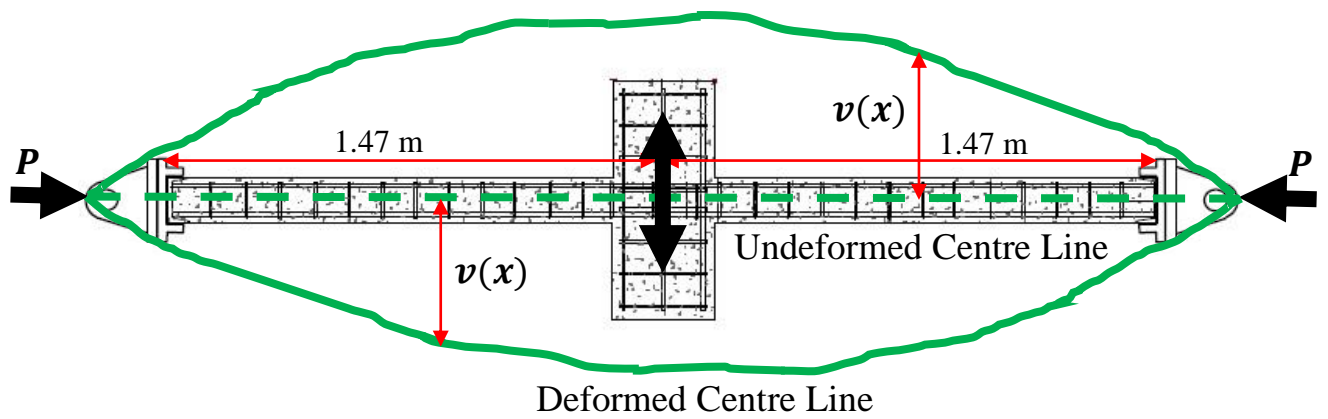


Figure 7-11. Geometry of Column Specimen

The cross-section details of this specimen are shown in Figure 7-12. The specimen has width and depth of 150 mm and 260 mm respectively.

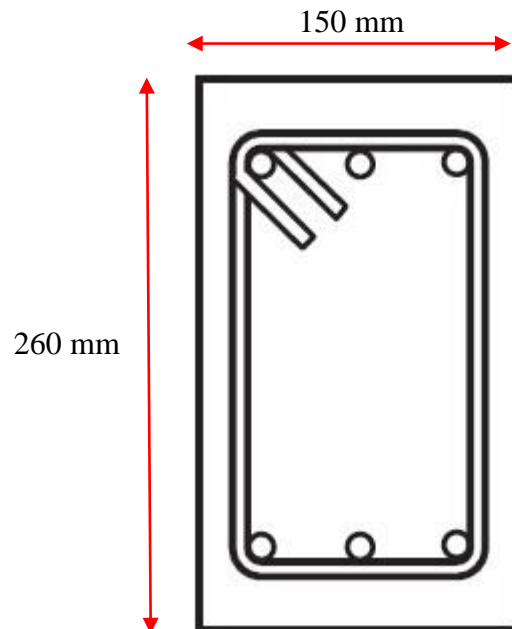


Figure 7-12. Cross-section of Column NF60L05V2S600

6 longitudinal reinforcements of diameter 12 mm are uniformly spaced at the top and bottom perimeter of the column. Rectangular hoops of diameter 8 mm are placed at a spacing of 600 mm along the length of the columns. Concrete compressive strength of the column is 32.12 MPa. Yield strengths of longitudinal and transverse reinforcements are 548.27 MPa and 541.57 MPa respectively.

Two elements have been used to model the entire column specimen with 5 section integration points in each element. Figure 7-13 compares the shear force versus mid deflection response of the model using the proposed beam element with the experimental results of column NF60L05V2S600.

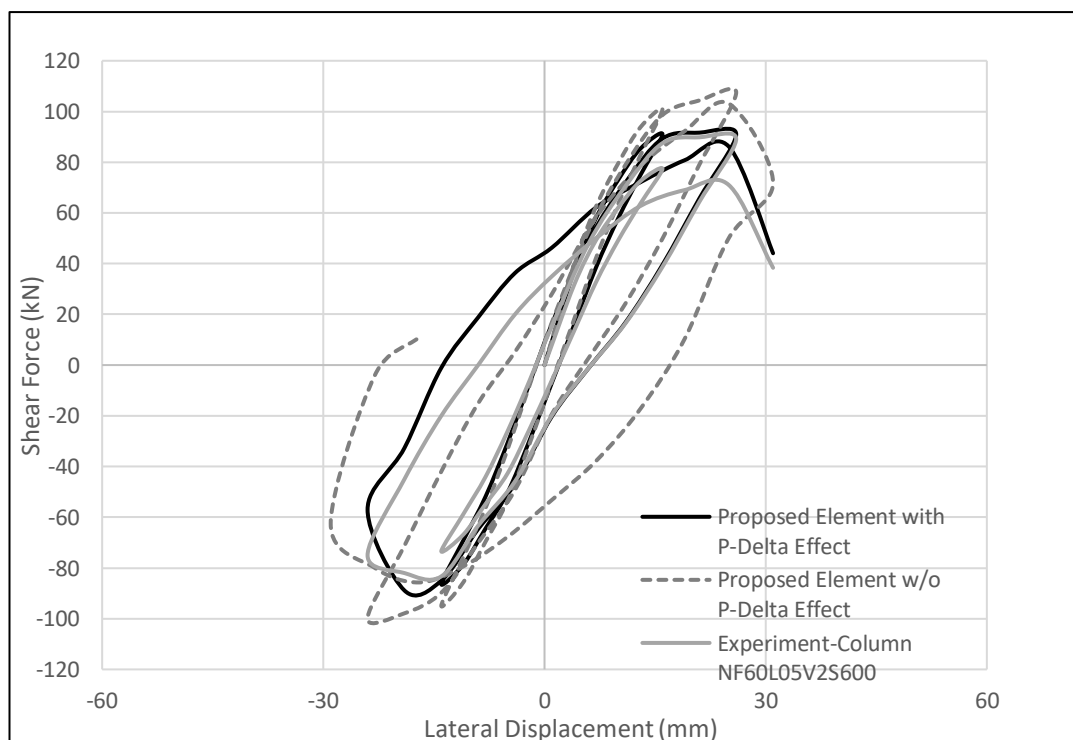


Figure 7-13. Load-Deflection Response of Column NF60L05V2S600

From the above plot, it can be observed that the proposed element with large displacement effect, reasonably reproduce the overall experimentally observed load-deflection response. Hysteretic energy and shear deformation capacity have been captured reasonably well. However, it has overestimated the shear resistance slightly at the last cycle as the proposed element does not include cover spalling and bar buckling observed in the experiment but predicted the failure at the correct displacement step. On the contrary, the proposed element without geometric nonlinearity effects, overestimated the shear strength, stiffness and hysteretic energy too. In addition, it has failed to detect the failure at the right displacement stage.

#### **7.2.4 Column by Bae and Bayrak (2008)**

Bae et al. (2008) performed tests on a series of 4 full scale cantilever reinforced concrete columns under constant axial compressive loading and reversed cyclic displacement excursions to investigate the effect of axial load and shear span to depth ratio on the plastic hinge length. The length of a plastic hinge depends on many factors such as the level of axial load, moment gradient, level of shear stress in the plastic hinge region, mechanical properties of longitudinal and transverse reinforcement, concrete strength and level of confinement and its effectiveness in the potential hinge region. The plastic hinge length is necessary to determine

the tip displacement of columns which consists of flexural deformation, fixed-end rotation resulting from the slip of longitudinal bars out of joints, shear deformation and additional displacement due to secondary moments generated by the P- $\Delta$  effect. In this study, column S17-3UT (shear span to depth ratio 7) has been chosen as large inelastic tie bar strains were observed in the experiment. The specimen has been subjected to a constant axial load of 4166.2 kN.

The cross-section details of this specimen are shown in Figure 7-14. The square specimen has width and depth of both 440 mm.

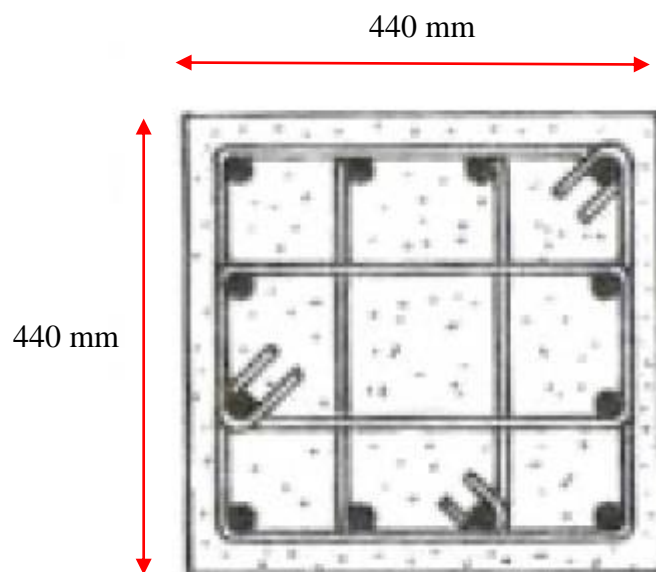


Figure 7-14. Cross-section of Column S17-3UT

12 numbers longitudinal reinforcements of diameter 16 mm are uniformly spaced along the perimeter of the columns. Square hoops of diameter 10

mm are placed at a spacing of 86 mm along the length of the column. Concrete compressive strength of the column is 43.4 MPa. Yield strengths of longitudinal and transverse reinforcements are both 496 MPa.

One element has been used to model the entire column specimen with 5 section integration points. Figure 7-15 compares the lateral load versus top end deflection response of the model using the proposed beam element with the experimental results.

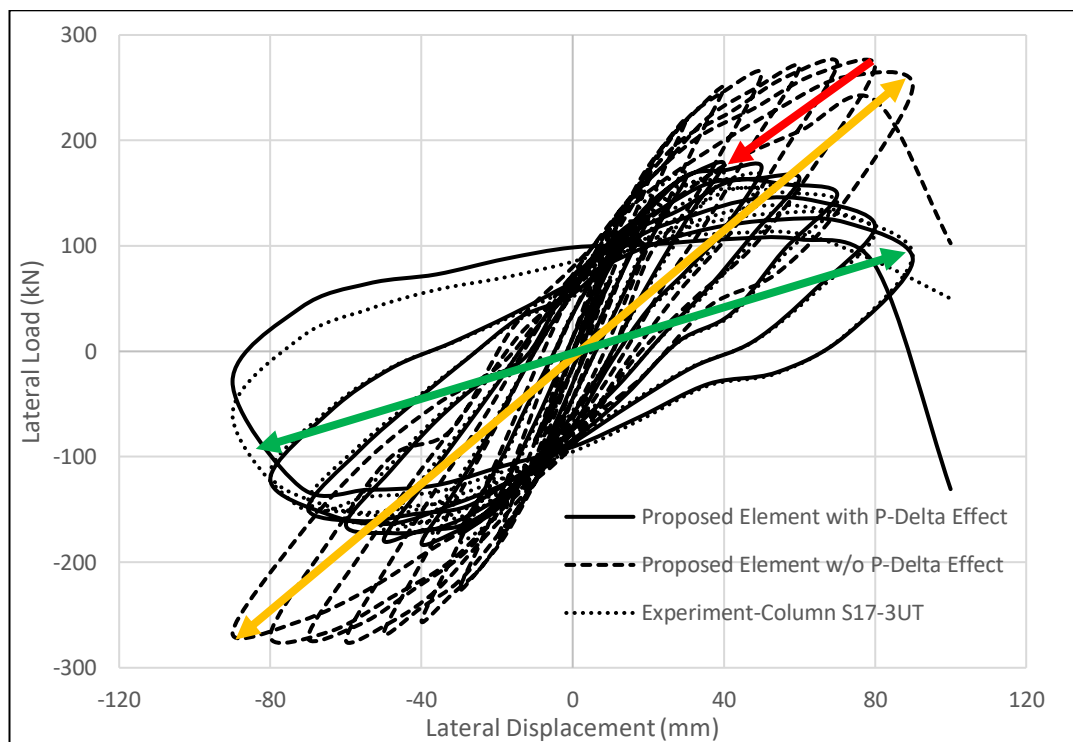


Figure 7-15. Load-Deflection Response of Column S17-3UT

From the above plot, it can be observed that the proposed element with large displacement effects, reasonably reproduce the overall experimentally observed load-deflection response. Hysteretic energy and shear deformation capacity have been captured reasonably well. It is to be noted that the element has reasonably simulated the post peak shear strength softening region. On the contrary, the proposed element without geometric nonlinearity effects, overestimated shear strength and stiffness in both unloading and reloading conditions. It is also to be noted that the attainment of peak shear strength with the element considering P-Delta effect was reached earlier than that of its counterpart as expected.

From the following Figure 7-16 of cyclic envelopes, it can be observed that the drop of shear resistance in positive and negative regions at the end of loading stages is not in symmetry which is in synchronization with experimental results.

From the following Figure 7-17, it can be also observed that the percentage drop of shear resistance is nonlinear with time and gets increased with the loading cycles. The contribution of P-Delta effects on shear strength degradation is huge in the later stage of loading i.e. after the attainment of peak shear resistance. Its effect again is higher in the negative region compared to that of the positive region during the last loading stage. It

signifies that the performance of the column in one direction depends on the experienced accumulated damage of the other direction in the later stage of lateral loading along with huge constant axial compressive load.

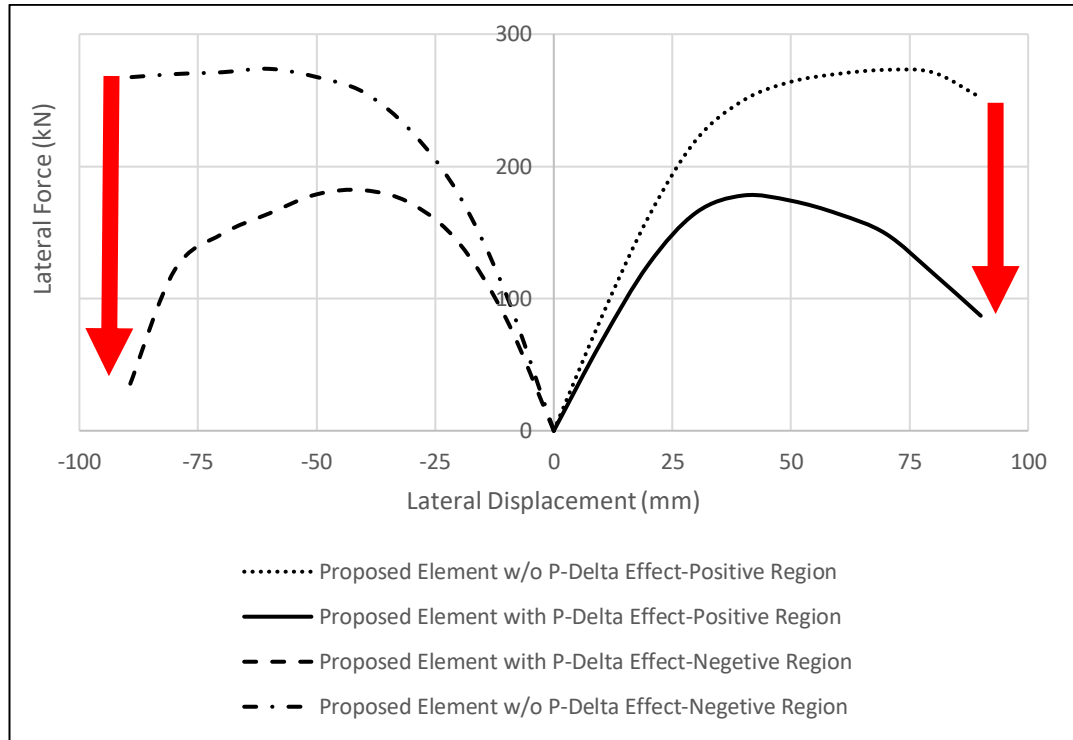


Figure 7-16. Cyclic Envelops

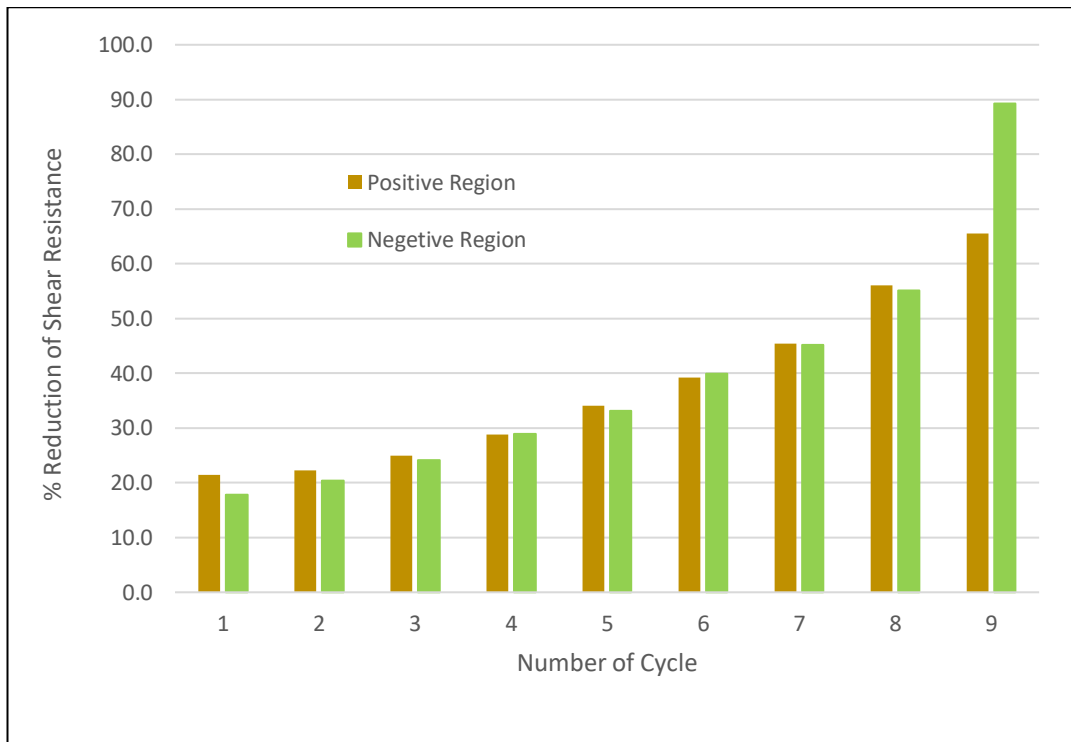


Figure 7-17. Reduction of Peak Shear Resistance due to P-Delta Effect (%)

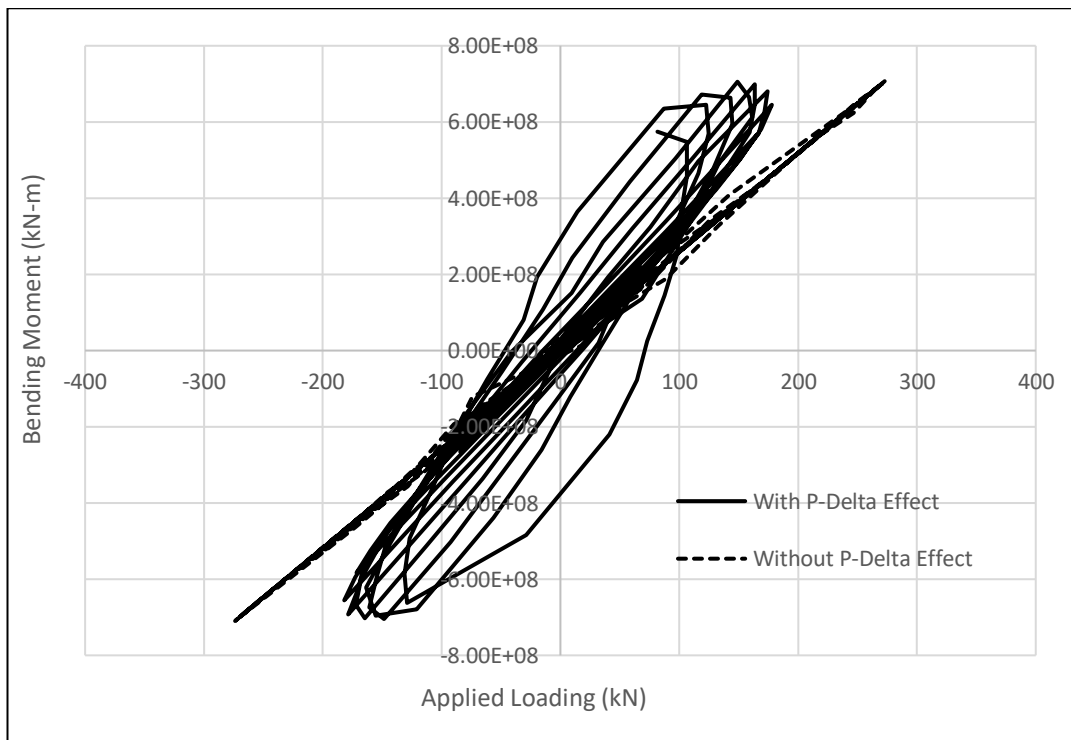


Figure 7-18. Moment-Loading Response at base section

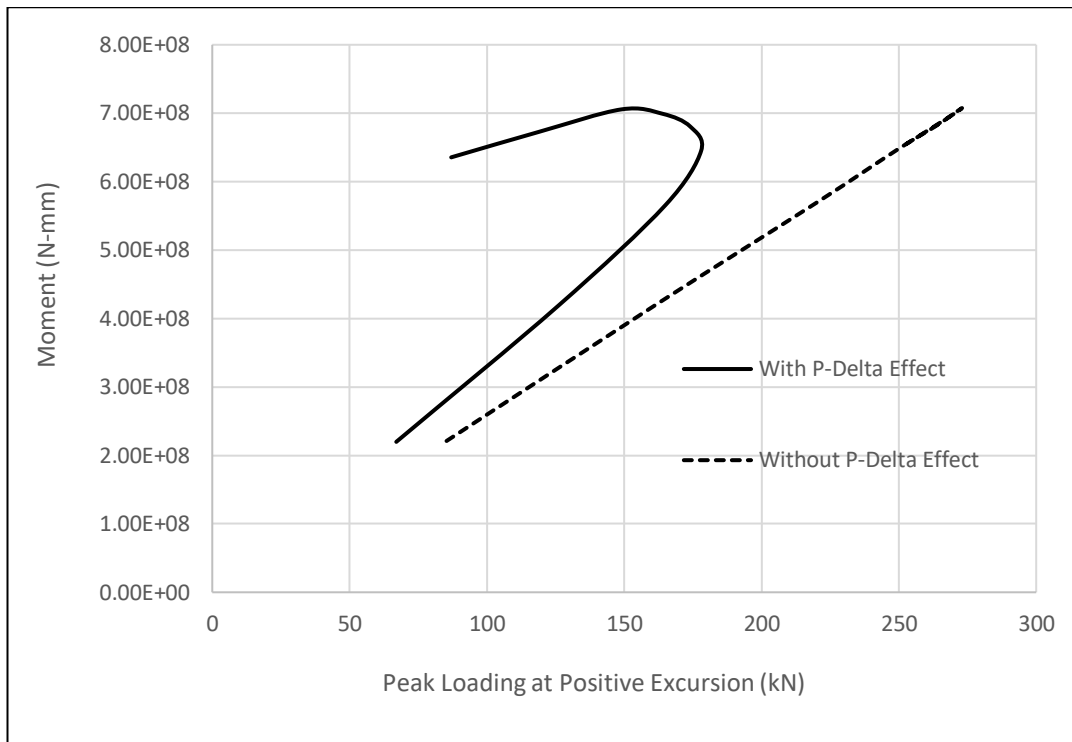


Figure 7-19. Moment-Peak Loading Response at base section for positive excursion

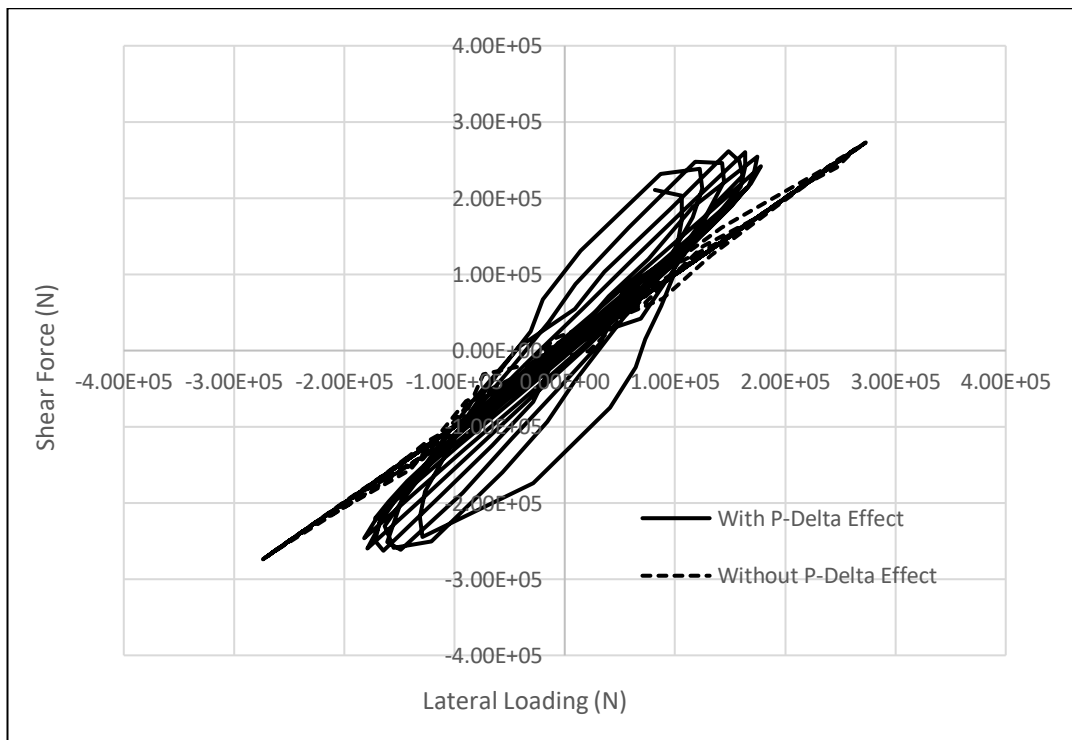


Figure 7-20. Shear Force-Loading Response at base section

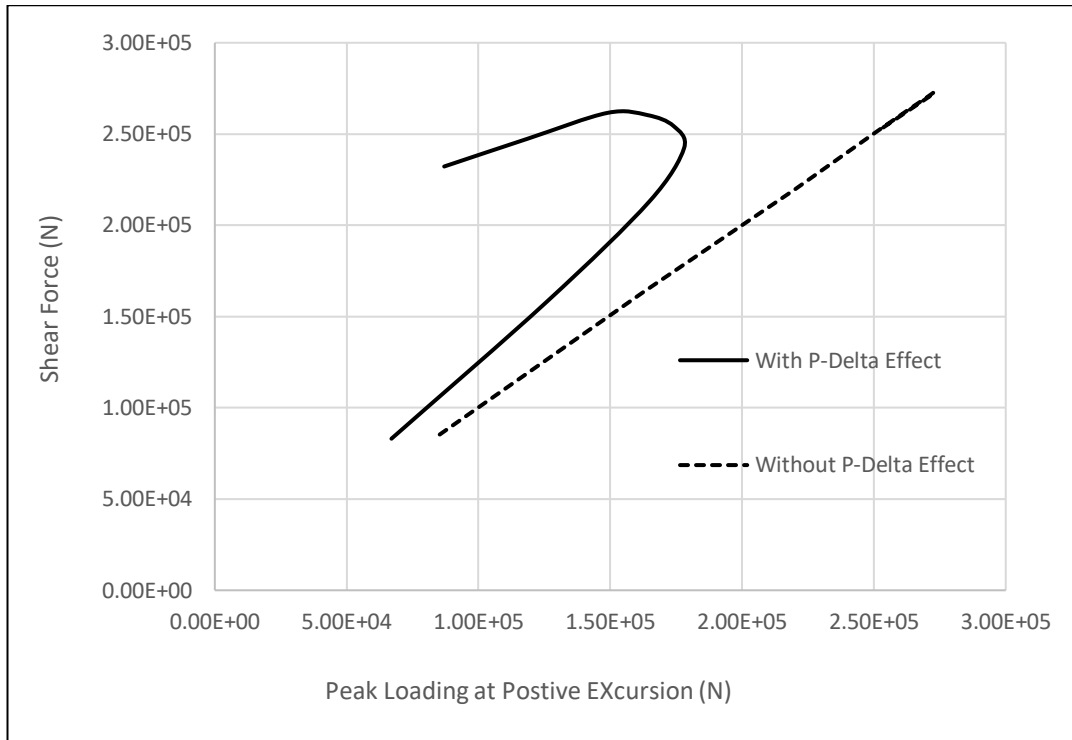


Figure 7-21. Shear Force-Peak Loading Response at base section for positive excursion

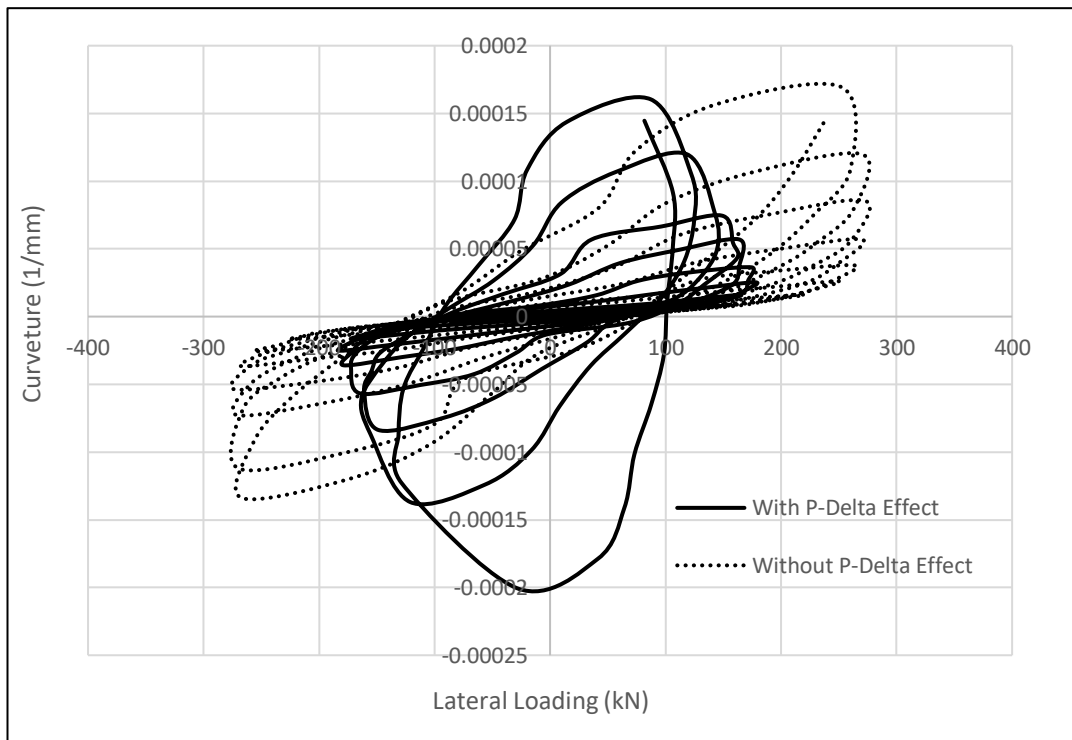


Figure 7-22. Curvature-Loading Response at base section

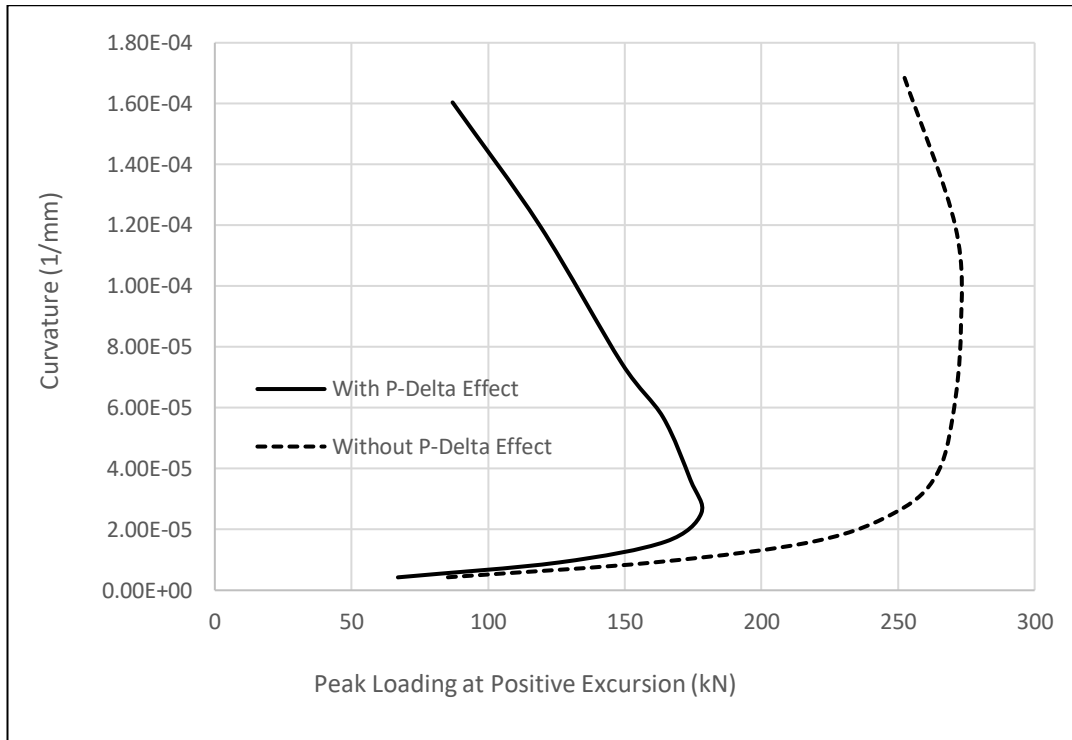


Figure 7-23. Curvature-Peak Loading Response at base section for positive excursion

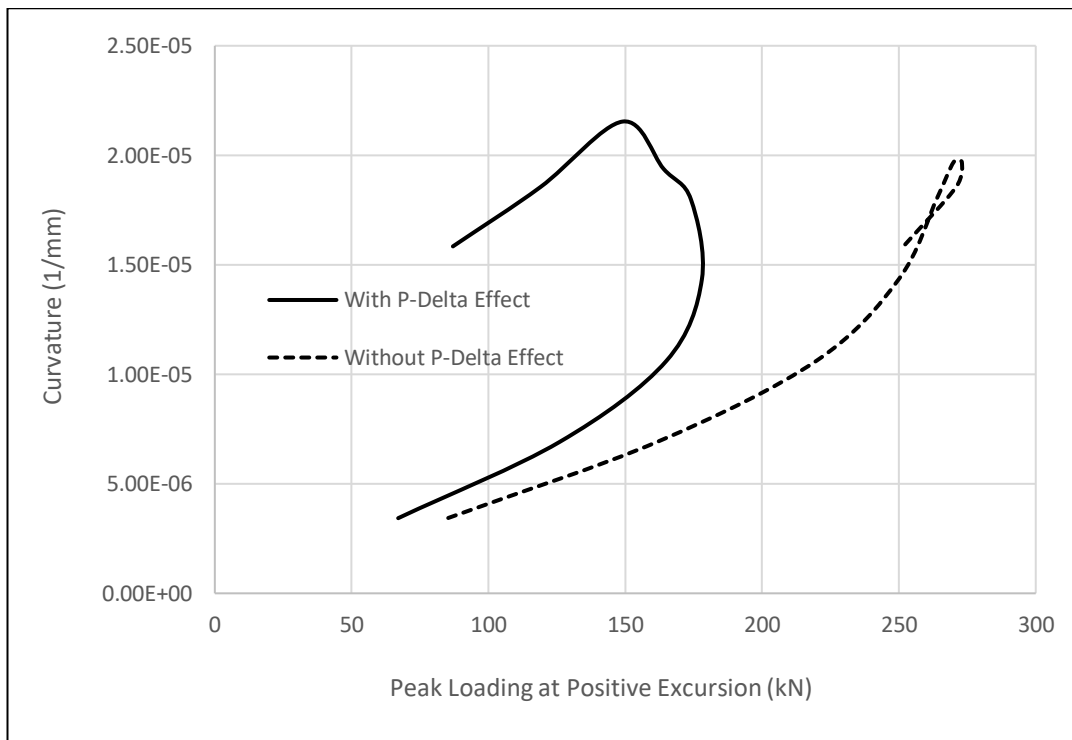


Figure 7-24. Curvature-Peak Loading Response at 447 mm from base section for positive excursion

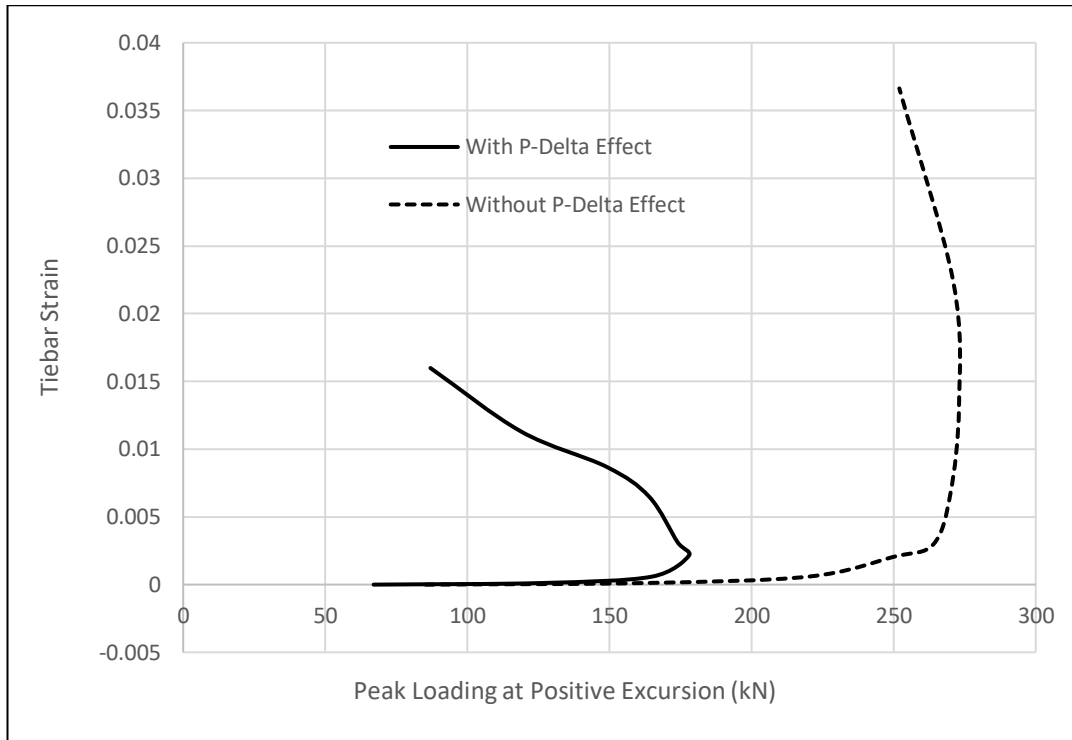


Figure 7-25. Stirrup Strain-Peak Loading Response at base section for positive excursion

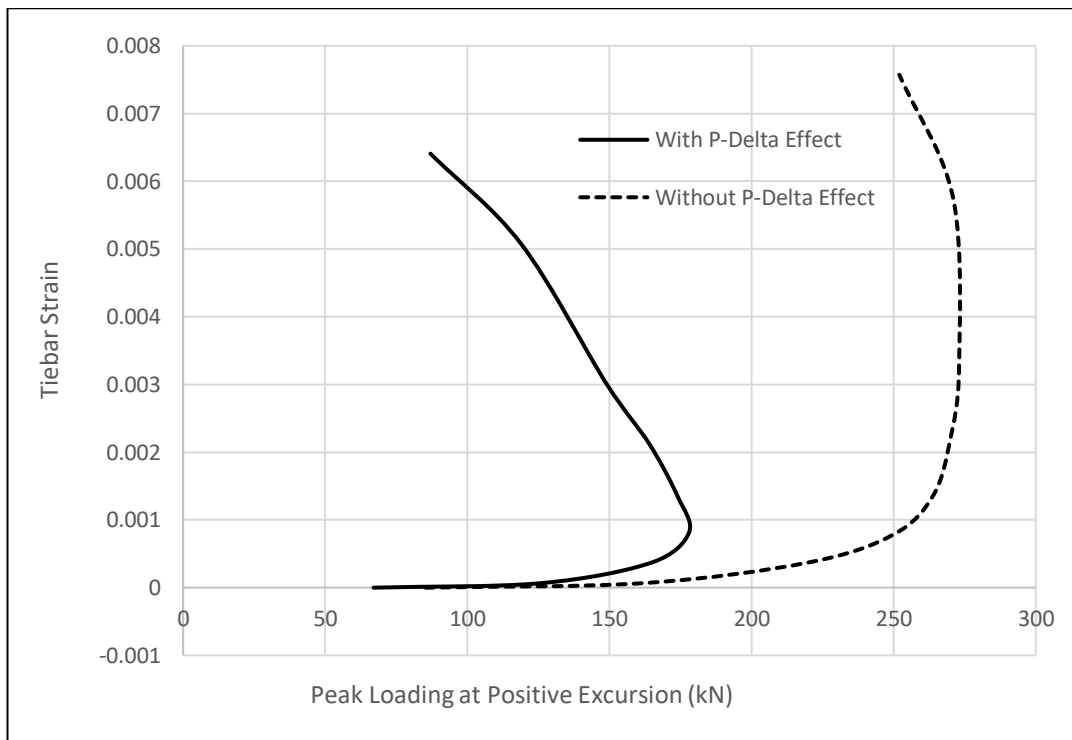


Figure 7-26. Stirrup Strain -Peak Loading Response at 447 mm from base section for positive excursion

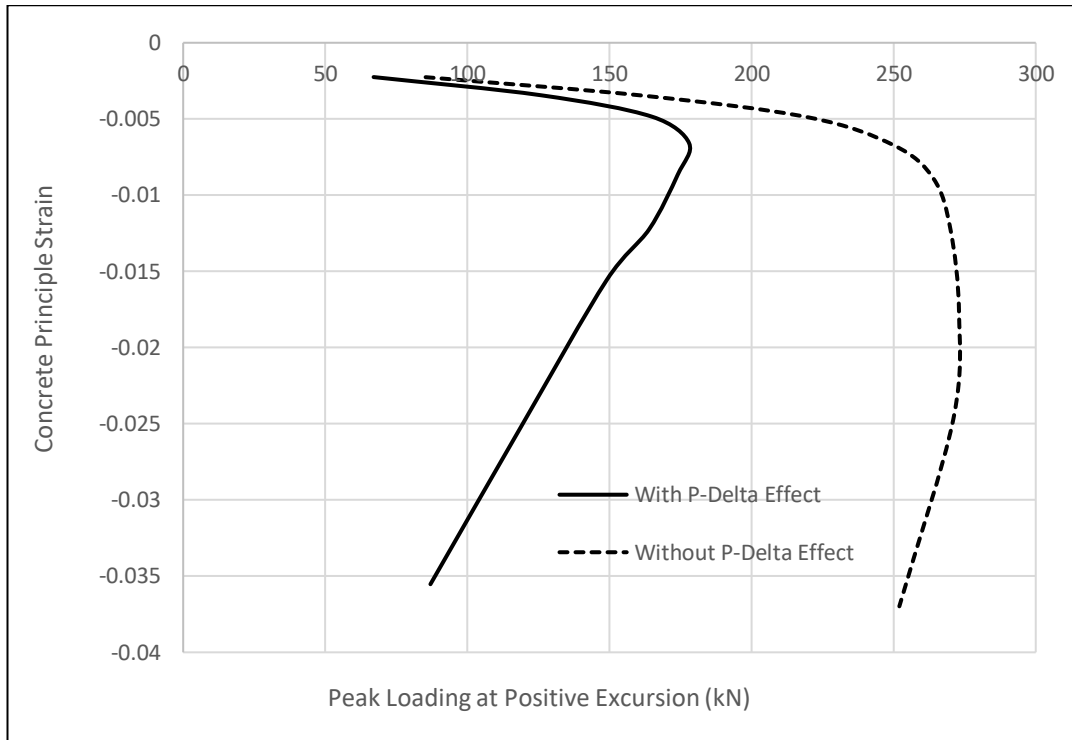


Figure 7-27. Principle Strain-Peak Loading Response of Rightmost Concrete Fibre at base section for positive excursion

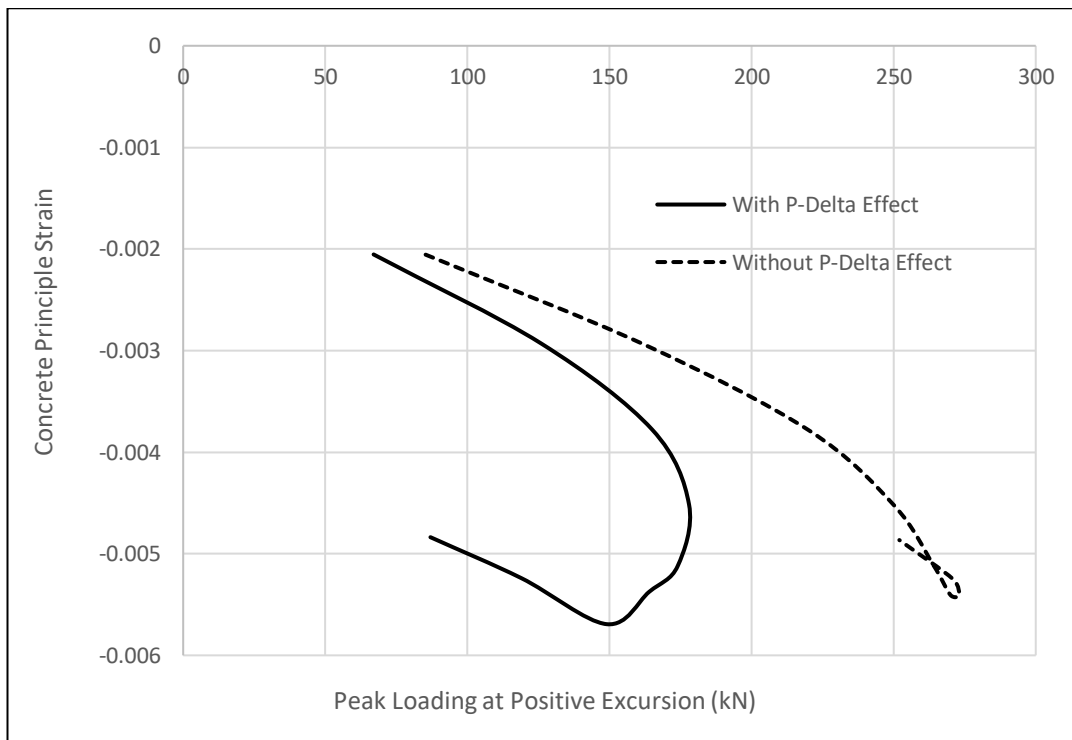


Figure 7-28. Principle Strain-Peak Loading Response of Rightmost Concrete Fibre at 447 mm from base section for positive excursion

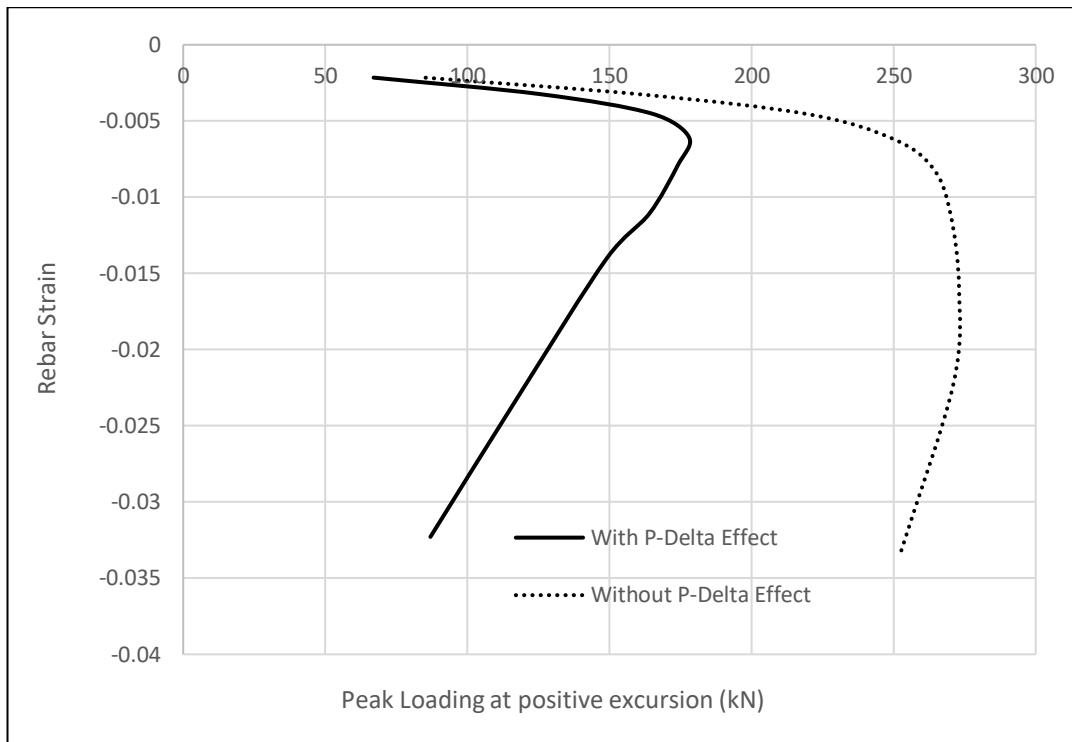


Figure 7-29. Axial Strain-Peak Loading Response of Rightmost vertical Steel Rebar at base section for positive excursion

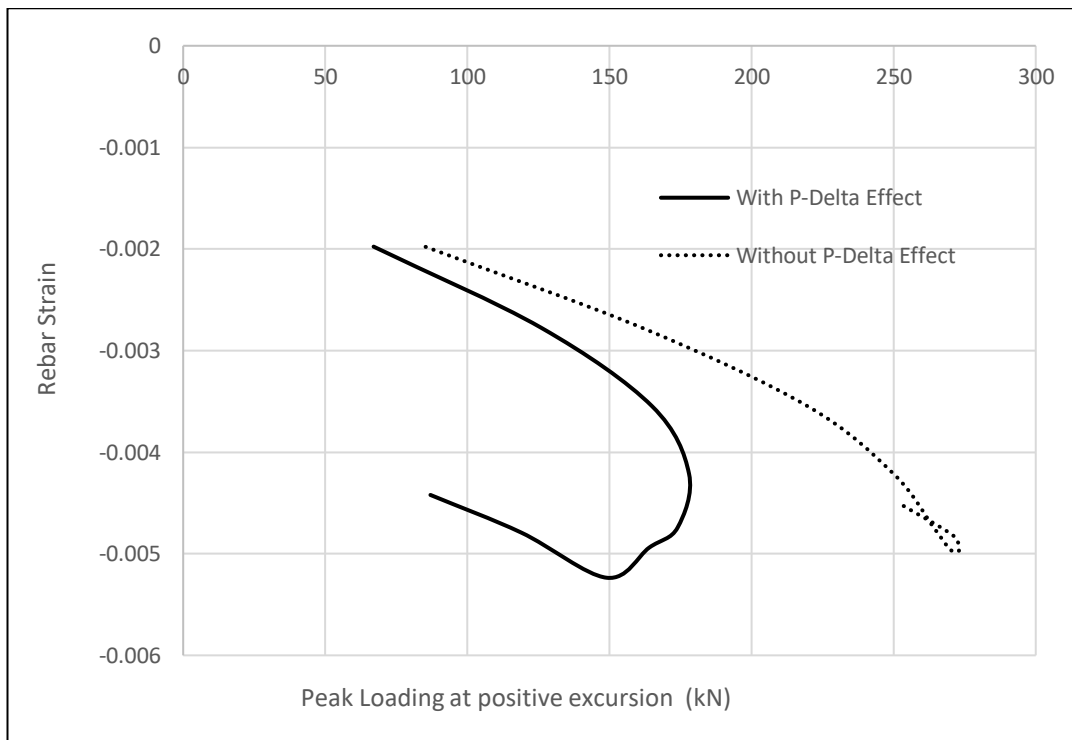


Figure 7-30. Axial Strain-Peak Loading Response of Rightmost vertical Steel Rebar at 447 mm from base section for positive excursion

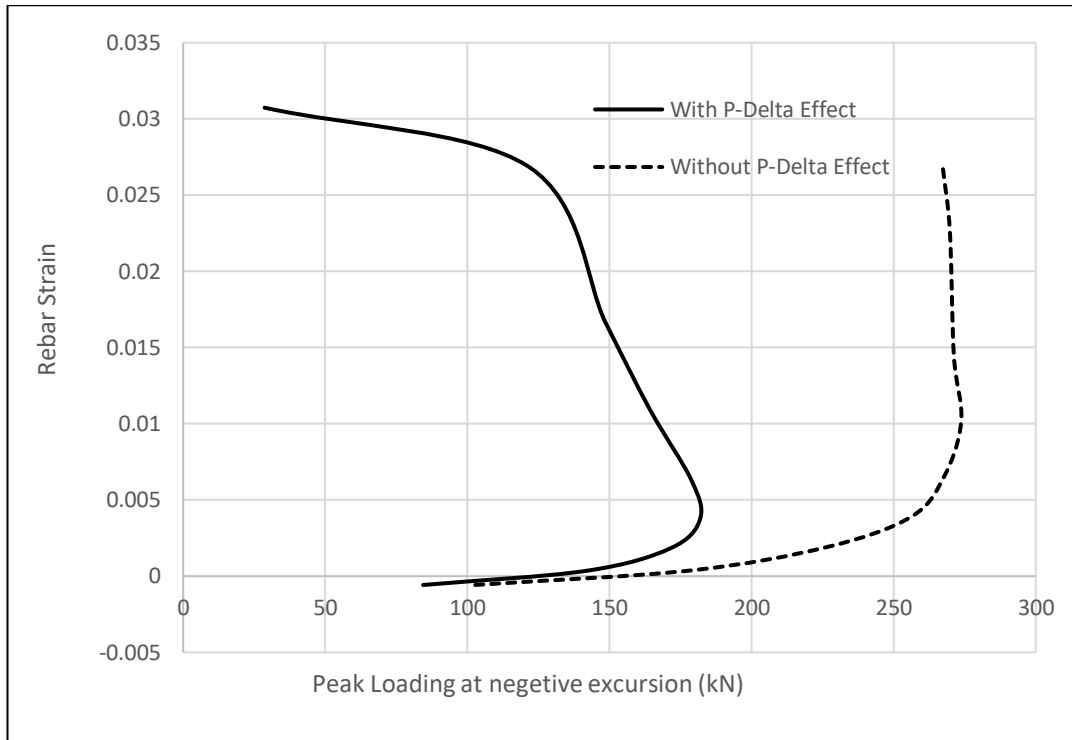


Figure 7-31. Axial Strain-Peak Loading Response of Rightmost vertical Steel Rebar at base section for negative excursion

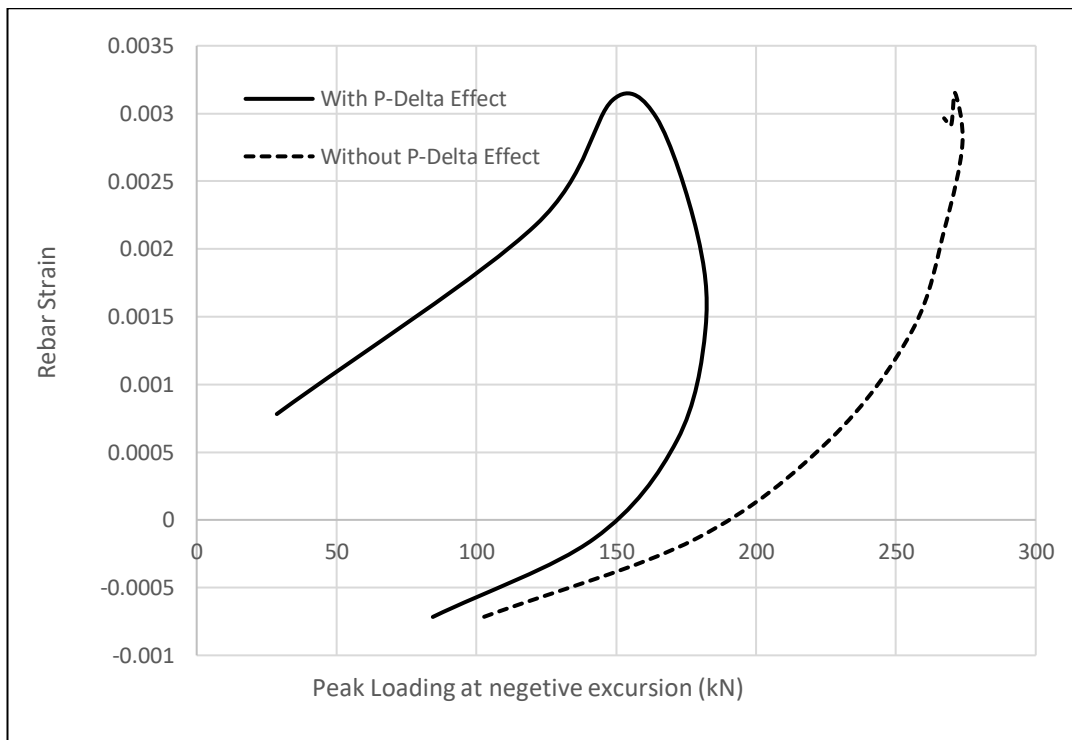


Figure 7-32. Axial Strain-Peak Loading Response of Rightmost vertical Steel Rebar at 447 mm from base section for negative excursion

Figure 7-18 shows the moment-peak loading response at positive excursion. It can be observed, the moment response is in 45 degree when we do not consider P-Delta effect as expected. However, if we consider P-Delta effect moment response gets deviated from the 45 degree response line, which indicates that the proposed element is able to successfully reproduce the geometric nonlinearity effect. This observation can also be supported from the Figure 7-19 where it has been clearly shown the effect of geometric nonlinearity on the moment response. P-Delta does not affect only on bending moment, it also similarly effect on shear force which can be seen from the Figures 7-20 and 7-21. Figure 7-22 shows the curvature-loading response at the base section. It can be observed that attainment of curvature is higher when we consider P-Delta effect in each loading cycle. Unlike bending moment and shear force, from Figure 7-23, it can be noted that curvature gets increased at later stage of loading which is consistent with the experimental observation. However, from Figure 7-24 it can be seen that curvature at 447 mm above the base section, gets unloaded which signifies that external input energy gets resisted almost fully by the shear energy i.e. failure gets controlled by shear mode. This phenomena can be again substantiated from the Figures 7-25 and 7-26 where stirrup strain gets increased at both base section and the section located 447 mm from the base section, which indicates that shear energy resists the external input

energy. It can also be observed from Figure 7-27 that concrete fibre reaches substantial amount of principle compressive strain. However, concrete compressive strain gets unloaded at the section located at 447 mm from the base section, which signifies that flexural action gets ceased i.e. shear mode fully controls the failure mode. This observation can also be supported from the Figures 7-29 and 7-30 where rightmost vertical rebar reaches substantial amount of strain at the base section but in the nearest section, the axial strain gets unloaded. Similar observations can also be seen from the Figures 7-31 and 7-32 for negative loading excursions.

From the above results, it can be concluded that the proposed mixed based shear beam element including geometric nonlinearity effect, successfully reproduce global and local behaviour along with the flexure and shear failure modes under both monotonic and cyclic loading conditions.

## **Chapter 8 Summary and Conclusions**

### **8.1 Summary**

The objective of this research work was the development of two dimensional frame finite element models for the analysis of shear critical reinforced concrete, steel and steel-concrete composite structural members considering the interaction of axial force, bending moment and shear force under monotonic and cyclic loading conditions. The frame elements are based on a two-field mixed formulation following Hellinger-Reissner variational principle where both section forces and displacements are simultaneously approximated within the element through independent interpolation functions. Force interpolation functions satisfy the differential section equilibrium equations in its strong form i.e. nodal equilibrium equations with externally applied concentrated loads in an internally statically determinate system under small deformation assumptions. The composite frame elements with partial interaction are based on both displacement and two-field mixed formulations where the slip field has been determined from the independent nodal displacement degree of freedoms to solve the governing differential equations of statically internally indeterminate system. Shear deformation has been considered through the Timoshenko based section kinematics. Distributed inelasticity

at the element level is considered through the integration of section response of various section integration points along the length of the element by Gauss-Lobatto integration scheme. Section response in a particular section integration point has been obtained by integration of material response of fibre discretization across the cross-section through the midpoint integration rule. The interaction between normal and shear stress has been considered through 2D material model at a single material point in a section. Response in the vertical direction of 2D material model has been statically condensed out by satisfying the vertical stress equilibrium equation.

For the analysis of reinforced concrete members, a fixed crack smeared softened membrane model which is based on the stress equilibrium, the strain compatibility and the constitutive relationships of materials, has been used to account for multi-axial stress states due to crack-induced anisotropy in reinforced concrete fibres. Softening effect on compressive strength of concrete due to perpendicular tensile strains, tension stiffening effects on concrete due to longitudinal reinforcement and effect of concrete on reinforcement stress-strain relations have been considered in the material constitutive models. Transverse equilibrium between concrete and stirrups of 2D material fibre has been used considering no bond-slip along the vertical direction, to constrain the vertical stress component to synchronize

the stress field of the frame element. The proposed frame element has been validated by comparing the numerical response with experimental measurements of different types of reinforced concrete members under monotonic and cyclic loading conditions. Different failure modes of reinforced concrete beams, columns and shear walls i.e. flexure, flexure-shear and shear modes have been simulated. The good agreement between experimental and numerical results validates the proposed element formulation.

For the analysis of steel members, 2D J2 plasticity and generalized plasticity models with radial return mapping algorithm are implemented for structural steel fibres under monotonic and cyclic loading conditions respectively to accommodate the interaction among the multi-axial stress states. The proposed frame element has been validated by comparing the numerical response with experimental measurements of shear critical shear links of eccentrically braced frame systems under monotonic and cyclic loading conditions. The good agreement between experimental and numerical results validates the proposed element formulation.

For the analysis of shear critical steel-concrete composite members with deformable shear connectors, the above mentioned material models are implemented to consider the multi-axial stress states. The transfer of forces

between steel and concrete due to partial interaction has been modelled by distributed spring elements. The element is validated through correlation studies with experimental results of shear critical SC composite beams for monotonic loading conditions. The good agreement between experimental and numerical results validates the proposed composite element formulations with partial interaction.

This research work concludes with the development of frame element under large displacements which is based on two-field mixed formulations following Hellinger-Reissner variational principle. The corotational formulation has been used to describe the large displacement at the element nodal level which has generated the external geometric stiffness matrix. Degenerated form of Green-Lagrange strain measure in the generalized section deformation has been used at the basic element level which has produced the internal geometric stiffness matrix. The proposed frame element has been validated through correlation studies with experimental results of flexure and flexure-shear critical slender reinforced concrete columns (shear slenderness ratio  $> 5$ ) under both monotonic and cyclic loading conditions. The good agreement between numerical and experimental results validates the proposed frame element considering both material inelasticity and geometric nonlinearity.

The proposed frame element formulations are not able to account for various experimentally observed limit states such as local buckling, the dowel actions of reinforcing steel and rebar fracture at the cracks.

## **8.2 Conclusions**

The strength and deformation capacity depend on cumulative damage experienced by the components under seismic loading excursions. Thus cyclic loading protocols used in the experiments should be able to create accurate cumulative damage in the component, to become the representative of the anticipated seismic time history (Krawinkler et al. (2001)). The proposed finite element models used memory or history dependent cyclic material constitutive laws, thus are able to capture the cumulative damage effect. Experimentally observed strength, deformation and energy dissipation capacity along with strength and stiffness degradation of various components have been reasonably reproduced by the proposed finite element models under cyclic loading conditions. Therefore, it can be concluded that the proposed frame elements formulations based on two-field Hellinger-Reissner functional, are suitable for seismic analysis of structures.

The following conclusions can be drawn from this research work.

## **Element Formulation**

- Consistent variational framework of frame element formulations for determining element tangent stiffness and resistance matrix has been developed by following four critical steps:
  1. Choosing of variational principle and development of functional at the section level
  2. Variation of chosen functional based on independent arguments
  3. Discretization of section level generalized degrees of freedom
  4. Linearization of variation of functional with respect to principle nodal arguments
- New stability criteria for two-field mixed based frame element formulations considering shear deformation have been proposed.
- Axial-flexure-shear interaction has been successfully captured by the proposed frame elements through the implementation of 2D material models.

## **Reinforced Concrete and Steel Members**

- Load deformation response of flexure-shear and shear critical reinforced concrete beams with various shear span to depth ratio, which fails in flexure compression and shear compression, has been simulated rationally well.
- The proposed frame element can reasonably simulate the load-deflection response, unloading and reloading stiffness, shear resistance and deformation capacity and pinching effect of reinforced concrete columns with various aspect ratios under cyclic loading conditions.
- The load deflection response of flexure-shear critical reinforced concrete shear walls along with hysteretic energy with pinching effect has been captured by the proposed frame element very well.
- The implemented J2 plasticity and generalized plasticity material models of steel have excellently simulated the monotonic and reverse cyclic load deformation response of shear critical shear links.

## **Composite Members with Partial Interaction**

- The numerical studies of the proposed composite frame element with partial interaction have proved the superiority of mixed based formulations over displacement based elements.
- The proposed composite elements with deformable shear connectors have successfully captured the load deflection response of steel-concrete-steel sandwiched beams under monotonic loading conditions.
- Various global and local response variables for steel-concrete composite decks such as the load-deflection response, inelastic curvature and shear deformation distribution along the length of the beam has been excellently captured by the proposed mixed based composite element.
- To represent the local behaviour of composite beams, displacement based formulations need a large number of elements compared to that for the global response simulation. In both cases, the number of required elements is much larger compared to the mixed based formulation to achieve a similar degree of convergence.

## **Reinforced Concrete Members with Geometric Nonlinearity**

- The proposed frame element considering both material and geometric nonlinearity can capture the load-deflection response and hysteretic behaviour of slender flexure critical reinforced concrete columns under both monotonic and cyclic loading conditions successfully.
- A consistent state determination process has been developed for mixed based frame element with large displacement effects through a corotational formulation.
- The experimentally observed post-peak softening region of shear force-shear deformation curve of slender reinforced concrete columns which fails in a flexure-shear mode has been simulated by the proposed frame elements satisfactorily.
- Shear strength degradation due to P-Delta effect in both positive and negative regions of reinforced concrete columns subjected to simultaneous axial compressive and lateral loading, has successfully been captured by the proposed frame element.

### **8.3 Recommendations for Future Research**

The following directions for future research work can be adopted to extend the capabilities of the proposed frame element formulations:

- The frame element formulations can be extended to enhance the material models by including longitudinal bar buckling, dowel actions, low cyclic fatigue and fracture, mechanisms related to the behaviour before and after the onset of axial failure, cyclic damage, robust crack opening and closing phenomena under cyclic loading condition.
- Integration of anchorage-slip phenomena following bond stress/strain variation inside the joints based on equilibrium, compatibility and constitutive law, with the proposed frame elements considering numerical and physical shear localization will help to accurately determine the load deformation response.
- The proposed frame elements can be extended for other loading scenarios such as impact, blast, temperature, creep and fatigue etc.
- 3D element formulations considering both material and geometric nonlinearity with section distortion and warping will certainly enhance the capability of the proposed frame elements to reach an esteemed level.

## Appendix A

The elements of external geometric stiffness matrix  $\mathbf{K}_{og}$  were first developed by Alemdar (2001). Here, the matrix has been modified to consider the effect of the middle degree of freedom.

$$\mathbf{K}_{og} = \begin{bmatrix} G_{11} & G_{12} & 0 & G_{14} & G_{15} & 0 & 0 \\ G_{21} & G_{22} & 0 & G_{24} & G_{25} & 0 & 0 \\ 0 & 0 & 0 & 0 & 0 & 0 & 0 \\ G_{41} & G_{42} & 0 & G_{44} & G_{45} & 0 & 0 \\ G_{51} & G_{52} & 0 & G_{54} & G_{55} & 0 & 0 \\ 0 & 0 & 0 & 0 & 0 & 0 & 0 \\ 0 & 0 & 0 & 0 & 0 & 0 & 0 \end{bmatrix}$$

$$G_{11} = -(Q_{ele}(2) + Q_{ele}(3) + Q_{ele}(4)) \frac{-(y_{21} + v_{21})2L \frac{\partial L}{\partial u_1}}{L^4} - Q_{ele}(1) \frac{-L - (x_{21} + u_{21}) \frac{\partial L}{\partial u_1}}{L^2}$$

$$G_{12} = (Q_{ele}(2) + Q_{ele}(3) + Q_{ele}(4)) \frac{-L^2 - (x_{21} + u_{21})2L \frac{\partial L}{\partial u_1}}{L^4} - Q_{ele}(1) \frac{-(y_{21} + v_{21}) \frac{\partial L}{\partial u_1}}{L^2}$$

$$G_{14} = (Q_{ele}(2) + Q_{ele}(3) + Q_{ele}(4)) \frac{-(y_{21} + v_{21})2L \frac{\partial L}{\partial u_1}}{L^4} + Q_{ele}(1) \frac{-L - (x_{21} + u_{21}) \frac{\partial L}{\partial u_1}}{L^2}$$

$$G_{15} = -(Q_{ele}(2) + Q_{ele}(3) + Q_{ele}(4)) \frac{-L^2 - (x_{21} + u_{21})2L \frac{\partial L}{\partial u_1}}{L^4} + Q_{ele}(1) \frac{-(y_{21} + v_{21}) \frac{\partial L}{\partial u_1}}{L^2}$$

$$G_{21} = -(Q_{ele}(2) + Q_{ele}(3) + Q_{ele}(4)) \frac{-L^2 - (y_{21} + v_{21})2L \frac{\partial L}{\partial v_1}}{L^4} - Q_{ele}(1) \frac{-(x_{21} + u_{21}) \frac{\partial L}{\partial v_1}}{L^2}$$

$$G_{22} = (Q_{ele}(2) + Q_{ele}(3) + Q_{ele}(4)) \frac{-(x_{21} + u_{21})2L \frac{\partial L}{\partial v_I}}{L^4} - Q_{ele}(1) \frac{-L - (y_{21} + v_{21}) \frac{\partial L}{\partial v_I}}{L^2}$$

$$G_{24} = (Q_{ele}(2) + Q_{ele}(3) + Q_{ele}(4)) \frac{-L^2 - (y_{21} + v_{21})2L \frac{\partial L}{\partial v_I}}{L^4} + Q_{ele}(1) \frac{-(x_{21} + u_{21}) \frac{\partial L}{\partial v_I}}{L^2}$$

$$G_{25} = -(Q_{ele}(2) + Q_{ele}(3) + Q_{ele}(4)) \frac{-(x_{21} + u_{21})2L \frac{\partial L}{\partial v_I}}{L^4} + Q_{ele}(1) \frac{-L - (y_{21} + v_{21}) \frac{\partial L}{\partial v_I}}{L^2}$$

$$G_{41} = -(Q_{ele}(2) + Q_{ele}(3) + Q_{ele}(4)) \frac{-(y_{21} + v_{21})2L \frac{\partial L}{\partial u_J}}{L^4} - Q_{ele}(1) \frac{L - (x_{21} + u_{21}) \frac{\partial L}{\partial u_J}}{L^2}$$

$$G_{42} = (Q_{ele}(2) + Q_{ele}(3) + Q_{ele}(4)) \frac{L^2 - (x_{21} + u_{21})2L \frac{\partial L}{\partial u_J}}{L^4} - Q_{ele}(1) \frac{-(y_{21} + v_{21}) \frac{\partial L}{\partial u_J}}{L^2}$$

$$G_{44} = (Q_{ele}(2) + Q_{ele}(3) + Q_{ele}(4)) \frac{-(y_{21} + v_{21})2L \frac{\partial L}{\partial u_J}}{L^4} + Q_{ele}(1) \frac{L - (x_{21} + u_{21}) \frac{\partial L}{\partial u_J}}{L^2}$$

$$G_{45} = -(Q_{ele}(2) + Q_{ele}(3) + Q_{ele}(4)) \frac{L^2 - (x_{21} + u_{21})2L \frac{\partial L}{\partial u_J}}{L^4} + Q_{ele}(1) \frac{-(y_{21} + v_{21}) \frac{\partial L}{\partial u_J}}{L^2}$$

$$G_{51} = -(Q_{ele}(2) + Q_{ele}(3) + Q_{ele}(4)) \frac{-L^2 - (y_{21} + v_{21})2L \frac{\partial L}{\partial v_J}}{L^4} - Q_{ele}(1) \frac{-(x_{21} + u_{21}) \frac{\partial L}{\partial v_J}}{L^2}$$

$$G_{52} = (Q_{ele}(2) + Q_{ele}(3) + Q_{ele}(4)) \frac{-(x_{21} + u_{21})2L \frac{\partial L}{\partial v_J}}{L^4} - Q_{ele}(1) \frac{L - (y_{21} + v_{21}) \frac{\partial L}{\partial v_J}}{L^2}$$

$$G_{54} = (Q_{ele}(2) + Q_{ele}(3) + Q_{ele}(4)) \frac{L^2 - (y_{21} + v_{21})2L \frac{\partial L}{\partial v_J}}{L^4} + Q_{ele}(1) \frac{-(x_{21} + u_{21}) \frac{\partial L}{\partial v_J}}{L^2}$$

$$G_{55} = -(Q_{ele}(2) + Q_{ele}(3) + Q_{ele}(4)) \frac{-(x_{21} + u_{21})2L \frac{\partial L}{\partial v_j}}{L^4} + Q_{ele}(1) \frac{L - (y_{21} + v_{21}) \frac{\partial L}{\partial v_j}}{L^2}$$

$$x_{21} = (x_2 - x_1)$$

$$u_{21} = (u_j - u_l)$$

$$y_{21} = (y_2 - y_1)$$

$$v_{21} = (v_j - v_l)$$

$$L = \sqrt{((x_2 - x_1) + (u_j - u_l))^2 + ((y_2 - y_1) + (v_j - v_l))^2}$$

$$\frac{\partial L}{\partial u_l} = -\frac{x_{21} + u_{21}}{L}$$

$$\frac{\partial L}{\partial u_j} = \frac{x_{21} + u_{21}}{L}$$

$$\frac{\partial L}{\partial v_l} = -\frac{y_{21} + v_{21}}{L}$$

$$\frac{\partial L}{\partial v_j} = \frac{y_{21} + v_{21}}{L}$$

## Appendix B

The Uniaxial material models for concrete and steel have been briefly described below.

The monotonic stress strain curve envelop of the concrete is represented by a parabolic curve as shown in Figure B-1.

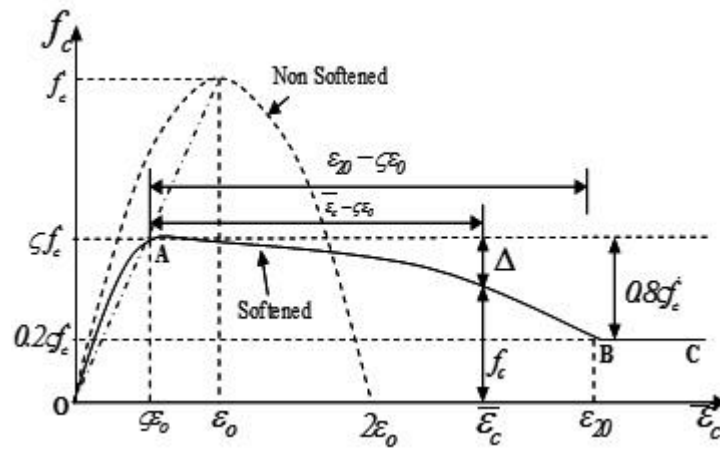


Figure B-1. Monotonic non-softened and softened stress–strain curve

The following equations are used for equivalent uniaxial strength  $f_c$  and tangent stiffness  $E_t$  at different regions of compressive stress-strain curve shown in Figure 2-6:

For region OA,

$$f_c = \zeta \dot{f}_c \left[ 2 \left( \frac{\bar{\varepsilon}_c}{\zeta \varepsilon_0} \right) - \left( \frac{\bar{\varepsilon}_c}{\zeta \varepsilon_0} \right)^2 \right] \quad (1)$$

$$E_t = \frac{2 \dot{f}_c}{\varepsilon_0} \left( 1 - \frac{\bar{\varepsilon}_c}{\zeta \varepsilon_0} \right) \quad (2)$$

For region AB,

$$f_c = \zeta \dot{f}_c \left[ 1 - 0.8 \left( \frac{\bar{\varepsilon}_c - \zeta \varepsilon_0}{\varepsilon_{20} - \zeta \varepsilon_0} \right)^2 \right] \quad (3)$$

$$E_t = -1.6 \zeta \dot{f}_c \left( \frac{\bar{\varepsilon}_c - \zeta \varepsilon_0}{(\varepsilon_{20} - \zeta \varepsilon_0)^2} \right) \quad (4)$$

For region BC,

$$f_c = 0.2 \zeta \dot{f}_c \quad (5)$$

$$E_t = 0 \quad (6)$$

For reverse cyclic loading condition, unloading and reloading behaviour represented by straight lines (Figure B-2), developed by Zulfiqar et al. (1990) has been used in this research work with the above mentioned softened stress-strain relationship. It has been observed from the experimental tests (Sinha et al. (1964) and Karsan et al. (1969)) of cyclic

compressive loading of concrete that the envelope curve for cyclic loading coincided with the stress-strain curve of monotonic loading.

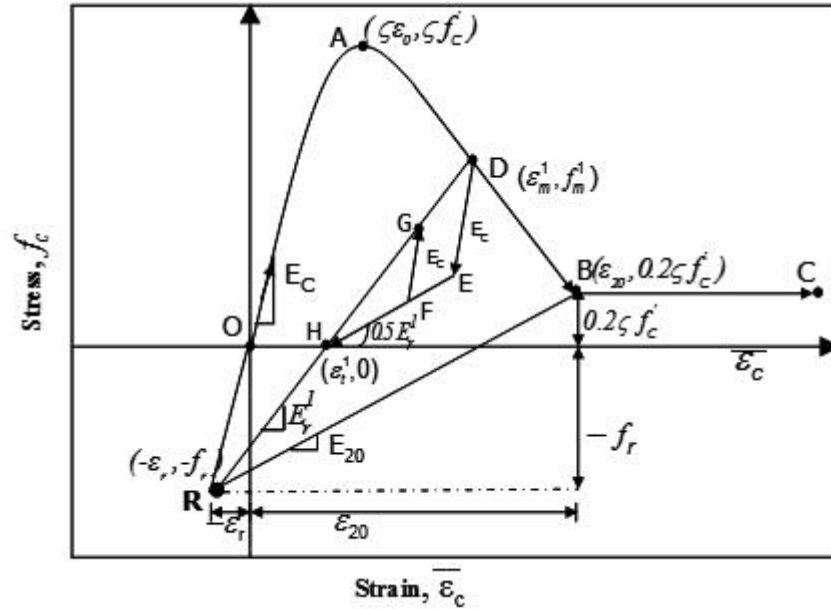


Figure B-2. Cyclic Softened Compression Stress-Strain Relation

Successive degradation of stiffness with increasing compressive strains is represented by projecting all reloading lines into the intersection point R which is determined by the intersection of the tangent to the monotonic envelope curve at the origin and the projection of the unloading line from point B that corresponds to the concrete strength of  $0.2\zeta f_c$ .

Strain and stress at the intersection point R is:

$$\varepsilon_r = \frac{0.2\zeta f_c - E_{20}\varepsilon_{20}}{E_c - E_{20}} \quad (7)$$

$$f_r = E_c \varepsilon_r \quad (8)$$

$$E_c = \frac{2f_c}{\varepsilon_0} \quad (9)$$

$E_{20}$  is determined from experimental data.

Stress at any point of unloading lines can be determined as follows.

On HD branch,

$$f_{hd} = f_m + E_r(\bar{\varepsilon}_c - \varepsilon_m) \quad (10)$$

On HE branch,

$$f_{he} = 0.5E_r(\bar{\varepsilon}_c - \varepsilon_t) \quad (11)$$

Where

$$E_r = \frac{f_m - f_r}{\varepsilon_m - \varepsilon_r}$$

$$\varepsilon_t = \varepsilon_m - \frac{f_m}{E_r}$$

Where  $f_m$  and  $\varepsilon_m$  are the stress and strain at the unloading point on the compressive monotonic envelope. It is to be noted that in this model, after reloading to compressive region, the reloading line re-joins the starting unloading point.

For partial unloading and reloading cycle, the model follows a straight line with modulus  $E_c$ . The following rules are adopted to determine the stress and stiffness of these branches:

For  $f_{he} \leq f_c^t \leq f_{hd}$

$$f_c = f_c^t \tag{12}$$

$$E_t = E_c \tag{13}$$

For  $f_c^t < f_{he}$

$$f_c = f_{he} \tag{14}$$

$$E_t = 0.5E_r \tag{15}$$

For  $f_c^t > f_{hd}$

$$f_c = f_{hd} \quad (16)$$

$$E_t = E_r \quad (17)$$

Where  $f_c^t$  is the trial stress determined from strain increment  $\Delta\bar{\epsilon}_c$ :

$$f_c^t \text{ at } (t + 1) = f_c^t \text{ at } (t) + E_c \Delta\bar{\epsilon}_c \quad (18)$$

The tensile unloading and reloading rules are independent of the compressive ones. It can be seen from Figure B-3 that model can simulate tensile stiffening, stiffness degradation for unloading and reloading branches. The tensile stress-strain relation is controlled by three points i.e. J, K and M.



$$\sigma_c = \sigma_n + E_t(\bar{\varepsilon}_c - \varepsilon_n) \quad (22)$$

On MN branch  $\bar{\varepsilon}_c > \varepsilon_u$

$$E_t = 0 \quad (23)$$

$$\sigma_c = 0 \quad (24)$$

Here,  $\varepsilon_n$  and  $\sigma_n$  are the strain and stress at the peak of the tensile stress-strain relation:

$$\varepsilon_n = \varepsilon_t + \Delta\varepsilon_t \quad (25)$$

$$\sigma_n = \hat{f}_t \left(1 + \frac{E_{ts}}{E_c}\right) - E_{ts}\Delta\varepsilon_t \quad (26)$$

$\Delta\varepsilon_t$  is determined as follows:

$$\Delta\varepsilon_t = \frac{\hat{f}_t}{E_c} \text{ before cracking} \quad (27)$$

After cracking:

$$\Delta\varepsilon_t = \text{previous maximum differential between tensile strain and } \varepsilon_t \quad (28)$$

$\varepsilon_u$  is the point where tensile stress is zero.

$$\varepsilon_u = \varepsilon_t + \hat{f}_t \left( \frac{1}{E_{ts}} + \frac{1}{E_c} \right) \quad (29)$$

$$\hat{f}_t = 0.31 \sqrt{\hat{f}_c} (MPa) \quad (30)$$

Here,  $E_{ts}$  is the tension stiffening modulus and  $E_c$  is the initial compressive modulus.

Uniaxial steel model is used for the rebars in the reinforced concrete members. There are many types of uniaxial models available. The bilinear steel model is the simplest one but is suitable for monotonic loading conditions only. In this study, nonlinear model developed by Menegotto et al. (1973) and later modified by Filippou et al. (1983) to include isotropic strain hardening has been adopted (Figure B-4). This model has been used by many researchers for modelling reinforcing stress-strain hysteretic behaviour under cyclic loading conditions as with this model through single equation both loading and unloading states can be described and it is computationally efficient and agrees very well with cyclic experimental

results on reinforcing bars. Rebar buckling and fracture has not been included in this research work. Interested readers are referred to Dhakal et al. (2002), Zong et al. (2014) and Kenawy et al. (2018).

The stress-strain relationship of the model is:

$$\sigma^* = b\varepsilon^* + \frac{(1-b)\varepsilon^*}{(1+\varepsilon^{*R})^{1/R}} \quad (31)$$

Where:

$$\varepsilon^* = \frac{\varepsilon - \varepsilon_r}{\varepsilon_0 - \varepsilon_r}$$

$$\sigma^* = \frac{\sigma - \sigma_r}{\sigma_0 - \sigma_r}$$

$$R = R_0 - \frac{a_1 \xi}{a_2 + \xi}$$

$$\xi = \left| \frac{(\varepsilon_m - \varepsilon_0)}{\varepsilon_y} \right|$$

$$b = \frac{E_h}{E}$$

$$E_h = \frac{\sigma_u - \sigma_y}{\varepsilon_0 - \varepsilon_y}$$

$$\varepsilon_y = \frac{\sigma_y}{E}$$

The tangent modulus can be determined as:

$$E_t = \left( \frac{\sigma_0 - \sigma_r}{\varepsilon_0 - \varepsilon_r} \right) \frac{d\sigma^*}{d\varepsilon^*} \quad (32)$$

Where,

$$\frac{d\sigma^*}{d\varepsilon^*} = b + \left( \frac{(1-b)}{(1+\varepsilon^{*R})^{\frac{1}{R}}} \right) \left( 1 - \frac{\varepsilon^{*R}}{1+\varepsilon^{*R}} \right)$$

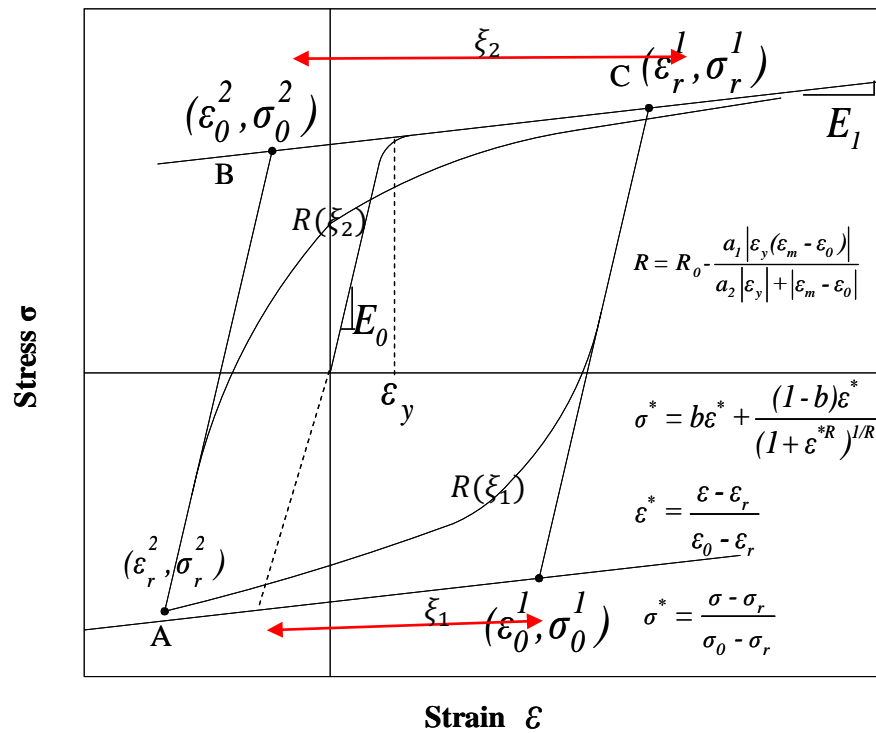


Figure B-4. Menegotto-Pinto model

Filippou et al. (1983) has modified this model to account for isotropic hardening by imposing a shift in stress through moving the yield asymptote through the following relation:

$$\sigma_{st} = a_3 \left( \frac{\varepsilon_{max}}{\varepsilon_y} - a_4 \right) \sigma_y \quad (33)$$

Here,  $E_0$  and  $E_h$  are elastic modulus and strain hardening modulus. The point  $(\sigma_r, \varepsilon_r)$  corresponds to the last reversal. The point  $(\sigma_0, \varepsilon_0)$  corresponds to the interaction point of initial and strain hardening modulus lines after strain reversal. Curvature of transition asymptote and Bauschinger effect is represented by the parameter  $R$ . The points  $(\sigma_r, \varepsilon_r)$  and  $(\sigma_0, \varepsilon_0)$  are updated after each strain reversal.  $\varepsilon_m$  is the strain at the previous maximum or minimum strain reversal point depending on whether the current strain is increasing or decreasing and  $\varepsilon_0$  is the strain at the current intersection point of two asymptotes. Therefore,  $\xi$  needs to be updated following a strain reversal.  $\varepsilon_{max}$  is the absolute strain at the maximum strain reversal point if the stress shift is applied to the negative yield asymptote or at the minimum strain reversal point if the stress shift is applied to the positive yield asymptote. The fixed parameters  $\sigma_y, E, b, R_0, a_1, a_2, a_3, a_4$  are determined from experimental data.

The effect of concrete on rebar needs to be accounted for as proposed by Belarbi et al. (1994, 1995):

For  $\bar{\epsilon}_s \leq \epsilon'_y$

$$\sigma_s = E_s \bar{\epsilon}_s \quad (34)$$

$$E_t = E_s \quad (35)$$

For  $\bar{\epsilon}_s > \epsilon'_y$

$$\sigma_s = (0.91 - 2B)f_y + (0.02 + 0.25B)E_s \bar{\epsilon}_s \quad (36)$$

$$E_t = (0.02 + 0.25B)E_s \quad (37)$$

For  $\bar{\epsilon}_s < \bar{\epsilon}_p$  during unloading

$$\sigma_s = f_p - E_s(\bar{\epsilon}_p - \bar{\epsilon}_s) \quad (38)$$

$$E_t = E_s \quad (39)$$

Where,

Smearred yield strain  $\hat{\epsilon}_y = \hat{f}_y E_s$

Smearred yield stress  $\hat{f}_y = (0.93 - 2B)f_y$

$$B = \frac{1}{\rho_{si}} \left( \frac{\hat{f}_t}{f_y} \right)^{1.5}$$

## Bibliography

### A

Alemdar, B.N. (2001). “Distributed plasticity analysis of steel building structural systems”, PhD thesis, Georgia Institute of Technology, Atlanta, GA.

Alemdar, B.N. and White, D.W. (2005). “Displacement, Flexibility and Mixed Beam-Column Finite element Formulations for Distributed Plasticity Analysis.” *Journal of structural engineering*, 10.1061/(ASCE)0733-9445; 131:12(1811).

Almeida, JP, Correia, AA, Rui, P (2015). “Force-based higher-order beam element with flexural-shear-torsional interaction in 3D frames. Part II: Applications” *Eng. Struct.* 89: 218–235.

Alsafadie, R., Hjiij, M. and Battini, J. M. (2001). “Three dimensional formulation of a mixed corotational thin-walled beam element incorporating shear and warping deformation.” *Thin Walled Structures*, 49(4), pp. 523-533.

Arakawa, T., Arai, Y., Mizoguchi, M., et al. (1989). “Shear resisting behavior of short reinforced concrete columns under biaxial bending–shear.” *Trans Jpn Conc Inst*;11:317–24.

Argyris, J., Tenek, L., Mattsson, A. (1988). “BEC: a 2-node fast converging shear-deformable isotropic and composite beam element based on 6 rigid-body and 6 straining modes.” *Comput Methods Appl Mech Eng* 152:281–336.

Armstrong, P.J., and Frederick, C.O. (1965). “A Mathematical Representation of the Multi-axial Baushinger Effect.” Tech. Report C.E.G.B. Report RD/B/N731, *Berkeley Nuclear Laboratories*, R&DDepartment.

Auricchio, F., Taylor, R. L. and Lubliner, J. (1992). “Application of a return map algorithm to plasticity models.” in: D.R.J. Owen et al., eds., *Computational Plasticity*, 3rd Int. Conf. (Pineridge) 2229-2248.

Auricchio, F., and Taylor, R. L. (1995). “2 material models for cyclic plasticity-Nonlinear kinematic hardening and generalized plasticity.” *Int. J. Plast.*, 11(1), 65–98.

Ayoub, A. S. (1999). “Mixed formulation for seismic analysis of composite steel-concrete frame structures.” Ph.D. thesis, *Univ. of California*, Berkeley, CA.

Ayoub, A. S., and Filippou, F. C. (1999). “Mixed formulation of bond slip problems under cyclic loads.” *J. Struct. Eng.*, 125 (6), 661-671.

Ayoub, A., and Filippou, F. C. (2000). “Mixed formulation of nonlinear steel-concrete composite beam element.” *J. Struct. Eng.*, 126 (3), 371-381.

Ayoub, A. (2001). “A two-field mixed variational principle for partially connected composite beams.” *Finite Elements in Analysis and Design*, 37 (11), 929-959.

Ayoub, A., and Filippou, F. C. (2002). “Discussion of “Reinforced Concrete Frame Element with Bond Interfaces. II: State Determinations and Numerical Validation by Suchart Limkatanyu and Enrico Spacone” *J. Struct. Eng.*, March 2002, Vol. 128, No. 3, pp. 356–364.

## B

Bae, S., Bayrak, O. (2008). “Plastic hinge length of reinforced concrete columns.” *ACI Struct J*; 105(3):290–300.

Bairan, J. M. and Mari, A. R. (2006a). “Coupled model for the non-linear analysis of anisotropic sections subjected to general 3D loading. Part 1: Theoretical formulation,” *Computers and Structures* 84, 2254–2263.

Bairan, J. M. and Mari, A. R. (2006b). “Coupled model for the non-linear analysis of anisotropic sections subjected to general 3D loading. Part 2: Implementation and validation,” *Computers and Structures* 84, 2264–2276.

Barrera, A., Bonet, J., Romero, M., Miguel, P. (2011). “Experimental tests of slender reinforced concrete columns under combined axial load and lateral force.” *Eng Struct* 33(12):3676–89.

Bathe, K.J. (1996). “*Finite Element Procedures*.” Prentice-Hall, Upper Saddle River, New Jersey.

Batista, J., Sousa, M. (2013). “Exact finite elements for multi-layered composite beam-columns with partial interaction.” *Comput Struct*; 123:48–57.

Bazant, Z. P. and Kim, S. S. (1979). "Plastic-Fracturing Theory for Concrete." *Journal of the Engineering Mechanics Division-ASCE* 105(3): 407-428.

Bazant, Z. P. and Oh, B. H. (1985). "Microplane model for progressive fracture of concrete and rock," *Journal of Engineering Mechanics*, ASCE 111(4), 559–582.

Bazant, Z. P. and P. C. Prat (1988). "Microplane Model for Brittle-Plastic Material .1.Theory." *Journal of Engineering Mechanics-ASCE* 114(10): 1672-1687.

Belarbi, A., Hsu, T.T.C. (1994). "Constitutive laws of concrete in tension and reinforcing bars stiffened by concrete." *Struct J Amer Concrete Institute*; 91(4):465–74.

Belarbi, A., Hsu, T.T.C. (1995). "Constitutive laws of softened concrete in biaxial tension-compression." *Struct J Amer Concrete Institute*;92(5):562–73.

Belega, B., Manglekar, H. C., and Ray, T. (2017). "Effects of axial-shear-flexure interaction in static and dynamic responses of steel beams." *J. Constr. Steel Res.* 131: 83–93.

Bentz, E. C. (2000). "Sectional analysis of reinforced concrete members," *PhD thesis*, University of Toronto, Toronto, Canada.

Bosco, M., Marino, E. M., and Rossi, P. P. (2015). "Modelling of steel link beams of short, intermediate or long length." *Eng. Struct.* 84: 406–418.

Bresler, B., and Scordelis, A. C. (1963). "Shear strength of reinforced concrete beams." *J. Am. Concr. Inst.*, 60(1), 51–72.

## C

Caballero-Morrison, K.E., Bonet, J.L., Navarro-Gregori, J., Martí-Vargas, J.R. (2012). "Behaviour of steel-fibre-reinforced normal-strength concrete slender columns under cyclic loading." *Eng Struct* 39:162–175.

Ceresa, P., Petrini, L., Rui, P. (2007). "Flexure–shear fiber beam-column elements for modeling frame structures under seismic loading-state of the art." *J Earthq Eng* 11(sup1):46–88

Ceresa, P., Petrini, L., Rui, P., Sousa, R. (2009). "A fibre flexure–shear model for seismic analysis of RC framed structures." *Earthq Eng Struct Dyn* 38(5):565–586.

Cervenka, J., Cervenka, V., Eligehausen, R. (1998). "Fracture-plastic material model for concrete. Application to analysis of powder actuated anchors." In: Proceedings of the 3rd international conference on fracture mechanics of concrete structures -*FraMCoS 3*. Gifu, Japan; p. 1107–16.

Chaboche, J. L. (1986). "Time-independent constitutive theories for cyclic plasticity." *Int. J. Plast.* 2 (2): 149–188.

Chakrabarti, A., Sheikh, A., Griffith, M., Oehlers, D. (2012). "Analysis of composite beams with longitudinal and transverse partial interactions using higher order beam theory." *Int. J. Mech. Sci.* 59; 115–125.

Chakrabarti, A., Sheikh, A., Griffith, M., Oehlers, D. (2012). "Dynamic response of composite beams with partial shear interaction using a higher-order beam theory," *J. Struct. Eng.* 139; 47–56.

Challamel, N., Girhammar, U.A. (2011). "Variationally-based theories for buckling of partial composite beam–columns including shear and axial effects." *Eng Struct* 33:2297–2319.

Chen, W.F. (1982). "Plasticity in Reinforced Concrete." McGraw-Hill, New York.

Cook, R. (1995). "Finite Element Modelling for Stress Analysis", John Wiley & Sons.

Correia, A.A., Almeida, J.P., Rui, P. (2015). "Force-based higher-order beam element with flexural-shear-torsional interaction in 3D frames. Part I: theory." *Eng Struct* 89:204–217.

Crisfield, M.A. (1991). "Non-linear Finite Element Analysis of Solids and Structures." volume 1-2. *John Wiley & Sons*.

## D

Dafalias, Y. F. & Popov, E. P. (1975). "A model of nonlinearly hardening materials for complex loading." *Acta Mechanica*, 21(3), pp. 173-192.

Dafalias, Y. F. (1986). "Bounding surface plasticity. I: Mathematical foundation and hypo plasticity." *Journal of Engineering Mechanics*, 112(9), pp. 966-987.

Das, D. and Ayoub, A. (2019). "Mixed formulation of Steel-Concrete Sandwiched Beam with partial Shear Slip", *Structural Congress*, Orlando, Florida, April 25-27.

Da Silva, A.R., Sousa, J.B.M. (2009). "A family of interface elements for the analysis of composite beams with interlayer slip." *Finite Elements in Analysis and Design* 45 (5); 305–314.

De Borst, R., Nauta, P. (1985). "Non-orthogonal cracks in a smeared finite element model." *Eng Comput*; 2:23–46.

De Souza, R.M. (2000). "Force-Based Finite Element for Large Displacement Inelastic Analysis of Frames." *University of California, Berkeley*.

De Veubeke, B. F. (1965). "Displacement and equilibrium models in the finite element method." *Stress Analysis*, Wiley, pp. 145-197.

De Veubeke, B. F. (1951). "Diffusion des inconnues hyper statiques dans les voilures a longer on couples." *Bulletin du Service Technique de L'Aeronautique* No. 24, Imprimerie Marcel Hayez, Bruxelles.

Dhakal, R. P., & Maekawa, K. (2002). "Modeling for post-yield buckling of reinforcement." *Journal of Structural Engineering*, ASCE, 128(9), 1139–1147.

Ding, R., Nie, J.G., Tao, M.X. (2018). "Fiber Beam–Column Element Considering Flange Contribution for Steel Links under Cyclic Loads." *J Struct Eng*; DOI: 10.1061/(ASCE)ST.1943-541X.0002072.

## E

Eligehausen, R., Popov, E.P., and Bertero, V.V. (1983). "Local Bond Stress-Slip Relationships of Deformed Bars Under Generalized Excitations". Report No. UCB/EERC 83-23, *Earthquake Engineering Research Center*, University of California, Berkeley, p. 178.

## F

Faria, R., Oliver, J. and Cervera, M. (1998). "A strain-based plastic viscous-damage model for massive concrete structures." *International Journal of Solids and Structures* 35(14): 1533-1558.

Feng, DC., Wu, G., Sun, ZY., Xu, JG. (2017). "A flexure–shear timoshenko fiber beam element based on softened damage-plasticity model." *Eng Struct* 140:483–497

Feng, DC., Xu, J. (2018). "An efficient fiber beam-column element considering flexure–shear interaction and anchorage bond-slip effect for cyclic analysis of RC structures." *Bull Earthquake Eng* 16:5425–5452.

Filippou, F.C., Fenves, G.L. (2004). "Methods of analysis for earthquake-resistant structures", in: Y. Bozorgnia, V.V. Bertero (Eds.), *Earthquake Engineering, From Engineering Seismology to Performance-Based Engineering*, CRC Press LLC.

Filippou, F.C., Popov, E.P., and Bertero, V.V. (1983). "Effects of Bond Deterioration on Hysteretic Behavior of Reinforced Concrete Joints". Report No. UCB/EERC-83/19, *Earthquake Engineering Research Center*, University of California, Berkeley, 191 pp.

Friedman, Z., Kosmatka, JB. (1993). "An improved two-node Timoshenko beam finite element." *Comput Struct* 47(3):473–481.

## G

Gendy, S.S.F. Mehanny., Ayoub, A. (2018). "Displacement and mixed fibre beam elements for modelling of slender reinforced concrete structures under cyclic loads." *Engineering Structures*; 173: 620–630.

Gregori, JN., Sosa, PM., Prada, MAF., Filippou, FC. (2007). "A 3D numerical model for reinforced and prestressed concrete elements subjected to combined axial, bending, shear and torsion loading." *Engineering Structures*; 29:3404–3419.

Guedes, J., Pegon, P., and Pinto, A. V. (1994). "A Fibre/Timoshenko Beam Element in CASTEM2000," Special Publication Nr. I.94.31 *Applied Mechanics Unit*, Safety Technology Institute, Commission of the European Communities, Joint Research Centre, Ispra Establishment, Italy.

Guner, S., and Vecchio, F. J. (2011). "Analysis of shear-critical reinforced concrete plane frame elements under cyclic loading." *J. Struct. Eng.*, 10.1061/(ASCE)ST.1943-541X.0000346, 834–843.

## H

Hellinger, E. (1914).“Die allgemeinen ansatze der mechanik der kontinua.”in: *Enzyklopadie der Mathematischen Wissenschaften*, pp. 654–655.

Hjelmstad, K. D., and Popov E. P. (1983). “Cyclic behavior and design of link beams.” *J. Struct. Eng.* 109 (10): 2387–2403.

Hjelmstad, K. D.,Taciroglu, E. (2005). “Variational basis of nonlinear flexibility methods for structural analysis of frames”, *Journal of Engineering Mechanics-ASCE* 131 (11)1157–1169.

Hjelmstad, K.D., Taciroglu, E. (2002).“Mixed methods and flexibility approaches for nonlinear frame analysis.” *Journal of Constructional Steel Research* 58 (5-8); 967–993.

Hjelmstad, K. D., and Taciroglu, E. (2003). “Mixed variational methods for finite-element analysis of geometrically non-linear, inelastic Bernoulli–Euler beams.” *Commun. Numer. Methods Eng.*, 19(10),809–832.

Hjiaj, M., Battini, J.-M., Nguyen, Q.H. (2012).“Large displacement analysis of shear deformable composite beams with interlayer slips.” *Int. J. Non-Linear Mech.* 47; 895–904.

Hsu, T.T.C., Belarbi, A. and Pang, X.B. (1995). “A Universal Panel Tester” *Journal of Testing and Evaluations, ASTM*, Vol 23, No 1, pp.41-49.

Hsu, T.T.C., and Zhu, R. H. (2001). “Softened Membrane Model for Reinforced Concrete Elements in Shear” *Structural Journal, American Concrete Institute*, Vol 99, No 4, pp.460-469.

Hsu, TTC., Zhang, LX. (1996). “Tension stiffening in reinforced concrete membrane elements.” *Struct J Amer Concrete Institute*;93(1):108–15.

Hsu, TTC., Zhang, LX. (1997). “Nonlinear analysis of membrane elements by fixed-angle softened-truss model.”*Struct J Amer Concrete Institute*;94(5):483–92.

Hsu, TTC., Zhu, RRH. (2002). “Softened membrane model for reinforced concrete elements in shear.” *Struct J Amer Concrete Institute*;99(4):460–9.

Hsu, TTC., Mansour, MY. (2005). “Stiffness, ductility, and energy dissipation of RC elements under cyclic shear.”*Earthquake Spectra, EERI*;21(4):1093–112.

Hu, H.-C. (1955). "On some variational methods on the theory of elasticity and the theory of plasticity." *Scientia Sinica* 4; 33–54.

## I

Imai, H., Yamamoto, Y. (1986). "A study on causes of earthquake damage of Izumi high school due to Miyagi-Ken-Okai earthquake in 1978." *Trans Jpn Conc Inst*;8:405–18.

Inoue, N., Suzuki, N. (1992). "Microscopic and macroscopic analysis of reinforced concrete framed shear walls." *In: Concrete shear in earthquake* (Proceedings of the international workshop on concrete shear in earthquake, Jan. 14–16, 1991, Houston). London-New York: Elsevier Science Publishers, Inc; p. 333–42.

Izumo, J., Shin, H., Maekawa, K., Okamura, H. (1992). "An analytical model for RC panels subjected to in-plane stresses." *In: Concrete shear in earthquake* (Proceedings of the international workshop on concrete shear in earthquake, Jan. 14–16, 1991, Houston). London-New York: Elsevier Science Publishers, Inc; p. 206–15.

Izzuddin, B.A. and Smith, D.L. (1996a). "Large-displacement analysis of elasto plastic thin-walled frames. I: formulation and implementation", *Journal of Structural Engineering (ASCE)*, Vol. 122 No. 8, pp. 905-14.

## J

Jiang, H., and Kurama, Y. C. (2010). "Analytical modeling of medium-rise reinforced concrete shear walls." *ACI Struct. J.*, 107(4), 400–410.

Ju, J. W. (1989). "On energy-based coupled elasto plastic damage theories: constitutive modeling and computational aspects." *International Journal of Solids and Structures*; 25:803-833.

## K

Kachanov, L. M. (1958). "Time of rupture process under creep conditions." *Izv.Akad. Nauk SSR, Otd. Tkh. Nauk* 8, 26-31.

Kagermanov, A., Ceresa, P. (2017). "Fiber-section model with an exact shear strain profile for two-dimensional rc frame structures." *J Struct Eng* 143(10):04017,132

Kagermanov, A., Ceresa, P. (2018). "3D Fiber-Based Frame Element with Multiaxial Stress Interaction for RC." *Advances in Civil Engineering*; Volume 2018, Article ID 8596970, <https://doi.org/10.1155/2018/8596970>.

Kanvinde, A. M., Marshall, K. S., Grilli, D. A., and Bomba, G. (2015). "Forensic analysis of link fractures in eccentrically braced frames during the February 2011 Christchurch earthquake: Testing and simulation." *J. Struct. Eng.* 141 (5): 04014146.

Karson, I.D., Jirsa, J.O., (1969). "Behaviour of concrete under compressive loadings." *Journal of Structure Division*, ASCE 95 (12), 2535-2563.

Keo, P., Nguyen, Q-H., Somja, H., Hji, M. (2016). "Derivation of the exact stiffness matrix of shear-deformable multi-layered beam element in partial interaction." *Finite Elements in Analysis and Design*, 112, 40-49.

Kenawy, M., Kunnath, S. K., Kolwankar, S., & Kanvinde, A. (2018). "Fiber-based nonlocal formulation for simulating softening in reinforced concrete beam-columns." *Journal of Structural Engineering*.

Klinkel, S., Govindjee, S. (2002). "Using finite strain 3D-material models in beam and shell elements." *Eng Comput* 19:902–921.

Kotronis, P. and Mazars, J. (2005) "Simplified modelling strategies to simulate the dynamic behaviour of R/C walls," *Journal of Earthquake Engineering* 9(2), 285–306.

Krawinkler H., Parisi F., Ibarra L., Ayoub A., Medina R. (2001). "Development of a testing protocol for wood frame structures." *CUREE* publication No. W-02.

Krieg, R. D. (1975). "A Practical Two Surface Plasticity Theory." *Journal of Applied Mechanics*, 42(3), 641.

Kupfer, H. B., Hildorf, H. K., & Rusch, H. (1969). "Behavior of concrete under biaxial stresses." *Structural Journal, American Concrete Institute*, 66(8), 656–666.

## L

Lee, J., Fenves, G.L. (1998). "Plastic-damage model for cyclic loading of concrete structures." *J Eng Mech*;124(8):892–900.

Lee, J. and Fenves, G. L. (2001). "A return-mapping algorithm for plastic-damage models: 3-D and plane stress formulation." *International Journal for Numerical Methods in Engineering* 50(2): 487-506.

Lee, C-L., and Filippou, F. C. (2015). "Frame Element with Mixed Formulations for Composite and RC Members with Bond Slip. I: Theory and Fixed-End Rotation." *J. Struct. Eng.*, DOI: 10.1061/(ASCE)ST.1943-541X.0001273.

Lemaitre, J. (1985). "A continuous damage mechanics model for ductile fracture." *J. Engng Mater. Technol.* 107,83-89.

Lefas, I. D., Kotsovos, M. D. and Ambraseys, N. N. (1990). "Behavior of Reinforced-Concrete Structural Walls - Strength, Deformation Characteristics, and Failure Mechanism." *ACI Structural Journal* 87(1): 23-31.

Le'geron, F., Paultre, P. (2000). "Behavior of high-strength concrete columns under cyclic flexure and constant axial load." *ACI Struct J* 97(4):591–601.

Leng, Y-B., Song, S-B. (2016). "Experimental study on shear performance of steel–concrete–steel sandwich beams." *J. Constr. Steel Res.* 120; 52–61.

Li, ZX., Gao, Y., Zhao, Q. (2016). "A 3D flexure–shear fiber element for modeling the seismic behavior of reinforced concrete columns." *Eng Struct* 117:372–383.

Li, N., Li, Z., Xie, L. (2013). "A fiber-section model based Timoshenko beam element using shear-bending interdependent shape function." *Earthq Eng & Eng Vib*; 12:421–432.

Long, X., Bao, J.Q., Tan, K.H., Lee, C.K.(2014). "Numerical simulation of reinforced concrete beam/column failure considering normal-shear stress interaction." *Eng Struct* 74:32–43.

Long, X., Tan, KH., Lee, CK. (2013). "A 3D co-rotational beam element for steel and RC framed structures." *Struct Eng Mech*;48(5):587–613.

Lubliner, J., Taylor, R. L., and Auricchio, F. (1993). "A new model of generalized plasticity and its numerical implementation." *Int. J. Solids Struct.*, 30-22, 3171–3184.

Lubliner, J., Oliver, J., Oiler, S. and Onate, E. (1989). "A Plastic-Damage Model for Concrete." *International Journal of Solids and Structures* 25(3): 299-326.

Luccioni, B. and Oller, S. (2003). "A directional damage model." *Comput. Methods Appl. Mech. Engrg.* 192; 1119–1145.

## M

Mansour, M. (2001). "Behavior of reinforced concrete membrane elements under cyclic shear: experiments to theory." Ph.D. dissertation. Houston (TX): *Department of Civil and Environmental Engineering*, University of Houston.

Mansour, M., Hsu, TTC. (2005a). "Behavior of reinforced concrete elements under cyclic shear: Part 1 – experiments." *J Struct Eng*, ASCE;131(1):44–53.

Mansour, M., Hsu, TTC. (2005b). "Behavior of reinforced concrete elements under cyclic shear: Part 2 - theoretical model." *J Struct Eng*, ASCE;131(1):54–65.

Marini, A. and Spacone, E. (2006). "Analysis of reinforced concrete elements including shear effects," *ACI Structural Journal* 103(5), 645–655.

Martinelli, L. (2002). "Numerical simulation of cyclic tests of R/C shear walls," *Proceedings of the Twelfth European Conference on Earthquake Engineering*, London, United Kingdom.

Martinelli, E., Nguyen, Q.H., Hji, M. (2012). "Dimensionless formulation and comparative study of analytical models for composite beams in partial interaction." *J. Constr. Steel Res.* 75(0); 21–31.

Mazars, J., Kotronis, P., Ragueneau, F., and Casaux, G. (2006). "Using multifibre beams to account for shear and torsion applications to concrete structural elements," *Computers Methods in Applied Mechanics and Engineering* 195(52), 7264–7281.

Mazars, J. (1986). "A Description of Microscale and Macroscale Damage of Concrete Structures." *Engineering Fracture Mechanics* 25(5-6): 729-737.

Mazars, J., Kotronis, P. and Davenne, L. (2002). "A new modelling strategy for the behaviour of shear walls under dynamic loading." *Earthquake Engineering & Structural Dynamics* 31(4): 937-954.

Menegotto, M. and Pinto, P. E. (1973). "Method of Analysis for Cyclically Loaded Reinforced Concrete Plane Frames Including Changes in Geometry and Non-Elastic Behavior of Elements under Combined Normal Force and

Bending.” *IABSE Symposium on Resistance and Ultimate Deformability of Structures Acted on by Well Defined Repeated Loads*, Lisbon.

Mohr, S., Bairán, JM., Mari, AR. (2010). “A frame element model for the analysis of reinforced concrete structures under shear and bending” *Eng Struct* 32(12):3936–3954.

Mullapudi, T., Ayoub, A. (2010). “Modeling of the seismic behavior of shear-critical reinforced concrete columns.” *Eng Struct*;32(11):3601–15.

Mullapudi, TR., Ayoub, AS. (2013). “Nonlinear analysis of reinforced concrete walls under three-dimensional loading.” *Mag Concr Res*;65(3):172–84.

## N

Neuenhofer, A., Filippou, F.C. (1997). “Evaluation of nonlinear frame finite-element models.” *Journal of Structural Engineering-ASCE*: 123; 958–966.

Nguyen, Q.-H., Hjjaj, M., Lai, V.-A. (2014). “Force-based FE for large displacement inelastic analysis of two-layer Timoshenko beams with interlayer slips.” *Finite Elem. Anal. Des.* 85; 1–10.

Nie, J., Xiao, Y., Chen, L. (2004). “Experimental Studies on Shear Strength of Steel–Concrete Composite Beams.” vol. 130; No. 8; 1206–13.

Noguchi, H., Inoue, N. (1983). “Analytical techniques of shear in reinforced concrete structures by finite element method.” In; Proceedings, JCI colloquium on shear analysis of RC structures. *Concrete Institute (C4E)*. p. 57–96.

Noguchi, H. (1992). “State-of-the-art of theoretical studies on membrane shear behavior in Japan.” *In: Concrete shear in earthquake* (Proceedings of the international workshop on concrete shear in earthquake, Jan. 14–16, Houston, 1991). London-New York: Elsevier Science Publishers, Inc; p. 196–205.

Nukala, PKVV., White, DW. (2004). “A mixed finite element for three-dimensional nonlinear analysis of steel frames.” *Computer Methods in Applied Mechanics and Engineering*; **193**(23–26):2507–2545.

Nukala, PKVV., White, DW. (2004). “Variationally consistent state determination algorithms for nonlinear mixed beam finite elements.”

*Computer Methods in Applied Mechanics and Engineering*; 193(33–35):3647–3666.

## O

Ottosen, N. S. (1977). "Failure Criterion for Concrete." *Journal of the Engineering Mechanics Division-ASCE* 103(4): 527-535.

Owen, D. R. J., Figueiras, J. A., and Damjanic, F. (1983). "Finite element analysis of reinforced and prestressed concrete structures including thermal loading." *Computer methods in applied mechanics and engineering* 41; 323-366.

## P

Pang, XB., Hsu, TTC. (1995). "Behavior of reinforced concrete membrane elements in shear." *Struct J Amer Concrete Institute*;92(6):665–79.

Pang, XB., Hsu, TTC. (1996). "Fixed-angle softened-truss model for reinforced concrete." *Struct J Amer Concrete Institute*;93(2):197–207.

Papachristidis, A., Fragiadakis, M., Papadrakakis, M. (2010). "A 3D fibre beam–column element with shear modelling for the inelastic analysis of steel structures." *Comput Mech*;45(6):553–72.

Petrangeli, M., Pinto, P. E., and Ciampi, V. (1999). "Fibre element for cyclic bending and shear of RC structures. I: theory," *Journal of Engineering Mechanics* 125 (9), 994, 1001.

Petrangeli, M. (1999). "Fibre element for cyclic bending and shear of RC structures. II: verification," *Journal of Engineering Mechanics* 125 (9), 1002–1009.

Prakash, V., Powell, G., and Campbell, S., (1993). "DRAIN-2DX Base Program Description and User Guide; Version 1.10," *Report No. UCB/SEMM-93/17*, University of California, Berkeley, CA, 90 pp.

Pugh, J. S., Lowes, L. N., & Lehman, D. E. (2015). "Nonlinear line-element modeling of flexural reinforced concrete walls." *Engineering Structures*, 104, 174–192.

## R

Rahal, K.N. and Collins, M.P. (1995). "Analysis of sections subjected to combined shear and torsion - a theoretical model." *ACI Structural Journal*, 92(4):459–469.

Rakowski, J. (1990). “The interpretation of the shear locking in beam elements.” *Comput Struct* 37(5):769–776.

Ranzi, G., Zona, A. (2007). “A steel–concrete composite beam model with partial interaction including the shear deformability of the steel component.” *Eng. Struct.* 29; 3026–3041.

Ranzo, G. and Petrangeli, M. (1998). “A fibre finite beam element with section shear modelling for seismic analysis of RC structures,” *Journal of Earthquake Engineering* 2, 443–473.

Re Di, P., Addessi, D., and Filippou, F. C, (2018). “Mixed 3D beam element with damage plasticity for the analysis of RC members under warping torsion,” *Journal of Structural Engineering*, vol. 144, no. 6, p. 04018064.

Reddy, J.N. (1984). “A simple higher-order theory for laminated composite plates.” *J. Appl. Mech.* 51; 745–752.

Reddy, JN. (1997). “On locking-free shear deformable beam finite elements.” *Comput Methods Appl MechEng*;149:113–32.

Reissner, E. (1950). “On a variational theorem in elasticity.” *Journal of Mathematical Physics* 29; 90–95.

Rezaiee-Pajand, M., Moghaddam, G. N. (2015). “Analysis of 3D Timoshenko frames having geometrical and material nonlinearities.” *Int. J. Mech Sci.* 94-95; 140–155.

Rots, JG., Nauta, P., Kusters, GMA., Blaawendraad, J. (1985). “Smearred crack approach and fracture localization in concrete.” *Heron*;30(1):1–48.

## S

Santos, H.A.F.A., Silberschmidt, V.V. (2014). “Hybrid equilibrium finite element formulation for composite beams with partial interaction.” *Comput. Struct.*, 108, 646–656.

Saritas, A., Filippou, FC. (2009). “Inelastic axial-flexure–shear coupling in a mixed formulation beam finite element.” *Int J Non-linear Mech* 44(8):913–922.

Saritas, A., and Filippou, F. C. (2009). “Frame element for metallic shear-yielding members under cyclic loading.” *J. Struct. Eng.* 135 (9):1115–1123.

Schnabl, S., Saje, M., Turk, G., Planinc, I. (2007). “Locking-free two-layer Timoshenko beam element with interlayer slip.” *Finite Elem. Anal. Des.* 43; 705–714.

Shin, H., Maekawa, K., Okamura, H. (1992). “Analytical models for reinforced concrete shear walls under reversed cyclic loading.” *In: Concrete shear in earthquake* (Proceedings of the international workshop on concrete shear in earthquake, Jan. 14–16, 1991, Houston). London-New York: Elsevier Science Publishers, Inc; p. 289–98.

Silva, G.L.R., Lavall, C.C.A., Costa, S.R., Viana, F.H.(2018). “Formulation for second-order inelastic analysis of steel frames including shear deformation effect.” *J. Constr. Steel Res.* 151: 216–227.

Simo, J. C., Hjelmstad, K. D., and Taylor, R. L. (1984). “Numerical formulations for finite deformation problems of beams accounting for the effect of transverse shear.” *Comput. Methods Appl. Mech. Eng.*, 42, 301–330.

Simo, J. C. and Hughes, T. J. R. (1998). “Computational Inelasticity.” New York, Springer-Verlag.

Sinha, E., Gerstle, K. and Tulin, L. (1964). “Stress-strain relations for concrete under cyclic loading.” *Journal of the American Concrete Institute* 62(2), 195-210.

Soydas, O., Saritas, A. (2013). “An accurate nonlinear 3d Timoshenko beam element based on Hu-Washizu functional.” *Int J Mech Sci* 74:1–14.

Spacone, E., Filippou, F. C., and Taucer, F. F. (1996). “Fiber beam-column model for nonlinear analysis of RC frames. I: Formulation.” *Earthquake Eng. Struct. Dyn.*, 25(7), 711–725.

Spacone, E., and El-Tawil, S. (2004). “Nonlinear analysis of steel-concrete composite structures: State of the art.” *J. Struct. Eng.*, 10.1061/(ASCE)0733-9445(2004)130:2(159), 159–168.

Spacone, E., Ciampi, V., and Filippou, F. C. (1996). “Mixed formulation of nonlinear beam finite element.” *Comput. Struct.*, 58(1), 71–83.

Stevens, N.J., Uzumeri, S.M., Collins, M.P. (1987). “Analytical modeling of reinforced concrete subjected to monotonic and reversed cyclic loadings.” *Dept. of Civil Engineering*, University of Toronto; Publication No. 87-1. Toronto (Canada).

Stramandinoli R. S.B., Rovere H. L. La.(2012). “FE model for nonlinear analysis of reinforced concrete beams considering shear deformation.” *Engineering Structures*, 35, 244–253.

## T

Taig, G., Ranzi, G., Dias-da-Costa, D., Piccardo, G., and Luongo, A. (2015). “A GBT Model for the Analysis of Composite Steel–Concrete Beams with Partial Shear Interaction.” *Structures*; 4:27–37.

Taylor, R.L., Filippou, F.C., Saritas, A., Auricchio, F. (2003). “Mixed finite element method for beam and frame problems.” *Comput Mech*; 31(1-2):192-203.

Tran, T.A., Wallace, J.W. (2015). “Cyclic testing of moderate-aspect-ratio reinforced concrete structural walls.” *ACI Struct J*;112(6):653–65.

Triantafyllou, P. S., Koumousis, K. V., (2011). “An inelastic Timoshenko beam element with axial–shear–flexural interaction.” *Comput. Mech.*, 48, 713–727.

## U

Uddin, M-A., Sheikh, A., Brown, D., Bennett, T., Uy, B. (2018). “Geometrically nonlinear inelastic analysis of steel–concrete composite beams with partial interaction using a higher-order beam theory.” *Int. J. Non-Linear Mech.* 100; 34–47.

## V

Vecchio, F.J., Collins, M.P. (1981). “Stress–strain characteristic of reinforced concrete in pure shear.” *In: IABSE colloquium, advanced mechanics of reinforced concrete*, Delft, Final Report, International Association of Bridge and Structural Engineering; p. 221–5.

Vecchio, F. J. and Collins, M. P. (1982). “The Response of Reinforced Concrete to In-Plane Shear and Normal Stress.” Toronto, Canada, Department of Civil Engineering, University of Toronto.

Vecchio, F. J. and Collins, M. P. (1986). "The Modified Compression Field Theory for Reinforced Concrete Elements Subjected to Shear." *ACI Structural Journal* 83(2):219-231.

Vecchio, F. J. and Collins, M. P. (1988). "Predicting the response of reinforced concrete beams subjected to shear using the modified compression field theory," *ACI Structural Journal* 85, 258–268.

Vecchio, F. J. (1992). "Finite element modeling of concrete expansion and confinement." *Journal of Structural Engineering, ASCE*, 118(9), 2390–2405.

Vecchio, F. J. (2000). "Disturbed stress field model for reinforced concrete: formulation," *Journal of Structural Engineering* 126(9), 1070–1077.

Vecchio, F. J. and Shim, W. (2004). "Experimental and analytical re-examination of classic concrete beam tests." *Journal of Structural Engineering-ASCE* 130(3): 460-469.

## W

Washizu, K. (1955). "On the Variational Principles of Elasticity and Plasticity." Technical Report 25-18, *Aeroelastic and Structures Research Laboratory*, MIT, Cambridge.

Washizu, K. (1982). "Variational Methods in Elasticity and Plasticity." Pergamon, Oxford.

Wilkins, M. L. (1964). "Calculation of elastic-plastic flow." In *Methods in Computational Physics* (Edited by B.Alder), Vol. 3, pp. 211-263. Academic Press, New York.

Wu, Y. J., Li, J. and Faria, R. (2006). "An energy release rate-based plastic-damage model for concrete." *International Journal of Solids and Structures* 43: 583-612.

## X

Xiao, Y., Priestley, M. J. N., and Seible, F. (1993). "Steel jacket retrofit for enhancing shear strength of rectangular short reinforced concrete columns." *Rep. No. SSRP 92/07*, Univ. of California, San Diego.

## Y

Yamada, Y., Yoshimura, N., Sakurai, T. (1968). "Plastic stress–strain matrix and its application for the solution of elastic–plastic problems by the finite element method." *Int J Mech Sci*; 10:343–354.

## Z

Zhu, R. H. (2000). "Softened Membrane Model for Cracked Reinforced Concrete Considering Poisson Effect" PhD dissertation, Dept. of Civil and Environmental Engineering, University of Houston, Houston, TX.

Zhu, RH., Hsu, TTC., Lee, JY. (2001). "Rational shear modulus for smeared crack analysis of reinforced concrete." *Struct J Amer Concrete Institute*;98(4):443–50.

Zhu, RRH., Hsu, TTC. (2002). "Poisson effect of reinforced concrete membrane elements." *Struct J Amer Concrete Institute*;99(5):631–40.

Zienkiewicz, O. C., and Taylor, R. L. (1989). "*The finite element method. Vol. 1, Basic formulation and linear problems*", McGraw-Hill, London.

Zimos, D.K. (2017). Modelling the Post-Peak Response of Existing Reinforced Concrete Frame Structures Subjected to Seismic Loading. (Unpublished Doctoral thesis, City, University of London).

Zimos, D.K., Mergos, P.E., Kappos, A.J. (2018). "Modelling of R/C members accounting for shear failure localization: Hysteretic shear model" *Journal of Earthquake Engineering and Structural Dynamics*; 47:1722-1741.

Zona, A., Ranzi, G. (2011). "Finite element models for nonlinear analysis of steel–concrete composite beams with partial interaction in combined bending and shear." *Finite Elem. Anal. Des.*47(2); 98–118.

Zong, Z., Kunnath, S. K., Monti, G. (2014). "Material model incorporating buckling of reinforcing bars in RC columns." *Journal of Structural Engineering*, ASCE, 140(1), 04013032.

Zulfiqar, N., and Filippou, F.C. (1990). "Models of Critical Regions in Reinforced Concrete Frames under Seismic Excitations". *Report No. UCB/EERC-90/06*, Earthquake Engineering Research Center, University of California, Berkeley.